(2)

ESL-TR-87-35

ATMOSPHERIC PHOTOCHEMICAL MODELING OF TURBINE ENGINE FUELS AND EXHAUST, PHASE II, COMPUTER MODEL DEVELOPMENT, VOLUME I OF II

DR. W.P.O. CARTER, A.M. WINER, R. ATKINSON,
S.E. HEFFRON, M.P. POE, DR. M.A. GOODMAN

UNIVERSITY OF CALIFORNIA
STATEWIDE AIR POLLUTION RESEARCH CENTER
UNIVERSITY OF CALIFORNIA
RIVERSIDE CA 92521

MAY 1988

FINAL REPORT

OCTOBER 1984 - DECEMBER 1986

AFESC

ENGINEERING & SERVICES LABORATORY
AIR FORCE ENGINEERING & SERVICES CENTER
TYNDALL AIR FORCE BASE, FLORIDA 32403

NOTICE

PLEASE DO NOT REQUEST COPIES OF THIS REPORT FROM HQ AFESC/RD (ENGINEERING AND SERVICES LABORATORY). ADDITIONAL COPIES MAY BE PURCHASED FROM:

NATIONAL TECHNICAL INFORMATION SERVICE
5285 PORT ROYAL ROAD
SPRINGFIELD, VIRGINIA 22161

FEDERAL GOVERNMENT AGENCIES AND THEIR CONTRACTORS REGISTERED WITH DEFENSE TECHNICAL INFORMATION CENTER SHOULD DIRECT REQUESTS FOR COPIES OF THIS REPORT TO:

DEFENSE TECHNICAL INFORMATION CENTER
CAMERON STATION
ALEXANDRIA, VIRGINIA 22314

UNCLASSIFIED

SECURITY CLASSIFICATION OF THIS PAGE

ADA198690

REPORT DOCUMENTATION PAGE

Form Approved OMB No. 0704-0188

1a. REPORT SECURITY CLASSIFICATION	1b. RESTRICTIVE MARKINGS
2a. SECURITY CLASSIFICATION AUTHORITY	3. DISTRIBUTION/AVAILABILITY OF REPORT: Approved for public release Distribution unlimited
2b. DECLASSIFICATION/DOWNGRADING SCHEDULE	
4. PERFORMING ORGANIZATION REPORT NUMBER(S)	5. MONITORING ORGANIZATION REPORT NUMBER(S): ESL-TR-87-35
6a. NAME OF PERFORMING ORGANIZATION: University of California Riverside CA; 6b. OFFICE SYMBOL (If applicable)	7a. NAME OF MONITORING ORGANIZATION: Air Force Engineering and Services Center
6c. ADDRESS (City, State, and ZIP Code): Statewide Air Pollution Research Center University of California Riverside CA 92521	7b. ADDRESS (City, State, and ZIP Code): HQ AFESC/RDVS Tyndall AFB FL 32403
8a. NAME OF FUNDING/SPONSORING ORGANIZATION; 8b. OFFICE SYMBOL (If applicable)	9. PROCUREMENT INSTRUMENT IDENTIFICATION NUMBER: F08635-83-0278
8c. ADDRESS (City, State, and ZIP Code)	10. SOURCE OF FUNDING NUMBERS

PROGRAM ELEMENT NO.	PROJECT NO.	TASK NO.	WORK UNIT ACCESSION NO.
62601F	1900	20	40

11. TITLE (Include Security Classification): Atmospheric Photochemical Modeling of Turbine Engine Fuels and Exhaust, Phase II, Computer Model Development, Volume I of II

12. PERSONAL AUTHOR(S): Drs William P.O. Carter, Arthur M. Winer, Roger Atkinson; Ms Susan E. Heffron, Ms Minn P. Poe, and Dr Mark A. Goodman

13a. TYPE OF REPORT	13b. TIME COVERED	14. DATE OF REPORT (Year, Month, Day)	15. PAGE COUNT
Final	FROM Oct 84 TO Dec 86	May 1988	248

16. SUPPLEMENTARY NOTATION: Availability of this report is specified on reverse of front cover

17. COSATI CODES			18. SUBJECT TERMS (Continue on reverse if necessary and identify by block number)
FIELD	GROUP	SUB-GROUP	Ozone formation, atmospheric reactivity, environmental chambers, alkanes, alkenes, photochemical models, acrolein (YES)
04	01		
07	04		

19. ABSTRACT (Continue on reverse if necessary and identify by block number)

A computer model capable of predicting photochemical reactivity of turbine engine fuel emissions and exhaust emissions from routine AF operations is developed. This Phase II report describes experimental work on engine exhaust components conducted in environmental chamber facilities. The results indicate that engine exhaust is significantly more reactive than the fuels themselves. The reaction mechanism incorporates new methods for "lumping" of complex reactive organic gas (ROG) mixtures when representing them in model simulations. This model can be run on Cyber or VAX computers and it provides a reliable and cost-effective means of a priori prediction of photochemical reactivity of AF fuels and exhaust. This technical report is divided into two volumes. Volume I explains the computer model development, while Volume II is the User's Manual.

Keywords:

20. DISTRIBUTION/AVAILABILITY OF ABSTRACT	21. ABSTRACT SECURITY CLASSIFICATION
☒ UNCLASSIFIED/UNLIMITED ☐ SAME AS RPT. ☐ DTIC USERS	UNCLASSIFIED

22a. NAME OF RESPONSIBLE INDIVIDUAL	22b. TELEPHONE (Include Area Code)	22c. OFFICE SYMBOL
SURENDRA B. JOSHI	(904) 283-4235	RDVS

DD Form 1473, JUN 86 — Previous editions are obsolete. — SECURITY CLASSIFICATION OF THIS PAGE: UNCLASSIFIED

(The Reverse of this page is blank.)

PREFACE

This report was prepared by the Statewide Air Pollution Research Center (SAPRC) of the University of California, Riverside, California 92521, under Contract No. F08635-80-C-0359, with the Air Force Engineering and Services Center, Air Force Engineering and Services Laboratory (AFESC/RDVS), Tyndall Air Force Base, Florida 32403.

This report describes the second phase of a two-phase program aimed at developing experimentally tested models for the atmospheric reactions of turbine engine fuels. This phase consisted primarily of the model development and testing and software development, although additional environmental chamber experiments were conducted for several jet engine exhaust constituents.

Volume I of this technical report describes the model development, validation and testing. A user's manual and necessary documentation is being submitted separately as Volume II.

This work was carried out between October 1984 and December 31, 1986 under the direction of Dr William P. L. Carter and Dr Arthur M. Winer, Co-principal Investigators, and Dr Roger Atkinson, Program Manager. The principal research staff on this program was Ms Susan E. Heffron, Ms Minn P. Poe, and Dr Mark A. Goodman. The environmental chamber experiments were carried out with the assistance of Ms Li Li N. Parker and Mr William D. Long. Assistance in preparation of this report was provided by Ms Christy J. LaClaire and Ms Diane L. Skaggs.

Mr Surendra Joshi, AFESC/RDVS, was Project Officer for Phase II of this contract.

This report has been reviewed by the Public Affairs Office (PA) and is releasable to the National Technical Information Service (NTIS). At NTIS, it will be available to the general public, including foreign nationals.

This report has been reviewed and is approved for public release.

SURENDRA B. JOSHI
Project Officer

THOMAS J. WALKER, Lt Col, USAF, BSC
Chief, Environics Division

KENNETH T. DENBLEYKER, Maj, USAF
Chief, Environmental Sciences Branch

LAWRENCE D. HOKANSON, Colonel, USAF
Director, Engineering and Services Laboratory

(The reverse of this page is blank)

TABLE OF CONTENTS

Section	Title	Page
I	INTRODUCTION	1
	A. OBJECTIVES	1
	B. BACKGROUND	1
	C. SCOPE	5
II	SUMMARY OF PHASE I ACTIVITIES AND RESULTS	7
III	ENVIRONMENTAL CHAMBER STUDIES IN PHASE II	11
	A. EXPERIMENTAL	11
	1. Chamber Employed	11
	2. Experimental Procedures and Materials	12
	3. Analytical Techniques	16
	B. RESULTS	24
	1. Characterization Runs	24
	2. Single Component Runs	33
	3. JP-4 Fuel Runs	35
	4. Synthetic Exhaust Runs	40
IV	PHOTOCHEMICAL MODEL DEVELOPMENT AND TESTING	43
	A. DERIVATION OF THE MECHANISM AND DISCUSSION OF UNCERTAINTIES	43
	1. General Representation of Organic Peroxy and Acyl Peroxy Radical Reactions	44
	2. General Alkane Reaction Mechanism	56
	3. Aromatic Reaction Mechanisms	62
	4. Reactions of Furan, Thiophene, and Pyrrole	79
	5. 1-Hexene and General Higher Alkene Reaction Mechanisms	85
	6. Representation of Acrolein in the Model	90
	B. LUMPING TECHNIQUES USED TO REPRESENT REACTIONS OF ROG SPECIES NOT EXPLICITLY IN THE MECHANISM	93
	1. Combined Lumping Approach	94
	2. Pure "Lumped Molecule" Representations	104
	C. MODEL SIMULATIONS OF THE ENVIRONMENTAL CHAMBER EXPERIMENTS	106

TABLE OF CONTENTS
(CONCLUDED)

Section	Title	Page
	1. Representation of Chamber-Dependent Parameters	108
	2. Simulations of Air Force Experiments with Single Organics and Known Mixtures	109
	3. Simulations of Experiments Employing the Reference JP-4 Fuel	148
	4. Summary of Model Performance in Simulations of Our Full EPA and USAF Environmental Chamber Data Base	171
V	ATMOSPHERIC PHOTOCHEMICAL REACTIVITY MODEL	177
	A. OVERVIEW OF THE MODEL	177
	B. EXAMPLES OF ATMOSPHERIC REACTIVITY ASSESSMENT APPLICATIONS	181
	C. MAJOR COMPONENTS OF THE MODEL SOFTWARE	188
	1. User Interface Program	188
	2. Plotting Program	191
	3. Model Integration Program	192
	4. Model Preparation Program	193
VI	CONCLUSIONS AND RECOMMENDATIONS	195
REFERENCES		199
APPENDIX		
A	COMPUTER TAPE CONTAINING RESULTS OF THE AIR FORCE CHAMBER EXPERIMENTS	207
	A. DATA SETS IN "PRINTOUT" FORMAT	212
	B. DATA SETS IN "COMPRESSED" FORMAT	215
B	FULL LISTING OF THE CHEMICAL MECHANISM	221

LIST OF FIGURES

Figure	Title	Page
1	The SAPRC Indoor Teflon® Chamber with Associated Analytical Instruments	13
2	Comparison of Ozone Formation Observed in Environmental Chamber Experiments Employing Four Fuels at Two Different Initial Fuel and NO_x Concentrations	38
3	Experimental and Calculated Concentration-Time Profiles for Selected Species Observed in the Methylcyclohexane-NO_x-Air Experiment ITC-767	130
4	Experimental and Calculated Concentration-Time Profiles for Selected Species Observed in the n-Octane-NO_x-Air Experiment ITC-762	131
5	Experimental and Calculated Concentration-Time Profiles for Selected Species Observed in the 1-Hexene-NO_x-Air Experiment ITC-931	133
6	Experimental and Calculated Concentration-Time Profiles for Selected Species Observed in the 1,3,5-Trimethylbenzene-NO_x-Air Experiment ITC-706	135
7	Experimental and Calculated Concentration-Time Profiles for Selected Species Observed in the Naphthalene-NO_x-Air Experiment ITC-756	136
8	Experimental and Calculated Concentration-Time Profiles for Selected Species Observed in the Furan-NO_x-Air Experiments ITC-711 and ITC-715	139
9	Experimental and Calculated Concentration-Time Profiles for Selected Species Observed in the Acrolein-NO_x-Air Experiment ITC-944	141
10	Experimental and Calculated Concentration-Time Profiles for Selected Species Observed in the "Standard" Synthetic Fuel Experiment ITC-784	142
11	Comparison of Experimental and Calculated Ozone Concentration-Time Profiles for Three Experiments Employing Three Synthetic Fuels, with Initial NO_x = ~0.5 ppm and Initial Fuel = ~100 ppmC	144
12	Comparison of Experimental and Calculated Ozone Concentration-Time Profiles for Three Experiments Employing Three Synthetic Fuels, with Initial NO_x = 0.5 ppm and Initial Fuel = 50 ppmC	145

LIST OF FIGURES
(CONCLUDED)

Figure	Title	Page
13	Comparison of Experimental and Calculated Effects on Ozone Concentration-Time Profiles of Addition of ~(2-5) Percent of Furan, Thiophene, or Pyrrole to a Synthetic Fuel Mixture	147
14	Experimental and Calculated Concentration-Time Profiles for Selected Species Observed in the Synthetic Jet Exhaust Experiment ITC-967	149
15	Experimental and Calculated Concentration-Time Profiles for Selected Species Observed in the "Reference" JP-4 Experiment ITC-966	169
16	Experimental and Calculated Concentration-Time Profiles for Selected Species Observed in the "Reference" JP-4 Experiment EC-492	170
17	Components of the SAPRC-USAF Atmospheric Photochemical Modeling System and their Interrelationship	189

LIST OF TABLES

Table	Title	Page
1	REPRESENTATIVE CHEMICAL COMPOSITION OF JP-4 (REFERENCE 1)	5
2	SUMMARY OF EXPERIMENTS CARRIED OUT FOR TESTING CHEMICAL MECHANISMS FOR TURBINE ENGINE FUELS AND REPRESENTATIVE FUEL CONSTITUENTS	8
3	CHRONOLOGICAL SUMMARY OF ENVIRONMENTAL CHAMBER EXPERIMENTS CARRIED OUT DURING PHASE II	25
4	SUMMARY OF RESULTS OF THE TRACER-NO_x-AIR IRRADIATIONS	31
5	INITIAL REACTANT CONCENTRATIONS AND SELECTED RESULTS OF THE SINGLE ORGANIC-NO_x-AIR IRRADIATIONS CARRIED OUT DURING PHASE II	34
6	INITIAL REACTANT CONCENTRATIONS AND SELECTED RESULTS OF THE JP-4 FUEL-NO_x-AIR AND THE SYNTHETIC EXHAUST-NO_x-AIR IRRADIATIONS CARRIED OUT DURING PHASES I AND II	37
7	COMPOSITION OF THE SYNTHETIC JET EXHAUST MIXTURE, AND MEASURED INITIAL CONCENTRATIONS OF ITS CONSTITUENTS, FOR THE SYNTHETIC JET EXHAUST EXPERIMENTS CARRIED OUT IN THIS PROGRAM	41
8	PEROXY RADICAL PSEUDOSPECIES USED IN THE MECHANISM TO REPRESENT OVERALL PROCESSES COMMON TO PEROXY RADICAL REACTIONS	48
9	KINETIC AND MECHANISTIC PARAMETERS USED IN THE REPRESENTATIONS OF THE REACTIONS OF THE ALKANES	63
10	KINETIC AND MECHANISTIC PARAMETERS USED IN THE REPRESENTATIONS OF THE REACTIONS OF THE AROMATIC HYDROCARBONS	70
11	PARAMETERS ADJUSTED TO FIT ENVIRONMENTAL CHAMBER DATA USING NONLINEAR LEAST SQUARES OPTIMIZATION, AND DATA USED IN THE OPTIMIZATION IN THE DERIVATIONS OF THE REACTION MECHANISMS FOR THE AROMATIC HYDROCARBONS	75
12	KINETIC AND MECHANISTIC PARAMETER USED IN THE REPRESENTATIONS OF THE REACTIONS OF THE ALKENES	91
13	LIST OF ROG SPECIES INCLUDED IN THE MECHANISM, AND THEIR REPRESENTATION IN THE MODEL USING THE COMBINED "LUMPED MOLECULE"-"LUMPED PARAMETER" APPROACHES	95

LIST OF TABLES
(CONTINUED)

Table	Title	Page
14	OH RADICAL RATE CONSTANT RANGES USED TO DETERMINE LUMPED SPECIES GROUPS WHEN REPRESENTING THE REACTIONS OF ALKANES AND AROMATICS USING THE "LUMPED PARAMETER" APPROACH	100
15	LIST OF MODEL SPECIES USED IN THE PURE "LUMPED MOLECULE" REPRESENTATIONS, AND THE TYPES OF COMPOUNDS THEY ARE USED TO REPRESENT	105
16	SUMMARY OF ENVIRONMENTAL CHAMBER RUNS CARRIED OUT UNDER USAF FUNDING WHICH WERE USED FOR MODEL TESTING	107
17	SUMMARY OF CHAMBER-DEPENDENT INPUT PARAMETERS USED IN THE MODEL SIMULATIONS OF THE USAF AND RELATED ITC CHAMBER RUNS	110
18	SUMMARY OF CHAMBER-DEPENDENT INPUT PARAMETERS USED IN THE MODEL SIMULATIONS OF THE USAF AND RELATED EC CHAMBER RUNS	112
19	SUMMARY OF THE INITIAL REACTANT CONCENTRATIONS, AND THE PERFORMANCE OF THE MODEL IN SIMULATING THE OZONE YIELDS AND OZONE FORMATION AND NO OXIDATION RATES IN THE AIR FORCE RUNS USED FOR MODEL TESTING	115
20	SUMMARY OF PERFORMANCE OF THE MODEL IN SIMULATING THE REACTANT HALF-LIVES AND THE PAN AND FORMALDEHYDE YIELDS IN THE AIR FORCE RUNS FOR WHICH SUCH DATA WERE USEFUL FOR MODEL TESTING	124
21	COMPOSITION OF THE REFERENCE JP-4 FUEL, GIVEN IN TERMS OF MILLIGRAMS PER MILLILITER ASSOCIATED WITH MONSANTO'S GC-MS FEATURE NUMBERS (REFERENCE 29)	151
22	LISTING OF THE AFGC.PRM DATA SET, GIVING THE MONSANTO GC-MS FEATURE NUMBERS, THE MONSANTO FEATURE IDENTIFICATIONS AND RELATED DATA, AND THE MODEL COMPOUNDS ASSIGNED TO EACH FEATURE	152
23	COMPOSITION OF THE "REFERENCE" JP-4 FUEL, GIVEN IN TERMS OF THE SPECIES NAMES USED IN THIS MODEL	166
24	AVERAGES OF PERCENTAGE BIASES AND ERRORS IN MODEL SIMULATIONS OF MAXIMUM OZONE YIELDS, AVERAGE NO OXIDATION AND OZONE FORMATION RATES, AND MAXIMUM PAN YIELDS FOR ALL RUNS USED FOR MODEL EVALUATION	172
25	SUMMARY OF THE INPUT DATA FOR THE "EKMA" SCENARIOS USED IN THE REACTIVITY ASSESSMENT EXAMPLES	182

LIST OF TABLES
(CONCLUDED)

Table	Title	Page
26	COMPOSITION OF ALOFT MIXTURE USED IN THE REACTIVITY ASSESSMENT EXAMPLES	183
27	COMPOSITION OF THE SURROGATE MIXTURE USED TO REPRESENT BASE CASE ROG EMISSIONS IN THE REACTIVITY ASSESSMENT EXAMPLES	185
28	COMPOSITIONS OF THE REPRESENTATIVE SURROGATE JET FUELS USED IN THE REACTIVITY ASSESSMENT EXAMPLES	186
29	MAXIMUM BASE CASE OZONE LEVELS CALCULATED FOR THE EXAMPLE EKMA SCENARIO, AND CALCULATED CHANGES IN MAXIMUM OZONE CAUSED BY THE ADDITION OF REPRESENTATIVE TEST MIXTURES	186
A-1	RUN NUMBERS, RUN TYPES, AND FILE NUMBERS FOR ALL CHAMBER RUNS ON THE DATA TAPE	208
A-2	REPRESENTATIVE ABBREVIATIONS USED IN THE DATA TABULATIONS	214
A-3	ORGANIZATION OF THE COMPRESSED DATA FILES FOR CHAMBER RUNS	216
B-1	REACTIONS AND RATE CONSTANTS USED IN THE PHOTOCHEMICAL MODEL	223
B-2	LIST OF SPECIES USED IN THE PHOTOCHEMICAL MODEL	237
B-3	ABSORPTION COEFFICIENT x QUANTUM YIELD PRODUCTS USED TO CALCULATE THE PHOTOLYSIS REACTION RATE CONSTANTS	242
B-4	PHOTOLYSIS RATE CONSTANTS CALCULATED FOR INDOOR TEFLON® CHAMBER (ITC) RUNS WHERE K1 = 0.235 MIN^{-1}, AND FOR REPRESENTATIVE EVACUABLE CHAMBER (EC) RUNS	247
B-5	PHOTOLYSIS RATE CONSTANTS CALCULATED FOR AMBIENT AIR SIMULATIONS FOR SOLAR ZENITH ANGLES OF 0, 30, 60, AND 80 DEGREES	248

(The reverse of this page is blank)

SECTION I

INTRODUCTION

A. OBJECTIVES

The objective of this two-phase program was to develop an experimentally validated chemical kinetic computer model which can be used by the United States Air Force to predict atmospheric impacts of groundlevel emissions of present and future turbine engine fuels and jet exhausts. The model was also designed to predict the atmospheric impacts of changes in fuel and exhaust composition. The model was expected to represent the state of the art in our knowledge of atmospheric chemistry, to be consistent with current detailed knowledge of the atmospheric reaction mechanisms of representative components of current and potential future jet fuels and exhausts, and to be able to satisfactorily simulate results of environmental chamber experiments involving such compounds, both singly and in mixtures. This necessitated carrying out appropriate environmental chamber experiments to develop and test the model. Subsequently, appropriate computer software was developed for the Air Force which allows utilization of the model.

The objective of the first phase of this program was to carry out most of the environmental chamber experiments required to develop the model. The results of that phase of the program were described in an earlier technical report. The overall objective or the second phase of this program was to complete the necessary experimental work, and to develop and test the computer model and the software. The results of this second and final phase of the program, in which the major overall objectives have been achieved, are documented in this report.

B. BACKGROUND

Normal operations of military aircraft involve the use of large quantities of turbine engine fuels. Some release of these fuels into the atmosphere must result from their storage and handling. Further emissions of fuel vapor into the atmosphere occur through in-flight fuel jettisoning

(Reference 1), where operational situations call for the aircraft's gross weight to be reduced to facilitate safe landing, and through the emission of unburned fuel components in jet exhaust (Reference 2). In the presence of oxides of nitrogen (emitted from aircraft engines and other anthropogenic sources), these vaporized fuel components can react in sunlight to form ozone and other secondary pollutants, as well as aerosols. To comply with federal, state, and local air quality regulations, it is necessary to know the impacts of direct emissions of current jet fuels on air quality, and to be able to predict how future changes in fuel composition may affect air quality.

Significant changes in fuel composition may occur in the future since continued dependence on foreign oil as a source of these fuels is economically and militarily unacceptable, and alternate domestic sources such as coal- or shale-oil are likely to be developed during the 1990s. Such a change in derivation will almost certainly involve significantly broadened specifications for future fuels (Reference 3), which, in turn, may affect their atmospheric reactivity. In addition, fuels derived from coal- or shale-oil may also include sulfur-, oxygen-, or nitrogen-containing impurities at levels significantly higher than in present fuels, and this may also affect the extent to which fuel releases affect air quality. However, the nature and magnitude of these effects are presently highly uncertain, and no reliable means exist by which they can be predicted.

Previous studies concerning atmospheric impacts of vaporized aircraft fuels are few, and have been highly limited in scope. Thus, while Bouble et al. (Reference 4) and Scott (Reference 5) dealt with fuel emissions from aircraft and Clewell (Reference 1) discussed fuel jettisoning, these studies did not address the atmospheric reactions occurring after the fuel was emitted or released. However, two recent studies carried out in our laboratories were more directly related to the problem of atmospheric reactions of vaporized fuels. In one of these, a series of multiday outdoor chamber experiments were conducted in which nine different military turbine engine or commercial motor vehicle fuels were vaporized and irradiated in sunlight in the presence of NO_x (Reference 6). This study showed that differences in fuel composition can significantly affect

atmospheric reactivity, and data were obtained concerning the relative reactivities of the nine fuels studied. In the second program, the effects of temperature and pressure on the NO_x-air irradiations of petroleum-derived JP-4 and (to a lesser extent) JP-8 were studied in an indoor environmental chamber (Reference 7) to investigate the effects of altitude on the atmospheric reactivity of these fuels. The reactivity of these fuels in terms of rates of NO oxidation and O_3 formation increased with altitude. This effect was apparently caused by reduced pressure.

However, in terms of being able to predict the effects of future changes in fuel composition on their atmospheric reactivities, the approach employed in our previous studies, i.e., to carry out chamber experiments under a variety of representative conditions for each of the many different present or potential future fuels or fuel types, is neither practical nor cost-effective. For example, to compare the reactivities of nine different fuels required over 130 single- and multiday experiments, and only for two fuels were such experiments carried out under a variety of temperatures and lighting conditions. A much more effective approach would be to develop reliable computer models for the atmospheric reactions for each of the major classes of fuel constituents and potential future impurities, and to use these models to predict the atmospheric reactivity of any present or future fuel whose composition is known. This approach was employed in the study described in this report.

Developing reliable computer models for the atmospheric reactions of fuels involves the following tasks: (1) identifying the major constituents, including S-, N- and O-atom containing fuel impurities, of the fuels of interest; (2) reviewing the kinetic, mechanistic and product data available for the atmospheric reactions of members of the various major classes of fuel constituents and impurities, and using this information to develop chemically valid reaction mechanisms for these processes; (3) carrying out environmental chamber experiments under carefully controlled conditions to test and refine these chemical mechanisms; (4) using the data from these experiments to test the mechanisms and to allow values of uncertain mechanistic or kinetic parameters to be refined to be consistent with the data; and (5) incorporating this tested and refined chemical mechanism into computer software suitable for use by Air Force planners

and others to predict effects of changes in fuel composition on air quality under various idealized scenarios. The work conducted on each of these tasks, during both Phase I and II of this program, is briefly discussed below.

The major constituents of turbine engine fuels have already been identified. As presently used, military jet fuels are multicomponent hydrocarbon mixtures, as exemplified by the petroleum- and shale-derived JP-4 and JP-8 fuels (Reference 6). The major individual components of these fuels are alkanes (straight chain, branched, and cycloalkanes) together with lesser amounts of aromatic hydrocarbons and very small amounts of alkenes (Reference 6). As an example, Table 1 gives a representative composition of JP-4, based on an analysis administered by the Air Force Aeropropulsion Laboratory (Reference 1). In addition, if future military aircraft fuels are derived from coal or shale-oil, they may also contain small (< 2 percent) amounts of sulfur-, oxygen-, and, less likely (Reference 4), nitrogen-containing organics. These heteroatom-containing organics are anticipated to include such compounds as thiophenes, furans, and pyrroles (Reference 8), but detailed analyses of these fuels will be necessary to identify these components.

In addition to a knowledge of the composition of a given fuel, an adequate knowledge of the atmospheric chemistry of its major components is required before reliable chemical mechanisms for its atmospheric reactions can be developed. At the present time, many aspects of the kinetics and reaction mechanisms of O_3 and OH radicals with the simple organic compounds are known or are becoming known from a combination of laboratory, environmental chamber, and computer modeling studies (References 9-26). In particular, the available kinetic data indicate that the essentially sole reaction of the alkane and aromatic fuel constituents occurs via reaction with the hydroxyl radical (Reference 25) and, based on our knowledge of the atmospheric chemistry of the simpler organics, reaction mechanisms for several of the major fuel constituents can be formulated. However, significant gaps still remain in our understanding of the atmospheric chemistry of the aromatics and the larger alkanes (including the cycloalkanes). No data exist concerning the atmospheric chemistry of the heteroatom-containing organics, the naphthalenes, and the other bicyclic aromatic hydrocarbons subsequent to the initial OH radical reaction.

TABLE 1. REPRESENTATIVE CHEMICAL COMPOSITION OF JP-4 (REFERENCE 1).

Component	Mass percentage
Isopentane	3.2
Isohexane	7.1
Cyclohexane	2.2
Benzene	0.3
3-Methylhexane	8.6
Methylcyclohexane	7.3
Toluene	0.8
4-Methylheptane	9.4
cis-1,4-Dimethylcyclohexane	7.7
m-Xylene	1.8
4-Methyloctane	8.7
Isopropylcyclohexane	4.6
1-Ethyl-2-methylbenzene	2.8
2,7-Dimethyloctane	7.0
p-Menthane (cis)	3.9
p-Cymene	2.1
Naphthalene	0.3
Undecane	4.7
3-Methylbutylcyclohexane	2.7
3-Methylenedecalin (trans)	4.0
1-Butyl-3-methylbenzene	1.2
1-Methylnaphthalene	0.3
Dodecane	2.8
3-Ethylbutylcyclohexane	1.3
1,3,5-Triethylbenzene (mesitylene)	0.6
2,3-Dimethylnaphthalene	0.3
Tridecane	1.1
3-Isopropylbutylcyclohexane	0.4
3,5-Diethyl-1-propylbenzene	0.1
Tetradecane	0.2
Pentadecane	0.1
Perhydrophenanthrene	2.2
Residual	0.2

C. SCOPE

To improve our understanding of the atmospheric chemistry of the classes of compounds discussed above, and to develop reliable predictive computer models for the turbine engine fuels, the Air Force Engineering and Services Laboratory contracted the Statewide Air Pollution Research

Center (SAPRC) of the University of California at Riverside to carry out the tasks required for model development. This program consisted of two phases. The first phase (Phase I) involved conducting environmental chamber experiments to provide a data base suitable for testing and refining chemical mechanisms for representative fuel components and representative surrogate and whole fuels (Task 3, above). This phase was completed in June 1984 and the results are briefly summarized in Section II of this report. By far the major effort of Phase I consisted of the environmental chamber experiments. In addition, experimental measurements of the rate constants for the reactions of (a) OH radicals and O_3 with pyrrole, 2-methylnaphthalene, and 2,3-dimethylnaphthalene, and (b) NO_3 radicals with furan, thiophene, and pyrrole were carried out at no added cost to the Air Force. The methods employed and the results obtained are given in the Phase I Final Report, ESL-TR-84-32 (Reference 27).

The second phase of this program (Phase II) involved using these and other available data to develop and test the chemical mechanisms (Tasks 2 and 4) and to develop the necessary software so that the final chemical model can be used by the Air Force for planning purposes (Task 5). A limited number of environmental chamber experiments were also conducted for representative jet engine exhaust constituents and a synthetic jet exhaust mixture, as well as for a preproduction sample of shale-oil derived JP-4 fuel. These experiments allow the model developed for this program to predict the impacts of emissions of jet exhaust, as well as fuel constituents, on air quality. The experimental procedures employed and results obtained in these Phase II environmental chamber studies are described in Section III of this report. Phase II was conducted from October 1, 1984 to December 31, 1986. Phase II of this program is the subject of the present report, which contains a full discussion of the chemical mechanism development, as well as the additional experiments which were conducted, and the results, and conclusions from this study. In addition, a Model User's Manual and other needed documentation has been developed and supplied separately to the Air Force under this contract (Reference 28).

SECTION II

SUMMARY OF PHASE I ACTIVITIES AND RESULTS

The development and testing of chemical mechanisms for inclusion into airshed models for the prediction of worst-case potentials for air quality degradation resulting from use of current and potential future turbine engine (jet) fuels requires an extensive data base derived from environmental chamber and laboratory studies. In Phase I of this two-phase program, 131 environmental chamber experiments were carried out in a ~6400-liter, all-Teflon® indoor environmental chamber, and several kinetic measurements were made to obtain data required for mechanism development. The chamber experiments included 47 single component-NO_x-air irradiations of various representative fuel constituents and potential future fuel-impurities, 15 fuel-NO_x-air irradiations employing one whole and six synthetic surrogate fuels, and 69 control or characterization runs. The number of experiments of the various types which were conducted in the Phase I program are summarized in Table 2.

NO_x-air irradiations of single representative fuel constituents are generally the most useful for testing chemical mechanisms for individual compounds or classes of compounds. The single compounds studied were benzene and the representative alkylbenzenes toluene, m-xylene, and mesitylene (1,3,5-trimethylbenzene), tetralin, naphthalene, and 2,3-dimethylnaphthalene, the representative alkanes n-octane and methylcyclohexane, and the representative potential future heteroatom-containing fuel impurities furan, pyrrole, and thiophene. These compounds constituted a reasonably good representation of the various classes of compounds present in current turbine engine fuels, or which are anticipated as possible impurities in future fuels.

NO_x-air irradiations of synthetic "surrogate" fuels, whose exact compositions are known, are useful for testing chemicals for the complete fuels, since uncertainties in the exact fuel composition are avoided. The specific synthetic fuel mixtures studied in this program consisted of the following: (1) a "standard" 15-component synthetic fuel whose composition was specified by the Air Force before the beginning of this program, and was taken to represent military jet fuels currently in use; (2) a "high-

TABLE 2. SUMMARY OF EXPERIMENTS CARRIED OUT FOR TESTING CHEMICAL MECHANISMS FOR TURBINE ENGINE FUELS AND REPRESENTATIVE FUEL CONSTITUENTS.

Type of experiment	No. runs (total = 131)
Single Constituent	
Benzene	3
Toluene	2
m-Xylene	2
Mesitylene (1,3,5-Trimethylbenzene)	5
Tetralin	5
Naphthalene	5
2,3-Dimethylnaphthalene	4
n-Butane	1
n-Octane	4
Methylcyclohexane	4
Furan	4
Thiophene	4
Pyrrole	4
Synthetic Fuel	
Standard fuel	4
Standard fuel + furan	1
Standard fuel + pyrrole	1
Standard fuel + thiophene	1
Fuel #2 (high aromatics)	2
Fuel #3 (modified aromatics)	2
Whole Fuel	
Pre-production shale-derived JP-4	4
Control and Characterization	
NO_x-air irradiations	[a]31
NO_2 actinometry runs	25
Propene-NO_x irradiations	10
O_3 dark decays	2
Acetaldehyde irradiations	1

[a]Not counting the 13 NO_x-air + alkane or aromatic experiments, which also give chamber characterization data.

aromatics" fuel which had the same components as the "standard" fuel but in which the percentage of aromatics (on a mole carbon basis) was increased from 27 percent to 38 percent; (3) a "modified aromatics" fuel which had the same relative amounts of the alkanes and aromatics as did the standard fuel, but in which the ratio of the alkylbenzenes to the bicyclics tetralin, naphthalene, and 2,3-dimethylnaphthalene was increased by a factor of 2, relative to that in the other fuels; and (4) the "standard" fuel with 1-2 percent (on a mole carbon basis) of either furan, pyrrole, or thiophene added as an "impurity." These different formulations were useful for testing the effects of changing fuel composition on their atmospheric reactivity, and for testing models designed to predict these effects.

In addition to the above, it is also necessary to test the predictions of the chemical model against experiments employing real fuels. Since environmental chamber data were already available concerning NO_x-air irradiations of various whole fuels from our previous USAF-funded programs (References 6 and 7), obtaining such data was not a major effort in this program. However, to further expand the available data base concerning whole fuels, a series of experiments employing a preproduction batch of shale-oil derived JP-4 fuel was carried out in this program.

In addition to the runs discussed above, a number of control and characterization runs were carried out so that the conditions of the various experimental runs would be sufficiently well-characterized to be used for mechanism testing. These included runs of the following type: (1) NO_2 actinometry experiments to monitor the light intensity, (2) organic tracer-NO_x-air irradiations to monitor the magnitude of the chamber radical source and contamination by reactive organics (Reference 21), (3) propene-NO_x-air control runs to condition the chamber (when required) and to test for overall chamber performance [since the atmospheric chemistry of propene is reasonably well understood] (References 11, 15, and 17), and (4) O_3 dark decay rate determinations.

Pyrrole, furan, and the methylbenzenes were found to be the most reactive in terms of rates of O_3 formation, with benzene, tetralin, the naphthalenes, and thiophene having intermediate reactivity, and the alkanes being by far the least reactive. The large differences in

reactivity observed between these classes of compounds is primarily due to the differing effects their photooxidations have on radical levels in NO_x-air irradiations, with the OH radical rate constant determining the relative reactivities within a given class of compounds.

The fuel-NO_x-air runs showed that changes in the composition of the turbine engine fuels can significantly affect their atmospheric reactivity. Thus, increasing the total level of aromatics in the 15-component synthetic fuel resulted in increased rates of O_3 production, but also resulted in lower maximum O_3 yields. In contrast, increasing the ratio of alkylbenzenes to bicyclic aromatics (with the total aromatic concentrations remaining unchanged) increased both the O_3 formation rates and the maximum O_3 yields. The addition of small amounts (1-2 percent on a mole carbon basis) of furan or pyrrole to the fuel resulted in dramatic increases in O_3 production rates and also suppressed O_3 yields, but the addition of comparable amounts of thiophene to the fuel had a relatively minor effect. The implications of these results for the photooxidation mechanisms of these compounds were discussed in our Final Report to Phase I of this program.

In associated kinetic studies, OH radical and O_3 rate constants were obtained for pyrrole, 2-methylnaphthalene, 2,3-dimethylnapthalene, and NO_3 radical rate constants were determined for furan, thiophene, and pyrrole for the first time.

The results of this program provided an important and necessary data base required for the development of a chemical mechanism for the atmospheric reactions of current and future turbine engine fuels which was carried out in Phase II of this two-part program.

SECTION III

ENVIRONMENTAL CHAMBER STUDIES IN PHASE II

Although most of the environmental chamber experiments used to derive data necessary for model development and testing were carried out under Phase I of this program, a limited number of experiments were also conducted in Phase II. These experiments were aimed primarily at obtaining data necessary to extend the applicability of the model being developed to simulations of jet exhaust reactivity, though several experiments with samples of JP-4 fuel were also carried out. The specific types of experiments conducted during this phase of the program were as follows: (1) NO_x-air irradiations of the representative jet exhaust constituents ethene, propene, 1-butene, 1-hexene, and acrolein; (2) NO_x-air irradiations of a synthetic jet exhaust mixture; (3) NO_x-air irradiations of a sample of JP-4 fuel obtained from a USAF storage tank; (4) NO_x-air irradiations of the "reference" sample of JP-4 fuel (Reference 29) employed in previous chamber studies (References 6, 7) and (5) various associated chamber characterization and control runs similar to those carried out in association with the Phase I experiments. The experiments conducted, the facility and procedures employed, and a summary of the results obtained are described in this section.

Detailed tabulations of the data obtained from the experiments carried out during both phases of this program are available on tape in computer readable format. A copy of this tape has been submitted to AFESC/RDVS at Tyndall AFB, and copies are available from the authors of this report for the cost of duplication. The contents and format of this data tape are described in Appendix A of this report.

A. EXPERIMENTAL

1. Chamber Employed

The ~6400-liter SAPRC indoor Teflon® chamber was employed for all of the chamber experiments conducted in this study. The chamber consisted of a reaction bag which was constructed of 2-mm thick FEP Teflon® panels

heat-sealed together using a double-lap seam and externally reinforced with Mylar® tape. The reaction bag was fitted inside an aluminum frame of dimensions of 8 feet x 8 feet x 4 feet. One edge was hinged to allow the bag to collapse to less than one-fifth of its maximum volume. This chamber is shown schematically in Figure 1.

The light source for this indoor Teflon® chamber consisted of two diametrically opposed banks of 40 Sylvania 40-W BL blacklamps backed by arrays of Alzak-coated reflectors. The light intensity could be controlled by switching on or off sets of lights as previously described (Reference 30) although for all the indoor runs reported here, the light intensity was held constant at 70 percent of its maximum. The intensity and spectral characteristics of this light source are discussed elsewhere (References 26, 27, 31).

Pure air for these experiments was provided by an air purification system which has been described in detail (Reference 32). This system can produce both dry and humidified pure air, and reduced the hydrocarbon levels (as measured in the chamber) to ~800 ppb methane, <5 ppb of C_2 hydrocarbons and propane and <1 ppb of all higher hydrocarbons.

2. Experimental Procedures and Materials

Before each experiment, the chamber was flushed with purified air for at least 3 hours with the lights on and then for at least 2 hours with the lights off. For the final flush purified air humidified to ~50 percent relative humidity (RH) was employed. Before any reactant injections, background samples were analyzed using all of the gas chromatographic instruments to be employed during the run. NO, NO_2 and the various surrogate components were then injected individually, as described below. Gas chromatographic (GC) samples were then taken on all instruments before the beginning of the irradiations.

Techniques used to inject the reactants depended on the type of reactant, and are as follows:

NO and NO_2. In the case of NO, the calculated volume of gaseous NO was taken from a cylinder of Matheson, C.P. grade nitric oxide with a

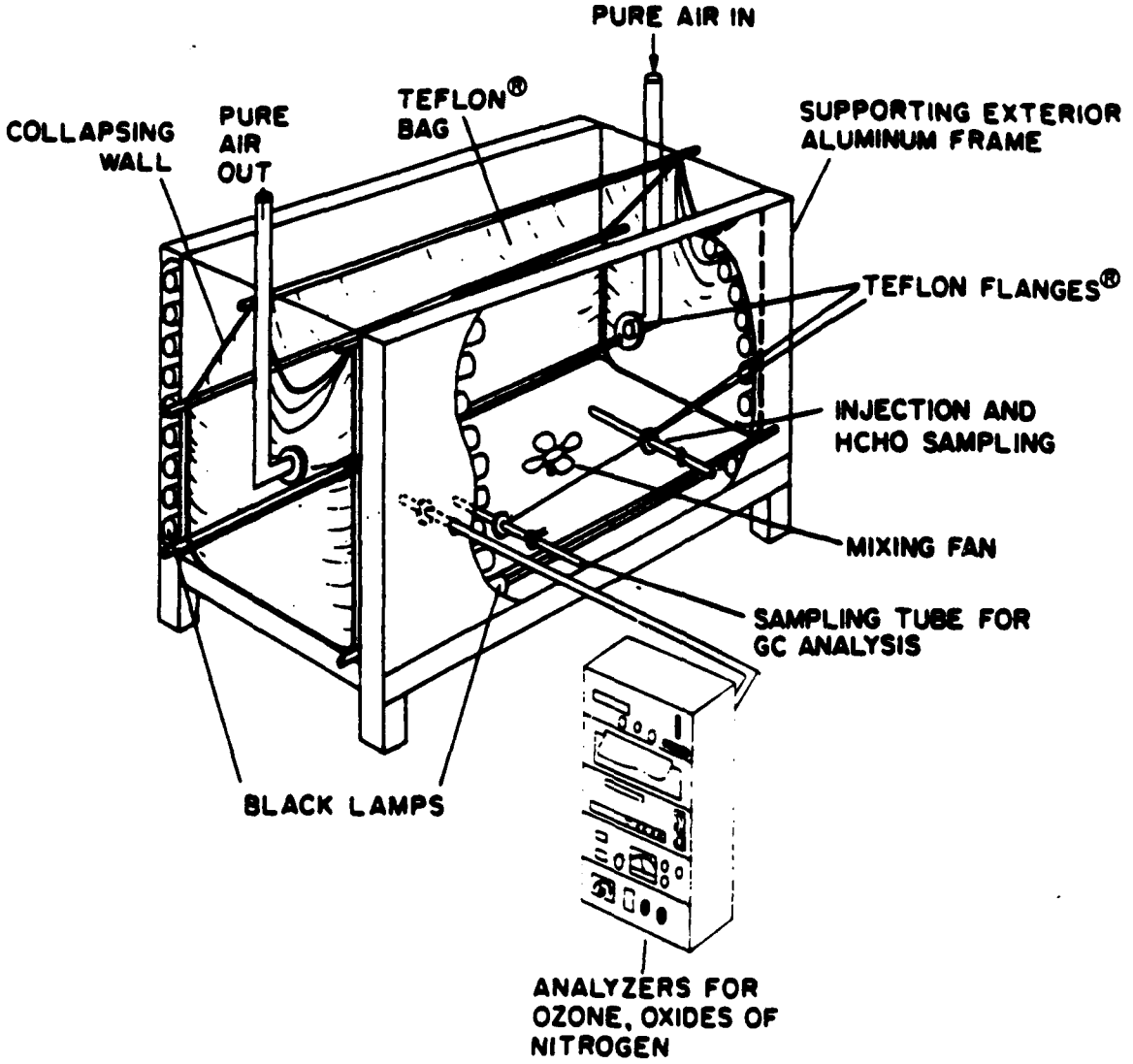

Figure 1. The SAPRC Indoor Teflon® Chamber with Associated Analytical Instruments.

20-mL gas-tight, all-glass syringe (with a stainless steel tip), and diluted to 100-mL with N_2 using a separate 100-mL syringe. The NO_2 was prepared in a similar manner, except that the NO was diluted with an excess of O_2 to yield NO_2. The contents of these syringes were then injected into the chamber through the Pyrex® tube running into the chamber through the injection and formaldehyde sampling port (see Figure 1), and then flushed into the chamber with N_2.

Gaseous Hydrocarbons. Gaseous hydrocarbon reactants were injected using 100 mL glass syringes and flushed into the chamber using the same general procedure as employed for NO.

Liquid Reactants. Pure liquid reactants used in these experiments were injected into the chamber as follows: The desired amount of the liquid was injected, using a microsyringe, into a 5-liter Pyrex® bulb equipped with stopcocks on each end and a port for the injection of the liquid. The port was then closed, and one end of the bulb was attached to the injection port of the chamber and the other to a nitrogen source. The stopcocks were then opened, and the vaporized contents of the bulb were flushed into the chamber for approximately 20 minutes. Acetaldehyde (used in acetaldehyde-air irradiations) was purified by vapor transfer before use.

Solid Reactants. Solid reactants employed in this study consisted of the naphthalenes which were included among the components of the synthetic exhaust mixture. These were injected as described in the Phase I report (Reference 27). Briefly, the solids were packed into 0.25-inch o.d. Pyrex® tubes, held in place with glass wool, and their vapors were flushed into the chamber with N_2 at 2 liters min^{-1} for the amount of time required to attain the desired concentration in the chamber. This amount of time was calculated based on their known vapor pressures.

JP-4 Fuels. Two samples of JP-4 fuel were used in the experiments carried out during this phase of the program: (1) an aged sample of JP-4 obtained from a normal USAF storage tank at Tyndall AFB, and (2) a sample of the "reference" JP-4 (Reference 29) which was employed in previous chamber programs carried out under funding from AFESC/RDVS (References 6 and 7). The latter sample had been stored in a sealed Pyrex® bottle in a freezer since the time it has been obtained from the Air Force. These

fuels were injected into the chamber using the same procedure as described above for pure liquids, except that a heat gun was used to heat the bulb during the injection of the JP-4 fuel, to assist in its volatilization.

Synthetic Exhaust Mixture. The mixture used in the synthetic exhaust experiments consisted of a number of liquids, solids, and gases, including formaldehyde and methylglyoxal. The gases, other than formaldehyde and methylglyoxal, and the solids were injected as described above. The liquids, other than benzene and acetaldehyde, were all mixed together on the day before the experiment according to their desired relative amounts (measured using microsyringes), and injected as described above for pure liquids. Benzene and acetylene were injected separately, as described above. Formaldehyde was prepared on the day of the experiment by heating paraformaldehyde in an evacuated vacuum line attached to a 5-liter bulb of accurately known volume, until the pressure in the bulb corresponded to the amount desired. The contents of this bulb were then flushed into the chamber with N_2. Methylglyoxal was prepared as described previously (Reference 33), and measured and injected using vacuum techniques similar to that used for formaldehyde. Methylglyoxal was stored under liquid N_2, in an evacuated bulb when not being used.

The procedures during the irradiations were generally the same for most experiments. Data from the continuous monitoring instruments (see below) were collected every 15 minutes using a computerized data acquisition system, and GC samples were taken at least hourly, and sometimes more frequently, depending on the type of experiment and compound being monitored. Irradiation time varied with the type of experiment, but most were 6-hour irradiations. The irradiation times, special procedures employed, and approximate initial reactant concentrations are given in the chronological listing of these runs given at the beginning of Section III. The detailed data tabulations described in Appendix A include comments giving the specific procedures employed for each run, taken from the laboratory notebooks.

3. Analytical Techniques

This section describes the analytical procedures employed for each set of compounds or physical parameters monitored in this program and discusses the calibration technique and estimated accuracy for each.

a. Continuous Monitoring Instruments

Ozone, nitrogen oxides and temperature were monitored continuously, using the instruments described below. Except as noted, samples for analysis by these systems were taken directly from a probe inserted ~18 inches into the chamber, using Teflon® or Pyrex® sampling lines.

- Ozone was monitored using a Dasibi Model 1003AH UV absorption ozone monitor. Calibrations were carried out every 2 months against a Dasibi Model 1003AH ozone monitor transfer standard which, in turn, was routinely calibrated by the California Air Resources Board. The ozone source was a Monitor Labs Calibrator Model 8500, with four different ozone concentrations, and the dilution gas was Liquid Carbonic Company Medical Air. The analyzer being calibrated was first zeroed using Medical Air, then the calibrator was turned on to produce the highest concentration of ozone, ~0.3 ppm. Both analyzers were allowed to equilibrate before any readings were recorded. The ozone concentration was then reduced, and the output from both instruments was observed to verify that the response was linear, this being repeated at two lower ozone concentrations. If the response was not linear, then corrective action was taken. Finally, the analyzer being calibrated was again zeroed with Medical Air. The precision and accuracy were both better than 5 percent.

- Nitric oxide and total oxides of nitrogen (NO_x + organic nitrates) were monitored with a Columbia Scientific Instruments Series 1600 chemiluminescence oxides of nitrogen analyzer. Calibrations, using a Monitor Labs, Inc. Model 8500 calibrator as the dilution system, and a National Bureau of Standards cylinder of 97.4 ppm of NO in nitrogen, were performed bimonthly. The dilution gas was Liquid Carbonic Company Medical Air. The analyzer was first zeroed using Medical Air, then calibrated for NO by

diluting NO in Medical Air and measuring the flow of each gas with a bubble flowmeter. The analyzer was allowed to equilibrate at each concentration for 30 minutes. The first concentration used was ~0.30 ppm. The potentiometers in the analyzer were adjusted, if necessary, to match the NO output of the analyzer with the actual concentration. Two lower concentrations were used to verify linearity of the analyzer. The converter efficiency was checked by setting up an NO concentration of about 0.30 ppm, and reacting this with a lesser concentration of ozone. If the converter was operating properly, the NO_2 would equal the difference in NO. The linearity of the converter was verified by using three different concentrations of ozone. After this procedure was completed, the analyzer was rezeroed with Medical Air. The accuracy and precision of this instrument in the absence of interfering nitrates (see below) was estimated to be comparable to those for the ozone monitors, i.e., better than 5 percent.

The analyses of NO_2 and NO_x are complicated by the fact that for such instruments the converters have been shown (Reference 34) to convert PAN, organic nitrates and HNO_3 to NO, and thus, such species yield a positive interference in the NO_2 analysis cycle. (The NO data are unaffected.) Conversion of PAN and organic nitrates is essentially quantitative for molybdenum converters employed in some types of NO_x analyzers (Reference 34), but this is not the case for the converter employed in the Columbia Scientific Industries instrument. Preliminary data from our laboratories have indicated that the conversion of PAN is not quantitative on this instrument. Thus, no correction for this interference on the NO_2 data was attempted.

- Temperatures were monitored with an Analogic Model AN 2572 Digital thermocouple indicator using iron-constantan thermocouples. The thermocouple was installed in a probe inserted into the center of the chamber. This instrument was calibrated, periodically, using ice water as the source for 0°C and boiling water as the source for 100°C. The accuracy was better than 5 percent, and the precision was better than 1 percent.

b. Gas Chromatographic Analyses

Organic reactants and products were monitored using six different gas chromatographic systems, each suitable for a particular set of compounds. Samples for chromatographic analyses were withdrawn from the chamber using 100 mL gas-tight, all-glass syringes. The syringes were flushed at least three times with the sample gas before the sample for analysis was taken. A syringe was attached to the sample port of the chamber to withdraw a sample. The sample port was an ~18-inch by 0.25-inch Pyrex® tube with a Becton-Dickinson stainless steel lever-lok stopcock manifold. Depending on the gas chromatographic analysis system, the contents of the syringe were either: (1) flushed through ~2-mL stainless steel or ~10-mL heated glass loops and injected onto the column by turning a gas-sample valve, (2) condensed in a trap cooled with liquid argon, and injected onto the column by simultaneously turning the gas-sample valve and heating the loop with boiling water or ice water, or (3) flushed through a purged Tenax® tube. The various gas chromatographic systems used, and the compounds they monitored, are briefly described below.

- Oxygenates such as acetaldehyde, acetone, 2-butanone, and acrolein, organic nitrates such as 2- and 3-pentyl nitrates and aromatic hydrocarbons such as toluene and m-xylene were monitored using the "C-600" gas chromatograph (GC). This system consisted of a Varian 1400 GC with a flame-ionization detector (FID) and a 10-feet by 0.125-inch stainless steel column packed with 10 percent Carbowax® 600 on C-22 Firebrick (30/60 mesh). The flow through this column was set at 50 mL min^{-1} and, as was the case with all of the GCs, the carrier gas was nitrogen. The hydrogen flow was kept at 45 mL min^{-1}, and the oxygen, used in the place of air to enhance sensitivity, was set at 250 ml min^{-1}. The detector was heated to 200°C, and the column was maintained at 75°C. One hundred mL samples drawn from the chamber were trapped by pushing the gas sample through a 10-inch by 0.125-inch stainless steel tube packed with glass beads (80 mesh) and immersed in liquid argon. The sample was carried onto the column by immersing the trap in boiling water while actuating the gas-sampling valve which was heated to 95°C to prevent adsorption of compounds.

• Methane, ethane, ethene, and acetylene were monitored using the "PN" GC which consisted of a Varian 1400 GC with a flame-ionization detector and a 5-feet by 0.125-inch stainless steel column packed with Porapak® N, 80/100 mesh. The nitrogen carrier flow was set at 80 mL min^{-1}, the hydrogen at 60 mL min^{-1} and the oxygen at 400 mL min^{-1}. The column was maintained at 60°C, while the detector was heated to 180°C. When a sample was to be analyzed for methane, 100 mL of the sample was pushed through a 3-mL stainless steel loop. The sample in the loop was then transferred onto the column by actuating the gas sampling valve. Sampling for ethene, ethane and acetylene was accomplished by trapping the sample in a 11-inch by 0.125-inch stainless steel column packed with 10 percent Carbowax® 400 on Firebrick, 30/60 mesh, immersed in liquid argon. The sample was thawed by immersing the trap in ice water while turning the valve so that the sample was transferred to the column.

• C_2-C_5 alkanes and alkenes were monitored using the "DMS" GC, which consisted of the electrometer and flame-ionization detector from a Varian 1400 GC with a 34.5-feet x 0.125-inch stainless steel column packed with 10 percent 2,4-dimethylsulfolane on acid-washed 60/80 mesh Firebrick. At the end of this column, before the detector, was a 2-feet x 0.125-inch stainless steel "soaker" column packed with 10 percent Carbowax® 600 on Firebrick. The carrier nitrogen flow through these two columns was set at 50 mL min^{-1}, as was the hydrogen flow. The oxygen flow was 330 mL min^{-1}. The columns were maintained at 0°C and the detector was heated to 115°C. The 100-mL gas samples were trapped on a 10-inch by 0.125-inch stainless steel column packed with 10 percent 2,4-dimethylsulfolane on Firebrick, 60/80 mesh, immersed in liquid argon. The sample was then introduced to the column by simultaneously thawing the trap in ice water and turning the gas sampling valve. In some experiments, where these compounds were monitored at higher concentrations, sampling was carried out by flushing a ~2 mL loop with the sample from the chamber, with the contents of the loop then being injected into the column.

Some problems were experienced with this instrument during the course of this program. In some experiments, where propene, 1-butene, or n-butane were injected, their concentrations, as monitored by this instrument were inconsistent with the amount injected. In many cases the

measured values were high by approximately a factor of two. This was probably caused by an incorrect setting of the recorder sensitivity. The calibration factors were adjusted by a factor of two, to bring the reported concentrations within the expected range. In addition, in the n-butane and 1-butene experiments where the loop sampling technique was employed, the initial concentrations were found to be 25-50 percent higher than expected. In those cases, initial concentration used in the model simulations were estimated, based on the volume of gas injected and the estimated ~5800-liter volume of the chamber, but the data on the detailed data tabulations were not changed. The comments on the data tabulations for the runs indicate when these problems arose, and how they were treated in each individual case.

- C_5 of higher alkanes and alkenes, aromatic hydrocarbons and some oxygenates and alkyl nitrates were monitored by a Hewlett-Packard 5711A gas chromatograph with a flame ionization detector and a 97.5-feet by 0.013-inch fused silica capillary column. This column, manufactured by J&W Scientific, Inc., had a film thickness of 1 μm composed of the bonded, liquid phase DB-5. The nitrogen carrier flow was set at 1.1 mL min^{-1} and the makeup gas, also nitrogen, was set to 30 mL min^{-1}. The hydrogen and oxygen flows were maintained at 30 mL min^{-1} and 230 mL min^{-1}, respectively. Before a sample was taken, the column oven was cooled to -90°C. Sampling was accomplished by flushing 100 mL of sample through a dichlorodimethylsilane treated 10.2-mL glass loop. The GC gas-sampling valve, which was maintained at 145°C, was then actuated, and the sample was transferred onto the head of the column (at -90°C) over 12 minutes. The column was then heated from -90 to -50°C over a 1.3-minute duration. The temperature program was then started with the column being heated from -50 to 200°C at a rate of 8°C min^{-1}.

- Peroxyacetyl nitrate (PAN) was monitored using an Aerograph gas chromatograph with electron capture detector (ECD). The detector was equipped with a standing current control, and since the response was directly influenced by the standing current, it was maintained to within 2 percent of a constant value during all experiments and calibrations. The GC used a 12-inch x 0.125-inch FEP Teflon® column containing 5 percent

Carbowax® 400 on Chromosorb G (80/100 mesh) operating at room temperature with a nitrogen carrier flow of 75 mL min^{-1}.

Calibrations of all GCs were performed at approximately 2- to 3-month intervals, and, except for the gas chromatographs used to monitor PAN, were carried in the same general manner. First, all gas flows were measured to verify that no changes had occurred that would indicate previous measurements were erroneous. After measuring these flow rates, a calibration mixture was made up, using one of the two methods described below. The calibration mixture, composed of known quantities of various compounds, was then injected into the appropriate GC. The elution time and height of each peak were recorded. The height of each peak was multiplied by the attenuation and the response in millivolts was obtained.

For gaseous compounds, two 2000-mL flasks, whose volumes had been determined by measuring with water, were flushed with nitrogen for 20 minutes, and then 2 mL of each pure gas was injected into the first flask with a 5 mL syringe. This flask was allowed to mix for 20 minutes, and 2 mL from this flask was transferred into the second flask. The contents of this second flask were allowed to mix for 20 minutes. This resulted in a concentration of 1 ppm of the gas in the second flask. Loop calibrations were performed by connecting this second flask directly to the loop and flushing the loop with the contents of the flask. Trap calibrations were accomplished by diluting a 5 mL sample from the second flask with nitrogen in a 100 mL syringe, and passing the contents of the syringe through the trap. For a flask containing 1 ppm of the compound, this was equivalent to sampling 100 mL of gas containing 50 ppb of the compound.

Calibration of compounds that were liquid in a pure state at room temperature was carried out using an ~50-L all-glass carboy, which was first cleaned by being heated from the inside with a heat gun, then cooled with the heat gun with the heat off until the carboy reached room temperature, and finally flushed with nitrogen for one hour. The carboy was then dosed with 1 μL of each pure liquid to be calibrated using a 10 μL syringe. These were allowed to mix for 1 hour before samples were taken. Trap and loop calibrations were both accomplished in the same way. A 1 mL sample was taken from the carboy with a 5 mL syringe and

diluted with 99 mL of nitrogen. The samples were injected in the manner described previously. The exact concentration of each compound was calculated knowing the amount of liquid injected and its density.

Calibration samples of PAN were prepared in pressurized cylinders as described previously (Reference 35), and the PAN concentration was determined by infrared absorption of the 8.6μ band [absorption cross section = 13.9 by 10^{-4} ppm^{-1} (Reference 36)]. The contents of the cylinder were diluted using a flow manifold with calibrated rotometers to yield PAN concentrations in the range 5-50 ppb, and 100-mL samples were taken directly from the flow manifold using gas-tight, all-glass syringes.

The expected accuracy and precision of concentration measurements of most of the compounds determined by the above systems were, with the exception of PAN and acetaldehyde, ~5 percent or better. Because of varying peak widths, acetaldehyde concentrations were precise and accurate to ~20 percent. Peroxyacetyl nitrate measurements were estimated to have ~10 percent precision and ~25 percent accuracy, while acrolein measurements were estimated to have similar precision and accuracy.

c. Formaldehyde Analysis

Formaldehyde was monitored using the chromatropic acid technique. Samples for analysis by this technique were obtained by drawing (at 1 liter min^{-1}) 20 liters of air from the chamber through a single bubbler containing 10 mL of doubly distilled water. The sample probe for the indoor chamber consisted of a 0.5-inch Pyrex® tube with the internal tip located 18 inches from the chamber wall. A metal bellows pump at the downstream end of the bubbler, with a calibrated flowmeter and needle valve, was used to pull the sample through the bubbler. The samples were developed by adding 0.10 mL of chromatropic acid (4,5-dihydroxy-2,7-naphthalenedisulfonic acid disodium salt) to a 4.0 mL aliquot of the sample. The solution was acidified by diluting it to 10.0 mL with concentrated sulfuric acid. The chromatropic acid solution was prepared by dissolving 0.10 g of the salt in 10.0 mL of doubly distilled water. The developed solutions were purple and the absorbances were measured at 580

nm by a Beckman Model 35 spectrophotometer, after zeroing the instrument using a prepared blank. Instrumental drift was also checked periodically during the measurements using the same blank.

Periodic calibrations of the spectrophotometer and flowmeters were carried out. The spectrophotometer was calibrated by exposing a known concentration of formaldehyde salt to the same procedure as outlined above.

The accuracy and precision of this formaldehyde analysis technique depended upon a number of factors, including the calibration of the spectrometer and the efficiency of the bubbler in collecting formaldehyde from the air passing through it. In the past, the accuracy and precision of this technique had been quite variable, ranging from an optimum accuracy and precision of ~30 percent, to periods of anomalously low readings (apparently due to problems with the bubbler), to periods of anomalously high and variable readings apparently caused by contamination. Although attempts had been made to improve the reliability of this technique for routine use, they have been met with variable success.

d. Light Intensity Determination

The light intensity was measured periodically in separate experiments using the quartz tube NO_2 actinometry technique of Zafonte et al. (Reference 37). In this technique, the reactor cell consisted of a 100-cm, 21.44-mm i.d. quartz tube with blackened extensions at each end. NO_2 was fed through this tube at a flow rate of typically 37 mL s^{-1}. This corresponded to an approximate residence time of 9 seconds in the exposed portion of the tube, allowing a measurable amount of NO to build up under irradiation, from which the NO_2 photolysis rate can be calculated (Reference 37). The NO_2 used in these experiments was obtained from a Scott-Marrin, Inc. tank mixture of 1.5 ppm NO_2 in nitrogen, and was not diluted further. The NO_2 flow entered and exited the reactor cell via blackened FEP Teflon® tubing. The NO and NO_2 were measured using a chemiluminescence $NO-NO_2-NO_x$ monitor and a Teco Model 14-B, which was calibrated every other month using the same procedure as described above for the NO_x analyzer used to sample the contents of the chamber.

The precision of these NO_2 actinometry measurements was generally ~5-10 percent. The accuracy of the NO_2 actinometry measurements was determined by a number of factors, including: (1) the accuracy of the NO_x analyzer, (2) the extent to which plug flow conditions in the tube had been established, and (3) whether the tube was placed in a location in which the light intensity and spectral distribution accurately reflected that in the chamber.

B. RESULTS

A total of 51 environmental chamber irradiations were carried out in this phase of this program, including 15 NO_x-air irradiations of various representative alkenes representative of those in jet exhaust, five runs employing the representative exhaust constituent acrolein, four NO_x-air irradiations of a synthetic jet exhaust mixture, seven NO_x-air irradiations of various JP-4 fuels, 15 chamber characterization and control runs, and five NO_2 actinometry experiments. Detailed tabulations of the data from all these runs are available in computer-readable format, as discussed in Appendix A in this report. A chronological listing of the runs carried out is given in Table 3. The results of these experiments are discussed in the following sections.

1. Characterization Runs

Several different types of runs were carried out for characterization and conditioning purposes. The purpose of these runs, and the results obtained as they apply to the interpretation and modeling of the experimental runs carried out in this study, are briefly summarized below. For more detailed discussions of the types of characterization runs carried out at SAPRC, and how the data are analyzed, the reader should refer to other recent reports from this laboratory (References 27, 31, 38). In general, the results of the characterization runs carried out in this study were consistent with results of previous such experiments carried out in this chamber.

TABLE 3. CHRONOLOGICAL SUMMARY OF ENVIRONMENTAL CHAMBER EXPERIMENTS CARRIED OUT DURING PHASE II.

ITC run no.	Run type	Comments and results
		New reaction bag installed and lights cleaned
923	NO_2 Actinometry	NO_2 photolysis rate (k_1) = 0.337 min^{-1}, which is slightly higher than previous and subsequent determinations, where values in the 0.30 - 0.32 range are more typical. Slightly high value may be due to cleaning of lights.
924	Tracer-NO_x	Characterization run. Initial NO_x = 0.62 ppm. 2-Hour run. Results summarized in Table 4.
925	Propene-NO_x	Initial propene = 0.92 ppm, NO_x = 0.54 ppm. 7-Hour run. Results summarized in Table 5.
926	Ethene-NO_x	Initial ethene = 3.9 ppm, NO_x = 0.51 ppm. 6-Hour run. Results summarized in Table 5.
927	1-Butene-NO_x	Initial 1-butene = 0.96 ppm[a], NO_x = 0.51 ppm. 6-Hour run. Results summarized in Table 5.
928	Tracer-NO_x + 1-Butene	Initial NO_x = 0.98 ppm. 0.96 ppm 1-butene added at t=2 hours. 6-Hour run. Results summarized in Tables 4 and 5.
929	1-Hexene-NO_x	Initial 1-hexene = 0.84 ppm, NO_x = 0.51 ppm. 6-Hour run. Results summarized in Table 5.
930	1-Butene-NO_x	Initial 1-butene = 1.8 ppm[a], NO_x = 0.51 ppm. 6-Hour run. Results summarized in Table 5.
931	1-Hexene-NO_x	Initial 1-hexene = 1.7 ppm, NO_x = 0.49 ppm 6-Hour run. Results summarized in Table 5.
932	Tracer-NO_x	Characterization run. Initial NO_x = 0.49 ppm. 2-Hour run. Results summarized in Table 4.
933	NO_2 Actinometry	NO_2 photolysis rate = 0.317 min^{-1}.
934	1-Hexene-NO_x	Initial 1-hexene = 1.6 ppm, NO_x = 0.98 ppm. 7-Hour run. Results summarized in Table 5.

TABLE 3. CHRONOLOGICAL SUMMARY OF ENVIRONMENTAL CHAMBER EXPERIMENTS CARRIED OUT DURING PHASE II (CONTINUED).

ITC run no.	Run type	Comments and results
935	1-Butene-NO_x	Initial 1-butene = 1.9 ppm[a], NO_x = 0.98 ppm. 6-Hour run. Results summarized in Table 5.
936	Ethene-NO_x	Initial Ethene = 1.9 ppm, NO_x = 0.49 ppm. 7-Hour run. Results summarized in Table 5.
937	Tracer-NO_x + 1-Hexene	Initial NO_x = 0.98 ppm. 0.93 ppm 1-hexene added at t=2 hours. 6-Hour run. Results summarized in Tables 4 and 5.
938	Propene-NO_x	Initial propene = 0.93 ppm[a], NO_x = 0.51 ppm. 7-Hour run. Results summarized in Table 5.
939	n-Butane-NO_x	Run for control and characterization purposes. Initial n-butane = 3.7 ppm[a], NO_x = 0.51 ppm. 6-Hour run. NO declined from 0.34 to 0.25 ppm. No ozone formed.
940	Pure Air Irrad.	Characterization run. 72 ppb ozone formed in 6-hour irradiation. Results consistent with prediction of chamber characterization model.
941	Acrolein-NO_x	Initial acrolein = 0.7 ppm, NO_x = 0.51 ppm. 6-Hour run. Results summarized in Table 5.
942	Tracer-NO_x	Characterization run. Initial NO_x = 0.49 ppm. 2-Hour run. Results summarized in Table 4.
943	Acrolein-NO_x	Initial acrolein estimated to be 2.7 ppm based on amount injected, and initial acrolein in other runs. Initial NO_x = 0.50 ppm. 7-Hour run. Results summarized in Table 5. Acrolein data rejected because they were anomalously low.
944	Acrolein-NO_x	Initial acrolein = 1.6 ppm, NO_x = 0.26 ppm. 6-Hour run. Results summarized in Table 5.
945	Tracer-NO_x + Acrolein	Initial NO_x = 0.52 ppm. 0.62 ppm acrolein added at t=2 hours. 5-Hour run. Results summarized in Tables 4 and 5.

TABLE 3. CHRONOLOGICAL SUMMARY OF ENVIRONMENTAL CHAMBER EXPERIMENTS CARRIED OUT DURING PHASE II (CONTINUED).

ITC run no.	Run type	Comments and results
946	Acrolein + Propene -NO_x	Initial acrolein = 0.72 ppm, propene = 0.93 ppm[a], NO_x = 0.52 ppm. 6-hour run. Results summarized in Table 5.
947	Propene-NO_x	Initial propene = 0.93 ppm[a], NO_x = 0.52 ppm. 7.5-Hour run. Results summarized in Table 5.
948	n-Butane-NO_x	Characterization and control run. Initial n-butane = 3.8 ppm[a], NO_x = 0.26 ppm. 6-Hour run. NO declined from 0.19 ppm to 0.07 ppm. 54 ppb ozone formed.
949	Tracer-NO_x	Characterization run. Initial NO_x = 0.27 ppm. Results summarized in Table 4.
950	NO_2 Actinometry	NO_2 photolysis rate = 0.316 min^{-1}, in good agreement with other recent actinometry results in this chamber.
951	JP-4(ST)-NO_x	Estimated initial JP-4 (from USAF storage tank) = 40.6 ppmC. Initial NO_x = 0.49 ppm. 6-Hour run. Results summarized in Table 6. Initial ppmC fuel estimated as discussed in text.
952	JP-4(ST)-NO_x	Estimated initial JP-4 (from USAF storage tank) = 40.6 ppmC. Initial NO_x = 0.26 ppm. 6-Hour run. Results summarized in Table 6.
953	Tracer-NO_x	Characterization run. Initial NO_x = 0.50 ppm. 2-Hour run. Results summarized in Table 4.
954	JP-4(ST)-NO_x	Estimated initial JP-4 (from USAF storage tank) = 81.2 ppmC. Initial NO_x = 0.47 ppm. 6-Hour run. Results summarized in Table 6. Problems encountered with GC analysis of fuel constituents.
955	Pure Air Irrad.	Characterization run. 64 Ppb ozone formed in 6-hour irradiation. Results consistent with prediction of chamber characterization model.

TABLE 3. CHRONOLOGICAL SUMMARY OF ENVIRONMENTAL CHAMBER EXPERIMENTS CARRIED OUT DURING PHASE II (CONTINUED).

ITC run no.	Run type	Comments and results
956	JP-4(ST)-NO_x	Repeat of run ITC-954. Estimated initial JP-4 (from USAF storage tank) = 81.2 ppmC. Initial NO_x = 0.47 ppm. 6-Hour run. Results summarized in Table 6. Results were a good replication of ITC-954.
957	Acetaldehyde-Air Irradiation	Characterization run to determine NO_x offgassing rate. Initial acetaldehyde = 0.55 ppm. 6-Hour run. Final ozone = 76 ppb, PAN = 12 ppb. Results in good agreement with predictions of our chamber characterization model.
958	Tracer-NO_x	Characterization run. Initial NO_x = 0.50 ppm. 2-Hour run. Results summarized in Table 4.
959	NO_2 Actinometry	NO_2 photolysis rate = 0.309 min^{-1}, in good agreement with usual values observed.
960	Propene-NO_x	Control run. Initial propene = 0.96 ppm[a], NO_x = 0.50 ppm. 6-Hour run. Results summarized in Table 5.
961	JP-4(ST)-NO_x	Estimated initial JP-4 (from USAF storage tank) = 81.2 ppmC. Initial NO_x = 0.48 ppm. 6-Hour run. Results summarized in Table 6.
962	Syn. Jet Exhaust -NO_x Trial Run	Preliminary run to test synthetic exhaust reactivity and injection technique. Nominal initial exhaust = 100 ppmC, nominal initial NO_x = 0.5 ppm. Methylglyoxal not injected. 6.5-Hour irradiation. No continuous monitoring data for first 2 hours. Run was highly reactive, with ozone maximum occurring almost immediately, indicating that runs should be conducted at lower ROG/NO_x ratios. Run not suitable for model testing.
963	Syn. Jet Exhaust -NO_x	Estimated initial exhaust = 4.55 ppm; initial NO_x =0.48 ppm. Methylglyoxal not injected since the sample was found to be impure.

TABLE 3. CHRONOLOGICAL SUMMARY OF ENVIRONMENTAL CHAMBER EXPERIMENTS CARRIED OUT DURING PHASE II (CONTINUED).

ITC run no.	Run type	Comments and results
		6.75-Hour run. Results summarized in Table 6. Method used for estimating initial ppmC exhaust discussed in text.
964	Tracer-NO_x	Characterization run. Initial NO_x = 0.50 ppm. 2-Hour run. Results summarized in Table 4.
965	Syn. Jet Exhaust -NO_x	Estimated initial exhaust = 5.19 ppm; initial NO_x = 0.46 ppm. 6-Hour run. Results summarized in Table 6.
966	JP-4(1A)-NO_x	Estimated initial JP-4 ("reference" fuel) = 40.6 ppmC; initial NO_x = 0.26 ppm. 6-Hour run. Results summarized in Table 6.
967	Syn. Jet Exhaust -NO_x	Estimated initial exhaust = 4.44 ppm; initial NO_x = 0.26 ppm. 6-Hour run. Results summarized in Table 6.
968	Syn. Jet Exhaust -NO_x	Estimated initial exhaust = 8.70 ppm; initial NO_x = 0.48 ppm. 6-Hour run. Results summarized in Table 6.
969	JP-4(1A)-NO_x	Estimated initial JP-4 ("reference" fuel) = 81.2 ppmC; initial NO_x = 0.50 ppm. 6-Hour run. Results summarized in Table 6.
970	Tracer-NO_x	Characterization run. Initial NO_x = 0.49 ppm. Irradiation was for 4 hours, but tracer data only obtained during first 2 hours. Results summarized in Table 4.
971	NO_2 Actinometry	Measured NO_2 photolysis rate = 0.378 min^{-1}, which is anomalously high. It was determined that an inappropriate NO_x analyzer was employed, and the results were rejected.
972	Propene-NO_x	Control run. Initial propene = 0.79 ppm, NO_x = 0.50 ppm. 6-Hour run. No ozone data due to disconnected signal lead, so this run was not used for model testing.

TABLE 3. CHRONOLOGICAL SUMMARY OF ENVIRONMENTAL CHAMBER EXPERIMENTS CARRIED OUT DURING PHASE II (CONCLUDED).

ITC run no.	Run type	Comments and results
973	Pure Air Irrad.	Characterization run. 6.25 hour irradiation. No ozone data taken until end of run, when 167 ppb observed, which is somewhat higher than the final values observed in previous runs.
974	Acetaldehyde-Air Irradiation	Characterization run to determine NO_x offgassing rate. Initial acetaldehyde = 0.6 ppm. 6-Hour run. Final ozone = 84 ppb, PAN = 6 ppb. Results in fair agreement with predictions of our chamber characterization model.

[a]Initial concentration determined by GC analysis was inconsistent with amount injected. Initial concentration given was estimated based on amount injected.

Tracer-NO_x-Air Irradiations were carried out for the purpose of characterizing the chamber radical source and excess NO oxidation caused by the presence of reactive organic contaminants. The purpose of these runs, and the details of how the results are analyzed are discussed elsewhere (References 39, 40) and are not detailed here, except to note that they provide chamber characterization data needed in model simulations of the chamber experiments. These runs consist of 2-hour irradiations of ~10 ppb each of propene and n-butane (whose relative rates of decay yield an estimate of the OH radical concentration, which reflects the magnitude of the chamber radical source), in NO_x-air mixtures. The initial NO_x levels are generally similar to those used in associated experiments. In some experiments, a test compound (e.g., 1-hexene or acrolein) was injected after 2 hours of the irradiation, to obtain a direct indication of the effect of adding the compound in NO_x-air irradiations. In this case, the part of the irradiation following the addition of the test compound is

classified as a test compound-NO_x-air run, whose results are discussed in the following section.

The initial NO_x concentrations, average estimated t = 1-2 hour OH radical concentrations, and t = 1-2 hour and the chamber radical input rates and NO oxidation rates derived from the data of the tracer-NO_x-air runs are given in Table 4. As discussed in detail elsewhere (References 27, 39, 40), the OH radical concentrations are estimated from the rates of decay of the propene tracer relative to those for the n-butane tracer, and the radical input rate is obtained based on the assumption that the major radical termination process is the reaction of OH radicals with NO_2, and the fact that radical input rates (which under the conditions of these experiments reflects primarily the chamber radical source) and radical termination rates must balance. The NO oxidation rates shown are the negative rates of change of NO observed in the second hour of the irradiation. The data for the second hour are used to avoid complications from the role of initial nitrous acid when it is not present in its photoequilibrium concentration (References 39, 40).

TABLE 4. SUMMARY OF RESULTS OF THE TRACER-NO_x-AIR IRRADIATIONS.

ITC run no.	Initial conc. NO (ppm)	Initial conc. NO_2 (ppm)	Average[a] [OH] (10^6 cm^{-1})	Rates[a] (ppb min^{-1}) Radical input	Rates[a] (ppb min^{-1}) NO oxidation
924	0.32	0.31	<0.3	<0.04	-0.22
928	0.65	0.34	b	b	0.17
932	0.32	0.20	0.59	0.07	-0.11
937	0.66	0.33	0.48	0.10	-0.17
942	0.32	0.15	0.98	0.10	-0.04
945	0.34	0.18	0.56	0.07	0.05
949	0.18	0.09	0.93	0.05	0.01
953	0.33	0.18	0.92	0.10	-0.11
958	0.34	0.17	b	b	0.00
964	0.34	0.17	0.90	0.09	-0.19
970	0.31	0.19	0.62	0.07	-0.10

[a]Data are given for t = 1-2 hours.
[b]Tracer data too scattered to determine radical levels.

The average radical input rate for these runs (excluding the runs where the tracer data were too scattered to derive the OH radical concentrations) is 0.083 ± 0.019 ppb min^{-1}, which corresponds to a k_{RS} [radical input rate divided by the NO_2 photolysis rate (Reference 26)] value of approximately 0.25 ppb, which corresponds very closely to the 0.3 ppb value which is used as the default radical input parameter in the model simulations recently carried out for the EPA (Reference 26). This value was used in the model simulations of these experiments, discussed in Section IV of this report.

The NO oxidation rates observed in these experiments reflect the extent of contamination by reactive organics, which, if present in significant quantities, would cause anomalously high values of these rates. The NO oxidation rates observed in these runs were quite low, in many cases being negative (reflecting conversion of NO_2 to NO due to inorganic reactions), indicating that contamination by reactive organics is not a problem during these experiments. However, the pure air irradiations give a more sensitive indication of this.

Two acetaldehyde-air irradiations were carried out to obtain data reflecting the rates of NO_x offgassing in the chamber experiments. This must also be specified in model simulations of the chamber experiments. These experiments consist of 6-hour irradiations of ~0.5 ppm acetaldehyde in air, and the formation of PAN and ozone which result in a direct indication of the rate of NO_x input into the chamber, presumably from NO_x offgassing from the walls. The 6-hour ozone and PAN yields observed in these experiments are given with the summary of runs in Table 4. The results obtained are in reasonable agreement with model predictions, assuming the default NO_x offgassing rate established for this chamber as discussed in our previous EPA report (Reference 26).

Two pure air irradiations were carried out to determine the ozone formation rate in the chamber in irradiations with the absence of added reactants. Model simulations of the results of these experiments are very sensitive to assumed levels of NO_x offgassing and to excess NO-to-NO_2 conversion caused by background or contaminant organics. The results of the first experiment (ITC-955), carried out around the middle of this program, were in good agreement with model predictions using the ITC

chamber characterization values developed in our EPA study (Reference 26), though the ozone formed in the second run (ITC-973), carried out near the end of the study, was approximately twice that predicted by the model. However, this does not indicate a sufficient level of background reactivity to affect model simulations of experiments with added reactive organics.

Several NO_2 actinometry experiments were was carried out periodically during this program to establish the light intensity in this chamber. The results are summarized with the run tabulation in Table 4. Other than the very first actinometry experiment, which was carried out right after the lights were cleaned, and one experiment where the results were rejected, the results of these experiments yield an average NO_2 photolysis rate of $0.315 + 0.004\ min^{-1}$. This is the value used in the model simulations of all the experiments carried out during this phase of the program.

Several Propene-NO_x-air and n-butane-NO_x-air experiments were also carried out periodically during this program. These are used in chamber programs as standard control runs. The results of the n-butane experiments are summarized with the run listing in Table 4. The results of the propene experiments are summarized in the following section, along with the results of the other alkene-NO_x-air runs. The results of model simulations of these runs are discussed in Section IV.

2. Single-Component Runs

Runs where a single organic is irradiated in NO_x-air mixtures are essential in the development and testing of models for the atmospheric reactions of organics. During this phase of this program, such experiments were carried out for the representative jet exhaust components ethene, 1-butene, 1-hexene, and acrolein, as well as control experiments employing propene and n-butane. The initial reactant concentrations, maximum ozone yields, and average rates of NO oxidation and ozone formation of the runs employing the alkenes and acrolein are summarized in Table 5. Several of these experiments consisted of tracer-NO_x-air irradiations with the organic reactant added at t = 2 hours of the run, but for the purpose of summarizing the results in Table 5 they are treated

TABLE 5. INITIAL REACTANT CONCENTRATIONS AND SELECTED RESULTS OF THE SINGLE ORGANIC-NO_x-AIR IRRADIATIONS CARRIED OUT DURING PHASE II.

ITC Run	Organic	Initial concentrations NO (ppm)	NO_2 (ppm)	Organic (ppm)	Irrad. time (hours)	Maximum ozone (ppm)	(hrs.)	Avg. d/dt $[O_3]$-$[NO]^a$ (ppb min^{-1})
926	Ethene	0.32	0.19	3.92	6.0	0.98	3.4	6.96
936		0.32	0.17	1.93	7.0	0.94	b	2.72
925	Propene	0.35	0.19	0.92	7.0	0.78	b	3.72
938		0.34	0.19	[c]0.93	7.0	0.73	6.75	3.61
947		0.35	0.19	[c]0.93	7.5	0.71	b	3.34
960		0.33	0.18	0.96	6.0	0.72	b	4.23
927	1-Butene	0.31	0.20	0.96	6.0	0.65	b	3.24
930		0.32	0.18	[c]1.8	6.0	0.72	2.25	7.91
928		0.67	0.31	0.96	[d]4.0	0.02	b	1.36
935		0.66	0.36	[c]1.9	6.0	0.87	5.5	5.39
929	1-Hexene	0.33	0.19	0.84	6.0	0.30	b	1.27
931		0.31	0.18	1.71	6.0	0.60	4.25	2.82
934		0.66	0.34	1.61	7.25	0.43	b	1.84
937		0.69	0.31	0.93	[d]4.24	0.01	b	0.33
941	Acrolein	0.33	0.19	0.67	6.0	0.09	b	1.10
943		0.34	0.17	[c]~2.7	7.25	0.72	6.75	2.88
944		0.18	0.09	1.66	6.0	0.49	b	1.84
945		0.33	0.19	0.62	[d]3.5	0.05	b	0.61
946	Acrolein + Propene[e]	0.35	0.18	? [f]	6.0	0.78	4.25	5.21

[a]This quantity, which reflects the overall rates of NO oxidation and ozone formation in these experiments, is defined as one half the maximum change in the quantity ($[O_3]$-[NO]), divided by the time required to achieve one half the maximum ($[O_3]$-[NO]).

[b]Ozone still increasing at the end of the run. The ozone concentration given is the final value observed in the run.

[c]Initial concentration estimated based on amount injected.

[d]Irradiation time after organic reactant added.

[e]Initial acrolein = 0.72 ppm, propene = 0.93 ppm. Initial propene estimated based on amount injected.

[f]Total initial propene + acrolein.

as beginning at the time the organic reactant was added. Except for the propene and ethene runs, for which environmental chamber data are available from previous programs (Reference 26), runs were carried out with both varying initial concentrations of both NO_x and the organic reactant, to provide data to test the model under a range of initial reactant concentrations.

Since the purpose of carrying out these runs is to test the photochemical transformation mechanism, the results of these experiments are discussed in Section IV of this report. These were the first environmental chamber experiments employing 1-hexene and acrolein carried out for this specific purpose. These experiments are, thus, necessary for determining whether longer chain alkenes such as 1-hexene can be represented in "lumped" models by the same species as used for lower alkenes such as propene and 1-butene, and whether acrolein and related compounds can be represented by the same species as used for propionaldehyde and other $>C_3$ aldehydes. In addition, although ethene and 1-butene-NO_x-air runs have been carried out in other chambers (see, for example, Reference 26), they have never previously been carried out in this chamber. The inclusion of these runs, along with the standard propene control runs and the 1-hexene experiments, provides data for the homologous series of 1-alkenes from experiments in the same chamber carried out using the same experimental techniques, which is useful for testing model predictions of reactivity trends as the size of the 1-alkene increases.

3. JP-4 Fuel Runs

Several chamber experiments consisting of NO_x-air irradiations of two samples of JP-4 fuel were carried out during the period covered by this report. One of the two JP-4 samples studied consisted of fuel taken from a storage tank at Tyndall AFB, and represents fuels currently in use by the Air Force, as opposed to special research or preproduction fuel samples employed in some of the other experiments. The other JP-4 sample employed was the "reference" JP-4 fuel whose composition is given in detail in the Monsanto report (Reference 29), and which was employed in previous chamber experiments at SAPRC carried out for the Air Force

(References 6, 7). (Experiments with this "reference" fuel were carried out because this is the only fuel sample available to us for which detailed composition data are available.) The results of the runs with these JP-4 fuels are summarized in Table 6, along with the results of similar runs carried out during Phase I using a preproduction batch of shale-derived JP-4, and using the USAF-specified "standard" synthetic fuel mixture.

Since we did not analyze all of the fuel constituents in the experiments employing the whole fuels, the total initial concentrations of the fuel constituents had to be estimated. These were estimated from the volume of liquid fuel injected into the chamber, based on the assumption that the ratio of total initial gas phase concentration of the fuel constituents, to the volume of fuel injected, was the same in the runs with the whole fuels as it was in the runs with the synthetic fuels. This ratio could be determined in the synthetic fuel runs since the initial gas-phase concentration of all the constituents were experimentally determined (Reference 27). The initial gas-phase concentrations of the fuel constituents are required inputs when using the results of these experiments for model testing.

In addition to providing data for testing model predictions of fuel reactivity, the results of these experiments give an indication of the relative atmospheric reactivities of the three fuel samples studied and of the synthetic fuel mixture. A visual comparison of the relative reactivities of these fuels with respect to ozone formation is shown in Figure 2, which gives the ozone concentration-time profiles for the runs carried out with initial fuel and NO_x concentrations of ~0.25 ppm and ~50 ppmC, and of ~0.5 ppm and ~100 ppmC, respectively. These results indicate that the relative reactivities of these fuels depend somewhat on the initial reactant concentrations, with the principal difference in their reactivities being the rate at which ozone is formed, and not the final amount ultimately formed, given sufficient irradiation time. In the latter regard, the fuels appear to be quite similar.

TABLE 6. INITIAL REACTANT CONCENTRATIONS AND SELECTED RESULTS OF THE JP-4 FUEL-NO_x-AIR AND THE SYNTHETIC EXHAUST-NO_x-AIR IRRADIATIONS CARRIED OUT DURING PHASES I AND II.

ITC run	Mixture	Initial concentrations NO (ppm)	NO_2 (ppm)	Organic (ppmC)	Maximum ozone (ppm)	(hrs.)	Avg. d/dt ($[O_3]$-[NO])[a] (ppb min^{-1})
785	Synthetic Fuel	0.21	0.05	45	0.60	6.0	2.74
781	(Phase I)	0.41	0.10	43	0.75	b	2.77
784		0.43	0.06	88	0.75	5.5	3.93
805		0.40	0.12	98	0.79	5.75	3.27
725	Shale JP-4	0.18	0.05	45	0.45	b	1.64
722	(Phase I)	0.39	0.15	45	0.45	b	2.17
721		0.41	0.13	91	0.68	b	3.17
768		0.43	0.10	91	0.82	b	2.61
952	Tank JP-4	0.19	0.07	41	0.53	b	2.62
951		0.34	0.16	41	0.62	b	2.66
954		0.32	0.16	81	0.80	4.75	5.84
956		0.31	0.17	81	0.79	5.0	5.88
961		0.33	0.16	81	0.80	5.25	6.47
966	Reference JP-4	0.17	0.09	41	0.56	5.25	4.00
969		0.34	0.17	81	0.85	4.5	7.00
967	Syn. Exhaust	0.18	0.08	4.4	0.59	3.38	5.79
963		0.32	0.16	4.6	0.82	6.5	4.00
965		0.32	0.15	5.2	0.86	5.63	5.10
968		0.32	0.17	8.7	0.85	2.5	11.76

[a]This quantity, which reflects the overall rates of NO oxidation and ozone formation in these experiments, is defined as one half the maximum change in the quantity ($[O_3]$-[NO]), divided by the time required to achieve one half the maximum ($[O_3]$-[NO]).

[b]Ozone still increasing at the end of the run. The ozone concentration given is the 6-hour value.

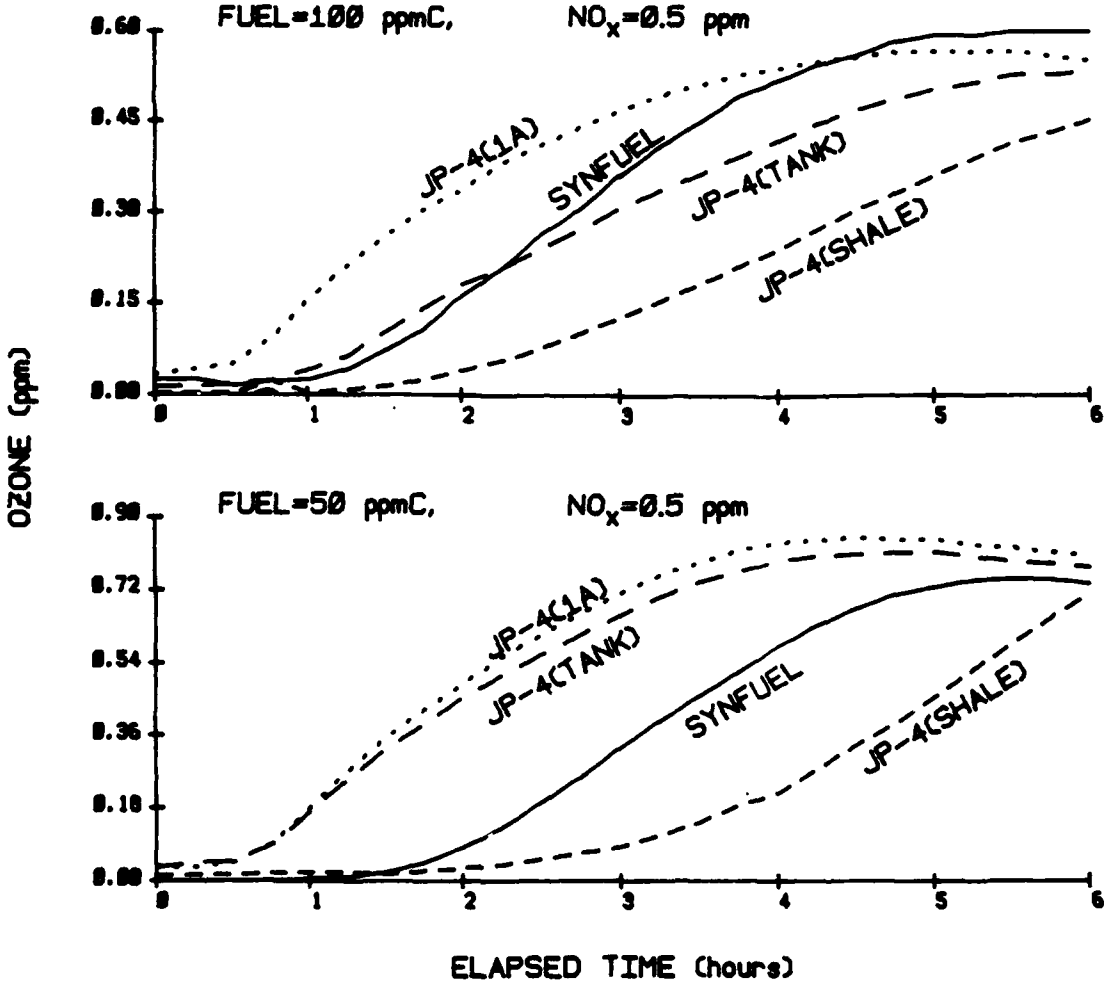

Figure 2. Comparison of Ozone Formation Observed in Environmental Chamber Experiments Employing Four Fuels at Two Different Initial Fuel and NO_x Concentrations.

Of the four whole or synthetic fuels studied, the preproduction shale-derived JP-4 was the least reactive, and that the "reference" JP-4 was the most reactive. This ordering of reactivity of these two fuels is consistent with results of outdoor chamber experiments carried out under a previous program, where it was found that this same "reference" JP-4 was consistently more reactive than another shale-derived JP-4 fuel (Reference 6). However, although none of the experiments with shale-derived JP-4 resulted in a "true" ozone maximum (since ozone was still increasing when the run was terminated), the results suggest that the ultimate ozone formation potential in NO_x-air irradiations of the shale-derived JP-4 may be at least as much, if not more, than those of the other fuels studied. This could be due to lower total alkylbenzene content of the shale-derived fuel relative to the reference fuel (Reference 6), which would result in lower ozone formation rates but similar or even higher final ozone yields. However, without detailed composition data on the shale-derived fuel, it is not clear whether this is the case, or whether there are other reasons for the differences in reactivities of these fuels.

The sample of JP-4 fuel from the Air Force storage tank appears to be similar in reactivity to the "reference" JP-4 fuel in the experiments with the lower initial reactant concentrations, but was somewhat less reactive at the higher concentrations. However, they appear to be similar in maximum ozone formation under both conditions. It is not clear whether the differences between these fuels are due to effects of "aging" of the fuel taken from the tank, or to lot-to-lot variability in JP-4 fuels, although we suspect that the latter is more likely to be the case.

The synthetic fuel was found to be less reactive than both petroleum-derived fuels at the lower concentrations but still more reactive than the shale-derived fuel, while at the higher concentrations, the reactivity of the synthetic fuel was roughly between those of the two samples of petroleum-derived JP-4. Under both sets of conditions, the synthetic fuel was similar in maximum ozone formation potential to the two petroleum-derived fuels. Thus, although in terms of atmospheric reactivity with respect to ozone formation the synthetic fuel is not a perfect representation of any of the specific samples of JP-4 fuel studied in this program, its overall reactivity in general appears to be within the range of variability observed between these samples.

4. Synthetic Exhaust Runs

Several NO_x-air irradiations of a synthetic jet exhaust mixture were also carried out as part of phase of this program, and the results of these experiments are included along with the results of the jet fuel runs in Table 6, above. The composition of this synthetic exhaust mixture was determined by scientists at AFESC/RDVS based on the results of jet exhaust analyses carried out at Battelle (Reference 41). The composition of this mixture is given in Table 7, along with the measured initial concentrations of those constituents for which experimental data are available.

Since the initial concentrations of all of the synthetic exhaust constituents used in these experiments were not determined experimentally, these had to be estimated for purposes of carrying out model simulations of these runs. This was done by assuming that the relative initial gas phase concentrations of the exhaust constituents attained in these experiments were the same as that shown in Table 7, i.e., the same as calculated, based on the relative amounts of each injected. The total amounts of synthetic exhaust injected were then determined, based on the total measured initial concentrations of the species for which the data are considered to be the most reliable, and the total assumed percentage of those in the mixture. The measured initial concentration values used for these estimates were all those shown in Table 7 except for those for 1-nonene and n-octane, which were consistently high, based on the amounts expected; benzene and styrene in run ITC-967, since these were both a factor of ~2 higher than expected based on the amount injected; and the values for the oxygenates, which are considered to be experimentally much more uncertain than those for the hydrocarbons. The total ppmC synthetic exhaust concentrations estimated in this way are given in Table 7 (as well as in Tables 3 and 5, above), from which it can be seen to agree with the expected values to within 13 percent.

The data in Table 6 show that the synthetic exhaust mixture is significantly more reactive than any of the fuels studied in this program. For example, comparative results of runs ITC-969 and ITC-965 show that in the presence of ~0.5 ppm NO_x, only ~5 ppmC of the synthetic exhaust mixture is required to form ozone at a similar rate and yield as

TABLE 7. COMPOSITION OF THE SYNTHETIC JET EXHAUST MIXTURE, AND MEASURED INITIAL CONCENTRATIONS OF ITS CONSTITUENTS, FOR THE SYNTHETIC JET EXHAUST EXPERIMENTS CARRIED OUT IN THIS PROGRAM.

Compound[a]	Relative amount (ppb in 1 ppmC)	Measured ppb constituent			
		ITC-963	ITC-965	ITC-967	ITC-968
Ethene	137.	600.	718.	574.	1213.
Propene	37.				299.
1-Butene	10.5				87.7
1,3-Butadiene	6.1				46.9
1-Hexene (DB)	15.9	70.3	78.8	58.4	
1-Nonene (DB)	0.48	5.4	6.7	6.6	15.4
Acetylene (PN)	37.	185.	190.	173.	343.
Methyl Cyclohexane(DB)	7.5	37.1	40.9	39.7	80.0
n-Octane (DB)	9.8	73.9	93.3	58.4	191.
n-Tetradecane (DB)	1.7				
Benzene (C-600)	4.8			50.2	41.0
Toluene (C-600)	4.1	17.5	16.2	18.3	32.7
m-Xylene (C-600)	5.8	29.2	29.5	38.0	72.5
Naphthalene	1.2				
2-Methyl Naphthalene	0.85				
Styrene	0.85		9.6		
Formaldehyde	36.	85.	255.	340.	386.
Acetaldehyde	13.6	37.	53.5	43.6	62.8
Acrolein	5.8	21.	18.		
Methyl Glyoxal	2.9				
Nominal Total ppmC[b]		5.00	5.00	5.00	10.00
Estimated Total ppmC[c]		4.55	5.19	4.44	8.70

[a]Notations in parentheses indicate instrument used to monitor the constituent, for compounds which were monitored using more than one instrument.

[b]Desired total amount used to calculate the amounts of constituents injected in the experiments.

[c]Total initial ppmC of organic reactants used in the model simulations. Estimated as described in the text.

observed in irradiations, at the same NO_x levels, of almost ~100 ppmC of the most reactive of the JP-4 fuels studied. Thus, under the conditions of these experiments, the synthetic exhaust mixture is almost 20 times more reactive than the most reactive JP-4 fuel. This high reactivity of the exhaust mixture can be attributed to the relatively high levels of alkenes and aldehydes, which are highly reactive, and the lower levels (relative to the fuels) of the higher molecular weight alkanes, which inhibit atmospheric reactivity, at least with respect to ozone formation.

As with the single component and the fuel runs, the primary purpose of the synthetic exhaust experiments is to provide data to determine if the model can simulate the reactivity of jet exhaust mixtures under atmospheric conditions. The results of the model simulations of these experiments are discussed in Section IV.D.

SECTION IV

PHOTOCHEMICAL MODEL DEVELOPMENT AND TESTING

This section discusses the photochemical transformation mechanism incorporated in the model developed under this program. In Section IV.A, the sources used to derive this mechanism, the ways in which it differs from the previously published precursor mechanisms, and the specific portions of this mechanism which were developed under this program are discussed. This discussion assumes that the reader has a general knowledge of atmospheric photochemical reaction mechanisms. If this is not the case, the reader should consult published general reviews of atmospheric chemistry (e.g., References 42, 43) and published references for the previous mechanisms from which this was derived (References 11, 13, 15, 17, 18, 21, 26). A discussion of the "lumping" techniques used to represent reactions of those species not explicitly represented in the mechanism, which is necessary in simulations of complex mixtures such as fuel or exhaust mixtures, is given in Section IV.B, and a full listing of the mechanism is given in Appendix B. This mechanism has been tested against the data from the environmental chamber experiments carried out in both phases of this program, and against the data from over 400 other experiments carried out at SAPRC or the University of North Carolina under other programs. The performance of the model in simulating the results of those experiments is summarized in Section IV.C, below.

A. DERIVATION OF THE MECHANISM AND DISCUSSION OF UNCERTAINTIES

The development and testing of many portions of the chemical mechanism incorporated in the model developed for this program was carried out under a separate EPA-funded contract, and is documented in detail in an EPA report (Reference 26). That report should be consulted for a complete documentation of the portions of chemical mechanism not developed specifically for this program, since that discussion is not reproduced here. In particular, this previous report includes discussions of the inorganic reactions and the reactions of the alkenes and the oxygenated

products, as well as the chamber-dependent reactions which must be included in the model when testing it against environmental chamber data. The major differences between the mechanism described in this report and that documented in the previous EPA report (Reference 26) are: (1) minor modifications in the general alkane reaction mechanism, particularly with regard to the representation of the reactions of their photooxidation products; (2) modifications in the reaction mechanism for the benzene and the alkylbenzenes to represent more efficiently the overall processes which occur; (3) the inclusion of reactions of the naphthalenes, furan, thiophene, pyrrole, and the long-chain alkenes in this model, which are not in the EPA model; and (4) modifications in the approach employed to represent the reactions of the peroxy radicals, to allow for a more efficient representation of their reactions in the absence of NO_x or at night. These differences, and the derivation of the mechanisms for the species not in the EPA model (Reference 26), are discussed in this section.

1. General Representation of Organic Peroxy and Acyl Peroxy Radical Reactions

Before discussing the specific areas where this mechanism differs from the previous mechanisms from which it was derived, it is useful to first discuss the representation of the organic peroxy radical reactions used in this mechanism, since this affects how many of the reactions are presented in the reaction list given in Appendix B. Atmospheric photochemical reaction mechanisms involve the formation of a large number of different organic peroxy and acyl peroxy radicals, since most organic compounds form at least one, and in most cases several, unique peroxy or acyl peroxy radicals, in their atmospheric photooxidation reactions. The major removal processes for these peroxy radicals are either reaction with NO, NO_2, HO_2, or with other peroxy or acyl peroxy radicals,

$$RO_2 + NO \rightarrow \text{products}$$

$$RCO_3 + NO \rightarrow \text{products}$$

$$RO_2 + NO_2 \rightarrow RO_2NO_2$$

$$RCO_3 + NO_2 \rightarrow RCO\text{-}OONO_2$$

$$RO_2 + HO_2 \rightarrow ROOH + O_2$$

$$RCO_3 + HO_2 \rightarrow RCO\text{-}OOH + O_2$$

$$RO_2 + RO_2 \rightarrow \text{products}$$

$$RO_2 + RCO_3 \rightarrow \text{products}$$

$$RCO_3 + RCO_3 \rightarrow \text{products}$$

The relative importance of these removal processes depends primarily on whether or not NO_x is present. Because a large number of different kinds of peroxy and acyl peroxy radicals are involved in the reactions of a realistic "urban surrogate" hydrocarbon mixture, explicit representation of all of these processes would require inclusion of a large number of species and reactions in the model, particularly if all the possible cross-combination reactions of the various different organic peroxy and acyl peroxy radicals were included. In practice, to keep the total mechanism down to a practical and manageable size, atmospheric photooxidation mechanisms for realistic "surrogate" mixtures have incorporated approximations concerning these reactions, and the present mechanism is no exception.

Most current atmospheric photooxidation mechanisms reduce the total number of peroxy radical reactions by neglecting the $RO_2 + NO_2$ reactions. This is justified since the organic peroxynitrates formed undergo rapid thermal back-decomposition (Reference 17), resulting in no net loss process. (On the other hand, acyl peroxy nitrates, e.g. PAN, are much more stable, and thus, no current models neglect $RCO_3 + NO_2$ reactions and the subsequent PAN chemistry.) Test calculations indicate that this approximation introduces no significant inaccuracies in the overall predictions in the mechanism, at least for temperatures greater than 270 K

(Reference 21). Therefore, these RO_2 + NO_2 reactions are also neglected in this mechanism.

A much more severe approximation, incorporated in many previous chemical mechanisms (such as those in References 11, 13, 15) is to neglect all the peroxy + peroxy and peroxy + HO_2 radical reactions because, under daytime conditions when NO_x levels are high enough to promote ozone formation, these reactions are much less important than reaction of peroxy radicals with NO. This not only allows all the possible peroxy + peroxy cross-combination reactions, and the formation and reactions of the various ROOH species, to be ignored, but also permits the peroxy radicals themselves to be removed from the mechanism, since under this approximation, the sequence of reactions forming and consuming a peroxy radical are of the type

$$\text{organic} + OH \xrightarrow{O_2} RO_2$$

$$RO_2 + NO \rightarrow \text{products},$$

which can be represented by

$$\text{organic} + OH \xrightarrow{O_2,\ NO} \text{products} - NO,$$

since in this model reaction with NO is the only consumption process for the peroxy radical. This results in a significant reduction of the number of species, as well as the number of reactions, in the mechanism.

However, the neglect of peroxy + peroxy and peroxy + HO_2 reactions is not a good approximation under conditions when NO_x is limited, nor is it acceptable for multiday simulation purposes, as employed in long-range transport and acid deposition modeling studies. Thus, mechanisms designed for the purpose of such studies, such as those of Lurmann et al. (Reference 21) and Stockwell (Reference 44), as well as the updated mechanism discussed in this report, include some provision for representing these processes, although approximate approaches are

employed. Neglecting these reactions has a significant effect on the ozone and PAN profiles (Reference 26), because, when the peroxy + peroxy radical reactions are included, PAN is removed via:

$$CH_3CO\text{-}OONO_2 \rightleftarrows CH_3CO\text{-}O_2\cdot + NO_2$$

$$CH_3CO\text{-}O_2\cdot + RO_2/RCO_3/HO_2 \rightarrow \text{products}$$

thus, releasing NO_2 to be photolyzed to yield additional O_3. It was also found that the inclusion of the peroxy + HO_2 reactions alone does not account for this effect, and that the organic peroxy + peroxy cross reactions must also be included (Reference 26). Therefore, this mechanism includes representations for both these types of reactions, though, as indicated above, an approximate approach is employed to keep the mechanism at a reasonable size.

Before discussing how peroxy + HO_2 and peroxy + peroxy radical reactions are represented in this mechanism, it is necessary to discuss the condensation technique employed to represent their reactions in the presence of NO_x, the dominant processes under conditions where ozone formation occurs. To minimize the number of species which have to be integrated in the mechanism, most individual peroxy radicals formed in the photooxidations of the various organics are not included explicitly in the mechanism. Instead, in any reaction which forms them, they are replaced by the set of stable products expected to be ultimately formed when they react in the presence of NO, together with one or more generalized peroxy radical pseudospecies, which are used to represent the effects of the reactions of the individual peroxy radicals common to large groups of peroxy radicals, such as the conversion of NO to NO_2 when they react with NO, etc. (This is applied not only to individual peroxy radicals, but to groups of peroxy radicals formed from the same species, whose overall reactions are lumped together in the mechanism). The specific peroxy pseudospecies used in this mechanism, and the overall common processes they represent, both in the presence and absence of NO, are indicated in Table 8.

TABLE 8. PEROXY RADICAL PSEUDOSPECIES USED IN THE MECHANISM TO REPRESENT OVERALL PROCESSES COMMON TO PEROXY RADICAL REACTIONS.

Pseudo-species name	Products formed		
	Reaction with NO	Reaction with HO_2	Reaction with RO_2/RCO_3
RO2-R.	NO_2 + HO_2	-OOH	0.5 HO_2
R2O2.	NO_2	none	none
RO2-N.	$RONO_2$	-OOH + MEK	0.5 HO_2 + MEK
RO2-NP.	Nitrophenol	-OOH + (inert)	0.5 HO_2 + (inert)

The representation of methyl peroxy radicals, and the representation of the overall reactions occurring in the photooxidation of n-butane in the presence of NO are given as examples of the application of this technique. Since the net effect of the reactions of methyl peroxy radicals in the presence of NO is to convert one NO to NO_2, and to form one HO_2 radical and one molecule of formaldehyde, the formation of methyl peroxy radicals is represented in this model by the formation of RO2-R. + HCHO, which has the same net effect. In the presence of NO at 300 K, the n-butane photooxidation process is as follows (see below and Reference 26):

$$\text{OH + n-butane} \xrightarrow{O_2} 0.15\ CH_3CH_2CH_2CH_2OO\cdot + 0.85\ CH_3CH(OO\cdot)CH_2CH_3$$

$$CH_3CH_2CH_2CH_2OO\cdot + NO \rightarrow 0.03\ RONO_2 + 0.97\ (NO_2 + CH_3CH_2CH_2CH_2O\cdot)$$

$$CH_3CH(OO\cdot)CH_2CH_3 + NO \rightarrow 0.08\ RONO_2 + 0.92\ (NO_2 + CH_3CH(O\cdot)CH_2CH_3)$$

$$CH_3CH_2CH_2CH_2O\cdot \xrightarrow{O_2} 0.78\ HOCH_2CH_2CH_2CH_2OO\cdot + 0.22\ (RCHO + HO_2\cdot)$$

$$CH_3CH(O\cdot)CH_2CH_3 \xrightarrow{O_2} 0.63\ (MEK + HO_2) + 0.37\ (CH_3CHO + C_2H_5OO\cdot)$$

$$HOCH_2CH_2CH_2CH_2OO\cdot + NO \xrightarrow{O_2} NO_2 + HO_2\cdot + \text{(bifunctional product, represented by RCHO + 0.25 MEK)}$$

$$C_2H_5OO\cdot + NO \xrightarrow{O_2} NO_2 + HO_2\cdot + CH_3CHO$$

If the steady state approximation is applied to the peroxy and alkoxy radical intermediates (which test calculations have shown to be a good approximation under conditions when NO_x and light are present), then the above reactions have the same net effect as the following overall process:

$$\begin{aligned} OH + \text{n-butane} \rightarrow\ & 0.08\ (RONO_2 - NO) + 0.92\ (NO_2 + HO_2 - NO) + \\ & 0.40\ (NO_2 - NO) + 0.57\ CH_3CHO + 0.53\ MEK + \\ & 0.14\ RCHO \end{aligned}$$

Table 8 shows that in the presence of NO, the above is the same as

$$\begin{aligned} OH + \text{n-butane} \rightarrow\ & 0.08\ RO2\text{-}N\cdot + 0.92\ RO2\text{-}R\cdot + 0.40\ R2O2 + \\ & 0.57\ CH_3CHO + 0.53\ MEK + 0.14\ RCHO \end{aligned}$$

which is how the photooxidation of n-butane at 300 K is represented in this model. The representations of the reactions of other radicals or groups of radicals are entirely analogous.

Because the reactions of acyl peroxy radicals with NO_2 cannot be ignored in this mechanism, the products ultimately formed when they react in the presence of NO_x and sunlight depend on the NO/NO_2 ratio, thus, the representation described above cannot be employed. Therefore, the four acyl peroxy radicals formed from the species in this mechanism, and their corresponding PAN analogues, are represented explicitly.

To represent peroxy + HO_2 and peroxy + peroxy radical reactions, the following approximations and assumptions are employed: (1) The set of stable oxygenated products ultimately formed when a given peroxy or acyl peroxy radical reacts with itself or when another peroxy or acyl peroxy radical is represented by the same set of stable oxygenated products as they form when they react in the presence of NO, excluding PAN analogues

(in the case of acyl peroxy radicals) or alkyl nitrates (in the case of $>C_4$ unsubstituted peroxy radicals); (2) Peroxy + peroxy, and peroxy + acyl peroxy radical - radical reactions are assumed to react 50 percent of the time to form nonradical products, and to form radical products the other 50 percent of the time. The formation of radicals in these reactions are represented in this model by the formation of 0.5 HO_2 for each radical so reacting; (3) Acyl peroxy + acyl peroxy radical reactions are assumed to occur only through radical-forming pathways, with this being represented by the formation of an HO_2 for each such radical reacting; (4) The organic hydroperoxide species believed to be formed when a peroxy or acyl peroxy radical reacts with HO_2 is not included explicitly in the mechanism. Instead, it is represented by the same set of oxygenated compounds used to represent their reaction products when they react with other peroxy or acyl peroxy radicals, plus the pseudospecies designated "-OOH," which represents the effects of photolysis at the hydroperoxide group, as discussed below; (5) The rate constants for the reactions of a peroxy radical with NO, with HO_2, with other peroxy radicals, or with acyl peroxy radicals are assumed to be unaffected by the nature of the peroxy radical. A similar assumption is made for the reactions of acyl peroxy radicals with NO, NO_2, HO_2, peroxy radicals, or with other acyl peroxy radicals; and (6) The reactions of a given peroxy radical with itself and with other peroxy radicals can be represented by a reaction of the peroxy radical with a pseudospecies whose concentration is given by the sum of all peroxy radical concentrations, and likewise for acyl peroxy + acyl peroxy reactions. Although these approximations are not totally accurate, if they are assumed, they allow the effects of the peroxy + peroxy and peroxy + HO_2 reactions to be represented in the model without having to employ an excessive number of reactions or species.

The assumption that the oxygenated organic products formed in the reactions of the peroxy radicals are the same whether or not they react with NO, HO_2, or peroxy or acyl peroxy radicals mean that the peroxy + HO_2 and peroxy + peroxy reactions can be represented by considering only the reactions of the pseudospecies listed above in Table 1, and the four individual acyl peroxy radicals. In addition, assumption (6), above, means that it is not necessary to include all of the possible radical -

radical reaction combinations; instead they can be represented by including in the model two additional pseudospecies representing the sum of all peroxy radicals (designated $RO_2.$ in listing in Appendix B) and the sum of all acyl peroxy radicals (designated $RCO_3.$), and using these as reactants with the individual peroxy radicals. Furthermore, if $RO_2.$ and $RCO_3.$ are integrated explicitly, the steady state approximation can be employed on all the peroxy pseudospecies listed in Table 8, and on the four individual acyl peroxy radicals represented in the mechanism, without adverse effects on the results of the model simulation.

The concentrations of $RO_2.$ and $RCO_3.$ are calculated by having each reaction in this mechanism which forms a peroxy radical also form $RO_2.$, and likewise with acyl peroxy radicals and $RCO_3.$ The following pseudo reactions, which represent the net consumption processes for these species are included in the mechanism:

$$RO_2. + NO \rightarrow NO \qquad (B1)$$

$$RCO_3. + NO \rightarrow NO \qquad (B2)$$

$$RCO_3. + NO_2 \rightarrow NO_2 \qquad (B4)$$

$$RO_2. + HO_2 \rightarrow HO_2 \qquad (B5)$$

$$RCO_3. + HO_2 \rightarrow HO_2 \qquad (B6)$$

$$RO_2. + RO_2. \rightarrow \qquad (B8)$$

$$RO_2. + RCO_3. \rightarrow \qquad (B9)$$

$$RCO_3. + RCO_3. \rightarrow \qquad (B10)$$

These are not true chemical reactions, but are included in the mechanism so the computer modeling software can calculate the loss rates of RO_2 and RCO_3, the lumped total peroxy and peroxyacetyl radical species. These pseudo reactions are thus, written in the incomplete form shown above because the effects of the reactions of peroxy and peroxy acetyl radicals on (for example) HO_2, NO, and NO_2 concentrations are accounted for in the reactions for the individual peroxy species which are already in the mechanism.

The assumptions which permit use of this highly condensed representation of peroxy + HO_2 and peroxy + peroxy reactions are obviously highly approximate; though because of our lack of explicit information concerning

the reactions of all but the simplest of the peroxy radicals, some of these would need to be incorporated even in explicit mechanisms. For example, the assumption that the rate constants for peroxy radical reactions with NO, NO_2, and HO_2 would not be affected by the nature of the radical would have to be made in developing explicit mechanisms, since no data are available to indicate that this assumption is incorrect (see Reference 17). On the other hand, the assumption that the rate constants for peroxy radical reactions with other peroxy radicals are independent of the nature of the radical is known to be grossly incorrect, since the rates for these reactions depend significantly on whether the peroxy radical is primary, secondary or tertiary, with tertiary + tertiary radical reactions being approximately four orders of magnitude slower than primary + primary reactions. The rate constant assigned for these reactions in this model is based on those for secondary peroxy radicals, since these are commonly formed in the reactions of most of the organics represented in this model. Although this is obviously a gross approximation, it is preferable to the alternatives of ignoring peroxy + peroxy reactions entirely, as is the case in the ALW mechanism), or ignoring reactions of peroxy radicals with different types of peroxy radicals, as is the case in the "detailed" version of the mechanism of Lurmann et al. (Reference 21).

Although there is very little information concerning the products formed in the cross reactions of most peroxy radicals, it is probable that the assumption that they are the same as those formed in the presence of NO_x is not totally accurate. As discussed by Atkinson and Lloyd (Reference 17), the most information available concerns the self-reaction of methyl peroxy radicals, which they recommend as occurring approximately equally via molecular and radical forming routes:

$$CH_3O_2\cdot + CH_3O_2\cdot \rightarrow CH_3OH + HCHO \qquad (\sim 60\%)$$

$$\xrightarrow{O_2} 2\ CH_3O\cdot \rightarrow 2\ (HCHO + HO_2\cdot) \qquad (40\text{-}50\%)$$

This corresponds to the overall process, for each $CH_3O_2\cdot$, being

$$CH_3O_2\cdot \xrightarrow{RO_2} 0.75\ HCHO + 0.25\ CH_3OH + 0.5\ HO_2$$

Data concerning the products formed in the self reactions of higher peroxy radicals are much more limited, but it is reasonable to assume that they react via analogous routes, provided that they have α-hydrogens. For example, in the case of the 2-butyl peroxy radical [formed in the n-butane system (see the example above)] reacting with another peroxy radical, the analogous processes would be expected to be

$$CH_3CH(OO\cdot)CH_2CH_3 + RO_2\cdot \rightarrow CH_3\text{-}CO\text{-}C_2H_5\ (MEK) + ROH \qquad (\sim 25\%)$$

$$\rightarrow CH_3CH(OH)C_2H_5 + R'CHO \qquad (\sim 25\%)$$

$$\rightarrow CH_3CH(O\cdot)C_2H_5 + RO\cdot \qquad (\sim 50\%)$$

$$CH_3CH(O\cdot)CH_2CH_3 \xrightarrow{O_2} 0.63\ (MEK + HO_2) + 0.37\ (CH_3CHO + C_2H_5OO\cdot)$$

$$C_2H_5OO\cdot + RO_2\cdot \rightarrow 0.25\ CH_3CHO + 0.25\ C_2H_5OH + 0.5\ C_2H_5O\cdot + (\text{corresponding products from } RO_2)$$

$$C_2H_5O\cdot + O_2 \rightarrow CH_3CHO + HO_2$$

or overall,

$$CH_3CH(OO\cdot)CH_2CH_3 \xrightarrow{RO_2} 0.57\ MEK + 0.25\ CH_3CH(OH)C_2H_5 + 0.32\ CH_3CHO + 0.05\ C_2H_5OH + 0.41\ HO_2$$

These can be compared with the representation in this model, which implies that the overall processes for the above two examples are:

$$CH_3O_2\cdot \xrightarrow{RO_2} HCHO + 0.5\ HO_2$$

$$CH_3CH(OO.)CH_2CH_3 \xrightarrow{RO_2} 0.63\ MEK + 0.74\ CH_3CHO + 0.5\ HO_2$$

In the case of these representative primary and secondary peroxy radicals, the representation used in this mechanism is reasonably consistent with the known or estimated explicit mechanism in terms of the numbers of HO_2 radicals ultimately regenerated, but the distribution of the organic products is somewhat different. However, for the larger radicals, the estimated "explicit" mechanism may also be incorrect, therefore, the exact extent of how inaccurate this representation is in terms of overall model predictions is not known.

In the case of reaction of acyl peroxy radicals with other acyl peroxy radicals, the route forming the corresponding alkoxy radical is the only possible one. For that reason, acyl peroxy radicals are represented as forming one HO_2 radical when they react with RCO_3. Otherwise, the products formed in their reactions with peroxy or other acyl peroxy radicals are derived in a manner analogous to those for peroxy radicals. In general, for both peroxy and acyl peroxy radical-radical interactions, the accuracy of the representation used in this model depends on the specific pairs of species reacting, and can be assessed in a manner analogous to the discussion given for the examples above.

The reactions of HO_2 with organic peroxy radicals have not been well studied, but it is expected that they would result in the formation of organic hydroperoxides. These species are expected to photolyze, giving rise to OH and alkoxy radicals, or react with OH radicals, in both cases resulting in the formation of oxygenated products which are similar to, though in general not exactly the same as, the products ultimately formed when the parent peroxy radical reacts in the presence of NO. For example, in the case of the reaction of ethylperoxy radicals with HO_2, the expected processes are:

$$CH_3CH_2OO. + HO_2 \rightarrow CH_3CH_2OOH + O_2$$

$$CH_3CH_2OOH + h\nu \rightarrow CH_3CH_2O. + OH$$

$$CH_3CH_2O. + O_2 \rightarrow CH_3CHO + HO_2$$

$$CH_3CH_2OOH + OH \xrightarrow{-H_2O} CH_3CH_2OO. \xrightarrow{NO,\ O_2} \rightarrow \rightarrow CH_3CHO + HO_2$$

$$\rightarrow CH_3CH(.)OOH \rightarrow CH_3CHO + OH$$

$$\rightarrow .CH_2CH_2OOH \xrightarrow{O_2,\ NO} \rightarrow \rightarrow \rightarrow 2\ HCHO + OH$$

with the reactions with larger radicals being analogous, although in general more complex. Clearly, representing these processes accurately would require a large number of species and reactions (with one hydroperoxy species for each of the many kinds of peroxy radicals formed, and with the lumping of peroxy radicals, as discussed above, not being possible). This approach would be inappropriate considering that under conditions when ozone formation occurs they are relatively minor. Therefore, in this mechanism, the hydroperoxides are not represented explicitly, but instead are represented by the same set of species the peroxy radicals form when they react with NO, plus the pseudospecie -OOH, which is used to represent the regeneration of radicals formed when the hydroperoxides photolyze. Thus, the set of reactions above for the ethyl peroxy case are represented in the model simply by,

$$CH_3CH_2OO. + HO_2. \rightarrow -OOH + CH_3CHO + O_2$$

$$-OOH + h\nu \rightarrow OH + HO_2 \qquad (B7)$$

where the photolysis rates for "-OOH" are calculated using the absorption coefficients and quantum yields for CH_3OOH (Reference 45). Thus, CH_3CHO + -OOH is used as a "surrogate" for CH_3OOH in this mechanism, and likewise for the other hydroperoxides which are expected to be formed when peroxy radicals react with HO_2.

Although, as indicated above, this representation for peroxy + peroxy and peroxy + HO_2 reactions has a number of significant approximations and

oversimplifications, at least for the simplified propene + n-butane test problem, it gives predictions essentially in agreement with predictions using a model where the individual reactions are treated explicitly (Reference 26). The main difference between the predictions of this model and the more explicit mechanism is that this mechanism predicts somewhat higher oxygenate yields at the end of the irradiation (0.50 ppm formaldehyde + acetaldehyde vs. 0.46 ppm in the more explicit mechanism), due to the use of these species as surrogates for the hydroperoxides. [However, there is no difference in the calculated aldehyde formation rates when NO_x and sunlight are present, since peroxy + HO_2 (as well as peroxy + peroxy) reactions are negligible under those conditions.] Therefore, although approximate, this representation appears to be satisfactory in terms of overall model performance, at least for the test problems run by us previously (Reference 26). Because of the limited knowledge concerning atmospheric reactions of peroxy radicals in the absence of NO_x, and because the available chamber data are not well-suited for testing this aspect of the mechanism, more explicit and detailed mechanisms for these processes would be based on speculation, and may be no more accurate in their predictions than models employing this highly simplified representation. More research in this area is needed before more detailed models for the atmospheric photooxidations of organics in the absence of NO_x can be developed and adequately tested.

2. General Alkane Reaction Mechanism

The alkanes are consumed in the atmosphere almost entirely by hydrogen abstraction reactions by hydroxyl (OH) radicals, with the subsequent reactions involving the interconversions and competing reactions of various peroxy and alkoxy radicals, resulting in the conversion of NO to NO_2, the formation of organic nitrates and various mono-, bi-, and polyfunctional oxygenates (Reference 17, 24). The net effect of these processes is represented in this model by a single "lumped" reaction, shown below:

$$OH + Alkane \rightarrow p_{RR}\ RO2\text{-}R\cdot + p_{NR}\ RO2\text{-}N\cdot + p_{R2}\ R2O2\cdot + p_{A1}\ HCHO + p_{A2}\ CH_3CHO + p_{A3}\ (C_{3+}\ aldehyde) + p_{K3}\ acetone + p_{K4}\ (C_{4+}\ ketone) + p_{CO}\ CO + p_{C2}\ CO_2$$

where RO2-R., R2O2., and RO2-N. are generalized species which react with NO to form NO_2 + HO_2, NO_2 only, or the lumped $>C_4$ organic nitrate (see below), respectively, as discussed in the previous section. This representation is analogous to that employed in the previous model of Atkinson et al. (Reference 15), except for the use of the generalized species to represent the effects of the reactions of peroxy radicals with HO_2 or other peroxy or acyl peroxy radicals. The mechanistic and product yield parameters p_{RR}, p_{NR}, etc., and the rate constants for the initial OH radical reaction were obtained based on our current knowledge of alkane reaction mechanisms (Reference 24) and kinetic data for OH radical reactions (Reference 25), as indicated below.

A detailed discussion and evaluation of the current knowledge of atmospheric chemistry of the alkanes is given by Carter and Atkinson (Reference 24), and the reaction mechanisms derived for all alkanes in this model are based on the recommendations of this evaluation. In particular, Carter and Atkinson (Reference 24) and Atkinson (Reference 25) give methods for estimating the initial rates of OH radical attack on the various positions of the alkanes (the only significant atmospheric fate for the alkanes [Reference 25]); and Carter and Atkinson (Reference 24) give recommendations and estimates for all the peroxy and alkoxy radical branching ratios (in the presence of NO) which are necessary to derive the mechanistic and product yield parameters for any acyclic or monocyclic alkane. Based on the estimates and recommendations of Carter and Atkinson (Reference 25), a computer program was written which inputs the structure of any acyclic or monocyclic alkane and outputs the kinetic and mechanistic parameters needed to represent the atmospheric reactions of the alkane, and this computer program was used to derive the parameters for the reactions of the alkanes represented in this model.

Since the principles and estimates used to derive the alkane photooxidation mechanisms are already published and documented in detail elsewhere (References 24-26), these are not discussed in detail here.

However, there are a number of areas of uncertainty in the photooxidation mechanisms of the higher alkanes, and some modifications had to be made to the initially estimated mechanism to provide acceptable fits of the model simulation to the results of environmental chamber experiments carried out in this and previous programs. In addition, the photooxidations of the higher alkanes are expected to result in the formation of a large number of products, including many bi- and poly-functional species, and it is not practical to represent the explicit reactions of all of these species in this model. The major areas of uncertainty in the current alkane photooxidation mechanism, and the method used in this model to represent the reactions of their expected products, are summarized below.

The atmospheric reactions of the alkanes involve the intermediacy of a number of different types of peroxy and alkoxy radicals which can often react by more than one route. The ultimate products they form, and their overall effects on the photochemical smog system, can be significantly affected by what is assumed for these branching ratios. Although Carter and Atkinson (Reference 24) give values for all the branching ratios believed to be important, most of these estimates are derived from an extremely limited data base, and in many cases have extremely large uncertainty ranges. For example, the estimates of the branching ratios for the various possible reactions of the larger alkoxy radicals could be in error by factors of ≥ 5. However, in terms of affecting the atmospheric reactivity predicted for an alkane, the most important mechanistic parameters are those determining the alkyl nitrate yields from the reactions of NO with the peroxy radicals,

$$RO_2 + NO \rightarrow RO + NO_2 \qquad (a)$$

$$\xrightarrow{M} RONO_2 \qquad (b)$$

since this branching ratio determines the relative importance of radical propagation (process a) and radical inhibition and NO_x removal (process b) in the overall alkane photooxidation process. Although this ratio is reasonably well-characterized in the case of the reactions of NO with the

unsubstituted peroxy radicals initially formed following the OH attack on the alkane (References 24, 25, 46), no information is available concerning the alkyl nitrate yield from the reactions of NO with the hydroxy-substituted peroxy radicals presumed to be formed following the hydrogen shift isomerizations of the longer chain, C_4+ alkoxy radicals. For example, the major reactions following OH attack on the 2-position of n-pentane are expected to be the following,

$$CH_3CH_2CH_2CH_2CH_3 + OH \xrightarrow{O_2} CH_3\underset{\displaystyle OO\cdot}{C}HCH_2CH_2CH_3 \begin{cases} \xrightarrow{NO} CH_3\underset{\displaystyle ONO_2}{C}HCH_2CH_2CH_3 & (a) \\ \xrightarrow{NO} CH_3\underset{\displaystyle O\cdot}{C}HCH_2CH_2CH_3 + NO_2 & (b) \end{cases}$$

$$CH_3\underset{\displaystyle O\cdot}{C}HCH_2CH_2CH_3 \xrightarrow{\text{isom, } O_2} CH_3\underset{\displaystyle OH}{C}HCH_2CH_2CH_2OO\cdot \begin{cases} \xrightarrow{NO} CH_3\underset{\displaystyle OH}{C}HCH_2CH_2CH_2ONO_2 & (a') \\ \xrightarrow{NO} CH_3\underset{\displaystyle OH}{C}HCH_2CH_2CH_2O\cdot + NO_2 & (b') \end{cases}$$

$$CH_3\underset{\displaystyle OH}{C}HCH_2CH_2CHO\cdot \xrightarrow{\text{isom, } O_2} CH_3\overset{\displaystyle O}{\overset{\|}{C}}CH_2CH_2CHO + HO_2$$

which yields an overall regeneration efficiency for these reactions given by $[k_a/(k_a+k_b)][k_{a'}/(k_{a'}+k_{b'})]$. Although $k_a/(k_a+k_b)$ for the above system has been measured to be 0.13 (Reference 47) there is no information concerning the value of $k_{a'}/(k_{a'}+k_{b'})$, which is equally important in affecting model predictions of termination to propagation ratios.

The alkane mechanistic parameters in the earlier photochemical mechanisms, used as the starting point of this model (References 15, 18, 21), were derived, based on the assumption that alkyl nitrate from the reaction of NO with the substituted peroxy radicals formed following alkoxy radical isomerization, is the same as for a nonsubstituted radical

with the same number of carbons. In the above example, this is equivalent to the assumption that $k_{a'}/(k_{a'}+k_{b'}) = k_a/(k_a+k_b)$. However, if this assumption is made, then the model has a significant tendency to underpredict the overall rates of NO oxidation and ozone formation in model simulations of C_5-C_9 n-alkane-NO_x-air environmental chamber experiments (see Reference 26). On the other hand, if it is assumed the reactions of NO with substituted peroxy radicals do not result in significant organic nitrate formation [e.g., that $k_{a'}/(k_{a'}+k_{b'}) = 0$], then, although there is still a wide distribution in the quality of fits of the model to the experiments with many experiments being poorly simulated by the model (as shown in Section IV.C), there is much less of a consistent tendency for the model to underpredict reactivity. For that reason, the assumption that alkyl nitrate from NO + substituted peroxy radicals is the same as for nonsubstituted radicals with the same number of carbons, is incorporated in the general alkane mechanism used in this model. However, in view of the wide distribution of the quality of fits of the model predictions to the results of the alkane-NO_x-air experiments, as well as the consistent tendency to underpredict final ozone yields for those experiments in which "true" ozone maxima are obtained, the possibility that this adjusted general alkane mechanism could be in error cannot be entirely ruled out.

Using environmental chamber data to test models for the reactions of alkanes is subject to significantly more uncertainties than is the case for many other classes of organics, because results of model simulations of alkane-NO_x-air runs are extremely sensitive to assumptions incorporated in the model about the magnitude of the chamber radical source, which tends to be uncertain and to vary from run to run (Reference 39, 40). Alkane-NO_x-air runs are particularly sensitive to the chamber radical source because alkanes, unlike (for example) alkenes and aromatics, do not have important radical sources in their homogeneous reactions, and thus, the chamber radical source is the major source of radicals driving the photooxidations in alkane experiments. Because of this, unless the magnitude of the chamber radical source is adjusted from run-to-run to optimize the fits (a procedure which would invalidate the model testing process, since it could mask errors in the homogeneous reaction

mechanism), the variability of the radical source results in a wide variability in the quality of fits of the model to the experiment, regardless of the details of the reaction mechanism employed. Therefore, the validity of our alkane reaction mechanisms, and the assumptions and estimations they incorporate, cannot be considered to be unambiguously established by the existing chamber data set.

As discussed by Carter and Atkinson (Reference 24), the reactions of the larger alkanes can involve a large number of intermediates and result in the formation of a large number of (presumably) reactive products, many (mostly) being bi- or polyfunctional in nature. To minimize the total number of species in the model, the reactions of the many possible alkane photooxidation products were represented using a much smaller set of compounds, as indicated below: (1) formaldehyde, acetaldehyde, and acetone are represented explicitly; (2) "RCHO", i.e., propionaldehyde, is used to represent all the $>C_3$ aldehydes and the aldehyde groups in the bi- and polyfunctional products, with its yield being calculated by summing up the total number of -CHO groups other than those in formaldehyde or acetaldehyde; (3) methyl ethyl ketone (MEK) is used to represent the $>C_4$ ketones and the ketone and -OH groups in the bi- and polyfunctional products, provided this could be done without having more carbons in the species representing the oxygenated products than in those actually predicted to be formed; if not, the MEK is determined such that all the carbons in the oxygenated products are conserved; and (5) "$RONO_2$" (see below) was used to represent all the $>C_4$ alkyl nitrates, with the reactions of the C_3 or smaller alkyl nitrates being ignored. This representation of the alkane photooxidation products is consistent with the philosophy behind the "lumped molecule" approach (Reference 48) used to represent complex mixtures in models with a limited number of species, as discussed in Section V.B.

With the exception of the lumped organic nitrate species "$RONO_2$," the mechanisms employed for the reactions of all the species used to represent the alkane photooxidation products are the same as documented in our EPA report (Reference 26), and thus, are not discussed here. The EPA mechanism used two lumped organic nitrate species, 2-butyl nitrate and 7-heptyl nitrates, while subsequent test calculations have shown that the

results of the calculations are not significantly affected if only a single lumped nitrate species is employed. The reaction mechanism derived for "$RONO_2$" in this model is based on averaging the kinetic and mechanistic parameters estimated for the 2-butyl nitrate and the 4-heptyl nitrate used in the EPA model (Reference 26).

The kinetic and mechanistic parameters for all the alkanes included in the initial distribution of this model (Reference 28) are given in Table 9. The values are given for three temperatures: 270, 300, and 330 K. For intermediate temperatures, the model software obtains the parameters and rate constants by linear interpolation.

3. Aromatic Reaction Mechanisms

Like the alkanes, the aromatic hydrocarbons are consumed in the atmosphere, predominantly by reaction with the hydroxyl radical (Reference 25). However, the details of the subsequent reactions are often more uncertain. Although reaction mechanisms have been published for the reactions of benzene (Reference 26) and the methylbenzenes (e.g., References 12, 13, 15, 16, 18, 20-23, 26, 44, 49), no atmospheric reaction mechanism has been published for the atmospheric reactions of tetralin and the naphthalenes, which are also included in this model. With benzene and the methylbenzenes, the current understanding is that in the initial reaction (benzene) the OH radical can either add to the aromatic ring, ultimately giving rise primarily to phenols and aromatic ring opening products, or (with methylbenzenes) abstract an H atom from the methyl group, ultimately giving rise primarily to aromatic aldehydes (References 13, 15, 16, 20, 26). The net effect of these processes are represented in the model using a "lumped reaction" approach analogous to that employed for the alkanes, where the overall reaction is as follows:

$$\begin{aligned} \text{OH + aromatic} \rightarrow\ & p_{RR}\ \text{RO2-R.} + p_{RH}\ HO_2\cdot + p_{NP}\ \text{RO2-NP.} + \\ & p_{BZ}\ \text{benzaldehyde} + p_{PH}\ \text{phenol} + p_{CR}\ \text{cresols} + \\ & p_{GL}\ \text{glyoxal} + p_{MG}\ \text{(methylglyoxal)} + p_{U1}\ \text{HCOCHO(X)} + \\ & p_{U2}\ \text{CCOCHO(X)} \end{aligned}$$

TABLE 9. KINETIC AND MECHANISTIC PARAMETERS USED IN THE REPRESENTATIONS OF THE REACTIONS OF THE ALKANES.

Name	k_{OH}[a]	P_{RR}	P_{NR}	P_{R2}	P_{A1}	P_{A2}	P_{A3}	P_{K3}	P_{K4}	P_{CO}	P_{C2}
T = 270 K											
ETHANE	2.09E-13	1.000	0.000	0.000	0.000	1.000	0.000	0.000	0.000	0.000	0.000
PROPANE	9.68E-13	0.940	0.000	0.000	0.000	0.000	0.277	0.662	0.000	0.000	0.000
N-C4	2.11E-12	0.880	0.120	0.085	0.000	0.056	0.124	0.000	0.758	0.000	0.000
N-C5	3.32E-12	0.798	0.202	0.240	0.000	0.000	0.060	0.000	0.952	0.000	0.000
N-C6	4.53E-12	0.682	0.318	0.459	0.000	0.000	0.042	0.000	0.992	0.000	0.000
N-C7	5.75E-12	0.561	0.439	0.513	0.000	0.000	0.027	0.000	0.961	0.000	0.000
N-C8	6.96E-12	0.470	0.530	0.500	0.000	0.000	0.001	0.000	0.940	0.000	0.000
N-C9	8.17E-12	0.413	0.587	0.445	0.000	0.000	0.001	0.000	0.858	0.000	0.000
N-C10	9.38E-12	0.379	0.621	0.413	0.000	0.000	0.001	0.000	0.791	0.000	0.000
N-C11	1.06E-11	0.357	0.643	0.394	0.000	0.000	0.001	0.000	0.751	0.000	0.000
N-C12	1.18E-11	0.343	0.657	0.378	0.000	0.000	0.000	0.000	0.721	0.000	0.000
N-C13	1.30E-11	0.333	0.667	0.367	0.000	0.000	0.000	0.000	0.700	0.000	0.000
N-C14	1.42E-11	0.326	0.674	0.360	0.000	0.000	0.000	0.000	0.685	0.000	0.000
N-C15	1.54E-11	0.321	0.679	0.353	0.000	0.000	0.000	0.000	0.673	0.000	0.000
ISO-C4	2.24E-12	0.964	0.036	0.789	0.789	0.000	0.175	0.789	0.000	0.000	0.000
ISO-C5	3.75E-12	0.904	0.096	0.670	0.000	0.614	0.101	0.614	0.245	0.000	0.000
NEO-C5	5.53E-13	0.915	0.085	0.000	0.000	0.000	0.915	0.000	0.000	0.000	0.000
2-ME-C5	4.97E-12	0.805	0.193	0.605	0.003	0.000	0.499	0.100	0.759	0.000	0.000
3-ME-C5	5.46E-12	0.831	0.169	0.696	0.000	0.540	0.054	0.000	0.933	0.000	0.000
23-DMB	5.40E-12	0.852	0.088	0.887	0.000	0.000	0.089	1.587	0.064	0.000	0.000
4-ME-C6	6.67E-12	0.726	0.272	0.693	0.000	0.078	0.377	0.000	0.950	0.000	0.000
24-DM-C5	6.61E-12	0.815	0.185	0.741	0.000	0.000	0.717	0.089	0.749	0.000	0.000
23-DM-C5	7.10E-12	0.807	0.174	0.935	0.023	0.146	0.235	0.332	0.936	0.000	0.000
ISO-C8	4.33E-12	0.733	0.266	0.659	0.012	0.000	0.620	0.062	0.699	0.000	0.000
CYCC6	7.28E-12	0.670	0.330	0.000	0.000	0.000	0.000	0.000	0.670	0.000	0.000
ME-CYCC6	9.41E-12	0.667	0.333	0.749	0.075	0.000	0.264	0.000	0.942	0.000	0.035
ET-CYCC6	1.14E-11	0.613	0.387	1.309	0.209	0.335	0.268	0.000	0.691	0.000	0.209
3-ME-C6	6.67E-12	0.726	0.272	0.693	0.000	0.078	0.377	0.000	0.950	0.000	0.000

TABLE 9. KINETIC AND MECHANISTIC PARAMETERS USED IN THE REPRESENTATIONS OF THE REACTIONS OF THE ALKANES (CONTINUED).

Name	k_{OH}[a]	P_{RR}	P_{NR}	P_{R2}	P_{A1}	P_{A2}	P_{A3}	P_{K3}	P_{K4}	P_{CO}	P_{C2}
4-ME-C7	7.88E-12	0.638	0.360	0.663	0.000	0.000	0.378	0.000	0.923	0.000	0.000
4-ET-C7	9.84E-12	0.608	0.390	0.644	0.001	0.036	0.353	0.000	0.862	0.000	0.000
4-PR-C7	1.10E-11	0.562	0.436	0.594	0.000	0.001	0.351	0.000	0.804	0.000	0.000
BR-C6	4.97E-12	0.805	0.193	0.605	0.003	0.000	0.499	0.100	0.759	0.000	0.000
BR-C7	6.67E-12	0.726	0.272	0.693	0.000	0.078	0.377	0.000	0.950	0.000	0.000
BR-C8	7.88E-12	0.638	0.360	0.663	0.000	0.000	0.378	0.000	0.923	0.000	0.000
BR-C9	9.84E-12	0.608	0.390	0.644	0.001	0.036	0.353	0.000	0.862	0.000	0.000
BR-C10	1.10E-11	0.562	0.436	0.594	0.000	0.001	0.351	0.000	0.804	0.000	0.000
BR-C11	1.39E-11	0.661	0.339	0.891	0.004	0.000	0.030	0.000	1.519	0.000	0.000
BR-C12	1.51E-11	0.629	0.371	1.283	0.001	0.457	0.012	0.000	1.441	0.000	0.000
BR-C13	1.64E-11	0.602	0.398	0.914	0.001	0.000	0.038	0.000	1.477	0.000	0.000
BR-C14	1.76E-11	0.578	0.422	1.011	0.001	0.000	0.001	0.000	1.587	0.000	0.000
BR-C15	1.88E-11	0.559	0.441	0.966	0.001	0.000	0.001	0.000	1.522	0.000	0.000
CYC-C6	7.28E-12	0.670	0.330	0.000	0.000	0.000	0.000	0.000	0.670	0.000	0.000
CYC-C7	9.41E-12	0.667	0.333	0.749	0.075	0.000	0.264	0.000	0.942	0.000	0.035
CYC-C8	1.14E-11	0.613	0.387	1.309	0.209	0.335	0.268	0.000	0.691	0.000	0.209
CYC-C9	1.35E-11	0.657	0.343	1.840	0.297	0.276	0.405	0.000	0.891	0.000	0.282
CYC-C10	1.55E-11	0.635	0.365	1.725	0.224	0.400	0.143	0.000	1.140	0.003	0.224
CYC-C11	1.76E-11	0.682	0.318	1.617	0.209	0.345	0.033	0.000	1.317	0.000	0.195
CYC-C12	1.96E-11	0.668	0.332	1.813	0.180	0.392	0.033	0.000	1.520	0.000	0.178
CYC-C13	2.08E-11	0.643	0.356	1.330	0.078	0.200	0.056	0.000	1.481	0.001	0.076
CYC-C14	2.20E-11	0.621	0.378	0.987	0.034	0.021	0.316	0.000	1.165	0.001	0.033
CYC-C15	2.32E-11	0.601	0.396	1.135	0.024	0.012	0.431	0.000	1.220	0.001	0.025
T = 300 K											
ETHANE	2.94E-13	1.000	0.000	0.000	0.000	1.000	0.000	0.000	0.000	0.000	0.000
PROPANE	1.23E-12	0.962	0.000	0.000	0.000	0.000	0.303	0.659	0.000	0.000	0.000
N-C4	2.56E-12	0.924	0.076	0.400	0.002	0.573	0.140	0.000	0.532	0.000	0.000

TABLE 9. KINETIC AND MECHANISTIC PARAMETERS USED IN THE REPRESENTATIONS OF THE REACTIONS OF THE ALKANES (CONTINUED).

Name	k_{OH}[a]	P_{RR}	P_{NR}	P_{R2}	P_{A1}	P_{A2}	P_{A3}	P_{K3}	P_{K4}	P_{CO}	P_{C2}
N-C5	3.97E-12	0.873	0.127	0.515	0.006	0.073	0.163	0.000	0.930	0.000	0.000
N-C6	5.38E-12	0.801	0.199	0.711	0.000	0.020	0.103	0.000	1.115	0.000	0.000
N-C7	6.79E-12	0.728	0.272	0.719	0.000	0.000	0.055	0.000	1.233	0.000	0.000
N-C8	8.19E-12	0.674	0.326	0.713	0.000	0.000	0.002	0.000	1.347	0.000	0.000
N-C9	9.60E-12	0.640	0.360	0.688	0.000	0.000	0.001	0.000	1.327	0.000	0.000
N-C10	1.10E-11	0.620	0.380	0.677	0.000	0.000	0.001	0.000	1.295	0.000	0.000
N-C11	1.24E-11	0.607	0.393	0.673	0.000	0.000	0.001	0.000	1.279	0.000	0.000
N-C12	1.38E-11	0.598	0.402	0.665	0.000	0.000	0.001	0.000	1.262	0.000	0.000
N-C13	1.52E-11	0.592	0.408	0.659	0.000	0.000	0.001	0.000	1.250	0.000	0.000
N-C14	1.66E-11	0.588	0.412	0.655	0.000	0.000	0.001	0.000	1.242	0.000	0.000
N-C15	1.80E-11	0.585	0.415	0.651	0.000	0.000	0.001	0.000	1.236	0.000	0.000
ISO-C4	2.40E-12	0.976	0.024	0.747	0.747	0.000	0.229	0.747	0.000	0.000	0.000
ISO-C5	4.02E-12	0.934	0.064	0.733	0.000	0.612	0.132	0.609	0.307	0.000	0.000
NEO-C5	7.59E-13	0.946	0.054	0.023	0.023	0.000	0.935	0.011	0.000	0.000	0.000
2-ME-C5	5.43E-12	0.868	0.127	0.740	0.006	0.021	0.541	0.229	0.717	0.000	0.000
3-ME-C5	5.79E-12	0.885	0.115	0.844	0.004	0.519	0.087	0.000	1.003	0.000	0.000
23-DMB	5.47E-12	0.906	0.056	0.950	0.000	0.000	0.127	1.595	0.095	0.000	0.000
4-ME-C6	7.20E-12	0.818	0.180	0.839	0.000	0.129	0.329	0.000	1.123	0.000	0.000
24-DM-C5	6.88E-12	0.874	0.124	0.851	0.000	0.000	0.776	0.268	0.682	0.000	0.000
23-DM-C5	7.24E-12	0.868	0.121	1.070	0.036	0.184	0.180	0.401	1.003	0.000	0.000
ISO-C8	4.71E-12	0.823	0.176	0.956	0.117	0.000	0.747	0.260	0.655	0.000	0.000
CYCC6	8.44E-12	0.793	0.207	0.311	0.003	0.000	0.292	0.000	0.803	0.000	0.003
ME-CYCC6	1.03E-11	0.784	0.216	0.960	0.100	0.001	0.454	0.000	0.994	0.002	0.046
ET-CYCC6	1.22E-11	0.748	0.252	1.470	0.189	0.316	0.387	0.000	0.939	0.009	0.189
3-ME-C6	7.20E-12	0.818	0.180	0.839	0.000	0.129	0.329	0.000	1.123	0.000	0.000
4-ME-C7	8.60E-12	0.764	0.233	0.816	0.000	0.000	0.360	0.000	1.220	0.000	0.000
4-ET-C7	1.06E-11	0.743	0.254	0.823	0.002	0.063	0.308	0.000	1.193	0.000	0.000
4-PR-C7	1.20E-11	0.715	0.282	0.797	0.000	0.004	0.336	0.000	1.172	0.000	0.000

TABLE 9. KINETIC AND MECHANISTIC PARAMETERS USED IN THE REPRESENTATIONS OF THE REACTIONS OF THE ALKANES (CONTINUED).

Name	k_{OH}[a]	P_{RR}	P_{NR}	P_{R2}	P_{A1}	P_{A2}	P_{A3}	P_{K3}	P_{K4}	P_{CO}	P_{C2}
BR-C6	5.43E-12	0.868	0.127	0.740	0.006	0.021	0.541	0.229	0.717	0.000	0.000
BR-C7	7.20E-12	0.818	0.180	0.839	0.000	0.129	0.329	0.000	1.123	0.000	0.000
BR-C8	8.60E-12	0.764	0.233	0.816	0.000	0.000	0.360	0.000	1.220	0.000	0.000
BR-C9	1.06E-11	0.743	0.254	0.823	0.002	0.063	0.308	0.000	1.193	0.000	0.000
BR-C10	1.20E-11	0.715	0.282	0.797	0.000	0.004	0.336	0.000	1.172	0.000	0.000
BR-C11	1.43E-11	0.776	0.224	1.289	0.020	0.057	0.089	0.000	1.899	0.000	0.000
BR-C12	1.58E-11	0.755	0.245	1.390	0.002	0.435	0.012	0.000	1.695	0.000	0.000
BR-C13	1.72E-11	0.737	0.263	1.252	0.002	0.009	0.113	0.000	1.865	0.000	0.000
BR-C14	1.86E-11	0.724	0.276	1.157	0.002	0.000	0.003	0.000	1.876	0.000	0.000
BR-C15	2.00E-11	0.712	0.288	1.138	0.001	0.000	0.003	0.000	1.846	0.000	0.000
CYC-C6	8.44E-12	0.793	0.207	0.311	0.003	0.000	0.292	0.000	0.803	0.000	0.003
CYC-C7	1.03E-11	0.784	0.216	0.960	0.100	0.001	0.454	0.000	0.994	0.002	0.046
CYC-C8	1.22E-11	0.748	0.252	1.470	0.189	0.316	0.387	0.000	0.939	0.009	0.189
CYC-C9	1.40E-11	0.774	0.226	2.004	0.290	0.271	0.505	0.000	1.087	0.000	0.271
CYC-C10	1.60E-11	0.759	0.241	1.917	0.214	0.401	0.230	0.000	1.392	0.011	0.214
CYC-C11	1.78E-11	0.790	0.210	1.890	0.240	0.384	0.138	0.000	1.510	0.001	0.190
CYC-C12	1.98E-11	0.780	0.220	2.092	0.205	0.447	0.107	0.000	1.762	0.001	0.174
CYC-C13	2.12E-11	0.762	0.238	1.671	0.104	0.246	0.194	0.000	1.706	0.002	0.076
CYC-C14	2.26E-11	0.748	0.251	1.536	0.071	0.070	0.440	0.000	1.574	0.002	0.051
CYC-C15	2.40E-11	0.737	0.261	1.673	0.041	0.028	0.475	0.000	1.788	0.002	0.038
T = 330 K											
ETHANE	3.90E-13	1.000	0.000	0.000	0.000	1.000	0.000	0.000	0.000	0.000	0.000
PROPANE	1.49E-12	0.975	0.000	0.021	0.021	0.021	0.320	0.634	0.000	0.000	0.000
N-C4	3.02E-12	0.950	0.050	0.819	0.009	1.337	0.154	0.000	0.164	0.000	0.000
N-C5	4.61E-12	0.916	0.083	0.807	0.014	0.281	0.385	0.000	0.713	0.000	0.000
N-C6	6.20E-12	0.870	0.130	0.857	0.001	0.054	0.205	0.000	1.124	0.000	0.000
N-C7	7.79E-12	0.824	0.176	0.836	0.000	0.000	0.093	0.000	1.371	0.000	0.000
N-C8	9.38E-12	0.790	0.210	0.836	0.000	0.000	0.002	0.000	1.578	0.000	0.000

TABLE 9. KINETIC AND MECHANISTIC PARAMETERS USED IN THE REPRESENTATIONS OF THE REACTIONS OF THE ALKANES (CONTINUED).

Name	k_{OH}[a]	P_{RR}	P_{NR}	P_{R2}	P_{A1}	P_{A2}	P_{A3}	P_{K3}	P_{K4}	P_{CO}	P_{C2}
N-C9	1.10E-11	0.769	0.231	0.830	0.000	0.000	0.002	0.000	1.597	0.000	0.000
N-C10	1.25E-11	0.756	0.244	0.834	0.000	0.000	0.002	0.000	1.589	0.000	0.000
N-C11	1.41E-11	0.748	0.252	0.842	0.000	0.000	0.002	0.000	1.589	0.000	0.000
N-C12	1.57E-11	0.743	0.257	0.838	0.000	0.000	0.001	0.000	1.580	0.000	0.000
N-C13	1.73E-11	0.739	0.261	0.837	0.000	0.000	0.001	0.000	1.574	0.000	0.000
N-C14	1.89E-11	0.736	0.264	0.836	0.000	0.000	0.001	0.000	1.571	0.000	0.000
N-C15	2.05E-11	0.734	0.266	0.834	0.000	0.000	0.001	0.000	1.567	0.000	0.000
ISO-C4	2.57E-12	0.984	0.016	0.710	0.710	0.000	0.274	0.709	0.000	0.000	0.000
ISO-C5	4.30E-12	0.950	0.044	0.892	0.018	0.710	0.161	0.690	0.193	0.000	0.000
NEO-C5	9.83E-13	0.963	0.037	0.250	0.250	0.000	0.839	0.124	0.000	0.000	0.000
2-ME-C5	5.89E-12	0.907	0.086	0.941	0.012	0.083	0.660	0.400	0.527	0.000	0.000
3-ME-C5	6.16E-12	0.918	0.082	0.977	0.014	0.588	0.113	0.000	0.997	0.000	0.000
23-DMB	5.59E-12	0.938	0.038	1.013	0.020	0.020	0.166	1.548	0.125	0.000	0.000
4-ME-C6	7.75E-12	0.876	0.123	0.959	0.004	0.192	0.314	0.000	1.203	0.000	0.000
24-DM-C5	7.18E-12	0.909	0.086	1.073	0.023	0.005	0.870	0.566	0.516	0.000	0.000
23-DM-C5	7.45E-12	0.907	0.085	1.219	0.052	0.409	0.147	0.450	0.939	0.000	0.000
ISO-C8	5.12E-12	0.878	0.121	1.331	0.293	0.001	0.815	0.536	0.563	0.000	0.000
CYCC6	9.54E-12	0.864	0.136	1.308	0.034	0.000	1.211	0.000	0.371	0.017	0.016
ME-CYCC6	1.11E-11	0.855	0.145	1.679	0.148	0.007	0.963	0.000	0.712	0.027	0.059
ET-CYCC6	1.31E-11	0.831	0.169	2.098	0.184	0.305	0.741	0.000	0.852	0.048	0.175
3-ME-C6	7.75E-12	0.876	0.123	0.959	0.004	0.192	0.314	0.000	1.203	0.000	0.000
4-ME-C7	9.34E-12	0.842	0.156	0.933	0.003	0.003	0.338	0.000	1.430	0.000	0.000
4-ET-C7	1.13E-11	0.827	0.171	0.960	0.005	0.085	0.268	0.000	1.429	0.000	0.000
4-PR-C7	1.29E-11	0.809	0.188	0.955	0.003	0.011	0.319	0.000	1.432	0.000	0.000
BR-C6	5.89E-12	0.907	0.086	0.941	0.012	0.083	0.660	0.400	0.527	0.000	0.000
BR-C7	7.75E-12	0.876	0.123	0.959	0.004	0.192	0.314	0.000	1.203	0.000	0.000
BR-C8	9.34E-12	0.842	0.156	0.933	0.003	0.003	0.338	0.000	1.430	0.000	0.000
BR-C9	1.13E-11	0.827	0.171	0.960	0.005	0.085	0.268	0.000	1.429	0.000	0.000
BR-C10	1.29E-11	0.809	0.188	0.955	0.003	0.011	0.319	0.000	1.432	0.000	0.000
BR-C11	1.49E-11	0.846	0.154	1.520	0.035	0.172	0.145	0.000	2.014	0.000	0.000

TABLE 9. KINETIC AND MECHANISTIC PARAMETERS USED IN THE REPRESENTATIONS OF THE REACTIONS OF THE ALKANES (CONCLUDED).

Name	k_{OH}[a]	P_{RR}	P_{NR}	P_{R2}	P_{A1}	P_{A2}	P_{A3}	P_{K3}	P_{K4}	P_{CO}	P_{C2}
BR-C12	1.65E-11	0.833	0.167	1.423	0.004	0.398	0.018	0.000	1.837	0.000	0.000
BR-C13	1.81E-11	0.820	0.180	1.409	0.003	0.056	0.177	0.000	1.994	0.000	0.000
BR-C14	1.97E-11	0.814	0.186	1.230	0.003	0.015	0.011	0.000	2.015	0.000	0.000
BR-C15	2.13E-11	0.806	0.194	1.232	0.002	0.013	0.005	0.000	2.017	0.000	0.000
CYC-C6	9.54E-12	0.864	0.136	1.308	0.034	0.000	1.211	0.000	0.371	0.017	0.016
CYC-C7	1.11E-11	0.855	0.145	1.679	0.148	0.007	0.963	0.000	0.712	0.027	0.059
CYC-C8	1.31E-11	0.831	0.169	2.098	0.184	0.305	0.741	0.000	0.852	0.048	0.175
CYC-C9	1.47E-11	0.847	0.153	2.420	0.279	0.260	0.738	0.000	1.088	0.002	0.258
CYC-C10	1.67E-11	0.837	0.163	2.210	0.194	0.385	0.394	0.000	1.499	0.030	0.194
CYC-C11	1.82E-11	0.857	0.143	2.379	0.296	0.462	0.395	0.000	1.669	0.005	0.172
CYC-C12	2.02E-11	0.850	0.150	2.339	0.263	0.526	0.244	0.000	1.821	0.003	0.164
CYC-C13	2.18E-11	0.833	0.166	2.179	0.174	0.350	0.466	0.000	1.819	0.004	0.076
CYC-C14	2.34E-11	0.824	0.175	2.144	0.125	0.157	0.679	0.000	1.838	0.006	0.064
CYC-C15	2.50E-11	0.821	0.176	2.034	0.061	0.047	0.538	0.000	2.115	0.004	0.045

[a]Rate constant given in units of cm^{-3} $molecule^{-1}$ sec^{-1}.

Analogous to the alkane mechanism, mechanism, RO2-NP. is used to represent the uncharacterized NO_x and radical processes used in the model for tetralin and the naphthalenes as discussed below, benzaldehyde is used to represent all of the aromatic aldehydes formed in these systems (such as the tolualdehydes formed from xylenes), and the pseudospecies HCOCHO(X) and CCOCHO(X) are used to represent the uncharacterized reactive aromatic ring-opening products, as discussed below.

The OH radical rate constants and the mechanistic and product yield parameters used for all the aromatic hydrocarbons in the present model are given in Table 10. Except as noted, the OH radical rate constants were obtained from the comprehensive review of Atkinson (Reference 25). The values derived for the mechanistic and product parameters were based on our current knowledge or estimates of aromatic reactions and product yields, or adjusted to fit the environmental chamber data obtained in this and previous programs, as discussed below.

Benzene and Alkylbenzenes. The parameters used in this model for the reactions of benzene, toluene, and the di- and tri-methyl benzenes are based to a large extent on the toluene and xylene mechanisms previously formulated by Atkinson and co-workers (References 13, 15, 17) and Leone et al. (References 16, 20). However, these mechanisms were updated and modified to be consistent with recent aromatic product yield data with results of the environmental chamber experiments, including those carried out in this program. Those papers, and the documentation of the aromatic mechanisms in our detailed EPA report (Reference 26), give a comprehensive discussion of the general features of aromatic photooxidation mechanisms as presently understood (other than the results of the most recent product studies and chamber experiments, discussed below), and this discussion is not reproduced here. In this section, we focus on: (1) the ways in which the aromatic photooxidation mechanisms in this model differ from those in the previous models of Atkinson and co-workers and Leone et al. (References 13, 15-17, 20) and from the mechanisms documented in our EPA report (Reference 26); (2) the reasons for these differences; and (3) the remaining major areas of uncertainty in the photooxidation mechanisms of these compounds.

TABLE 10. KINETIC AND MECHANISTIC PARAMETERS USED IN THE REPRESENTATIONS OF THE REACTIONS OF THE AROMATIC HYDROCARBONS.

Name	Kinetic parameters[a]		Mechanistic and product yield parameters[b]									
	k(300)	Ea	pRR	pRH	pNP	pBZ	pPH	pCR	pGL	pMG	pU1	pU2
BENZENE	1.30E-12	1.050	0.730	0.270	0.000	0.000	0.270	0.000	0.212	0.000	0.610	0.000
TOLUENE	6.14E-12	-0.640	0.840	0.160	0.000	0.080	0.000	0.160	0.114	0.144	0.000	0.420
C2-BENZ	7.50E-12	0.000										
I-C3-BEN	6.60E-12	0.000										
N-C3-BEN	5.70E-12	0.000										
S-C4-BEN	6.60E-12	0.000										
M-XYLENE	2.45E-11	-0.231	0.830	0.170	0.000	0.040	0.000	0.170	0.095	0.316	0.000	0.690
O-XYLENE	1.47E-11	0.000										
P-XYLENE	1.52E-11	0.000										
135-TMB	6.24E-11	0.000	0.830	0.170	0.000	0.020	0.000	0.170	0.000	0.860	0.000	0.540
123-TMB	3.33E-11	0.000										
124-TMB	4.00E-11	0.000										
TETRALIN	1.50E-11	0.000	0.790	0.090	0.120	0.000	0.090	0.000	1.000	0.000	0.240	0.000
NAPHTHAL	2.12E-11	-1.792	0.690	0.170	0.140	0.000	0.170	0.000	1.000	0.000	0.350	0.000
23-DMN	7.68E-11	0.000	0.800	0.040	0.160	0.000	0.000	0.040	0.000	0.400	0.690	0.070
ME-NAPH	5.23E-11	0.000	0.745	0.105	0.150	0.000	0.085	0.020	0.500	0.200	0.520	0.035

[a] K(300) is the OH radical rate constant at 300 K given in units of cm^{-3} $molecule^{-1}$ sec^{-1}. Ea is the Arrhenius activation energy in kcal $mole^{-1}$.

[b] If no mechanistc parameters are given, they are assumed to be the same as for the compound given above.

One way in which this aromatic mechanism differs from those in the earlier models from which this mechanism was developed (References 13, 15) is the earlier models assumed 25 percent benzyl nitrate formation from the reaction of the aromatic peroxy radicals with NO. This assumption was based on analogy with the observed formation of alkyl nitrates in the alkane photooxidation schemes (Reference 24), and because the radical and NO_x sink it caused was needed in the Atkinson et al. (Reference 13) model to adequately fit the chamber data. However, the aromatic mechanisms in the more recent mechanism of Lurmann et al. (References 18, 21), as well as the models of Leone and co-workers (References 16, 20), do not assume organic nitrate formation in these reactions to fit these data, and to be consistent with these more recent mechanisms, aromatic nitrate formation is also neglected in this mechanism.

However, Hoshino et al. (Reference 50) observed an ~10 percent yield of benzyl nitrate from the reaction of the benzyl peroxy radical with NO

$$C_6H_5CH_2OO\cdot + NO \xrightarrow{M} \begin{cases} C_6H_5CH_2ONO_2 & \sim 10\% \\ C_6H_5CH_2O\cdot + NO_2 & \sim 90\% \end{cases}$$

suggesting that some nitrate formation may indeed be occurring from this reaction, though at lower yields than assumed by Atkinson et al. (References 13, 15). Since a 10 percent nitrate yield in the reaction of benzyl peroxy radicals with NO corresponds to only 1 percent of the overall toluene photooxidation products, it is still ignored in the present model for all aromatic hydrocarbons. However, inclusion of some representation for nitrate formation from reactions of NO with aromatic peroxy radicals may be appropriate for future models, once more details of aromatic photooxidation mechanisms and the products formed are elucidated.

The major uncertainties, and the major areas where this mechanism differs from the previous mechanisms, concern the aromatic ring opening processes and the nature and reactions of the products ultimately formed. Despite continuing studies of aromatic photooxidation mechanisms, our current understanding in this area continues to be grossly inadequate.

The most recent experimental data have raised more questions than they have answered, giving results which are inconsistent with previously published aromatic photooxidation mechanisms. In particular, the recent experimental data concerning the yields of α-dicarbonyls from benzene and the methyl-substituted benzenes obtained by Tuazon et al. (Reference 51) and Bandow and co-workers (References 52-54) [which are in good agreement with each other for the methyl-substituted benzenes] indicate yields of α-dicarbonyls which are significantly lower than predicted by any of the previous mechanisms (References 12, 13, 15, 16, 18, 20-23, 26, 49). These experimental data, coupled with the observations of several unsaturated oxygenates as products from toluene (References 55, 56) and o-xylene (Reference 56), are not consistent with the ring-opening mechanisms proposed previously (References 13, 15-17, 20, 49).

Using toluene as an example, these mechanisms predict either the formation of three molecules of α-dicarbonyls for each molecule of toluene which undergoes ring opening [as predicted by the "recyclization" mechanism assumed by Killus and Whitten (Reference 49)] and incorporated into the latest carbon bond models (References 22, 23) or that one α-dicarbonyl molecule and one homologue to 2-butene-2,4-dial is formed [as predicted by the "cyclization" mechanism assumed in the review of Atkinson and Lloyd (Reference 17) and in the models of Atkinson et al. (Reference 13) and Leone et al. (References 16, 20)]. Both of these are inconsistent with the recent α-dicarbonyl product yield data, which indicate that these products (glyoxal and methylglyoxal) account for only 35 percent of the ring-opening reaction route from toluene if the cyclization mechanism is assumed, and only 12 percent of the reaction if recyclization is assumed. In addition, the qualitative product studies of Shepson et al. (Reference 56) and Dumdei and O'Brien (Reference 55) indicate that 2-butene-1,4-dial, or its methyl-substituted analogues 2-pentene-1,4-dial and 2-methyl-2-butene-1,4-dial, predicted to be formed from toluene by the cyclization mechanism, are not the only unsaturated ring-opening products. These studies show that the actual toluene ring-opening reaction mechanism is much more complex than previously assumed.

The formation and reactions of these uncharacterized products cannot be ignored in the aromatic models, because doing so results in the model

significantly and consistently underpredicting the reactivity observed in aromatic hydrocarbon-NO_x-air environmental chamber experiments. [This is particularly true for those experiments carried out in this program using the SAPRC ITC, since the wavelength distribution of the ITC blacklights is such that the α-dicarbonyls photolyze at significantly lower rates than is the case in the SAPRC EC or in outdoor chambers. The previous models which assumed the high α-dicarbonyl yields, which could simulate toluene runs carried out in the SAPRC EC and outdoor chambers (e.g., Reference 21), significantly underpredict reactivity in toluene runs carried out in the ITC, due to the lower calculated methylglyoxal photolysis rate (Reference 26).] However, because of our present lack of knowledge of the ring-opening reactions of the aromatic hydrocarbons, and of the nature and reactions of the non-α-dicarbonyl products formed, no attempt was made in this model to represent them explicitly. Instead, they were represented in a parameterized manner, as indicated below.

In the version of the aromatics mechanisms given in our detailed EPA report (Reference 26), the uncharacterized, non-α-dicarbonyl ring-opened products were lumped together and represented as "aromatic unknowns" (one for each aromatic hydrocarbon), whose subsequent reactions were represented as being analogous to the reaction mechanisms previously proposed (References 13, 17) for the 1,4-unsaturated dicarbonyls which had been assumed to be the coproducts to the α-dicarbonyls, but modified to conserve carbon and the number of methyl groups. In order for the model to simulate the observed reactivity of the aromatic hydrocarbons, each of these "unknowns" was assumed to photolyze to yield radicals, with the photolysis rate for the "unknown" for each aromatic being adjusted to fit the results of the single component aromatic-NO_x-air irradiations carried out in the SAPRC EC and the SAPRC ITC. If the same mechanism was to successfully simulate experiments in both the EC and the ITC, which have significantly different spectral distributions (Reference 26), it was necessary to assume that the "unknowns" photolyze (primarily by absorption of light in the wavelength region below 350 nm) significantly lower wavelengths than are responsible for the photolysis of the α-dicarbonyls. It was also necessary to assume that the reactions of the "unknowns" with OH radicals result in the formation of PAN analogues, since not assuming this

results in a consistent tendency for the model to overpredict final ozone yields in aromatic-NO_x-air irradiations (Reference 26). These aromatic mechanisms, optimized based on fits to SAPRC EC and ITC runs, gave satisfactory simulations, on the average, of toluene-NO_x-air and o-xylene-NO_x-air runs carried out in the UNC outdoor chamber (Reference 26).

Our current aromatic photooxidation mechanism uses a somewhat different parameterization of the reactions of the aromatic ring-opening products than that given in the previous EPA report (Reference 26), since we found that an alternative representation, with fewer species and reactions, could give equally good, and in some cases slightly better, fits of the model to the environmental chamber data. In this representation, two separate species were used to represent the unknown products of all the aromatic hydrocarbons in the model, instead of one for each aromatic. The PAN analogues they form were lumped with PAN analogues formed in other areas of the model, specifically those formed from the reactions of glyoxal and "RCHO," the lumped higher aldehyde. The specific set of reactions assigned for each was chosen to be analogous for those for the α-dicarbonyls, rather than the 1,4-unsaturated dicarbonyls as used in the previous representation of the unknown products. The photolysis rates and yields of these "lumped aromatic unknown products" in the photooxidations of benzene, toluene, m-xylene, and 1,3,5-trimethylbenzene were adjusted to obtain best fits to the results of selected aromatic-NO_x-air irradiations carried out in the SAPRC EC and ITC, using a nonlinear least squares optimization program. As was the case with the previous representation, in order to fit reactivity in EC and ITC experiments with the same model, the products were assumed to photolyze in the <350 nm wavelength region. The data were adequately fit by assigning one of the unknown products [designated HCOCHO(X) in the reaction list in Section IV.A.1] to represent the unknowns formed from benzene, and the other [designated CCOCHO(X)] to represent the unknowns from the methylbenzenes, with the latter photolyzing 13.3 times faster than the former. The parameters which were adjusted, and the specific sets of experimental data used by the optimization program to derive the adjusted parameters employed in the final model, are summarized in Table 11. The values of the parameters are given in Table 10.

TABLE 11. PARAMETERS ADJUSTED TO FIT ENVIRONMENTAL CHAMBER DATA USING NONLINEAR LEAST SQUARES OPTIMIZATION, AND DATA USED IN THE OPTIMIZATION IN THE DERIVATIONS OF THE REACTION MECHANISMS FOR THE AROMATIC HYDROCARBONS.

Compound	Mechanistic parameter(s) adjusted	Experiment	Data fit
Benzene	-Yield of HCOCHO(X) -HCOCHO(X) Photolysis Rates	ITC-560 ITC-561 ITC-562	Ozone, NO, NO_2[a]
Toluene	-Yield of CCOCHO(X) -CCOCHO(X) Photolysis rates[b]	EC-266 EC-270 EC-271 ITC-699	Ozone, NO, NO_2[a], PAN
m-Xylene[c]	-Yield of CCOCHO(X)	EC-344 EC-345 ITC-702	Ozone, NO, NO_2[a], PAN m-Xylene
135-TMB[d]	-Yield of CCOCHO(X)	EC-901 EC-903 ITC-703 ITC-706 ITC-709	Ozone, NO NO_2[a], PAN, 135-TMB
Tetralin	-Phenol Yield[e] -Nitrophenol Yield -Yield of HCOCHO(X)	ITC-739 ITC-747 ITC-748 ITC-750 ITC-832	Ozone, NO, NO_2[a], Propene[f]
Naphthalene	-Phenol Yield -Nitrophenol Yield -Yield of HCOCHO(X)	ITC-751 ITC-755 ITC-756 ITC-798 ITC-802	Ozone, NO, NO_2[a]
2,3-DMN[g]	-Phenol Yield -Nitrophenol Yield -Yield of HCOCHO(X) -Yield of CCOCHO(X) -Yield of Methyl Glyoxl	ITC-771 ITC-774 ITC-775 ITC-806	Ozone, NO NO_2[a], PAN 23-DMN

TABLE 11. PARAMETERS ADJUSTED TO FIT ENVIRONMENTAL CHAMBER DATA USING NONLINEAR LEAST SQUARES OPTIMIZATION, AND DATA USED IN THE OPTIMIZATION IN THE DERIVATIONS OF THE REACTION MECHANISMS FOR THE AROMATIC HYDROCARBONS (CONCLUDED).

[a]Only NO_2 data before time of NO_2 maximum used, because of nitrate interferences in the NO_2 analysis technique employed (Section III.A.3).

[b]The approximate magnitude of the CCOCHO(X) photolysis rate was adjusted in initial simulations, but the value used in the EPA model (Reference 26) was found to be satisfactory, and was held fixed in determining the optimum yield of CCOCHO(X) from toluene.

[c]Parameters optimized to fit results of runs with m-xylene were also used in simulations of runs with o-xylene.

[d]135-TMB = 1,3,5-trimethylbenzene.

[e]Phenol yield from tetralin was set to zero in final optimizations as a result of initial optimizations where this was allowed to vary.

[f]Present as a radical tracer in some of the runs.

[g]23-DMN = 2,3-dimethylnaphthalene.

As shown in Section IV.C, with this adjusted, parameterized representation of aromatic ring-opening products the current mechanism can simulate results of aromatic-NO_x-air experiments as well as, or better than, its simulations of single component experiments employing other classes of organics, such as alkanes and alkenes, whose reaction mechanisms are considered to have much fewer major areas of uncertainty. Although we do not claim that this representation necessarily has any degree of chemical accuracy, until more is known about the details of the aromatic ring-opening processes and the nature and reactions of the products formed, it is difficult to justify the use of more complex, and speculative mechanisms, which may not fit the available data any better.

Tetralin and the Naphthalenes. As with the other aromatics, tetralin and the naphthalenes are expected to be consumed in the atmosphere primarily by reaction with hydroxyl radicals. The rate constant used for the reaction of OH radicals with naphthalene was that recommended by Atkinson (Reference 25), and the rate constant for 2,3-dimethylnaphthalene was that measured by Atkinson and Aschmann (Reference 57). No rate constant has been measured for the reactions of OH radicals with tetralin, and it is assumed to be approximately 1.5×10^{-11} cm^3 $molecule^{-1}$ sec^{-1}, based on the recommended rate constant for o-xylene (Reference 25).

No data are available concerning the mechanisms or the products formed in the reactions of the tetralin and the naphthalenes under atmospheric conditions. Because of the still significant uncertainties concerning the atmospheric reactions of the more well studied aromatics, such as toluene, it appeared not to be profitable to attempt to speculate concerning the nature of the reactions of these compounds, where even fewer data are available. Rather, the reaction mechanism for tetralin and the naphthalenes were derived in a parameterized manner, using the general formulation, parameters, and products already used in our models for the alkylbenzenes, with the values of the parameters being adjusted based on model simulations of the chamber data.

In the initial set of simulations for naphthalene, the parameters employed were those involved in the photooxidation of benzene. Thus, in the initial set of simulations, the yields of phenol, glyoxal, and the generalized benzene fragmentation product HCOCHO(X) were adjusted. Based on assumptions implicit in the benzene and the alkylbenzene models (References 13, 15, 16, 20), it was assumed that the formation of all products involved the eventual generation of HO_2 radicals (at least in the presence of NO), that the formation of phenolic products involved no NO-to-NO_2 conversions, and that the formation of all other products involved one NO-to-NO_2 conversion before HO_2 is generated. In terms of our parameterized formulation, this means that $p_{RH} = p_{GL}$ and that $p^{RR} = 1 - p_{GL}$. However, model simulations based on these assumptions would not satisfactorily fit the results of the naphthalene experiments, regardless of what values of p_{GL}, p_{PH}, or p_{U1} were employed. In particular, models based on this assumption could not account for the fact that, as noted in our report on Phase I of this program (Reference 27), naphthalene and tetralin tend to suppress radical levels when added to NO_x-air mixtures. To represent this effect in the model, we arbitrarily represented this by the formation of species (designated RO_2-NP. in this model) which react with NO to form uncharacterized aromatic nitrogen-containing species, which are arbitrarily represented in this model as "nitrophenol." If the parameter giving the yield of RO_2-NP. is included in the optimization (see Table 11), then adequate fits of the model simulations to most of the experimental results were obtained. (In this context, "adequate" means the fits

were of the quality obtained for the alkylbenzenes.) The resulting optimized values for the mechanistic parameters derived are given in Table 10. A summary of these fits is given in Section IV.C.

The determination of the mechanistic parameters for 2,3-dimethylnaphthalene was obtained in an analogous manner, except that in this case the presence of methyl groups on this compound means that additional products might be formed. Thus, parameters giving yields of methylglyoxal and CCOCHO(X), the pseudospecies used to represent uncharacterized reactive methyl-containing aromatic ring-opening products, were also included in the optimization, and the observed measurements of PAN were partially used to determine these values. As with tetralin and naphthalene, adequate fits of the model simulations to the data were obtained. The resulting optimized values for the mechanistic parameters are given in Table 10, and a summary of the performance of the adjusted model in fitting the results of the 2,3-dimethylnaphthalene runs is given in Section IV.C

Although, in many respects, the structure of tetralin is similar to that of o-xylene and it is estimated to react in the atmosphere at a similar rate, the experiments with this compound have shown it to be much less reactive than o-xylene (Reference 27). Based on mechanistic considerations, this result is not unexpected since the additional ring could prevent some of the fragmentation routes causing reactive products in the reactions of the alkylbenzenes. Indeed, the overall reactivity of tetralin is more similar to that of naphthalene than to any of the alkylbenzenes and, if the mechanistic parameters adjusted for naphthalene are used, fair fits of the model simulation of the tetralin runs could be obtained. Thus, these parameters were used as the starting point in determining the optimum parameters for tetralin, and no additional parameters were employed. (In particular, since tetralin lacks methyl groups, methylglyoxal and CCOCHO(X) were not included among the products for tetralin.) The resulting fits of the optimized model for tetralin were similar to the other aromatics. The parameters so derived are given in Table 10, and the qualities of the fits are summarized in Section IV.C.

This model also includes the reactions of 2-methylnaphthalene, which is used to represent the reactions of all monoalkyl naphthalenes. The OH

radical rate constant used for this compound was determined as part of our Phase I program (References 26, 57), and is 5.23 x 10^{-11} cm^3 $molecule^{-1}$ sec^{-1}, as given in the evaluation of Atkinson (Reference 25). Since no single component environmental chamber experiments are available for any of the monoalkyl naphthalenes, the mechanistic and product yield parameters for this compound were estimated by averaging those for naphthalene and 2,3-dimethylnaphthalene. These values are tabulated in Table 10.

As with our parameterized representation of the formation and reactions of the ring-opening in the alkylbenzenes, no claim of chemical accuracy is made in our parameterized representation of the mechanisms of the reactions of tetralin and the naphthalenes, since even less is known of the nature of their reactions or the products formed. All that can be said is that the parameterized representation used in this model adequately fits most of the chamber data obtained in the first phase of this program (Reference 26), essentially the only data available concerning the atmospheric reaction mechanisms of these compounds. When more basic laboratory and product data about the reactions of these species become available, this model should be updated and reevaluated.

4. Reactions of Furan, Thiophene, and Pyrrole

The development of the reaction mechanisms for the heterocyclic compounds furan, thiophene and pyrrole, used to represent potential shale-oil derived fuel impurities, was analogous to the development of the mechanisms for tetralin and the naphthalenes, discussed above. As for tetralin and the naphthalenes, the rate constants for the major atmospheric removal processes for these heterocyclic organics appear to be well established. However, essentially nothing is known concerning their atmospheric reaction mechanisms, or the nature and reactions of the major products formed. Thus, mechanistic parameters for these compounds had to be estimated and adjusted so that model simulations could fit the results of the environmental chamber experiments carried out with these compounds under the first phase of this program (Reference 26). The derivations of

the mechanisms used in this model for these compounds are discussed below, in the order they were developed.

Furan. Based on available kinetic data (References 25, 27, 58, 59), the major loss processes for furan in the atmosphere are expected to be reactions with OH radicals, and sometimes reactions with NO_3 radicals. Both processes are represented in this model. The OH radical rate constant used in this model is recommended by Atkinson (Reference 25), and is given by (in cm^3 $molecule^{-1}$ sec^{-1}):

$$k(OH + furan) = 1.32 \times 10^{-11} \exp(0.664 \text{ kcal mole}^{-1}/RT)$$

In the case of the NO_3 radical reaction, the rate constant used in this model is 1.4×10^{-12} cm^3 $molecule^{-1}$ sec^{-1} (Reference 27, 59). The temperature dependence of this rate constant is not known, and is not represented in this model.

The parameterized reactions which were derived to represent the overall effects of the reactions of OH and NO_3 radicals with furan, and incorporated in this model, are those shown below:

$$OH + furan \rightarrow HO_2\cdot + 0.35\ R202. + 0.42\ HET\text{-}UNKN$$

$$NO_3 + furan \rightarrow HONO_2 + HO_2\cdot + (products\ whose\ reactions\ are\ ignored)$$

where R202. is the pseudospecies used to represent the conversion of NO-to-NO_2 by intermediate radicals, and HET-UNKN is used to represent reactive products formed in the furan system, which is assumed to react primarily by rapid photolysis, with a rate equal to that derived for the pseudo-species CCOCHO(X) used in the alkylbenzene system.

$$HET\text{-}UNKN + h\nu \rightarrow 2\ HO_2\cdot + (inert\ or\ unreactive\ products)$$

The yields of the pseudospecies R202. and HET-UNKN in the OH reaction, and the the assumption that HET-UNKN reacts primarily by rapid photolysis to form radicals, were determined by fitting model simulations to the results of the chamber experiments, as discussed below.

As discussed in the final report on Phase I of this program (Reference 26), the most obvious overall feature of the furan photooxidation mechanism, which is apparent even without the benefit of model simulations, is that the product(s) are highly reactive, and do not persist in the system. This is because, when furan is present, NO oxidation and (if NO is consumed) ozone formation occurs extremely rapidly, but once all the furan is consumed, the system is essentially "dead," i.e., is indistinguishable from a NO_x-air irradiation with no organic present. Experimentation with model simulations indicated that better results were obtained if it was assumed that relatively low yields of a highly photoreactive product were formed, with the photolysis rate being held at an arbitrary, high, value (arbitrarily assumed to be the same as that for the pseudospecies CCOCHO(X) used in the alkylbenzene mechanisms), with its yield being adjusted, rather than the alternative of assuming unit yield of some photoreactive product, with its photolysis rate being adjusted to fit the data. Best fits were also obtained if it was assumed that the photolysis of this product did not give rise to any secondary products, and that no reactive, or any moderately reactive products (such as glyoxal) were formed in the initial reaction. Only one reactive product was used in the model because that was all required for the model simulations to fit the data. Since it was represented as photolyzing so rapidly, its removal by other processes, such as reaction with OH radicals, was ignored.

The ozone, NO, and NO_2 profiles in the furan-NO_x-air chamber experiments were also extremely sensitive to the number of NO-to-NO_2 conversions assumed to occur in the furan photooxidation reactions. Thus, the yield of the pseudospecies R202., which as discussed in Section IV.A.1, was used to represent NO-to-NO_2 conversions, was also adjusted to fit the chamber data. With the adjustment of this parameter along with the adjustment of the yield used for the uncharacterized reactive species HET-UNKN, adequate fits to the results of the chamber experiments could be obtained using the parameterized mechanism as shown. The performance of this model in simulating the results of these runs is summarized in Section IV.C.

Furan is also consumed to some extent by reaction with NO_3 radicals, with this process becoming relatively more important later in the

experiments where ozone is formed. However, in the limited testing carried out, the model was not very sensitive to what is assumed concerning this reaction, so it was arbitrarily assumed that the overall process results in NO_x removal, as might occur if nitric acid were generated, and that radicals are not removed in the overall process.

The ozone yields in the furan-NO_x runs which this model was adjusted to fit, depended primarily on the NO-to-NO_2 conversions assumed and not the NO_x removal rates, since the availability of furan, not NO_x, was the limiting factor in all these runs. This model included no significant NO_x sinks in the OH + furan mechanism, and a 100 percent NO_x sink in the NO_3 + furan reaction, but this was assumed and could not be tested using only the data from the furan-NO_x runs. The results of the simulations of the experiment where furan was added to the synthetic fuel mixture (Section IV.C) suggested that the overall furan reactions may remove NO_x to a somewhat greater extent than assumed in this model, since the addition of furan caused a greater reduction in the maximum ozone yield than was predicted by this model. (NO_x removal processes cause reduced maximum ozone in experiments where a "true" ozone maximum is obtained, because in such runs the maximum amount of ozone formed is determined in part by the availability of NO_x.) However, no adjustments of this or any other other mechanisms were done on the basis of results of simulations of such complex experiments as synthetic fuel runs, since there are many other factors which might account for the observed discrepancies.

Pyrrole. As is the case with furan, pyrrole is consumed in the atmosphere primarily by reaction with OH and NO_3 radicals (References 27, 59, 60). The OH radical rate constant used in this model for pyrrole is 1.2×10^{-10} cm^3 $molecule^{-1}$ sec^{-1} (Reference 60), and the NO_3 radical rate constant is 4.9×10^{-11} cm^3 $molecule^{-1}$ sec^{-1} (Reference 59). These rate constants were measured at 295 K, but because of this large magnitude, their temperature dependencies are likely to be small, and are ignored in this model.

The parameterized mechanism used in this model to represent the net effects of the reactions of pyrrole is as follows:

$$OH + \text{pyrrole} \rightarrow HO_2\cdot + 0.23\ R2O_2\cdot + 0.23\ \text{HET-UNKN} + 1.0\ \text{HET-UNK2}$$

$$NO_3 + \text{pyrrole} \rightarrow HONO_2 + HO_2\cdot + \text{(products whose reactions are ignored)}$$

This mechanism is analogous to that given for furan, except for the formation of the additional pseudospecies designated HET-UNK2, which is included for reasons discussed below. The yields R2O2. and HET-UNKN were optimized (along with the parameters for HET-UNK2, discussed below) based on model simulations of the pyrrole-NO_x-air irradiations. The mechanism for pyrrole is similar to that used for furan because, as discussed in Reference 26, the major features of their reactions appear to be similar, other than the fact that pyrrole reacts significantly more rapidly. In particular, like furan, pyrrole-NO_x air systems are highly reactive as long as pyrrole is present, but become essentially "dead" once all the pyrrole has reacted. The mechanism shown above successfully simulates this effect.

Although optimized models based entirely on the formulation used for furan (i.e., without HET-UNK2) adequately simulated many of the observations in the pyrrole-NO_x-air runs, they did not successfully simulate the decay of ozone observed after its maximum was attained in run ITC-735. To fit this and the NO_2 data in that run, it was necessary to assume that some product is formed which reacts to convert NO_3 to NO. To represent this, the pseudospecies HET-UNK2 was added to the model, which reacts as shown below:

$$\text{HET-UNK2} + NO_3 \rightarrow NO + \text{(products whose reactions are ignored)}$$

whose NO_3 rate constant was optimized to fit the data at the same time the yields for $R2O_2\cdot$ and HET-UNKN were optimized. (The alternative representation of assuming a very rapid NO_3 + HET-UNK2 rate constant, and adjusting the yield of this pseudospecies in the initial OH + pyrrole reaction was explored, yielded less satisfactory results than this representation.) The best fit value for that rate constant was 1.36×10^{-13} cm^3 $molecule^{-1}$ sec^{-1}, and this is used in the model. This pseudospecies is not assumed to react via any other routes.

As for furan, the mechanism for the reaction of NO_3 radicals with pyrrole could not be unambiguously determined on the basis of the available experimental data, and thus, the same highly simplified and arbitrary mechanism for this reaction was used in both cases. Also, the simulation of the run in which furan was added to a synthetic fuel suggests that this pyrrole mechanism may not have sufficient NO_x sinks. This is suggested by the model overpredicting the ozone maximum in that run, while the model adequately predicted the ozone maximum in the run with the same synthetic fuel without pyrrole. However, the furan model was not adjusted to optimize the fits to that run, because of other uncertainties involved in the simulations of those complex mixtures.

Thiophene. Thiophene is the least reactive of the three heterocyclic organics studied in this program. As with the other two, it is consumed primarily by reactions with OH and NO_3 radicals (References 25, 27, 58, 59). The OH radical rate constant used was that that recommended by Atkinson (Reference 25), and given by (in cm^3 $molecule^{-1}$ sec^{-1}):

$$k(OH + \text{thiophene}) = 3.2 \times 10^{-12} \exp(0.644 \text{ kcal mole}^{-1}/RT)$$

while the NO_3 radical rate constant used was 1.26×10^{-13} cm^3 $molecule^{-1}$ sec^{-1} (References 26, 59). The temperature dependence of the NO_3 rate constant is not known, and is not represented in this model.

The parameterized mechanism used in this model to represent the overall effects of the OH and NO_3 reactions in the thiophene system are:

$$OH + \text{thiophene} \rightarrow HO_2\cdot + 0.145\ \text{HET-UNKN} + 0.55\ \text{HCOCHO(X)} + \text{HET-UNK2}$$

$$NO_3 + \text{thiophene} \rightarrow HONO_2 + HO_2\cdot + (\text{products whose reactions are ignored})$$

The initial calculations employed the mechanistic parameters used for the pyrrole system as the starting point, but better results were obtained if HCOCHO(X), the pseudospecies used to represent the benzene ring opening products, was included. This species, like HET-UNKN, is also photoreactive, but it is somewhat less so, and it also reacts to form glyoxal, which then reacts further. In initial calculations, the yield of HET-UNK2

was adjusted, but the optimized value obtained was sufficiently close to unity that a yield of 1 was assumed, consistent with the model used for pyrrole. The formation of R202. was not included in the above reaction, because best fits to the results of the thiophene-NO_x-air experiments were obtained if its formation was assumed to be unimportant. (The optimization software attempted to make its yield negative, indicating that the results of these runs would be even better fit if fewer NO to NO_2 conversions were involved than represented in the reactions shown above. The model optimization software also indicated that better fits would be obtained if the yield of HET-UNK2 was assumed to be greater than 1, but this was not incorporated in this model for consistency with the model used for pyrrole.) However, as shown in the comparisons of the model simulations to the experimental results given in Section IV.C, the scheme shown above was able to adequately simulate the results of the thiophene-NO_x-air experiments.

As with furan and pyrrole, the model predictions for the thiophene-NO_x-air runs were not very sensitive to the mechanism assumed for the NO_3 radical reaction. Therefore, the same simple mechanism as used for the other two heterocyclic organics was used in this model.

Obviously, these parameterized and, in many respects, arbitrary photooxidation mechanisms for furan, thiophene, and pyrrole have no claim to chemical accuracy beyond the fact that they can adequately simulate most of the major observations in the furan, thiophene, or pyrrole-NO_x-air experiments carried out in Phase I of this program. If any basic laboratory data concerning the reactions of this compound or the products formed and their reactions become available, this mechanism will be superseded. However, given the current state of knowledge concerning the reaction mechanisms of these species, this is probably about the best that can be done at present.

5. 1-Hexene and General Higher Alkene Reaction Mechanisms

Although reaction mechanisms for the C_2-C_4 monoalkenes have been included in previous models (e.g., References 11, 15, 18, 21), and are documented in detail in our recent EPA report (Reference 26), mechanisms

AD-A190 690 ATMOSPHERIC PHOTOCHEMICAL MODELING OF TURBINE ENGINE FUELS AND EXHAUSTS P..(U) CALIFORNIA UNIV RIVERSIDE STATEWIDE AIR POLLUTION RESEARCH CE.. 2/3

UNCLASSIFIED W O CARTER ET AL. MAY 88 F/G 4/1 NL

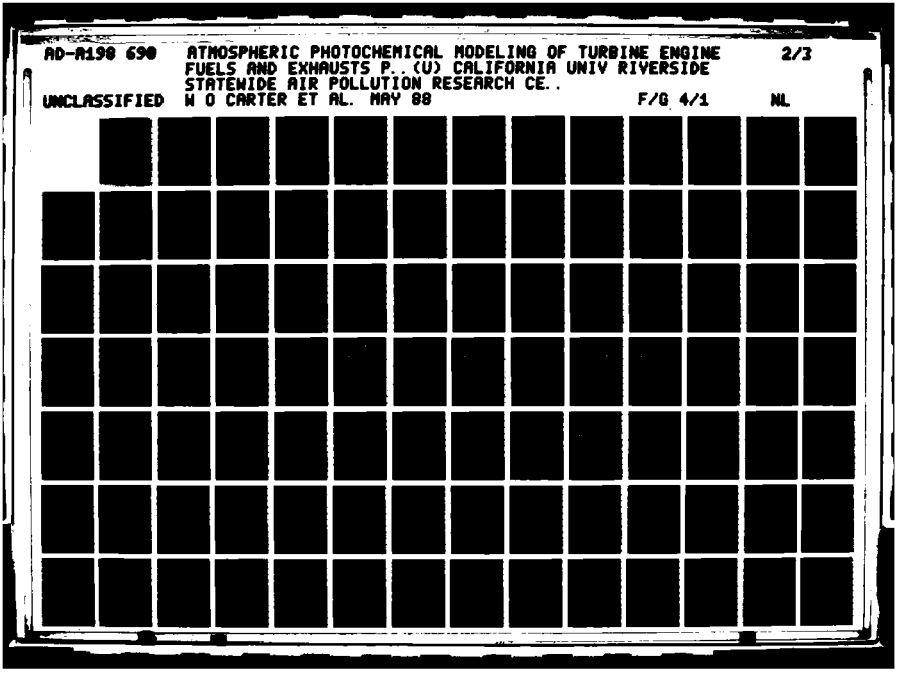

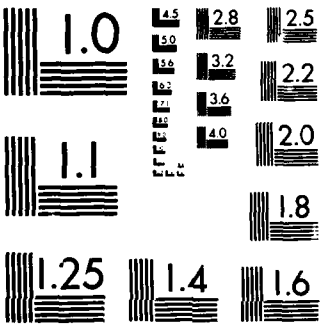
1.0
1.1
1.25
1.4
1.6
1.8
2.0
2.2
2.5
2.8
3.2
3.6
4.0
4.5
5.0
5.6
6.3
7.1
8.0
9.0

for reactions of the $>C_6$ monoalkenes, which are constituents of jet exhaust (Reference 41), have not been previously developed and tested. The model developed for the atmospheric reactions of 1-hexene, and tested using the results of the 1-hexene-NO_x-air chamber runs carried out under Phase II of this program, is discussed in this section. Extension of this model to include the reactions of higher monoalkenes is also discussed.

As with other alkenes, 1-hexene is expected to be consumed in the atmosphere by reaction with OH radicals, with ozone, and to a lesser extent by reaction with NO_3 radicals and $O(^3P)$ atoms, and all processes are represented in this model. The OH radical rate constants for 1-hexene have been measured at 295 and 303 K, and the average of these values, tabulated by Atkinson (Reference 25), is 3.5×10^{-11} cm^3 molecule^{-1} sec^{-1}, which is only around 10 percent higher than the 298 K value recommended by Atkinson (Reference 25) for 1-butene. Both propene and 1-butene have an effective "activation energy" of ~-1.0 kcal mole^{-1}, and if this is assumed for 1-hexene, the following expression for the OH + 1-hexene rate constant (in cm^3 molecule^{-1} sec^{-1}) is obtained:

$$k(OH + 1\text{-hexene}) = 6.52 \times 10^{-12} \exp(1.0 \text{ kcal mole}^{-1}/RT)$$

This was used in this model. Likewise, in the ozone + 1-hexene reaction, Atkinson and Carter (Reference 19) recommended a 298 K rate constant of 1.17×10^{-17} cm^3 molecule^{-1} sec^{-1}, which is also within 10 percent of the values for propene and 1-butene. If the preexponential factor recommended (Reference 19) for the ozone + 1-butene reaction is assumed for 1-hexene, this yields the following expression for the O_3 + 1-hexene rate constant (in cm^3 molecule^{-1} sec^{-1}),

$$k(O_3 + 1\text{-hexene}) = 3.56 \times 10^{-15} \exp(-3.369 \text{ kcal mole}^{-1}/RT)$$

which was used in this model. The rate constants for the NO_3 and $O(^3P)$ reactions with 1-hexene were assumed to be the same as those used in the model for 1-butene (Reference 26), and are given by the following expressions (in cm^3 molecule^{-1} sec^{-1})

$$k(NO_3 + \text{1-hexene}) = 5.0 \times 10^{-12} \exp(-3.698 \text{ kcal mole}^{-1}/RT)$$

$$k(O + \text{1-hexene}) = 1.25 \times 10^{-11} \exp(-0.648 \text{ kcal mole}^{-1}/RT)$$

Because 1-hexene is similar to 1-butene in both structure and reaction rates, a reasonable first estimate for the mechanisms for the 1-hexene reactions is to use those for 1-butene, which are documented in our EPA report (Reference 26), and shown in the mechanism listing in Appendix B. The 1-butene mechanism is based primarily on analogy with the corresponding reactions in the propene system, and if this mechanism works for 1-hexene, it would suggest that all of the 1-alkenes other than ethene react analogously. However, initial model simulations of the 1-hexene-NO_x-air runs carried out, based on this assumption showed that this model consistently overpredicted the reactivity observed in those runs. This overprediction in reactivity might be attributed to some process analogous to alkyl nitrate formation in the reaction of NO with the higher molecular weight peroxy radicals formed in the OH + $>C_5$ alkanes (discussed above) that might be occurring. In conjunction with the alkane photooxidation mechanisms, this process removes radicals and NO_x from the system, and, if important, will significantly reduce reactivity. This might account for the discrepancy observed in the initial model simulations of the 1-hexene runs, which were based on the assumption that such nitrate formation reactions are not important.

Therefore, the next series of calculations assumed that the OH-1-hexene-O_2 adducts formed in the OH + 1-hexene system react with NO to form alkyl nitrates, along with the "normal" process to form alkoxy radicals, and ultimately lead to products analogous to those in the 1-butene system. For example, if OH adds to the 1-position, the reactions assumed are:

$$\text{OH + 1-hexene} \rightarrow HOCH_2CH(\cdot)C_4H_9 \xrightarrow{O_2} HOCH_2CH(OO\cdot)C_4H_9$$

$$HOCH_2CH(OO.)C_4H_9 + NO \xrightarrow{M} HOCH_2CH(ONO_2)C_4H_9$$

$$\rightarrow HOCH_2CH(O.)C_4H_9 + NO_2$$

$$HOCH_2CH(O.)C_4H_9 \xrightarrow{O_2} HCHO + C_4H_9CHO + HO_2$$

and, analogously, if it adds to the 2-position. These are represented in the model as the following overall process:

$$OH + \text{1-hexene} \rightarrow p_N\ RO2\text{-}N. + (1-p_N)\ (HCHO + RCHO + RO2\text{-}R.)$$

where, as indicated above, RO2-N. is the pseudospecies representing processes which consume NO and form $RONO_2$, the lumped organic nitrate, RO_2-R. represents the psuedospecies representing processes which convert NO to NO_2 and generate HO_2, RCHO is the lumped higher aldehyde, and p_N is the nitrate yield parameter, which is adjusted to optimize the fits of the model simulations to the results of the 1-hexene-NO_x-air runs carried out in this program. No modifications were made to the ozone, NO_3, or $O(^3P)$ reaction mechanisms; they were still assumed to be the same as used for 1-butene.

Results of model simulations of these runs indicated that acceptable fits (i.e., of the same quality as observed for ethene, propene, and 1-butene) of model to experiment can be attained if $p_N = 0.225$ is assumed. Thus, no further adjustments of the model were carried out, and the 1-hexene mechanism incorporated in this model is based on this representation. Although it is probable that the ozone, NO_3, and $O(^3P)$ mechanisms in the 1-hexene may also have significant differences from those in the 1-butene (and propene) systems, the available data are not sufficient to indicate what the differences might be, and thus, for simplicity they are assumed to be the same. Thus, the only real difference between our model for 1-hexene and that for 1-butene is the assumed 22.5 percent nitrate formation in the OH radical reaction, though the results of the model simulations indicate that this difference is important, and that it is a

poor approximation to represent the higher 1-alkenes by propene and 1-butene.

The OH + 1-hexene mechanism, like the OH + 1-butene mechanism from which it is derived, is based on the assumption that the only significant mode of initial reaction is addition of OH radicals to the double bond, i.e., that H-atom abstraction, such as from the relatively weak allylic C-H bond, is not important. In the case of 1-butene, this is based on the results of experimental product studies, where products expected to result from abstraction from the allylic bond were not observed (Reference 61). The abstraction processes are calculated (Reference 25) to be relatively unimportant for 1-hexene, accounting for ~12 percent of the overall OH radical reactions. Since adequate fits of the model to the data can be attained without assuming that such processes are important, this possibility is ignored in this model.

The fact that, in the case of the alkanes, the alkyl nitrate yields increase monotonically with size of the molecule within a homologous series (Reference 24), suggests that this may also be the case for the 1-alkenes. Thus, in this model, we assume that alkyl nitrate formation in the OH + 1-alkene system also increases with the number of carbons in the alkene. The fact that the apparent 22.5 percent nitrate yield in the OH + 1-hexene system corresponds closely to the ~20 percent nitrate yield derived for the OH + n-hexane system (Reference 24) suggests that the yields derived for the alkanes can be used as a basis for estimating these for the structurally similar alkenes. The lumping technique for the higher alkanes, discussed in Section IV.B, is based on this assumption.

No data are available concerning whether alkyl nitrate formation may also be important in the reactions of OH radicals with the $>C_5$ internal alkenes, since no experiments with such compounds are available for model testing. We assume, in representing the reactions of such compounds in the models for complex mixtures, discussed below, that analogous processes occur in the OH + internal alkene systems as well. As with the 1-alkenes, we assume that the nitrate yields for $>C_5$ internal alkenes are the same as the yields estimated, using the techniques of Carter and Atkinson (Reference 24), for n-alkanes with the same number of carbon atoms. Until more

definitive data become available, the results for the 1-hexene system suggest that this is a reasonable assumption to make.

The kinetic parameters and estimated values of p_N used for all of the higher alkenes included in this model are summarized in Table 12. The sources of the rate constants used for these alkenes are given elsewhere (Reference 26). That table also includes parameters estimated for "lumped" species used to represent the reactions of the unspeciated $>C_5$ alkenes, which were used in the model simulations of the synthetic jet exhaust mixture and the "reference" JP-4 fuel, as discussed in Section IV.C. As indicated in the table, the kinetic parameters for the higher 1-alkenes are assumed to be the same as those for 1-hexene, while those for the higher internal alkenes are assumed to be the same as those for trans-2-butene. Table 12 also shows the structure parameters used in the lumping technique for the higher alkenes, as discussed in Section IV.C.

6. Representation of Acrolein in the Model

Acrolein is a constituent of jet exhaust (Reference 41) which has not been included in previous models, and thus, experiments employing that compound were carried out as part of Phase II of this program. Although because of its unsaturated nature, it is expected to have a different reaction mechanism than propionaldehyde (i.e., RCHO) [which is used in this model to represent the reactions of all $>C_3$ aldehydes], an initial series of simulations of the acrolein-NO_x-air runs (and the acrolein-propene-NO_x-air runs) was carried out with acrolein just being represented by RCHO. The results indicated that the RCHO model results in a moderate overprediction of the reactivity of acrolein, but this discrepancy was not judged to be sufficiently large to justify addition of an additional species in the model for the reactions of jet exhaust mixtures, especially since acrolein is not the dominant component of such mixtures (Reference 41). Thus, in this model, acrolein is just represented by RCHO, as is the other higher aldehydes. The acrolein runs carried out in this program have been useful in justifying the application of this assumption.

TABLE 12. KINETIC AND MECHANISTIC PARAMETER USED IN THE REPRESENTATIONS OF THE REACTIONS OF THE ALKENES[a].

Name	P_1	P_2	P_N	A(OH)	Ea(OH)	$A(O_3)$	$Ea(O_3)$	$A(NO_3)$	$Ea(NO_3)$	$A(O^3P)$	$Ea(O^3P)$
Alkenes Represented Explicitly											
Propene	1	2	0.000	4.85E-12	-1.001	1.32E-14	4.182	5.00E-12	3.843	1.18E-11	0.644
1-Butene	1	3	0.000	6.53E-12	-0.930	3.56E-15	3.403	5.00E-12	3.698	1.25E-11	0.648
T-2-Butene	2	2	0.000	1.01E-11	-1.091	9.08E-15	2.258	1.00E-11	1.937	2.26E-11	-0.020
C-2-Butene	2	2	0.000	1.09E-11	-0.970	3.52E-15	1.953	1.00E-11	2.002	1.21E-11	-0.235
Isobutene	1	4	0.000	9.51E-12	-1.000	3.55E-15	3.364	1.00E-11	2.139	1.76E-11	0.085
2-Me-2-Butene	2	4	0.000	1.92E-11	-0.894	6.17E-15	1.586	2.00E-11	0.461	2.50E-11	-0.380
2,3-Dime-2-butene	4	4	0.000	2.03E-11	-1.000	3.71E-15	0.690	2.00E-11	-0.608	5.58E-12	-1.570
1-Hexene	1	3	0.225	6.52E-12	-1.000	3.46E-15	3.369	5.00E-12	3.698	1.25E-11	0.648
Unspeciated 1-Alkenes[b]											
C5-OLE1	1	3	0.100	6.52E-12	-1.000	3.46E-15	3.369	5.00E-12	3.698	1.25E-11	0.648
C7-OLE1	1	3	0.270								
C8-OLE1	1	3	0.330								
C9-OLE1	1	3	0.360								
C10-OLE1	1	3	0.380								
C11-OLE1	1	3	0.395								
C12-OLE1	1	3	0.400								
C13-OLE1	1	3	0.410								
C14-OLE1	1	3	0.412								
C15-OLE1	1	3	0.415								
Unspeciated Internal Alkenes[c]											
C5-OLE2	2	3	0.100	1.01E-11	-1.091	9.08E-15	2.258	1.00E-11	1.937	2.26E-11	-0.020
C6-OLE2	3	3	0.225								
C7-OLE2	3	3	0.270								
C8-OLE2	3	3	0.330								
C9-OLE2	3	3	0.360								

TABLE 12. KINETIC AND MECHANISTIC PARAMETER USED IN THE REPRESENTATIONS OF THE REACTIONS OF THE ALKENES[a] (CONCLUDED).

Name	P_1	P_2	P_N	A(OH)	Ea(OH)	$A(O_3)$	$Ea(O_3)$	$A(NO_3)$	$Ea(NO_3)$	$A(O^3P)$	$Ea(O^3P)$
C10-OLE2	3	3	0.380								
C11-OLE2	3	3	0.395								
C12-OLE2	3	3	0.400								
C13-OLE2	3	3	0.410								
C14-OLE2	3	3	0.412								
C15-OLE2	3	3	0.415								

[a]Notation for parameters: P_1, P_2 = structure indices (see Section IV.B.1.b), P_N = nitrate yield assumed in the OH radical reaction, A(OH) = Arrhenius parameter for OH radical reaction (in cm^3 molecule^{-1} sec^{-1}), Ea(OH) = activation energy for OH radical reaction in kcal $mole^{-1}$, $A(O_3)$, $Ea(O_3)$, $A(NO_3)$, $Ea(NO_3)$, $A(O^3P)$ and $Ea(O^3P)$ are the corresponding values for ozone, NO_3 radical, and $O(^3P)$ atom reactions, respectively.

[b]Kinetic parameters of 1-hexene used. Nitrate yield estimated based on yields observed for corresponding n-alkanes.

[c]Kinetic parameters of trans-2-butene used. Nitrate yield estimated based on yields observed for corresponding n-alkanes.

B. LUMPING TECHNIQUES USED TO REPRESENT REACTIONS OF ROG SPECIES NOT EXPLICITLY IN THE MECHANISM

Although the chemical mechanism in this model includes explicit representation of a larger number of individual ROG species than included in any other previously published atmospheric transformation model, it is not practical to include all of the many individual reactive organic compounds emitted into real atmospheres. This is true even if the model was limited to turbine engine fuels or turbine engine exhaust mixtures. Therefore "lumping" techniques must be employed in which the relatively limited number of species explicitly included in the model can be used to represent the reactions of the much larger number of species emitted into the atmosphere.

Although several approaches have been employed in published models (Reference 48), probably the most common approach is that which McRae et al. (Reference 48) designate the "lumped molecule" approach, in which a given compound in the model is used to represent all other compounds which are both chemically similar, and react with similar rate constants. An example of this approach is using toluene to represent the reactions of all monoalkyl benzenes, and using propene to represent the reactions of all 1-alkenes. A modification and extension of this approach, which is used to some extent in some previously published models, is designated as the "lumped parameter" approach. In this approach, the kinetic, mechanistic, and product yield parameters of a lumped species in the model are derived, based on averaging the corresponding parameters of the individual compounds which that species is being used to represent. A third approach is the "lumped structure" (Reference 48) approach used in the "Carbon Bond" models (References 22, 23, 62), where fragments of the molecules are represented as reacting separately. This third approach is not employed in this model, and is not discussed further here.

The reactivity assessment model developed under this program allows the user to chose between three alternative lumping methods. Two of these are based entirely on the "lumped molecule" approach, but differ in the number of lumped species employed and thus, the level of accuracy possible in representing complex mixtures. The third method is based on a combination of the "lumped molecule" and the "lumped parameter"

approach. The combined approach is potentially the most accurate in representing the reactions of complex mixtures such as fuels and exhausts, and was the approach employed when testing the model against chamber data. The pure "lumped molecule" approach is more efficient to use in certain complex airshed model applications, and is probably suitable for representing "base case" ROG emissions (see Section V). The combined lumping approach will be discussed first, followed by a summary of the pure "lumped molecule" representation which can alternatively be employed in the airshed model.

1. Combined Lumping Approach

The lumping approach employed when testing this model against the results of the fuel and exhaust experiments, and recommended for use when assessing fuel and exhaust reactivities in reactivity assessment models (see Section V) is based on a combination of the "lumped molecule" and the "lumped parameter" approach. In this approach, some species are represented by the simple "lumped molecule" approach, while others are represented using the "lumped parameter" technique. Table 13 gives the list of the species used in the mechanisms employed in the simulations of the fuel and the synthetic exhaust runs (either represented explicitly in the model, or used to derive the kinetic, mechanistic, and product yield parameters for the "lumped parameter" representation), along with the groups of ROG species which they can be used to represent. The species, or groups of species, given in the second column of that table consist of all of the types of ROG species which this model is designed to simulate, and thus, includes groups which were not included in the synthetic fuel or synthetic exhaust runs against which the model was tested.

As indicated in the table, the "model species" in the first column of Table 13 fall into two categories: (1) those which are always represented in the the model either explicitly, or using the "lumped molecule" approach (e.g., RCHO, ETHENE, etc.), and (2) those which may be lumped with other species using the "lumped parameter" approach in simulations of complex mixtures. In the latter case, if the species is a $>C_3$ alkane or an aromatic, it is represented in the model by one of the seven lumped

TABLE 13. LIST OF ROG SPECIES INCLUDED IN THE MECHANISM, AND THEIR REPRESENTATION IN THE MODEL USING THE COMBINED "LUMPED MOLECULE"-"LUMPED PARAMETER" APPROACHES.

Model compound	L.P.[a] group	Compound or compounds represented
Compounds Represented as Unreactive		
INERT		C1-C2 alkanes, acetylene, and other compounds which are not more reactive than ethane
Compounds Represented Explicitly or by the "Lumped Molecule" Approach.		
ETHENE		Ethene
FORMALD		Formaldehyde
ACETALD		Acetaldehyde
PROPALD		Propionaldehyde and other $>C_3$ aldehydes, including acrolein, but not 1,2-dicarbonyls
ACETONE		Acetone
MEK		Methyl ethyl ketone and all >C4 ketones except α-dicarbonyls
GLYOXAL		Glyoxal
MEGLYOX		Methylglyoxal and other α-dicarbonyls
PHENOL		Phenol
CRESOL		Cresols and other alkylphenols
BFNZALD		Benzaldehyde and other aromatic aldehydes
NITROPHEN		Nitrophenols, nitrocresols, and other aromatic nitrocompounds
FURAN		Furan and compounds which can be represented by furan
THIOPHEN		Thiophene and related compounds
PYRROLE		Pyrrole and related compounds
Compounds or Groups of Compounds Represented by the "Lumped Parameter Approach"		
PROPANE	BZC3	Propane
N-C4	C4C5	n-Butane
ISO-C4	C4C5	Isobutane
N-C5	C4C5	n-Pentane
ISO-C5	C4C5	Isopentane
NEO-C5	BZC3	Neopentane
N-C6	AAR1	n-Hexane
2-ME-C5	AAR1	2-Methylpentane
3-ME-C5	AAR1	3-Methylpentane
23-DMB	AAR1	2,3-Dimethylbutane

TABLE 13. LIST OF ROG SPECIES INCLUDED IN THE MECHANISM, AND THEIR REPRESENTATION IN THE MODEL USING THE COMBINED "LUMPED MOLECULE"-"LUMPED PARAMETER" APPROACHES (CONTINUED).

Model compound	L.P.[a] group	Compound or compounds represented
BR-C6	AAR1	Unspeciated branched hexanes. Parameters of 2-Methyl pentane used.
CYC-C6	AAR2	Cyclohexane (also used for other C6 cycloalkanes)
N-C7	AAR1	n-Heptane
3-ME-C6	AAR1	3-Methylhexane
4-ME-C6	AAR1	4-Methylhexane
24-DM-C5	AAR1	2,4-dimethylpentane
23-DM-C5	AAR1	3,4-dimethylpentane
ME-CYCC6	AAR3	Methylcyclohexane
BR-C7	AAR1	Unspeciated branched heptanes. Parameters of 3-methyl hexane used.
CYC-C7	AAR3	Unspeciated C_7 cycloalkanes. Parameters of methyl cyclohexane used.
N-C8	AAR2	n-Octane
4-ME-C7	AAR2	4-Methylheptane
ISO-C8	AAR1	2,2,4-Trimethylpentane
ET-CYCC6	AAR3	Ethylcyclohexane
BR-C8	AAR2	Unspeciated branched octanes. Parameters of 4-methylheptane used.
CYC-C8	AAR3	Unspeciated C_8 cycloalkanes. Parameters of ethylcyclohexane used.
N-C9	AAR2	n-Nonane
4-ET-C7	AAR2	4-Ethylheptane
BR-C9	AAR2	Unspeciated branched nonanes. Parameters of 4-ethylheptane used.
CYC-C9	AAR3	Unspeciated C_9 cycloalkanes. Parameters of 1-ethyl-4-methylcyclohexane used.
N-C10	AAR3	n-Decane
4-PR-C7	AAR2	4-Propylheptane
BR-C10	AAR2	Unspeciated branched C_{10} alkanes. Parameters of 4-propylheptane used.
CYC-C10	AAR3	Unspeciated C_{10} cycloalkanes. Parameters of 1,3-diethylcyclohexane used.
N-C11	AAR3	n-Undecane
BR-C11	AAR3	Unspeciated branched C_{11} alkanes. Parameters of 3,5-diethylheptane used.
CYC-C11	AAR3	Unspeciated C_{11} cycloalkanes. Parameters of 1,3-diethyl-1-methylcyclohexane used.
N-C12	AAR3	n-Dodecane
BR-C12	AAR3	Unspeciated branched C_{12} alkanes. Parameters of 3,6-diethyloctane used.

TABLE 13. LIST OF ROG SPECIES INCLUDED IN THE MECHANISM, AND THEIR REPRESENTATION IN THE MODEL USING THE COMBINED "LUMPED MOLECULE"-"LUMPED PARAMETER" APPROACHES (CONTINUED).

Model compound	L.P.[a] group	Compound or compounds represented
CYC-C12	AAR3	Unspeciated C_{12} cycloalkanes. Parameters of ,3,5-triethylcyclohexane used.
N-C13	AAR4	n-Pentadecane
BR-C13	AAR3	Unspeciated branched C_{13} alkanes. Parameters of 3,7-diethyl nonane used
CYC-C13	AAR4	Unspeciated C_{13} cycloalkanes. Parameters of 1,3-diethyl-5-propylcyclohexane used.
N-C14	AAR4	n-Tetradecane
BR-C14	AAR3	Unspeciated branched C_{14} alkanes. Parameters of 3,8-diethyl decane used.
CYC-C14	AAR4	Unspeciated C_{14} cycloalkanes. Parameters of 1,3-dipropyl-5-ethylcyclohexane used.
N-C15	AAR4	n-Pentadecane
BR-C15	AAR3	Unspeciated branched $>C_{15}$ alkanes. Parameters of 3,9-diethylundecane used.
CYC-C15	AAR4	Unspeciated $>C_{15}$ cycloalkanes. Parameters of 1,3,5-tripropylcyclohexane used.
BENZENE	BZC3	Benzene
TOLUENE	AAR1	Toluene
M-XYLENE	AAR3	m-Xylene Benzenes
O-XYLENE	AAR2	o-Xylene (Uses mechanistic parameters of m-xlene.)
P-XYLENE	AAR2	p-Xylene (Uses mechanistic parameters of m-xlene.)
123-TMB	AAR5	1,2,3-Trimethylbenzene. (Uses mechanistic parameters of 1,3,5-trimethylbenzene.)
124-TMB	AAR5	1,2,4-Trimethylbenzene. (Uses mechanistic parameters of 1,3,5-trimethylbenzene.)
135-TMB	AAR5	1,3,5-Trimethylbenzene
ALK1BENZ	AAR1	Monoalkyl benzenes. Uses parameters of benzene.
ALK2BENZ	AAR3	Dialkylbenzenes. Uses parameters of m-xylene.
ALK3BENZ	AAR5	Tri- and poly-alkylbenzenes. Uses parameters of 135-TMB.
TETRALIN	AAR3	Tetralin. Also used for indans.
NAPHTHAL	AAR4	Naphthalene
ME-NAPH	AAR5	Monoalkylnaphthalenes. Rate constants of 2-methylnaphthalene. Mechanistic parameters averages of those for naphthalene and 2,3-DMN
DM-NAPH	AAR5	Di- and poly-alkylnaphthalenes. Uses parameters of 2,3-dimethylnaphthalene (23-DMN).

TABLE 13. LIST OF ROG SPECIES INCLUDED IN THE MECHANISM, AND THEIR REPRESENTATION IN THE MODEL USING THE COMBINED "LUMPED MOLECULE"-"LUMPED PARAMETER" APPROACHES (CONCLUDED).

Model compound	L.P.[a] group	Compound or compounds represented
PROPENE	OLE1	Propene
1-BUTENE	OLE1	1-Butene
C-2-BUTE	OLE2	cis-2-Butene
T-2-BUTE	OLE2	trans-2-Butene
ISOBUTEN	OLE1	Isobutene
1-PENTEN	OLE1	1-Pentene
2M-1-BUT	OLE1	2-Methyl-1-butene
2M-2-BUT	OLE2	2-Methyl-2-butene
1-HEXENE	OLE1	1-Hexene
23M2-BUT	OLE2	2,3-Dimethyl-2-butene
C6-OLE1	OLE1	Unspeciated C_6 1-alkenes. Parameters of 1-hexene used.
C6-OLE2	OLE2	Unspeciated C_6 2-alkenes. Parameters estimated.
C7-OLE1	OLE1	Unspeciated C_7 1-alkenes. Parameters estimated.
C7-OLE2	OLE2	Unspeciated C_7 2-alkenes. Parameters estimated.
C8-OLE1	OLE1	Unspeciated C_8 1-alkenes. Parameters estimated.
C8-OLE2	OLE2	Unspeciated C_8 2-alkenes. Parameters estimated.
C9-OLE1	OLE1	Unspeciated C_9 1-alkenes. Parameters estimated.
C9-OLE2	OLE2	Unspeciated C_9 2-alkenes. Parameters estimated.
C10-OLE1	OLE1	Unspeciated C_{10} 1-alkenes. Parameters estimated.
C10-OLE2	OLE2	Unspeciated C_{10} 2-alkenes. Parameters estimated.
C11-OLE1	OLE1	Unspeciated C_{11} 1-alkenes. Parameters estimated.
C11-OLE2	OLE2	Unspeciated C_{11} 2-alkenes. Parameters estimated.
C12-OLE1	OLE1	Unspeciated C_{12} 1-alkenes. Parameters estimated.
C12-OLE2	OLE2	Unspeciated C_{12} 2-alkenes. Parameters estimated.
C13-OLE1	OLE1	Unspeciated C_{13} 1-alkenes. Parameters estimated.
C13-OLE2	OLE2	Unspeciated C_{13} 2-alkenes. Parameters estimated.
C14-OLE1	OLE1	Unspeciated C_{14} 1-alkenes. Parameters estimated.
C14-OLE2	OLE2	Unspeciated C_{14} 2-alkenes. Parameters estimated.
C15-OLE1	OLE1	Unspeciated C_{15} 1-alkenes. Parameters estimated.
C15-OLE2	OLE2	Unspeciated C_{15} 2-alkenes. Parameters estimated.

[a]Pseudospecies used to represent this compound in the model using the "lumped parameter" method.

alkane/aromatic pseudo-species designated BZC3, C4C5, or AAR1 - AAR5, depending on how rapidly they react. If the species is an alkene other than ethene, it is represented by OLE1 or OLE2, depending on whether its double bond is internal or external. The lumping procedure for the alkanes, aromatics, and alkenes other than ethene is discussed in more detail below.

a. Lumped Parameter Approach for Alkanes and Aromatics

Despite the significant differences between the alkanes and the aromatics in the details of their reaction mechanisms and the types of products they produce, alkanes and aromatics which react at similar rates can be lumped together using the "lumped parameter" approach, because the reactions of either type of compound can be represented by the following overall process:

$$\begin{aligned} OH + aar \rightarrow\ & pn_{RR}\ RO2\text{-}R. + pn_{NR}\ RO2\text{-}N. + pn_{R2}\ R2O2. + pn_{RH}\ HO2. + \\ & pn_{NP}\ RO2\text{-}NP. + pn_{A1}\ HCHO + pn_{A2}\ CH3CHO + \\ & pn_{A3}\ (C_{3+}\ \text{aldehyde}) + pn_{K3}\ \text{acetone} + \\ & pn_{K4}\ (C_{4+}\ \text{ketone}) + pn_{CO}\ CO + pn_{C2}\ CO2 + \\ & pn_{BZ}\ \text{benzaldehyde} + pn_{PH}\ \text{phenol} + pn_{CR}\ \text{cresols} + \\ & pn_{GL}\ \text{glyoxal} + pn_{MG}\ (\text{methyl glyoxal}) + pn_{U1}\ HCOCHO(X) + \\ & pn_{U2}\ CCOCHO(X) \end{aligned}$$

where all the possible products which can be formed from either alkanes or aromatics, as represented in this model, are included. The symbol "aar" refers to the lumped species name, which in this model is either BZC3, C4C5, or AAR1 through AAR5, and the symbol "pn" refers to the prefix used for the lumped parameter for the various species, which in this model is either AZ, AL, or A1 through A5, respectively. The lumped group in which an alkane or aromatic is placed is determined by its OH radical rate constant. Table 14 indicates which of these groups the various types of alkanes and aromatics fall.

TABLE 14. OH RADICAL RATE CONSTANT RANGES USED TO DETERMINE LUMPED SPECIES GROUPS WHEN REPRESENTING THE REACTIONS OF ALKANES AND AROMATICS USING THE "LUMPED PARAMETER" APPROACH.

Group name	Parm name	k_{OH} Range (cm^3 $molecule^{-1}$ sec^{-1})
BC3	AB	$k_{OH} < 2.0 \times 10^{-12}$
C4C5	AL	$2.0 \times 10^{-12} \leq k_{OH} < 5.0 \times 10^{-12}$
AAR1	A1	$5.0 \times 10^{-12} \leq k_{OH} < 7.5 \times 10^{-12}$
AAR2	A2	$7.5 \times 10^{-12} \leq k_{OH} < 1.2 \times 10^{-11}$
AAR3	A3	$1.2 \times 10^{-11} \leq k_{OH} < 2.0 \times 10^{-11}$
AAR4	A4	$2.0 \times 10^{-11} \leq k_{OH} < 3.0 \times 10^{-11}$
AAR5	A5	$3.0 \times 10^{-11} \leq k_{OH}$

All the alkanes and aromatics within a given group, are represented in the model by the pseudospecies BZC3, C4C5, or AARn, whose OH radical rate constant, and kinetic and mechanistic parameters (pn_{RR}, pn_{BZ}, etc.) are determined by weighted averages of those for the group of alkanes and aromatics it is being used to represent. This approach involves no approximation if there is only one alkane or aromatic in a given group, since the kinetic and mechanistic parameters for the pseudospecies would be exactly the same as for the alkane or aromatic itself. Furthermore, there is no approximation if the set of alkane and aromatics grouped together react with exactly the same OH radical rate constant, provided that (in ambient air simulations) they also have the same emissions schedules, since their relative concentrations, and thus, the values of the weighted averages of their parameters, will not change with time.

However, this representation becomes more approximate as species with more disparate rate constants are lumped together, since the ratio of the concentrations of the more rapidly reacting species to those which react slower will decrease with time, and thus, the appropriate lumped parameters and rate constants would also change. The level of approximation in this representation is determined by the number of lumped groups which are employed, since with more groups, the ranges of rate constants of species which are lumped together can decrease. The choice of seven lumped groups in this model is based on what is considered to be

an appropriate compromise between accuracy in representation and minimizing the number of lumped species included in the model (since more species mean more computer time to carry out the calculations), and the specific ranges of rate constants used to define these groups is based on determining what is considered to be the best way to group the individual alkanes and aromatics in the model. Test calculations involving simulations of the chamber runs employing the synthetic fuel mixtures indicate that employing larger numbers of alkane/aromatic groups does not significantly change the results of the model simulations.

b. Lumped Parameter Approach for Alkenes

The alkenes cannot be lumped with the alkanes and aromatics because they also react to a nonnegligible extent with ozone and other species. Previous models which employed the "lumped molecule" approach, such as those of Atkinson and co-workers (References 15, 18, 21) and which have served as precursors to this model, generally lump the alkenes into three groups: (1) ethene; (2) the external alkenes other than ethene, generally represented by propene; and (3) the internal alkenes, generally represented by a 2-butene. This grouping is appropriate on kinetic grounds, since most non-ethene external alkenes react with similar rate constants, and most internal alkenes react so rapidly that differences in their rate constants are not significant. This model employs a similar lumping approach for the alkenes, except in this case, to more accurately represent the reactions of the higher alkenes present in jet exhaust mixtures, the "lumped parameter" approach is employed in determining the representation of the nonethene external alkenes and the internal alkenes. This permits an appropriate representation of the overall organic nitrate yield from the various mixtures of higher external and internal alkenes which are present.

Other than including provision for formation of alkyl nitrates in the OH radical reactions, the general parameterized lumping technique employed for the alkenes is similar to that discussed in detail in our recent EPA report (Reference 26). For both the lumped nonethene external alkenes and the lumped internal alkenes, the reactions employed in the model are as

follows:

$$OH + OLEn \rightarrow pn_N\ RO2\text{-}N. + (1-p_N)\ (RO2\text{-}R. + pn1\ HCHO + pn2\ acetaldehyde + pn3\ RCHO + pn4\ acetone + pn5\ MEK)$$

$$O3 + OLEn \rightarrow 0.5\ pn1\ (HCHO + (HCHO2)) + 0.5\ pn2\ (acetaldehyde + (CCHO2)) + 0.5\ pn3\ (RCHO + (C2CHO2)) + 0.5\ pn4\ (acetone + (C(C)CO2)) + 0.5\ pn5\ (MEK + (C(R)CO2))$$

$$NO3 + OLEn \rightarrow NO2 + R2O2. + pn1\ HCHO + pn2\ acetaldehyde + pn3\ RCHO + pn4\ acetone + pn5\ MEK)$$

$$O + OLEn \rightarrow 0.4\ HO2 + 0.5\ (MEK + RCHO)$$

where RO2-N., RO2-R., and R2O2. are defined as indicated above; (HCHO2), (CCHO2), (C2CHO2), (C(C)CO2), (C(R)CO2) are intermediates in the ozone + alkene reactions discussed in our recent EPA report (Reference 26); RCHO and MEK are the lumped C_{3+} aldehydes and the lumped C_{4+} ketones; pn_N is the nitrate yield mechanistic parameter discussed in Section IV.A.5; and pn1 through pn5 are parameters determined by the structure of the alkene. The parameter pn1 refers to the number of =CH2 groups; pn2 the number of =CHCH3 groups; pn3 the number of =CHR groups (where "R" is any alkyl group other than methyl); pn4 the number of =C(CH3)2 groups; and pn5 refers to the number of =CRCH3 or =CR2 groups in the alkene. These parameters are used to give the appropriate product distribution when alkenes are lumped using this approach. In the case of individual compounds, the parameters pn1 through pn5 are either 0, 1, or 2, and must sum up to 2, and although they may have noninteger values in lumped species representing a mixture of alkenes, they still must sum up to 2. In the case of the internal alkenes, pn1 is by definition always 0. The derivation of this representation is discussed in detail in our earlier EPA report (Reference 26) and in Section IV.A.5, above, and is not described further here.

This representation is only strictly valid for acyclic monoalkenes, but, in this model, it is still applied for all such alkenes. With dialkenes, reaction at only one of the double bonds is considered, i.e., 1,3-butadiene is treated as if it were 1-butene, and, if a dialkene has both internal and external double bonds, it is treated as internal alkene, since the internal double bond is generally more reactive. In addition, this model does not treat the cycloalkenes differently than acyclic alkenes, despite the different types of products formed; for example, cyclohexene would be represented in the model in the same way as 3-hexene. The level of inaccuracy in the model predictions for cyclic alkenes or dialkenes caused by this representation has not been determined.

c. Limitations of Applicability of "Lumped Parameter" Approach

When applied to airshed simulations (or simulations of "dynamic" chamber experiments) this "lumped parameter" approach, whether employed for alkenes or alkanes and aromatics, is only valid for lumping compounds with the same emissions schedules. It is not valid, for example, to lump together 1-butene and 1-hexene as a single species (namely OLE1) in an airshed simulation if most of the 1-butene is present initially, while most of the 1-hexene is emitted throughout the day, since the ratios of the concentrations of these two would change with time, despite their very similar atmospheric rates of reaction in the atmosphere. This means that the appropriate values of the mechanistic parameters of the lumped species (specifically the nitrate yield for OLE1 in this example) would also change with time. In such cases, either the strict "lumped molecule" approach, as discussed below, could be used, or alternatively separate "lumped parameter" species could be employed on groups of species which have different emissions schedules. For the alkene example, if the lumped molecule approach is used, several separate species could be used to represent the 1-alkenes depending on their nitrate yields, with the parameters in each lumped group being constant. Alternatively, the lumped parameter approach could be used to represent alkenes from different types of emissions sources, provided that different

groups are used to represent the alkenes from each of the different sources (e.g., alkenes from one source could be grouped in lumped groups OLE1A and OLE2A, while those from other sources, which are emitted at different times into the air parcel, could be lumped into separate groups OLE1B and OLD2B). Practical considerations are discussed further in the User's Manual for this model (Reference 28).

2. Pure "Lumped Molecule" Representations

As indicated above, although the "lumped parameter" approach is a potentially more accurate method to represent complex mixtures than the simple "lumped molecule" approach, it has limitations when being applied to complex airshed models where different groups of compounds are emitted at different times. Thus, we also include in this model, provision for using the pure "lumped molecule" approach, where lumped species in the model have fixed parameters which are independent of the species they are being used to represent. If a sufficient number of such species are included in the model, then the accuracy of this approach can approximate that of the "lumped parameter" approach, although in general a larger number of species are required. On the other hand, if the mixture being represented does not include in significant quantities all of the various types of organics which can be represented, then a "lumped molecule" representation involving a smaller number of species can be employed.

In the atmospheric reactivity airshed model developed under this program [discussed in Section V, and in the User's Manual for the model (Reference 28)], the user can choose from two alternative "lumped molecule" representations. The simpler representation, designated "LM1," is based on the lumping approach used in the version of this model which has previously been developed for use by the EPA for developing ozone control strategies (Reference 63), and is consistent with the level of detail used in other airshed models. This representation is, in most cases, suitable for representing "base case" ROG surrogate mixtures (i.e., ROG emissions into the airshed from all sources other than those whose reactivity is being assessed — see Section V), provided they do not contain significant levels of naphthalenes, C_{9+} alkanes, or C_{5+} alkenes. The more detailed

representation, designated "LM2," includes species representing the naphthalenes and the higher alkanes and alkenes, and is more appropriate for representing mixtures containing significant levels of such species in applications where use of the "lumped parameter" approach is not practical. Table 15 lists the lumped species employed in each approach, and the types of compounds they are used to represent.

TABLE 15. LIST OF MODEL SPECIES USED IN THE PURE "LUMPED MOLECULE" REPRESENTATIONS, AND THE TYPES OF COMPOUNDS THEY ARE USED TO REPRESENT.

Model species	Notes	Compound or compounds represented
INERT		C1 - C3 alkanes, acetylene, and other compounds which are less reactive than propane
FORMALD		Formaldehyde
ACETALD		Acetaldehyde
PROPALD		Propionaldehyde and other $>C_3$ aldehydes, including acrolein, but not 1,2-dicarbonyls
ACETONE		Acetone
MEK		Methyl ethyl ketone and all $>C_4$ ketones except α-dicarbonyls
GLYOXAL		Glyoxal
MEGLYOX		Methylglyoxal and other α-dicarbonyls
PHENOL		Phenol
CRESOL		Cresols and other alkylphenols
BENZALD		Benzaldehyde and other aromatic aldehydes
FURAN	(LM2 only)	Furan and related compounds
THIOPHEN	(LM2 only)	Thiophene and related compounds
PYRROLE	(LM2 only)	Pyrrole and related compounds
C4C5-ALK		C_4 - C_5 alkanes. Average of parameters for n-butane, isobutane, n-penatane, and isopentane. as "C4C5" in the lumping scheme used in the EPA model developed based on simulations of UNC auto exhaust irradiations (References 26, 63).
C6P-ALK		Unspeciated normal and branched C_6 - C_8 alkanes (LM2 model), or all $>C_6$ alkanes (LM1 model). Average of parameters for n-hexane, 2-methylpentane, 2,3-dimethylbutane, n-heptane, 2,3-dimethylpentane, n-octane, and iso-octane. Same as "C6PLUS" used in the lumping scheme used in the EPA model referenced above.

TABLE 15. LIST OF MODEL SPECIES USED IN THE PURE "LUMPED MOLECULE" REPRESENTATIONS, AND THE TYPES OF COMPOUNDS THEY ARE USED TO REPRESENT (CONCLUDED).

Model species	Notes	Compound or compounds represented
C9P-ALK	(LM2 only)	Unspeciated normal and branched $>C_9$ alkanes. Average of parameters for n-nonane, 4-ethylheptane, n-decane, 4-propylheptane, and n-undecane.
ETHENE		Ethene
1-ALKENE		$>C_3$ 1-Alkenes. Represented by propene.
2-ALKENE		2-Alkenes. Represented by trans-2-butene.
L-ALKENE	(LM2 only)	$>C_5$ Alkenes. Represented by 1-hexene.
BENZENE		Benzene
ALK1BENZ		Monoalkyl benzenes. Represented by toluene.
ALK2BENZ		Dialkyl benzenes (LM2 model) or di- and poly-alkyl benzenes and naphthalenes in the LM1 model. Represented by m-xylene.
ALK3BENZ	(LM2 only)	Tri- and poly-alkyl benzenes. Represented by 1,3,5-trimethylbenzene.
NAPHTHAL	(LM2 only)	Naphthalene
ME-NAPH	(LM2 only)	Monoalkyl naphthalenes. Represented by average of parameters of naphthalene and 2,3-dimethylnaphthalene.
DM-NAPH	(LM2 only)	Di- and poly-alkyl naphthalenes. Represented by 2,3-dimethylnaphthalene.

C. MODEL SIMULATIONS OF THE ENVIRONMENTAL CHAMBER EXPERIMENTS

The results of the computer model simulations of the environmental chamber experiments carried out in both phases of this program are summarized in this section. The number and types of runs carried out in this program which were used to test this model are listed in Table 16. With the exception of three runs carried out in the SAPRC Evacuable Chamber (EC) using mesitylene, and four runs carried out in the EC using the "reference" ("Fuel 1A") JP-4 fuel sample (Reference 29) as part of the previous Air Force Program (Reference 7), all of the Air Force chamber runs modeled were carried out in the SAPRC Indoor Teflon® Chamber (ITC).

TABLE 16. SUMMARY OF ENVIRONMENTAL CHAMBER RUNS CARRIED OUT UNDER USAF FUNDING WHICH WERE USED FOR MODEL TESTING.

Type of run		Number of runs ITC	EC
Indoor Teflon® Chamber Runs:			
Single Alkane	n-Butane	3	
	n-Octane	4	
	Methylcyclohexane	4	
Single Alkene	Ethene	2	
	Propene	[a]7	
	1-Butene	4	
	1-Hexene	4	
Single Aromatic	Benzene	[a]6	
	Toluene	2	[b]3
	m-Xylene	2	[b]2
	Mesitylene	5	3
	Tetralin	5	
	Naphthalene	5	
	2,3-Dimethylnaphthalene	4	
Other Single Component	Furan	4	
	Thiophene	4	
	Pyrrole	4	
	Acrolein	5	
Synthetic Fuel	"Standard" Fuel	4	
	"High Aromatics" Fuel	2	
	"Modified Aromatics" Fuel	2	
	Fuel + Heteroatom Impurity	3	
Synthetic Exhaust		4	
Whole Fuel[c]	"Reference" JP-4	2	4
TOTAL		91	12

[a]Includes three runs of this type carried out in the ITC under a previous program.

[b]These runs were carried out under previous programs, but are included here because they were employed, in part, to determine the optimum mechanistic parameters to use in the model.

[c]The runs carried out in this program employing the shale-derived JP-4, and the JP-4 fuel from the USAF storage tank were not modeled because no detailed composition data were available for these fuels.

In addition, several other aromatic-NO_x-air runs carried out in the EC for other programs are included in this set, since they were used, in part, to determine the optimum aromatic mechanistic parameters in the model (see Section IV.A.3). The methods used to represent chamber effects and other chamber-dependent parameters (such as light intensity, spectral distribution, etc.) in the simulations of the Air Force runs are summarized in Section IV.C.1, while the results of the simulations of the Air Force runs with known mixtures are summarized in Section IV.C.2. The methods used to represent the "reference" JP-4 fuel in the model, and the results of model simulations of experiments with that fuel, are discussed in Section IV.C.3.

This same photochemical model was also tested against the results of a wide variety of other experiments besides the Air Force runs discussed in Sections IV.C.2 and IV.C.3. This testing was conducted as a result of related and recently completed EPA-funded program for developing an updated photochemical mechanism for Air Quality Simulation Models (AQSMs), making this the most comprehensively tested single mechanism currently available. The results of testing this model against a full data base of almost 500 environmental chamber experiments, including runs modeled for this program along with those modeled for the EPA, are summarized in Section IV.C.4.

1. Representation of Chamber-Dependent Parameters

Model simulations of environmental chamber runs must include provisions for representing chamber dependent parameters such as the intensity and spectral characteristics of the light source, ozone wall loss and other heterogeneous processes, chamber-dependent radical sources, and dilution. A detailed discussion of the methods used to represent chamber-dependent parameters in simulations of experiments carried out in the SAPRC EC and ITC (the chambers used for the Air Force experiments modeled in this study), is discussed elsewhere (Reference 26). The methods used in this study are consistent with the methods discussed there, and therefore, are not discussed in detail here. The chamber-dependent input data used in the model simulations of the experiments in

this study are summarized in Table 17 for the ITC and in Table 18 for the EC, together with an indication of the sources of the individual parameter values employed. These chamber-dependent input parameters were tested by carrying out model simulations of appropriate chamber characterization runs, and the results indicated that the values used for these parameters were appropriate (Reference 26).

2. Simulations of Air Force Experiments with Single Organics and Known Mixtures

The performance of the model in simulating the results of the chamber experiments carried out at SAPRC as part of this and previous Air Force programs (with the exception of the runs employing whole fuels which are discussed in the following section) is summarized. As indicated in Table 16, these runs consist of NO_x-air irradiations of representative fuel and exhaust constituents, of several synthetic fuels, and of a synthetic exhaust mixture. Since, unlike the fuel runs discussed in the following section, the initial reactant concentrations are (in most cases) reasonably well characterized, these runs are the most useful for testing the accuracy of the photochemical model.

The performance of the model in simulating results of environmental chamber experiments can be measured in a number of ways, some more useful and generally applicable than others. In this assessment, the following measures of model performance, which we consider to be the most generally useful and applicable, are employed:

- Ability to Simulate Maximum Ozone Yields. This is one of the most important measures of performance for photochemical smog models, since ozone formation is generally regarded as one of the most serious problems in photochemical air pollution, and is a manifestation of air pollution this type of model is designed to simulate.

- Ability to Simulate Rates of Ozone Formation and NO Oxidation. An equally important measure of the performance of the model is its ability to accurately simulate the rates of photochemical transformations occurring. This can be measured in a number of ways, but the method we have found to be most useful (since it can be applied to essentially all such experiments regardless of what organic reactants are present and their

TABLE 17. SUMMARY OF CHAMBER-DEPENDENT INPUT PARAMETERS USED IN THE MODEL SIMULATIONS OF THE USAF AND RELATED ITC CHAMBER RUNS.

Parameter(s)	Value and derivation
NO_2 Photolysis Rate	Determined from NO_2 actinometry experiments. Generally ranged from 0.29 to 0.33 min^{-1} (Reference 27).
Other Photolysis Rates	Calculated from the NO_2 photolysis rate, the absorption coefficients and quantum yields of the photolysis reactions (Appendix B) and the ITC blacklight distribution given in the Phase I report (Reference 27).
Water Concentration	Based on measured temperature and humidity during the final pure air flush of the chamber. Typically 2.0×10^4 ppm.
Temperature	303 K. This is the typical average temperature in ITC chamber runs.
Dilution	No dilution, due to flexible nature of chamber walls.
Rates or Rate Constants of Chamber-Dependent Reactions:	
$O_3 \xrightarrow{\text{wall}}$ loss of O_3	1.3×10^{-4} min^{-1} (Reference 26)
$h\nu \xrightarrow{\text{wall}}$ OH	Rate given by $k_{RS} \times k_1$, where k_1 is the NO_2 photolysis rate, and k_{RS} is determined by averaging, for each reaction bag, the radical input rates measured using tracer-NO_x-air irradiations (References 26, 39, 40). If the average k_{RS} value from the tracer-NO_x runs was greater than 0.3 ppb, the value recommended in our previous evaluation (Reference 26), then a k_{RS} of 0.3 ppb was used. For the the experiments modeled here, the k_{RS} values used were 0.3 ppb for all runs except ITC-924 through ITC-174, for which k_{RS} = 0.25 ppb was used.

TABLE 17. SUMMARY OF CHAMBER-DEPENDENT INPUT PARAMETERS USED IN THE MODEL SIMULATIONS OF THE USAF AND RELATED ITC CHAMBER RUNS (CONCLUDED).

Parameter(s)	Value and derivation
wall + $h\nu$ → NO_2	Rate given by 0.15 ppb x k_1, the NO_2 photolysis rate (Reference 26).
$N_2O_5 \xrightarrow{wall,\ H_2O}$ Loss of N_2O_5	$2.5 \times 10^{-3} + 5.0 \times 10^{-8}$ $[H_2O]$ min^{-1} (Reference 26).
$NO_2 \xrightarrow{wall}$ 0.2 HONO + 0.8 loss of NO_2	1.4×10^{-4} min^{-1} (Reference 26).
$OH \xrightarrow{wall} HO_2$	250 min^{-1} (Reference 26). This "reaction" is used to simulate the effect of trace contamination by reactive organics.

overall reactivities) is the average rate of NO oxidation and ozone formation [i.e., the average of $d([O_3]-[NO])/dt$] during the time when ozone formation is still occurring. Ozone formation and NO oxidation rates are considered together because they reflect the same chemical processes; when NO is present in excess, they are manifested by NO consumption, and when most of the NO is consumed, they are manifested by ozone formation. (See Reference 26 for a more complete discussion of this.) For the purpose of this model evaluation, the statistic used is defined as one half the maximum change of the quantity $([O_3]-[NO])$, divided by the time required to achieve that change. Note that the time to the NO_2 maximum, which has been frequently used for this purpose, is not satisfactory because of analytical interferences in runs where PAN or other organic nitrates are formed (Reference 34).

- Reactant Half-Lives. Another measurement of the ability of the the model to simulate photochemical transformation rates is its ability to accurately predict reactant half-lives. For reactants such as alkanes and

TABLE 18. SUMMARY OF CHAMBER-DEPENDENT INPUT PARAMETERS USED IN THE MODEL SIMULATIONS OF THE USAF AND RELATED EC CHAMBER RUNS.

Parameter(s)	Value and derivation
NO_2 Photolysis Rate	Determined from NO_2 actinometry experiments. Generally ranged from 0.3 to 0.4 min^{-1}.
Other Photolysis Rates	Calculated from the NO_2 photolysis rate, the absorption coefficients and quantum yields of the photolysis reactions (Appendix B) and the solar simulator spectral distribution measured during the experiment (References 26, 64).
Water Concentration	Based on measured temperature and humidity during the final pure air fill of the chamber. Typically 2.0×10^4 ppm.
Temperature	303 K. This is a typical average temperature in EC chamber runs.
Dilution	3.0×10^{-4} min^{-1} (References 26, 64).
Initial Nitrous Acid (HONO)	Initial HONO = 7% of the initial NO_2, based on measured or estimated initial HONO concentrations in EC tracer-NO_x air irradiations (References 26, 39, 40).
Rates or Rate Constants of Chamber-Dependent Reactions:	
$O_3 \xrightarrow{\text{wall}}$ loss of O_3	1.1×10^{-3} min^{-1} (Reference 26)
$h\nu \xrightarrow{\text{wall}}$ OH	Rate given by 0.39 ppb x k_1, where k_1 is the NO_2 photolysis rate (References 26, 40). Derived based on results of tracer-NO_x-air runs carried out previously (References 39, 40).
$NO_2 + h\nu \xrightarrow{\text{wall}}$ 0.5 HONO + 0.5 loss of NO_2	Included to represent the NO_2-dependent component of the chamber radical source in this chamber (References 39, 40).

TABLE 18. SUMMARY OF CHAMBER-DEPENDENT INPUT PARAMETERS USED IN THE MODEL SIMULATIONS OF THE USAF AND RELATED EC CHAMBER RUNS (CONCLUDED).

Parameter(s)	Value and derivation
	Rate constant given by 2.16×10^{-3} ppm^{-1} x k_1, where k_1 is the NO_2 photolysis rate (Reference 26).
wall + $h\nu$ $\rightarrow$ NO_2	Rate given by 0.5 ppb x k_1, the NO_2 photolysis rate (Reference 26).
$N_2O_5 \xrightarrow{wall,\ H_2O}$ Loss of N_2O_5	$4.65 \times 10^{-3} + 7.21 \times 10^{-7}$ $[H_2O]$ min^{-1} (Reference 26)
$NO_2 \xrightarrow{wall}$ 0.5 HONO + 0.5 loss of NO_2	2.8×10^{-4} min^{-1} (References 26, 65).

aromatics, which are consumed in these irradiations primarily by reaction with hydroxyl radicals, this is an indication of the ability of the model to accurately predict OH radical levels. However, this is not as universally applicable a measure of model performance as is the ability to predict NO oxidation and ozone formation rates, since in some experiments the organic reactants are consumed too slowly for their rate of consumption to be a meaningful measure of reactivity. This is the case for all the alkane runs in this study. In other cases, such as the acrolein runs, the precision of the analytical data for the reactants is not sufficient for them not to be useful for this purpose. This measure of model performance is used only for runs containing alkenes, the more reactive aromatics, and the simple aldehydes.

• Yields of Organic Products. The ability of the model to simulate formation of other secondary pollutants besides ozone is also important, and in some cases can provide more precise information concerning the detailed accuracy of the model. A number of products are measured in these experiments, but those which are the most widely formed, and most routinely monitored, are PAN and formaldehyde. Thus, the performance of

this model in terms of predictions of yields of these products is also summarized. However, in assessing these results, it should be recognized that these products are more difficult to monitor precisely than ozone, NO, or the more reactive simple hydrocarbon reactants, thus a wider distribution in the discrepancies between the model predictions and the experimental results for these compounds is expected and observed.

• Visual Comparison of Experimental and Computed Concentration-Time Profiles. Comparison of concentration-time profiles is useful in obtaining a qualitative sense of how well the model can simulate the experimental results, and is probably the only way one can obtain a sense of the level of detail with which the model can simulate the experiment. When models are tested against results of a limited number of experiments, this is obviously the preferred way to assess its performance. However, it is less useful when a large number of experiments are being used to test the model, such as is the case in this study. If we were to present concentration-time plots for all experiments we used to test this model, the number of such plots would be so great that the reader could not assimilate the information presented, and the volume of this report would be increased significantly. In this report we present such plots for only a very limited number of runs, chosen based on how typical they appeared to be in terms of model performance. The specific runs chosen were neither the best nor the worst in terms of how well the model performed in simulating the types of runs they are chosen to represent.

A summary of the initial reactant concentrations and the performance of the model in simulating ozone yields and ozone formation and NO oxidation rates in the Air Force experiments is given in Table 19, and the performance of the model in simulating the reactant half lives and the PAN and formaldehyde yields are summarized in Table 20. Experimental and computed concentration-time plots for selected species are presented below, in conjunction with the discussion concerning the results of the simulations of the various types of experiments.

TABLE 19. SUMMARY OF THE INITIAL REACTANT CONCENTRATIONS, AND THE PERFORMANCE OF THE MODEL IN SIMULATING THE OZONE YIELDS AND OZONE FORMATION AND NO OXIDATION RATES IN THE AIR FORCE RUNS USED FOR MODEL TESTING.

Experiment	Initial concentrations			Maximum concentration OZONE				Average initial d([O_3]-[NO])/dt			
	NO_x (ppm)	HC (ppmC)	HC/NO_x	Expt (ppm)	Calc (ppm)	Calc -expt (ppm)	Calc -expt /expt[a]	Expt --	Calc (ppb/min)	Calc -expt --	Calc -expt /expt
n-Butane											
ITC770	0.52	37.9	72.8	0.042	0.054	0.012		1.56	2.03	0.47	0.30
ITC939	0.51	14.8	28.9	0.017	0.031	0.014		0.36	0.74	0.38	1.05
ITC948	0.26	10.0	38.2	0.054	0.179	0.125	2.31	0.53	1.18	0.64	1.20
Group Average	0.43	20.9	46.6	0.038	0.088	0.050	2.31	0.82	1.32	0.50	0.85
Avg. Abs. Value[b]						0.050	2.31			0.50	0.85
n-Octane											
ITC761	0.52	75.2	145.9	0.030	0.018	-0.012		1.08	0.89	-0.19	-0.18
ITC762	0.27	74.7	280.4	0.105	0.088	-0.017	-0.16	0.83	1.09	0.26	0.32
ITC763	0.28	7.7	27.7	0.041	0.042	0.002		0.68	1.11	0.43	0.63
ITC797	0.52	7.3	14.0	0.004	0.008	0.004		0.64	0.76	0.12	0.19
Group Average	0.39	41.2	117.0	0.045	0.039	-0.006	-0.16	0.81	0.96	0.15	0.24
Avg. Abs. Value						0.009	0.16			0.25	0.33
Methylcyclohexane											
ITC765	0.53	0.0	0.1	0.022	0.016	-0.006		0.86	0.96	0.10	0.12
ITC766	0.26	0.0	0.1	0.121	0.362	0.240	1.98	0.87	2.00	1.13	1.30
ITC767	0.55	0.1	0.1	0.041	0.097	0.055		1.09	1.52	0.43	0.39
ITC800	0.54	0.0	0.1	0.015	0.014	-0.001		0.86	1.04	0.19	0.22
Group Average	0.47	0.0	0.1	0.050	0.122	0.072	1.98	0.92	1.38	0.46	0.51
Avg. Abs. Value						0.076	1.98			0.46	0.51

TABLE 19. SUMMARY OF THE INITIAL REACTANT CONCENTRATIONS, AND THE PERFORMANCE OF THE MODEL IN SIMULATING THE OZONE YIELDS AND OZONE FORMATION AND NO OXIDATION RATES IN THE AIR FORCE RUNS USED FOR MODEL TESTING (CONTINUED).

Experiment	Initial concentrations			Maximum concentration OZONE				Average initial $d([O_3]-[NO])/dt$			
	NO_x (ppm)	HC (ppmC)	HC/NO_x	Expt (ppm)	Calc (ppm)	Calc -expt (ppm)	Calc -expt /expt[a]	Expt --	Calc (ppb/min)	Calc -expt --	Calc -expt /expt
Ethene											
ITC926	0.51	7.9	15.6	0.982	1.072	0.090	0.09	6.96	9.16	2.20	0.32
ITC936	0.50	3.9	7.8	0.940	1.039	0.099	0.11	2.72	3.62	0.90	0.33
Group Average	0.50	5.9	11.7	0.961	1.056	0.095	0.10	4.84	6.39	1.55	0.32
Avg. Abs. Value						0.095	0.10			1.55	0.32
Propene											
ITC693	0.49	3.5	7.2	0.779	0.709	-0.070	-0.09	5.07	5.72	0.65	0.13
ITC810	0.52	2.8	5.4	0.782	0.695	-0.088	-0.11	4.25	4.59	0.33	0.08
ITC860	0.52	3.0	5.8	0.585	0.662	0.078	0.13	3.57	5.08	1.51	0.42
ITC925	0.54	2.8	5.2	0.779	0.715	-0.064	-0.08	3.72	4.13	0.41	0.11
ITC938	0.52	2.8	5.3	0.729	0.717	-0.012	-0.02	3.61	4.27	0.66	0.18
ITC947	0.53	1.9	3.6	0.710	0.722	0.012	0.02	3.34	4.22	0.88	0.26
ITC960	0.50	2.8	5.5	0.721	0.688	-0.033	-0.05	4.23	4.38	0.15	0.04
Group Average	0.52	2.8	5.4	0.726	0.701	-0.025	-0.03	3.97	4.63	0.66	0.17
Avg. Abs. Value						0.051	0.07			0.66	0.17
1-Butene											
ITC927	0.31	3.8	12.3	0.646	0.713	0.067	0.10	3.24	4.66	1.42	0.44
ITC928	0.67	3.8	5.7	0.022	0.088	0.066		1.36	2.05	0.70	0.51
ITC930	0.32	7.2	22.2	0.717	0.793	0.076	0.11	7.91	11.44	3.53	0.45
ITC935	0.66	7.6	11.6	0.872	0.924	0.052	0.06	5.39	8.45	3.07	0.57
Group Average	0.49	5.6	12.9	0.564	0.629	0.065	0.09	4.47	6.65	2.18	0.49
Avg. Abs. Value						0.065	0.09			2.18	0.49

TABLE 19. SUMMARY OF THE INITIAL REACTANT CONCENTRATIONS, AND THE PERFORMANCE OF THE MODEL IN SIMULATING THE OZONE YIELDS AND OZONE FORMATION AND NO OXIDATION RATES IN THE AIR FORCE RUNS USED FOR MODEL TESTING (CONTINUED).

Experiment	Initial concentrations			Maximum concentration OZONE				Average initial $d([O_3]-[NO])/dt$			
	NO_x (ppm)	HC (ppmC)	HC/NO_x	Expt (ppm)	Calc (ppm)	Calc -expt (ppm)	Calc -expt /expt[a]	Expt --	Calc (ppb/min)	Calc -expt --	Calc -expt /expt
1-Hexene											
ITC929	0.51	5.1	10.0	0.298	0.280	-0.018	-0.06	1.27	1.38	0.11	0.08
ITC931	0.49	10.3	21.1	0.606	0.626	0.020	0.03	2.82	2.91	0.08	0.03
ITC934	1.00	9.7	9.7	0.428	0.432	0.004	0.01	1.84	2.20	0.36	0.20
ITC937	0.99	0.1	0.1	0.007	0.015	0.008		0.33	0.42	0.09	0.27
Group Average	0.75	6.3	10.2	0.335	0.338	0.004	-0.01	1.57	1.73	0.16	0.14
Avg. Abs. Value						0.013	0.04			0.16	0.14
Benzene											
ITC560	0.12	332.3	2874.4	0.323	0.350	0.027	0.08	7.01	9.32	2.31	0.33
ITC561	0.11	79.1	694.2	0.273	0.294	0.022	0.08	4.75	4.24	-0.51	-0.11
ITC562	0.56	83.8	149.7	0.412	0.402	-0.010	-0.02	2.85	3.07	0.22	0.08
ITC698	0.50	83.5	167.4	0.374	0.376	0.002	0.00	2.87	3.09	0.22	0.08
ITC710	0.55	83.6	151.0	0.367	0.390	0.023	0.06	2.70	2.94	0.24	0.09
ITC831	1.01	12.2	12.1	0.021	0.004	-0.016		0.17	0.28	0.11	0.65
Group Average	0.47	112.4	674.8	0.295	0.303	0.008	0.04	3.39	3.82	0.43	0.19
Avg. Abs. Value						0.017	0.05			0.60	0.22
Toluene											
ITC699	0.51	10.5	20.8	0.485	0.511	0.026	0.05	4.72	4.79	0.07	0.02
ITC828	1.02	3.0	3.0	0.021	0.006	-0.015		0.49	1.08	0.59	1.19

TABLE 19. SUMMARY OF THE INITIAL REACTANT CONCENTRATIONS, AND THE PERFORMANCE OF THE MODEL IN SIMULATING THE OZONE YIELDS AND OZONE FORMATION AND NO OXIDATION RATES IN THE AIR FORCE RUNS USED FOR MODEL TESTING (CONTINUED).

Experiment	Initial concentrations			Maximum concentration OZONE				Average initial $d([O_3]-[NO])/dt$			
	NO_x (ppm)	HC (ppmC)	HC/NO_x	Expt (ppm)	Calc (ppm)	Calc -expt (ppm)	Calc -expt /expt[a]	Expt --	Calc (ppb/min)	Calc -expt --	Calc -expt /expt
EC266	0.49	8.4	17.0	0.405	0.429	0.023	0.06	4.62	5.36	0.74	0.16
EC270	0.46	4.2	9.0	0.369	0.394	0.025	0.07	3.72	4.01	0.29	0.08
EC271	0.21	8.0	37.4	0.296	0.338	0.042	0.14	6.56	5.92	-0.64	-0.10
Group Average	0.54	6.8	17.5	0.315	0.335	0.020	0.08	4.03	4.23	0.21	0.27
Avg. Abs. Value						0.026	0.08			0.46	0.31
m-Xylene											
ITC702	0.52	4.0	7.8	0.627	0.481	-0.146	-0.23	7.79	8.51	0.73	0.09
ITC827	1.07	1.2	1.1	0.021	0.011	-0.010		1.12	1.89	0.77	0.69
EC344	0.67	4.0	5.9	0.589	0.524	-0.065	-0.11	10.72	9.95	-0.77	-0.07
EC345	0.28	3.7	13.3	0.396	0.381	-0.014	-0.04	11.35	10.90	-0.45	-0.04
Group Average	0.63	3.2	7.0	0.408	0.349	-0.059	-0.13	7.75	7.82	0.07	0.17
Avg. Abs. Value						0.059	0.13			0.68	0.22
1,3,5-Trimethylbenzene (mesitylene)											
ITC703	0.50	5.3	10.6	0.707	0.492	-0.215	-0.30	14.59	17.81	3.22	0.22
ITC706	0.49	2.7	5.4	0.641	0.483	-0.157	-0.25	7.20	8.54	1.33	0.18
ITC709	0.99	4.7	4.7	0.779	0.629	-0.150	-0.19	11.74	13.67	1.93	0.16
ITC742	0.48	4.6	9.7	0.773	0.493	-0.280	-0.36	13.14	14.64	1.50	0.11
ITC826	0.90	0.8	0.9	0.022	0.013	-0.009		1.68	2.33	0.66	0.39
EC900	0.53	5.4	10.2	0.381	0.443	0.062	0.16	(missing data)			
EC901	0.51	2.7	5.2	0.384	0.412	0.028	0.07	8.88	8.75	-0.13	-0.02
EC903	1.00	4.7	4.7	0.502	0.564	0.062	0.12	14.96	14.33	-0.63	-0.04
Group Average	0.68	3.9	6.4	0.524	0.441	-0.082	-0.11	9.50	134.88	1.13	0.15
Avg. Abs. Value						0.121	0.21			1.34	0.16

TABLE 19. SUMMARY OF THE INITIAL REACTANT CONCENTRATIONS, AND THE PERFORMANCE OF THE MODEL IN SIMULATING THE OZONE YIELDS AND OZONE FORMATION AND NO OXIDATION RATES IN THE AIR FORCE RUNS USED FOR MODEL TESTING (CONTINUED).

Experiment	Initial concentrations			Maximum concentration OZONE				Average initial $d([O_3]-[NO])/dt$			
	NO_x (ppm)	HC (ppmC)	HC/NO_x	Expt (ppm)	Calc (ppm)	Calc -expt (ppm)	Calc -expt /expt[a]	Expt --	Calc (ppb/min)	Calc -expt --	Calc -expt /expt
Tetralin											
ITC739	0.52	2.4	4.6	0.002	0.009	0.007		0.63	0.42	-0.20	-0.32
ITC747	0.50	93.2	187.4	0.508	0.555	0.046	0.09	2.73	2.24	-0.49	-0.18
ITC748	0.22	84.0	385.1	0.370	0.353	-0.017	-0.05	2.60	1.80	-0.80	-0.31
ITC750	0.53	44.5	84.6	0.482	0.332	-0.151	-0.31	2.10	1.94	-0.16	-0.08
ITC832	1.00	39.4	39.5	0.073	0.045	-0.028	-0.39	1.38	1.35	-0.03	-0.02
Group Average	0.55	52.7	140.2	0.287	0.259	-0.028	-0.16	1.89	1.55	-0.34	-0.18
Avg. Abs. Value						0.050	0.21			0.34	0.18
Naphthalene											
ITC751	0.52	7.5	14.3	0.113	0.096	-0.017	-0.15	1.08	1.16	0.08	0.07
ITC755	0.24	14.1	58.3	0.259	0.302	0.043	0.17	1.57	1.64	0.07	0.04
ITC756	0.26	27.4	106.8	0.282	0.327	0.044	0.16	2.20	1.93	-0.27	-0.12
ITC798	0.53	19.4	36.8	0.204	0.283	0.080	0.39	1.66	1.81	0.15	0.09
ITC802	0.53	8.4	15.9	0.124	0.079	-0.045	-0.36	1.42	1.26	-0.17	-0.12
Group Average	0.42	15.4	46.4	0.196	0.218	0.021	0.04	1.59	1.56	-0.03	-0.01
Avg. Abs. Value						0.046	0.25			0.15	0.09
2,3-Dimethylnaphthalene											
ITC775	0.29	1.7	5.8	0.274	0.190	-0.084	-0.31	1.73	1.51	-0.22	-0.13
ITC771	0.26	4.8	18.0	0.293	0.345	0.052	0.18	2.67	2.91	0.25	0.09
ITC806	0.33	5.9	17.7	0.360	0.392	0.032	0.09	2.69	3.15	0.46	0.17
ITC774	0.56	4.0	7.1	0.341	0.342	0.002	0.00	2.84	2.91	0.08	0.03
Group Average	0.36	4.1	12.2	0.317	0.317	0.000	-0.01	2.48	2.62	0.14	0.04
Avg. Abs. Value						0.042	0.14			0.25	0.10

TABLE 19. SUMMARY OF THE INITIAL REACTANT CONCENTRATIONS, AND THE PERFORMANCE OF THE MODEL IN SIMULATING THE OZONE YIELDS AND OZONE FORMATION AND NO OXIDATION RATES IN THE AIR FORCE RUNS USED FOR MODEL TESTING (CONTINUED).

Experiment	Initial concentrations			Maximum concentration OZONE				Average initial $d([O_3]-[NO])/dt$			
	NO_x (ppm)	HC (ppmC)	HC/NO_x	Expt (ppm)	Calc (ppm)	Calc -expt (ppm)	Calc -expt /expt[a]	Expt --	Calc (ppb/min)	Calc -expt --	Calc -expt /expt
Furan											
ITC711	0.52	1.6	3.0	0.471	0.442	-0.029	-0.06	9.01	7.80	-1.21	-0.13
ITC713	0.99	1.5	1.6	0.045	0.046	0.001		5.14	4.69	-0.45	-0.09
ITC715	0.50	0.8	1.7	0.059	0.078	0.019	0.33	2.93	3.32	0.39	0.13
ITC743	0.49	1.5	3.0	0.598	0.395	-0.203	-0.34	9.03	8.61	-0.43	-0.05
Group Average	0.63	1.4	2.3	0.293	0.240	-0.053	-0.02	6.53	6.10	-0.42	-0.03
Avg. Abs. Value						0.063	0.24			0.62	0.10
Thiophene											
ITC729	0.49	1.7	3.5	0.070	0.068	-0.002	-0.02	1.43	1.29	-0.13	-0.09
ITC730	0.47	7.1	15.1	0.405	0.481	0.076	0.19	5.24	5.72	0.48	0.09
ITC733	0.25	1.7	6.9	0.248	0.309	0.061	0.24	1.71	2.02	0.31	0.18
ITC744	0.52	6.5	12.5	0.479	0.471	-0.008	-0.02	6.51	5.76	-0.75	-0.11
Group Average	0.43	4.3	9.5	0.301	0.332	0.032	0.10	3.72	3.70	-0.02	0.02
Avg. Abs. Value						0.037	0.12			0.42	0.12
Pyrrole											
ITC735	0.49	2.1	4.3	0.319	0.284	-0.036	-0.11	19.33	20.90	1.56	0.08
ITC778	0.52	3.9	7.5	0.522	0.631	0.109	0.21	53.07	42.55	-10.52	-0.20
ITC779	0.53	1.1	2.0	0.069	0.050	-0.019	-0.27	8.79	7.78	-1.01	-0.11
ITC780	0.54	0.4	0.8	0.042	0.026	-0.015		0.92	0.76	-0.16	-0.18
Group Average	0.52	1.9	3.7	0.238	0.248	0.010	-0.06	20.53	17.99	-2.53	-0.10
Avg. Abs. Value						0.045	0.20			3.31	0.14

TABLE 19. SUMMARY OF THE INITIAL REACTANT CONCENTRATIONS, AND THE PERFORMANCE OF THE MODEL IN SIMULATING THE OZONE YIELDS AND OZONE FORMATION AND NO OXIDATION RATES IN THE AIR FORCE RUNS USED FOR MODEL TESTING (CONTINUED).

Experiment	Initial concentrations			Maximum concentration OZONE				Average initial $d([O_3]-[NO])/dt$			
	NO_x (ppm)	HC (ppmC)	HC/NO_x	Expt (ppm)	Calc (ppm)	Calc -expt (ppm)	Calc -expt /expt[a]	Expt --	Calc (ppb/min)	Calc -expt --	Calc -expt /expt
Acrolein											
ITC941	0.52	2.0	4.0	0.094	0.173	0.079	0.85	1.10	2.23	1.13	1.03
ITC943	0.51	8.1	15.8	0.722	0.597	-0.125	-0.17	2.88	4.53	1.65	0.57
ITC944	0.27	4.9	18.6	0.487	0.444	-0.043	-0.09	1.84	2.98	1.14	0.62
ITC945	0.52	1.9	3.6	0.046	0.088	0.042		1.33	2.40	1.06	0.80
ITC946	0.53	4.9	9.3	0.776	0.598	-0.178	-0.23	5.21	4.46	-0.75	-0.14
Group Average	0.47	4.4	10.3	0.425	0.380	-0.045	0.09	2.47	3.32	0.85	0.57
Avg. Abs. Value						0.093	0.33			1.15	0.63
Standard Synthetic Fuel											
ITC781	0.51	43.0	83.5	0.751	0.811	0.060	0.08	2.77	3.76	0.99	0.36
ITC784	0.50	88.0	177.6	0.746	0.821	0.075	0.10	3.93	4.72	0.79	0.20
ITC785	0.26	45.0	170.7	0.598	0.580	-0.018	-0.03	2.74	3.45	0.71	0.26
ITC805	0.52	98.0	189.5	0.791	0.848	0.057	0.07	3.27	4.55	1.28	0.39
Group Average	0.45	68.5	155.4	0.721	0.765	0.044	0.06	3.18	4.12	0.94	0.30
Avg. Abs. Value						0.053	0.07			0.94	0.30
High Aromatics Synthetic Fuel											
ITC795	0.50	45.0	89.8	0.761	0.747	-0.014	-0.02	3.05	5.26	2.21	0.72
ITC796	0.54	97.0	178.9	0.597	0.789	0.192	0.32	4.43	6.28	1.84	0.42
Group Average	0.52	71.0	134.3	0.679	0.768	0.089	0.15	3.74	5.77	2.03	0.57
Avg. Abs. Value						0.103	0.17			2.03	0.57

TABLE 19. SUMMARY OF THE INITIAL REACTANT CONCENTRATIONS, AND THE PERFORMANCE OF THE MODEL IN SIMULATING THE OZONE YIELDS AND OZONE FORMATION AND NO OXIDATION RATES IN THE AIR FORCE RUNS USED FOR MODEL TESTING (CONTINUED).

Experiment	Initial concentrations			Maximum concentration OZONE				Average initial $d([O_3]-[NO])/dt$			
	NO_x (ppm)	HC (ppmC)	HC/NO_x	Expt (ppm)	Calc (ppm)	Calc -expt (ppm)	Calc -expt /expt[a]	Expt --	Calc (ppb/min)	Calc -expt --	Calc -expt /expt
Modified Aromatics Synthetic Fuel											
ITC799	0.51	94.0	184.1	0.840	0.880	0.040	0.05	4.59	5.44	0.85	0.19
ITC801	0.55	41.0	75.1	0.881	0.873	-0.008	-0.01	2.98	4.09	1.11	0.37
Group Average	0.53	67.5	129.6	0.861	0.877	0.016	0.02	3.79	4.77	0.98	0.28
Avg. Abs. Value						0.024	0.03			0.98	0.28
Standard Synthetic Fuel + Heteroatom Impurities											
ITC786	0.49	72.0	146.7	0.637	0.808	0.172	0.27	6.59	7.24	0.65	0.10
ITC788	0.48	89.0	184.9	0.718	0.766	0.047	0.07	3.91	5.08	1.17	0.30
ITC807	0.48	77.0	159.4	0.641	0.779	0.138	0.21	7.47	8.45	0.98	0.13
Group Average	0.49	79.3	163.7	0.665	0.784	0.119	0.18	5.99	6.92	0.93	0.18
Avg. Abs. Value						0.119	0.18			0.93	0.18
Synthetic Jet Exhaust											
ITC963	0.49	4.4	9.1	0.822	0.746	-0.076	-0.09	4.00	3.89	-0.11	-0.03
ITC965	0.46	5.2	11.3	0.863	0.751	-0.112	-0.13	5.10	4.76	-0.33	-0.07
ITC967	0.26	4.4	17.2	0.586	0.605	0.019	0.03	5.79	5.07	-0.72	-0.12
ITC968	0.49	8.7	17.8	0.852	0.801	-0.051	-0.06	11.76	9.09	-2.67	-0.23
Group Average	0.42	5.7	13.8	0.781	0.726	-0.055	-0.06	6.66	5.70	-0.96	-0.11
Avg. Abs. Value						0.065	0.08			0.96	0.11

TABLE 19. SUMMARY OF THE INITIAL REACTANT CONCENTRATIONS, AND THE PERFORMANCE OF THE MODEL IN SIMULATING THE OZONE YIELDS AND OZONE FORMATION AND NO OXIDATION RATES IN THE AIR FORCE RUNS USED FOR MODEL TESTING (CONCLUDED).

Experiment	Initial concentrations			Maximum concentration OZONE				Average initial $d([O_3]-[NO])/dt$			
	NO_x (ppm)	HC (ppmC)	HC/NO_x	Expt (ppm)	Calc (ppm)	Calc -expt (ppm)	Calc -expt /expt[a]	Expt --	Calc (ppb/min)	Calc -expt --	Calc -expt /expt
Reference JP-4 Fuel (Simulated Assuming ~5% Alkenes in Fuel)											
ITC966	0.26	40.6	156.2	0.564	0.652	0.088	0.16	4.00	8.96	4.96	1.24
ITC969	0.51	81.2	158.6	0.849	0.939	0.090	0.11	7.00	16.00	9.00	1.29
EC489	0.46	50.0	108.8	0.515	0.804	0.289	0.56		(missing data)		
EC490	0.90	50.0	55.7	0.615	0.974	0.358	0.58	5.51	10.69	5.18	0.94
EC491	0.91	5.0	5.5	0.024	0.025	0.001		1.80	1.92	0.12	0.07
EC492	0.49	50.0	101.4	0.525	0.827	0.302	0.58	5.18	10.42	5.24	1.01
Group Average	0.59	46.1	97.7	0.515	0.703	0.188	0.40	4.70	9.65	4.90	0.91
Avg. Abs. Value						0.188	0.40			4.90	0.91
Reference JP-4 Fuel (Simulated Assuming "Alkenes" = Cycloalkanes)											
ITC966	0.26	40.6	156.2	0.564	0.725	0.161	0.29	4.00	2.81	-1.18	-0.30
ITC969	0.51	81.2	158.6	0.849	0.957	0.108	0.13	7.00	3.72	-3.28	-0.47
EC489	0.46	50.0	108.8	0.515	0.832	0.317	0.61		(missing data)		
EC490	0.90	50.0	55.7	0.615	1.006	0.391	0.63	5.51	7.88	2.37	0.43
EC491	0.91	5.0	5.5	0.024	0.024	0.000		1.80	1.91	0.11	0.06
EC492	0.49	50.0	101.4	0.525	0.854	0.329	0.63	5.18	6.20	1.03	0.20
Group Average	0.59	46.1	97.7	0.515	0.733	0.218	0.46	4.70	4.50	-0.19	-0.02
Avg. Abs. Value						0.218	0.46			1.59	0.29

[a]Relative discrepancies shown only for those runs with sufficiently high ozone yields to be useful for model testing.

[b]Average of absolute values.

TABLE 20. SUMMARY OF PERFORMANCE OF THE MODEL IN SIMULATING THE REACTANT HALF-LIVES AND THE PAN AND FORMALDEHYDE YIELDS IN THE AIR FORCE RUNS FOR WHICH SUCH DATA WERE USEFUL FOR MODEL TESTING.

Experiment	Half-life				Maximum concentration PAN				Maximum concentration HCHO			
	Expt (min)	Calc (min)	Calc -expt (min)	Calc -expt /expt	Expt (ppm)	Calc (ppm)	Calc -expt (ppm)	Calc -expt /expt	Expt (ppm)	Calc (ppm)	Calc -expt (ppm)	Calc -expt /expt
Ethene												
ITC926	227	206	-21	-0.09					1.308	1.258	-0.050	-0.04
ITC936	337	283	-54	-0.16					0.697	0.700	0.004	0.01
Group Average	282	244	-37	-0.13					1.002	0.979	-0.023	-0.02
Avg. Abs. Value[a]			37	0.13							0.027	0.02
Propene												
ITC693	126	126	0	0.00	0.311	0.253	-0.058	-0.19	0.416	0.502	0.086	0.21
ITC810	135	145	10	0.07	0.140	0.233	0.093	0.66	0.447	0.415	-0.032	-0.07
ITC860	142	131	-11	-0.08		0.216			0.617	0.411	-0.206	-0.33
ITC925	150	147	-3	-0.02	0.205	0.233	0.028	0.13	0.467	0.408	-0.059	-0.13
ITC938	137	142	5	0.04	0.296	0.249	-0.047	-0.16	0.416	0.413	-0.003	-0.01
ITC947	157	145	-12	-0.08	0.270	0.248	-0.022	-0.08		0.412		
ITC960	133	138	5	0.04	0.056	0.228	0.172	3.10	0.255	0.414	0.159	0.62
Group Average	140	139	0	0.00	0.213	0.237	0.028	0.58	0.436	0.425	-0.009	0.05
Avg. Abs. Value			6	0.05			0.070	0.72			0.091	0.23
1-Butene												
ITC927	168	131	-37	-0.22					0.331	0.387	0.056	0.17
ITC928									0.152	0.268	0.116	0.76
ITC930	92	75	-17	-0.18					0.762	0.702	-0.060	-0.08
ITC935	159	123	-36	-0.23					0.748	0.788	0.040	0.05
Group Average	139	109	-30	-0.21					0.498	0.536	0.038	0.23
Avg. Abs. Value			30	0.21							0.068	0.27

TABLE 20. SUMMARY OF PERFORMANCE OF THE MODEL IN SIMULATING THE REACTANT HALF-LIVES AND THE PAN AND FORMALDEHYDE YIELDS IN THE AIR FORCE RUNS FOR WHICH SUCH DATA WERE USEFUL FOR MODEL TESTING (CONTINUED).

Experiment	Half-life				Maximum concentration PAN				Maximum concentration HCHO			
	Expt (min)	Calc (min)	Calc -expt (min)	Calc -expt /expt	Expt (ppm)	Calc (ppm)	Calc -expt (ppm)	Calc -expt /expt	Expt (ppm)	Calc (ppm)	Calc -expt (ppm)	Calc -expt /expt
1-Hexene												
ITC929	295	292	-3	-0.01	0.002	0.006	0.005	2.40	0.186	0.242	0.056	0.30
ITC931	193	190	-3	-0.02	0.006	0.027	0.021	3.27	0.685	0.556	-0.128	-0.19
ITC934	328	311	-17	-0.05	0.002	0.020	0.019	10.93	0.358	0.468	0.110	0.31
ITC937						0.000			0.073	0.121	0.048	0.65
Group Average	272	264	-7	-0.03	0.003	0.014	0.015	5.53	0.326	0.347	0.021	0.27
Avg. Abs. Value			7	0.03			0.015	5.53			0.086	0.36
Toluene												
ITC699					0.145	0.111	-0.034	-0.24	0.091	0.032	-0.059	-0.65
ITC828					0.000	0.001	0.001		0.012	0.020	0.008	0.68
EC266					0.075	0.093	0.018	0.24	0.075	0.047	-0.028	-0.37
EC270	271	292	21	0.08	0.057	0.061	0.004	0.08	0.171	0.178	0.007	0.04
EC271					0.053	0.064	0.011	0.21	0.042	0.043	0.000	0.01
Group Average	273	292	21	0.08	0.066	0.066	0.000	0.07	0.078	0.064	-0.014	-0.06
Avg. Abs. Value			21	0.08			0.014	0.19			0.020	0.35
m-Xylene												
EC344	67	76	9	0.13	0.175	0.176	0.001	0.00	0.111	0.062	-0.049	-0.44
EC345	55	63	8	0.15	0.107	0.109	0.002	0.02	0.136	0.070	-0.066	-0.48
ITC702	87	90	3	0.03	0.390	0.159	-0.231	-0.59	0.053	0.064	0.010	0.20
ITC827					0.002	0.003	0.001	0.36	0.014	0.040	0.026	1.85
Group Average	69	106	6	0.10	0.168	0.112	-0.057	-0.05	0.079	0.059	-0.020	0.28
Avg. Abs. Value			6	0.10			0.059	0.24			0.038	0.74

TABLE 20. SUMMARY OF PERFORMANCE OF THE MODEL IN SIMULATING THE REACTANT HALF-LIVES AND THE PAN AND FORMALDEHYDE YIELDS IN THE AIR FORCE RUNS FOR WHICH SUCH DATA WERE USEFUL FOR MODEL TESTING (CONTINUED).

Experiment	Half-life				Maximum concentration PAN				Maximum concentration HCHO			
	Expt (min)	Calc (min)	Calc -expt (min)	Calc -expt /expt	Expt (ppm)	Calc (ppm)	Calc -expt (ppm)	Calc -expt /expt	Expt (ppm)	Calc (ppm)	Calc -expt (ppm)	Calc -expt /expt
1,3,5-Trimethylbenzene (mesitylene)												
ITC703	45	40	-5	-0.11	0.586	0.191	-0.395	-0.67	0.156	0.107	-0.049	-0.31
ITC706	45	40	-5	-0.11	0.440	0.182	-0.258	-0.59	0.069	0.068	-0.001	-0.01
ITC709	52	50	-2	-0.04	0.590	0.354	-0.236	-0.40	0.115	0.096	-0.019	-0.16
ITC742	42	40	-2	-0.05	0.470	0.186	-0.284	-0.60	0.127	0.097	-0.030	-0.24
ITC826	112	79	-33	-0.29	0.003	0.003	0.000	0.11	0.022	0.036	0.015	0.67
EC900					0.400	0.195	-0.205	-0.51	0.088	0.150	0.062	0.71
EC901	47	42	-5	-0.11	0.293	0.176	-0.117	-0.40	0.056	0.064	0.008	0.14
EC903	49	45	-4	-0.08	0.470	0.334	-0.136	-0.29	0.069	0.099	0.030	0.44
Group Average	56	47	-8	-0.11	0.407	0.203	-0.204	-0.42	0.088	0.090	0.002	0.15
Avg. Abs. Value			8	0.11			0.204	0.45			0.027	0.34
2,3-Dimethylnaphthalene												
ITC775					0.031	0.016	-0.015	-0.48				
ITC771					0.056	0.031	-0.025	-0.45				
ITC806					0.030	0.038	0.008	0.27				
ITC774					0.069	0.046	-0.023	-0.33				
Group Average					0.046	0.033	-0.014	-0.25				
Avg. Abs. Value							0.018	0.38				

TABLE 20. SUMMARY OF PERFORMANCE OF THE MODEL IN SIMULATING THE REACTANT HALF-LIVES AND THE PAN AND FORMALDEHYDE YIELDS IN THE AIR FORCE RUNS FOR WHICH SUCH DATA WERE USEFUL FOR MODEL TESTING (CONTINUED).

Experiment	Half-life				Maximum concentration PAN				Maximum concentration HCHO			
	Expt (min)	Calc (min)	Calc -expt (min)	Calc -expt /expt	Expt (ppm)	Calc (ppm)	Calc -expt (ppm)	Calc -expt /expt	Expt (ppm)	Calc (ppm)	Calc -expt (ppm)	Calc -expt /expt
Furan												
ITC711	36	45	9	0.25								
ITC713	65	74	9	0.14								
ITC715	62	58	-4	-0.06								
ITC743	36	40	4	0.11								
Group Average	49	54	4	0.11								
Avg. Abs. Value			6	0.14								
Thiophene												
ITC733	194	244	50	0.26								
ITC744	209	224	15	0.07								
Group Average	202	234	32	0.16								
Avg. Abs. Value			32	0.16								
Pyrrole												
ITC735	16	16	0	0.00								
ITC778	15	14	-1	-0.07								
ITC779	25	25	0	0.00								
Group Average	81	18	0	-0.02								
Avg. Abs. Value			0	0.02								

TABLE 20. SUMMARY OF PERFORMANCE OF THE MODEL IN SIMULATING THE REACTANT HALF-LIVES AND THE PAN AND FORMALDEHYDE YIELDS IN THE AIR FORCE RUNS FOR WHICH SUCH DATA WERE USEFUL FOR MODEL TESTING (CONCLUDED).

Experiment	Half-life				Maximum concentration PAN				Maximum concentration HCHO			
	Expt (min)	Calc (min)	Calc -expt (min)	Calc -expt /expt	Expt (ppm)	Calc (ppm)	Calc -expt (ppm)	Calc -expt /expt	Expt (ppm)	Calc (ppm)	Calc -expt (ppm)	Calc -expt /expt
Synthetic Jet Exhaust[b]												
ITC963	295	331	36	0.12	0.068	0.116	0.048	0.71				
ITC965	236	302	66	0.28	0.076	0.121	0.045	0.59				
ITC967	312	305	-7	-0.02	0.052	0.080	0.028	0.53				
ITC968	228	265	37	0.16	0.123	0.142	0.019	0.15				
Group Average	267	300	33	0.14	0.080	0.115	0.035	0.50				
Avg. Abs. Value			36	0.15			0.035	0.50				

[a]Average of absolute values.
[b]Half-lives shown are for ethene.

a. Alkane Runs

The single-component alkane experiments in this set of Air Force experiments consisted of runs with n-butane, n-octane, and methylcyclohexane. The performance of the model in simulating these runs showed a relatively large amount of variability, with the model, in most cases, overpredicting the reactivity observed. There did not appear to be any significant difference in quality of fits between the three different alkanes employed, though the fits for the n-butane runs were somewhat worse than the other two alkanes, despite the fact that the n-butane photooxidation mechanism is considered to be the most well-characterized of the three. Most of these alkane runs did not form sufficient ozone to be useful for model testing, so the primary statistic useful for model evaluation was the average rate of NO oxidation and ozone formation. Figures 3 and 4 shows experimental and calculated concentration-time plots for a representative methylcyclohexane-NO_x-air run, and for a representative n-octane-NO_x-air run.

In assessing the implications of these relatively poor fits in these runs, it should be recognized that model simulations of alkane-NO_x-air irradiations are extremely sensitive to the assumed magnitude of the chamber radical source. This arises since, unlike many other classes of organics, the alkanes have no significant homogeneous radical sources, and the overall processes in alkane-NO_x-air runs are driven almost entirely by the chamber radical source. This is a significant problem in testing models for alkanes against results of such experiments, since the chamber radical source tends to vary from run to run (References 26, 39, 40), making its precise value difficult to predict a-priori. Much better fits would be obtained if the magnitude of the chamber radical source were to be adjusted from run to run to optimize the fits. However, such run-to-run adjustment of parameters would invalidate using these runs for model testing, since it could also result in disguising possible errors in the mechanism. Thus, considering the variability of the chamber radical source and the sensitivity of simulations of these runs to its assumed magnitude, the quality of the fits in the simulations of the alkane-NO_x-air runs is probably as good as can reasonably be expected when testing the model with a consistent set of assumptions.

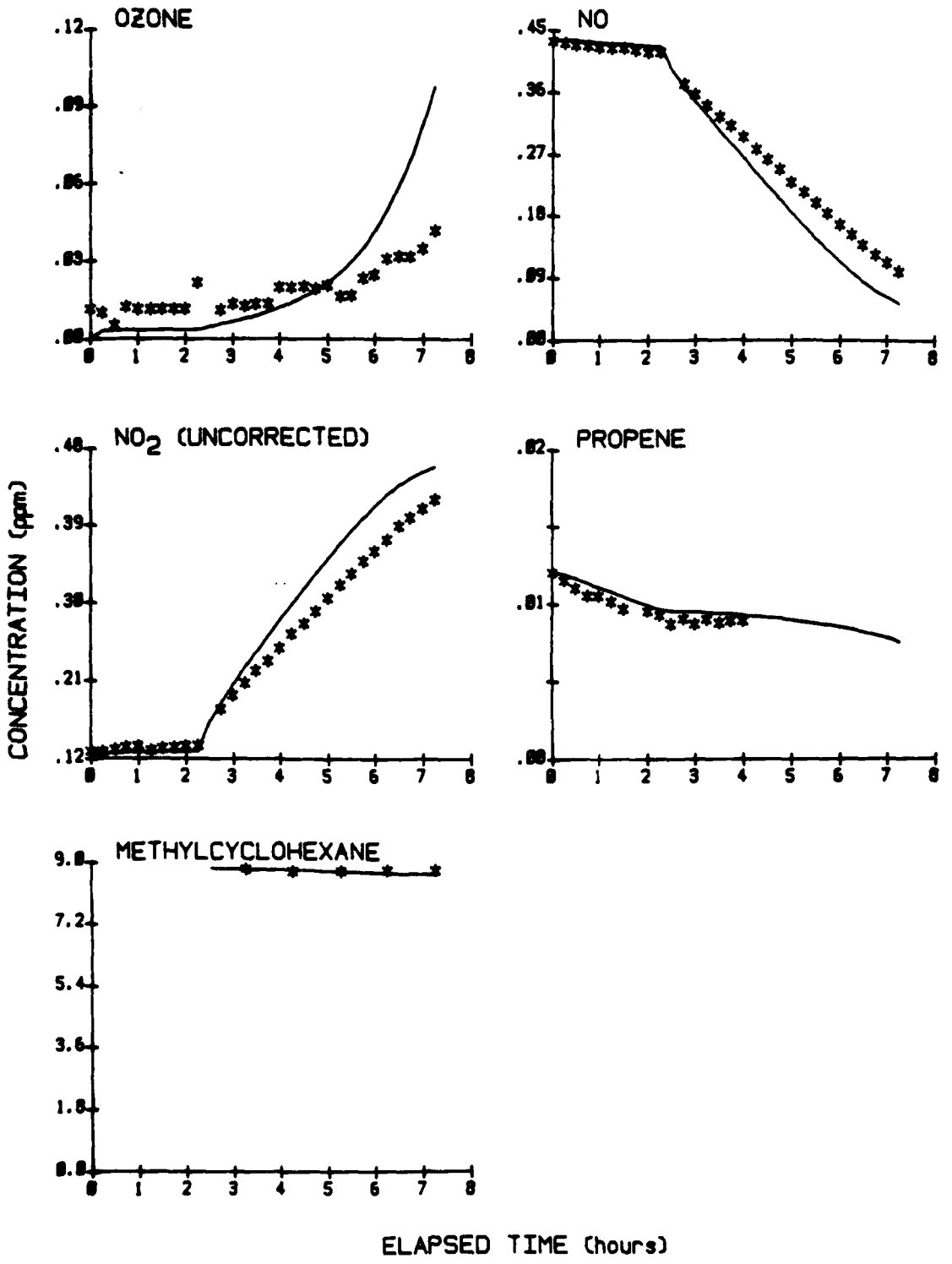

Figure 3. Experimental and Calculated Concentration-Time Profiles for Selected Species Observed in the Methylcyclohexane-NO_x-Air Experiment ITC-767.

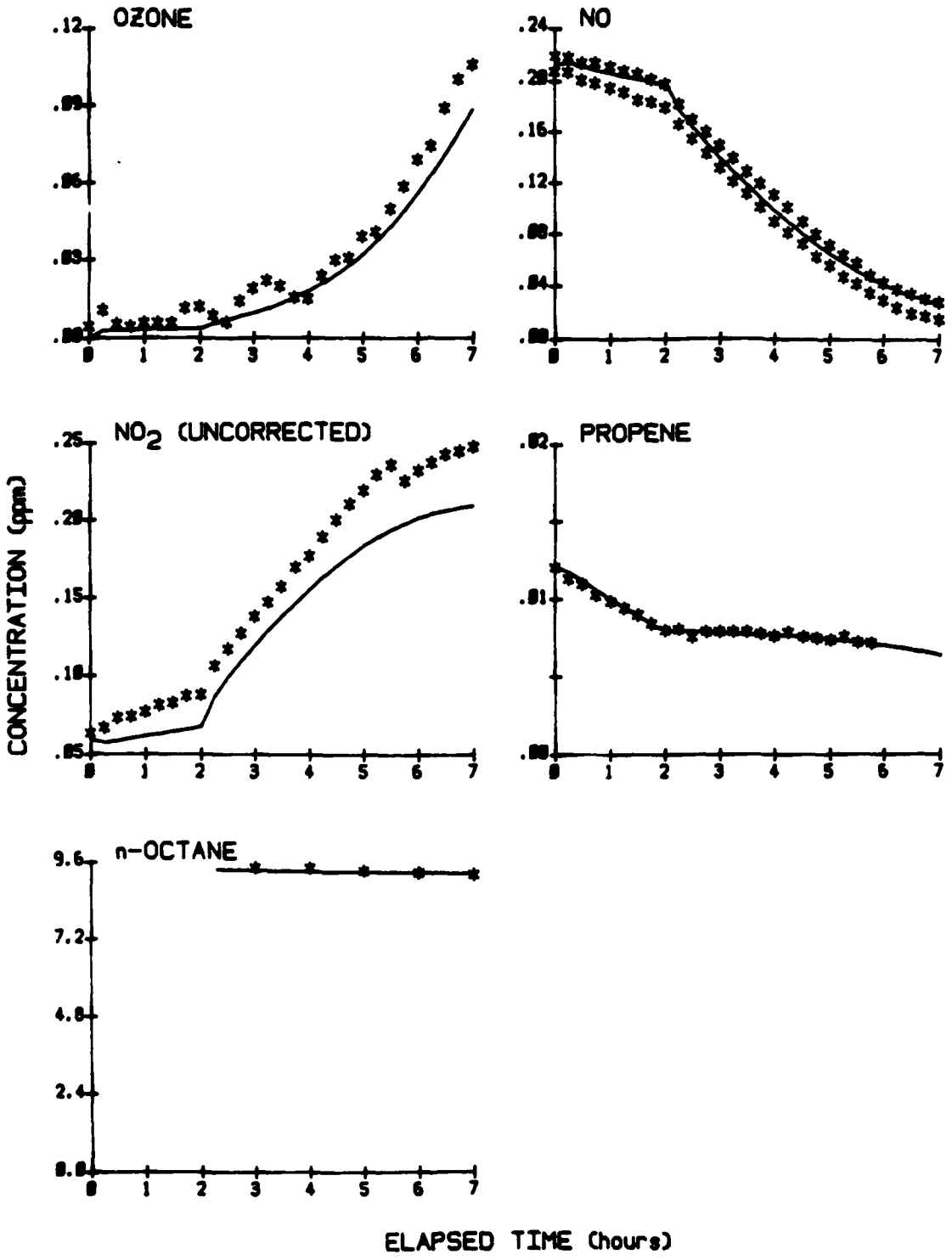

Figure 4. Experimental and Calculated Concentration-Time Profiles for Selected Species Observed in the n-Octane-NO_x-Air Experiment ITC-762.

b. Simulations of the Alkene Runs

The single-component alkene-NO_x-air runs in this set include runs with ethene, propene, 1-butene, and 1-hexene. The results of the simulations of the propene and ethene runs in general did not indicate systematic discrepancies between model predictions and experimental results, although [as is the case in simulations of all types of chamber experiments (Reference 26)], the quality of fits tended to vary from run to run, with some individual runs not being well simulated. In general, there was a greater variability in the performance of the model in simulating PAN and formaldehyde yields than in simulating ozone yields, NO oxidation or ozone formation rates, and reactant half-lives. This can be attributed, at least to some extent, to difficulties in precisely monitoring PAN and (especially) formaldehyde. The atmospheric chemistry of ethene and (to a lesser extent) propene are reasonably well-characterized, and thus the variability in the fits to these runs probably primarily reflects the variability in our ability to accurately characterize experimental conditions and chamber effects in our model simulations.

The model appeared to have a tendency to overpredict the reactivity observed in the 1-butene experiments carried out in this program, although it had the opposite tendency in the simulations of 1-butene runs previously carried out in the SAPRC EC (Reference 26). This model assumes that alkyl nitrate formation in the OH + 1-butene reaction is not important (despite the fact that it appears to be important in the 1-hexene case -- see Section IV.A.5), and if it were assumed to occur to some extent in this system, then the simulations of the ITC 1-butene experiments would probably be improved. However, because of the inconsistency with the results of the earlier EC runs, no modification of the 1-butene photooxidation mechanism was made.

The model performance was generally satisfactory with respect to predictions of the overall reactivities observed in the 1-hexene runs. This was, in part, a result of adjusting the assumed organic nitrate yield in the OH radical reaction (see Section IV.A.5) to optimize these fits. Experimental and predicted concentration-time plots for a representative 1-hexene-NO_x-air run are shown in Figure 5.

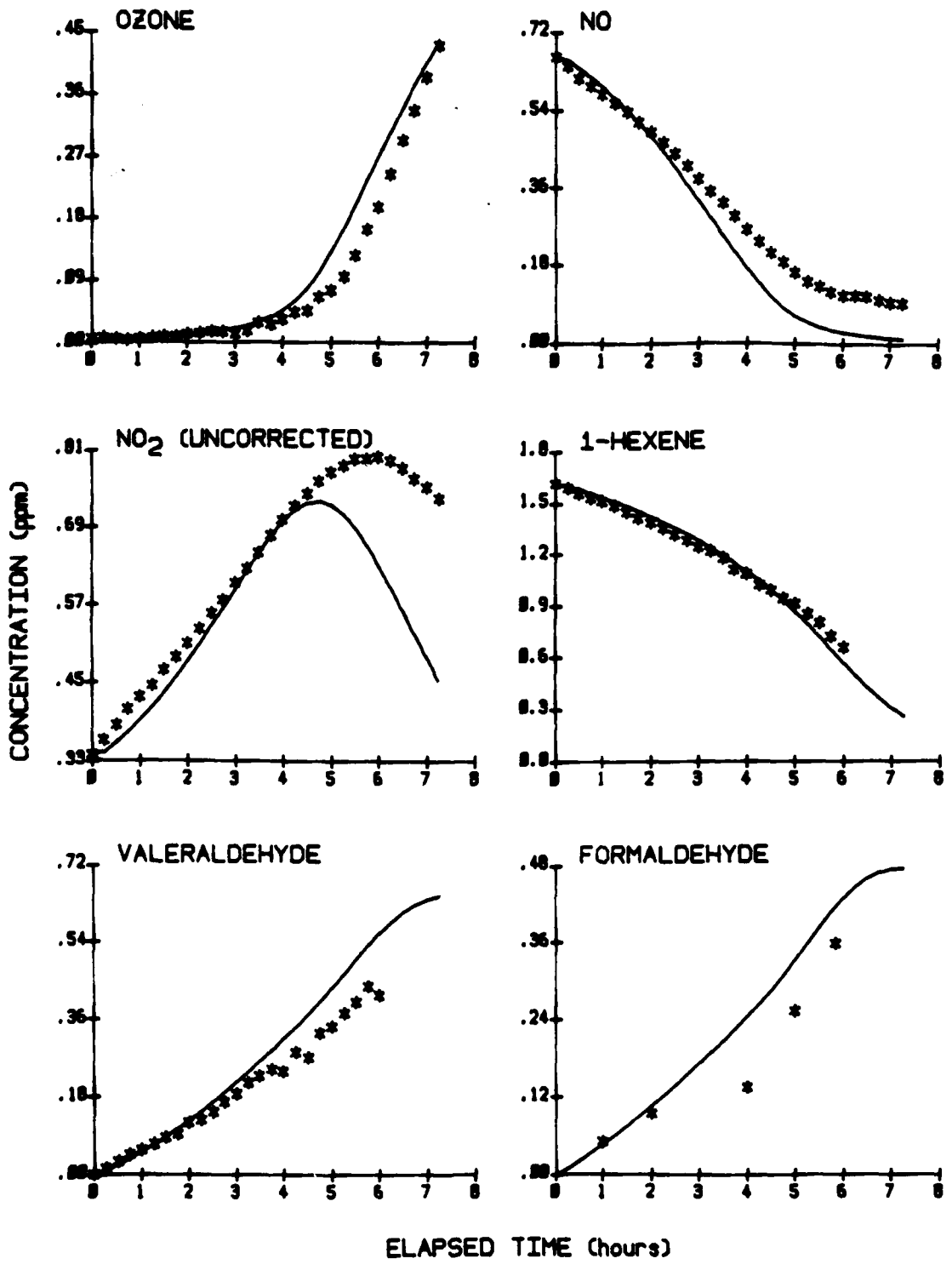

Figure 5. Experimental and Calculated Concentration-Time Profiles for Selected Species Observed in the 1-Hexene-NO_x-Air Experiment ITC-931.

[The apparent poor fit to the NO_2 maximum is attributable to analytical interferences in the NO_2 monitor (discussed in Section III.A.3.a), and does not necessarily indicate a problem with the model. This "discrepancy" is seen in most of the other NO_2 plots shown in this section.]

c. Simulations of the Aromatic Runs

The aromatic runs used for model testing in this program consisted of runs with benzene, toluene, m-xylene, 1,3,5-trimethylbenzene, tetralin, naphthalene, and 2,3-dimethylnaphthalene. Experimental and calculated concentration-time plots for selected species in a representative 1,3,5-trimethylbenzene experiment and in a representative naphthalene experiment are shown in Figures 6 and 7, respectively. With several exceptions, the results of the simulations of the aromatic runs were generally satisfactory, i.e., of similar quality as the results of the simulations of the propene and ethene runs. However, as discussed in Section IV.A.3, these fits were obtained as a result of optimizing parameters in the mechanism regarding the formation and reactions of the uncharacterized aromatic ring-opened products. If the formation and reactions of these products were ignored, then the model significantly underpredicted the reactivities observed in these experiments.

As discussed in Section IV.A.3, there are significant areas of uncertainty in the aromatic photooxidation mechanisms, and many aspects of the mechanisms of these compounds had to be represented in this model in a parameterized and highly simplified manner. Thus, despite the optimization of several mechanistic parameters in the model based on fits to these experiments, areas of discrepancy between model simulation and the experimental results are not unexpected. Specific systematic discrepancies observed which might be attributed to problems with the mechanism are indicated below:

- One experiment each was carried out in which benzene, toluene, m-xylene, or 1,3,5-trimethylbenzene was added to the chamber after 2 hours irradiation of a tracer-NO_x-air mixture. In all cases, the model significantly underpredicted the NO consumption rates after the addition

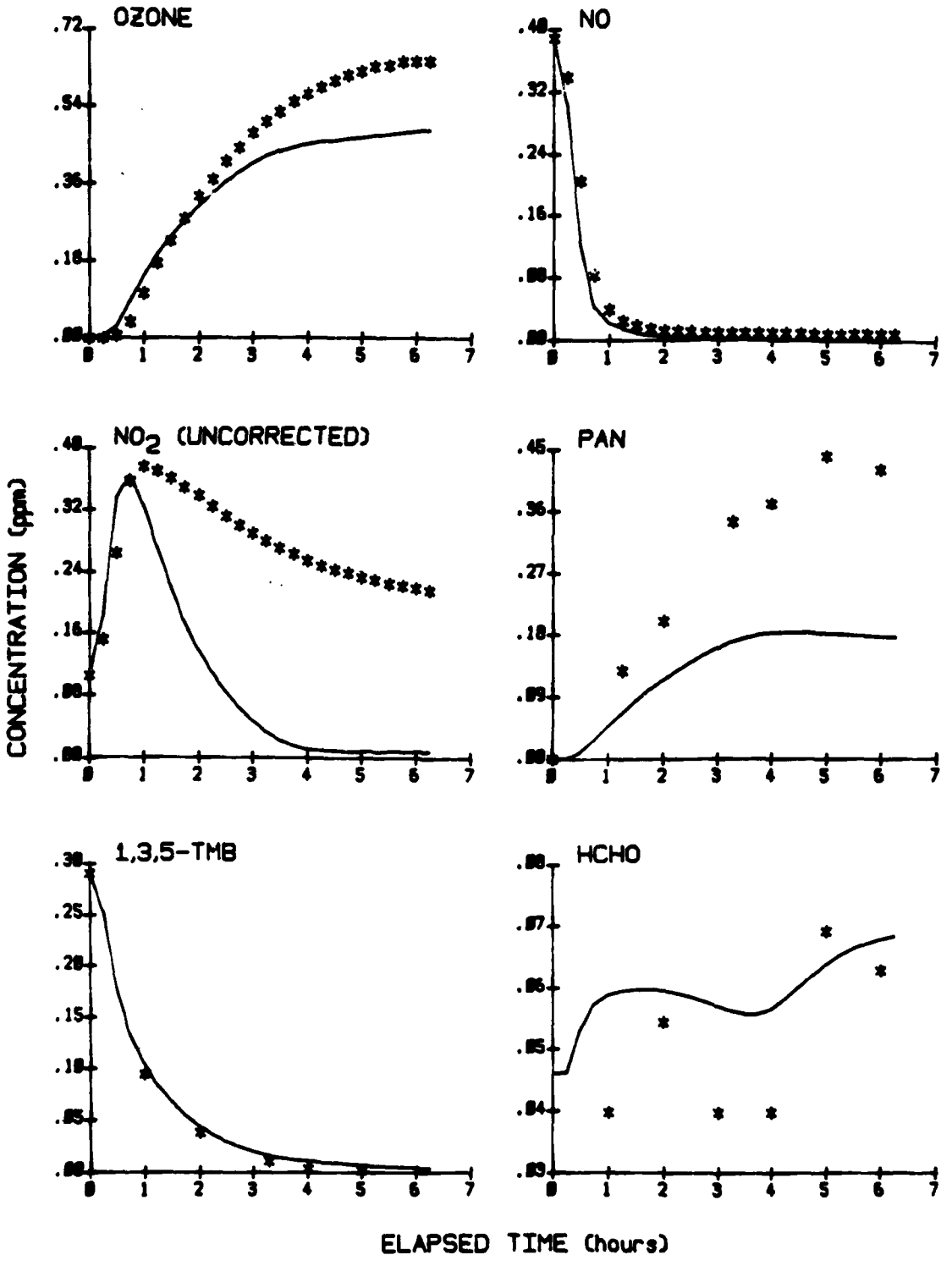

Figure 6. Experimental and Calculated Concentration-Time Profiles for Selected Species Observed in the 1,3,5-Trimethylbenzene-NO_x-Air Experiment ITC-706.

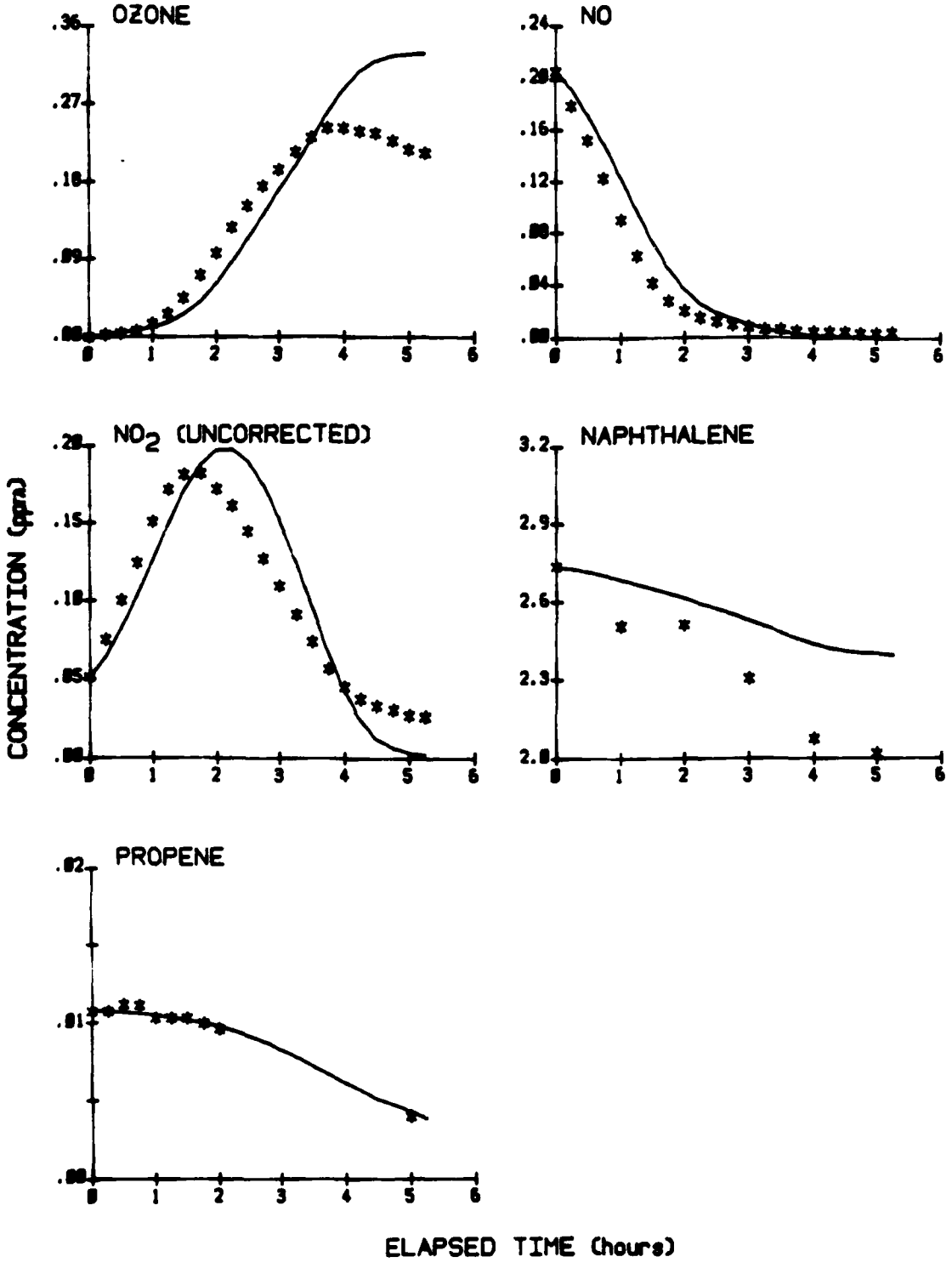

Figure 7. Experimental and Calculated Concentration-Time Profiles for Selected Species Observed in the Naphthalene-NO_x-Air Experiment ITC-756.

of the aromatic. These runs differed from most of the other runs with these aromatics in that the total NO_x levels were ~1 ppm, where in most of the others the total NO_x levels were ~0.5 ppm or less. This suggests that the method used to parameterize the unknown aspects of the atmospheric reactions of these alkylbenzenes did not accurately take into account the effects of NO_x on their overall reactivity, at least when NO_x is present at levels significantly above ~0.5 ppm. However, under atmospheric conditions, NO_x is usually present at much lower levels.

- The model had a consistent tendency to underpredict the ozone yields observed in the 1,3,5-trimethylbenzene experiments carried out in the ITC, despite the fact that it tended to overpredict the NO oxidation and ozone formation rates in those same experiments. The model fit reasonably well the ozone yields in the EC experiments for this aromatic, but propene runs carried out around the same time tended to give anomalously low ozone yields. Thus, these EC 1,3,5-trimethylbenzene runs may also be anomalous and this fit may be fortuitous. The model also consistently underpredicted the PAN yields in both the EC and the ITC experiments with this aromatic. These two discrepancies in the 1,3,5-trimethylbenzene system may be related since, if higher PAN yields were predicted, the resulting NO_x sinks would lead to lower total ozone yields. However, it is difficult to modify this mechanism in a chemically reasonable way to predict higher PAN yields.

- The model also had a tendency to underpredict the PAN yields in the 2,3-dimethylnaphthalene experiments, though this was not true in all such runs, and the discrepancy was not as large as for the 1,3,5-trimethylbenzene runs.

However, despite these problems, this model performs probably as well as can be expected, given our current relatively poor state of knowledge of atmospheric photooxidation reactions of aromatics. More basic laboratory studies are required before significantly better model performance can be expected in simulating results of NO_x-air irradiations with these compounds.

d. Furan, Thiophene, and Pyrrole Runs

A series of runs employing furan, thiophene, or pyrrole were also modeled as part of this program. As discussed in Section IV.A.5, essentially nothing is known about the mechanisms of the reactions of these compounds, beyond their initial OH and NO_3 radical reaction rate constants. Thus, as with the naphthalenes and (in part) the alkylbenzenes, empirical models were adjusted, based on fits to the results of these experiments.

With suitable parameterization, the adjusted model was able to simulate the major observations concerning the overall reactivities of these compounds. This includes, in the case of furan and pyrrole, the high reactivities of these compounds when present in NO_x-air systems, and the observation that when all the furan or pyrrole had reacted, the photochemical system became essentially unreactive. Examples of experimental and calculated concentration-time profiles for selected species in two furan runs, carried out at differing initial furan levels, where one formed essentially no ozone and the other was highly reactive, are shown in Figure 8. The results of the simulations of the runs with pyrrole were similar. Thiophene was found to be much less reactive than furan or pyrrole, though the results of the experiments with these compounds can be simulated using a parameterized mechanism similar to that used for the other two. The lower reactivity of thiophene is attributed primarily to its lower rate constant for reaction with OH radicals.

e. Acrolein Runs

Runs employing acrolein were also used to test the model developed in this program. However, unlike the other individual reactants discussed, no explicit mechanism for the reactions of acrolein was developed; instead it is lumped in this model with the other $>C_3$ aldehydes, which are represented in this model by propionaldehyde. The model simulations of the acrolein experiments were used to test the validity of the approximation that acrolein can be represented in atmospheric reactivity models by propionaldehyde.

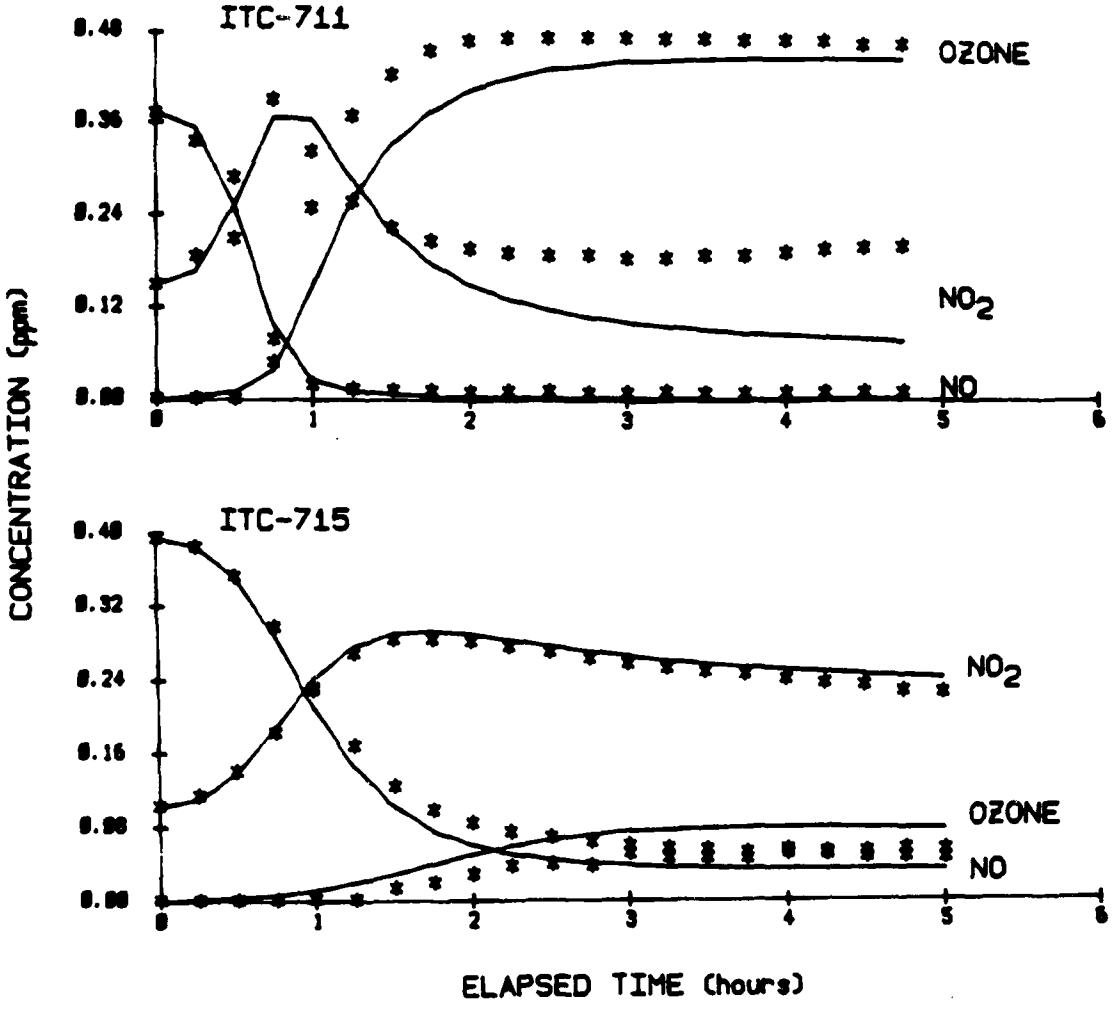

Figure 8. Experimental and Calculated Concentration-Time Profiles for Selected Species Observed in the Furan-NO_x-Air Experiments ITC-711 and ITC-715.

The results of the model simulations of the acrolein runs indicated the propionaldehyde model tends to consistently overpredict the rates of NO oxidation and ozone formation observed in the acrolein runs (except for the one run where significant amounts of propene was also present), but that it also tends to underpredict the maximum ozone yields in those experiments which are sufficiently reactive for a "true" ozone maximum yield to be observed. This is illustrated in Figure 9, which gives experimental and calculated concentration-time profiles for representative species in a typical acrolein experiment. Obviously, a mechanism designed to be more representative of acrolein would do a better job in simulating the results of these runs. However, because this propionaldehyde model is not grossly inaccurate in simulating the overall reactivity of acrolein, and because acrolein is not present in jet fuels to any significant extent and is only a relatively minor constituent in jet exhaust, it was judged not to be necessary to add a species to the model which only represents the reactions of acrolein.

f. Synthetic Fuel Runs

Experiments employing six different types of synthetic jet fuels were available for testing the ability of this model to simulate the reactivities of fuel mixtures whose exact compositions are known. The largest number of experiments (four) were carried out using the mixture designated the "standard" synthetic fuel, whose composition was determined by the scientists at AFESC/RDVS, and was designed to be approximately representative of JP-4. The model gave reasonably good fits to the maximum ozone yields observed in the experiments with this fuel, but tended to overpredict the NO oxidation/ozone formation rate in those runs by ~30 percent. This is within the variability of the performance of the model in simulating the results of experiments employing other complex mixtures (References 26, 63 -- See also Section IV.C.4, below). Experimental and calculated concentration-time plots for selected species in a representative "standard" synthetic fuel run are shown in Figure 10.

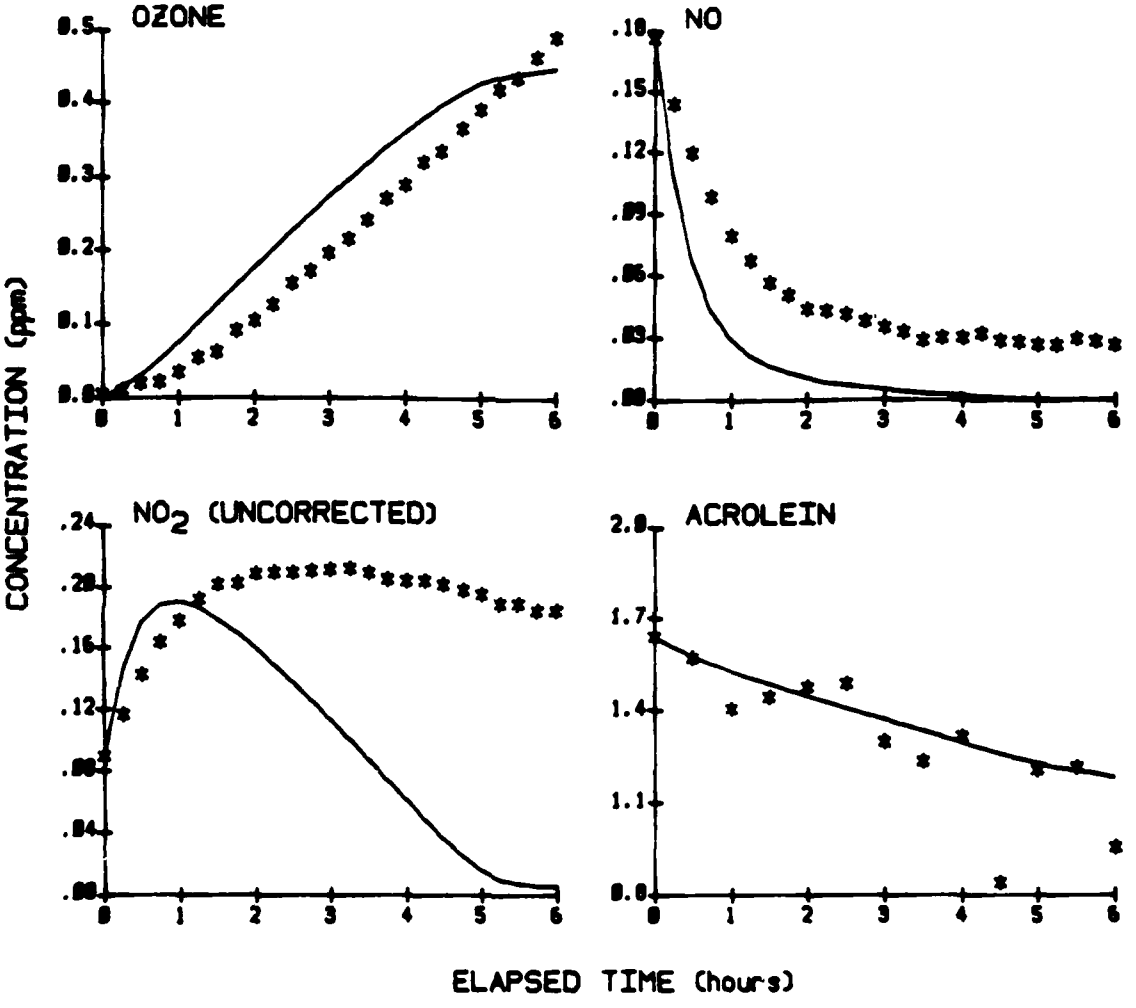

Figure 9. Experimental and Calculated Concentration-Time Profiles for Selected Species Observed in the Acrolein-NO_x-Air Experiment ITC-944.

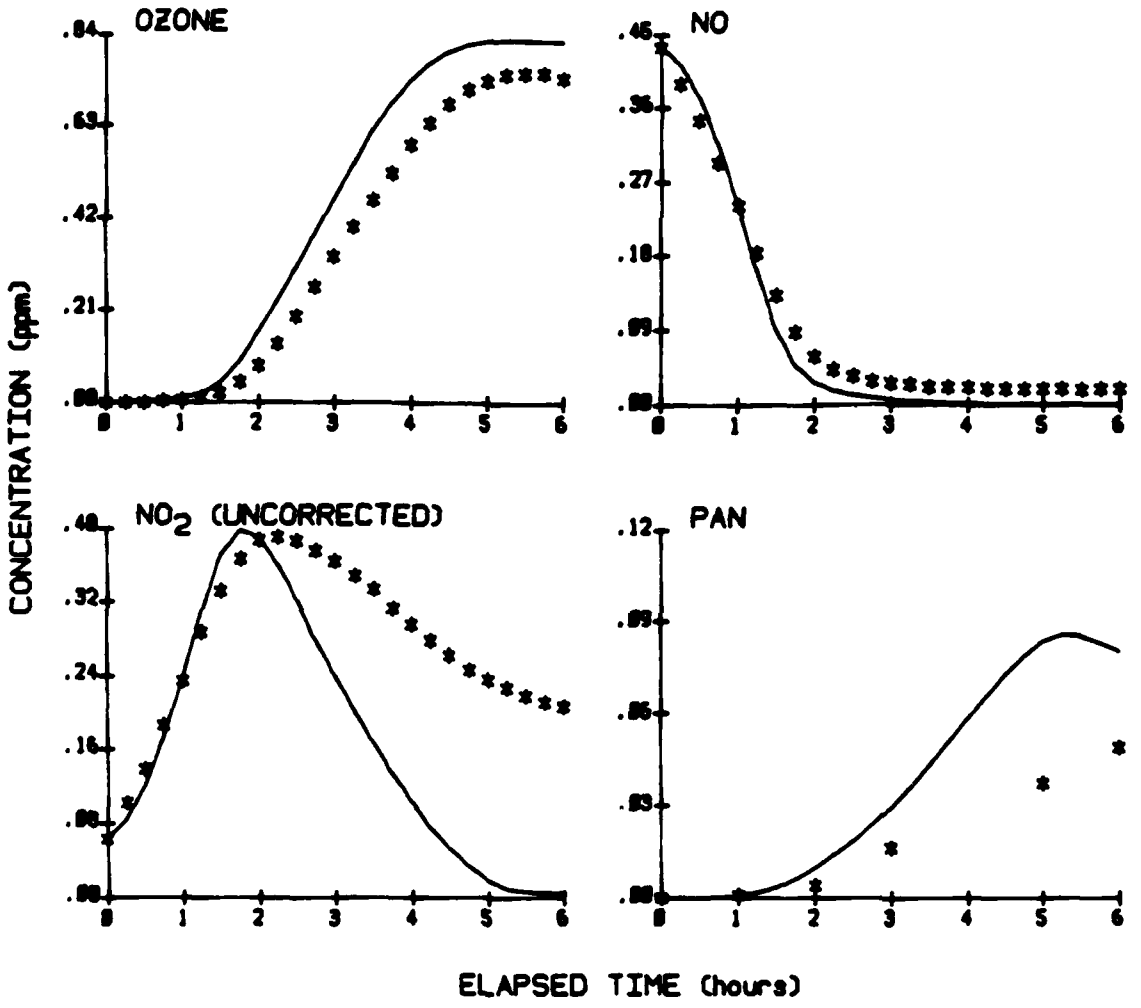

Figure 10. Experimental and Calculated Concentration-Time Profiles for Selected Species Observed in the "Standard" Synthetic Fuel Experiment ITC-784.

The simulations of the experiments employing the "high-aromatic" and "modified-aromatic" fuels are useful in testing the ability to simulate the effects of changing fuel compositions with respect to relative levels of aromatics. Both of these fuels are based on modifications of the "standard" fuel. The "high-aromatic" fuel having the total aromatic content increased from 27 to 38 percent. The "modified-aromatic" fuel has the same total aromatic content as the "standard" fuel, but the ratio of alkylbenzenes to tetralin and the naphthalenes was increased by a factor of ~2. The experimental and predicted ozone profiles from the three synthetic fuels in the ~0.5 ppm NO_x, ~100 ppmC fuel experiments are compared in Figure 11, and similar plots for the experiments using 50 ppmC fuel are shown in Figure 12.

These results show that the model simulations of the "modified aromatic" fuel are of comparable quality as the simulations of the "standard" fuel, while the model has a significantly greater tendency to overpredict the NO oxidation and ozone formation rates in the "high aromatic" fuel than it does with the other two. This indicates, at least for these three synthetic fuels, that the model is reasonably accurate in simulating the effects in changing the alkylbenzene/tetralin + naphthalene ratio, but tends to overpredict the extent to which increasing the total aromatic content enhances the reactivity of the fuel with regard to ozone formation and NO oxidation rates. The model also underpredicts the ozone yield in the "high-aromatic" synthetic fuel run with the ~100 ppmC fuel level.

The reason for these discrepancies in the predictions of the reactivity of the fuel with higher total aromatic content are not clear, though as indicated above the reaction mechanism for the aromatics are highly uncertain, and these results could well reflect these uncertainties. Of the aromatics, the mechanisms for tetralin and the naphthalenes are the most uncertain, and the "high-aromatic" fuel, where the model performance is the least satisfactory, is also the fuel with the highest content of these compounds. Without a more detailed understanding of the atmospheric chemistry of aromatics than is presently the case, it is doubtful that this situation will improve significantly. At least the current model is able to predict the qualitative reactivity trends

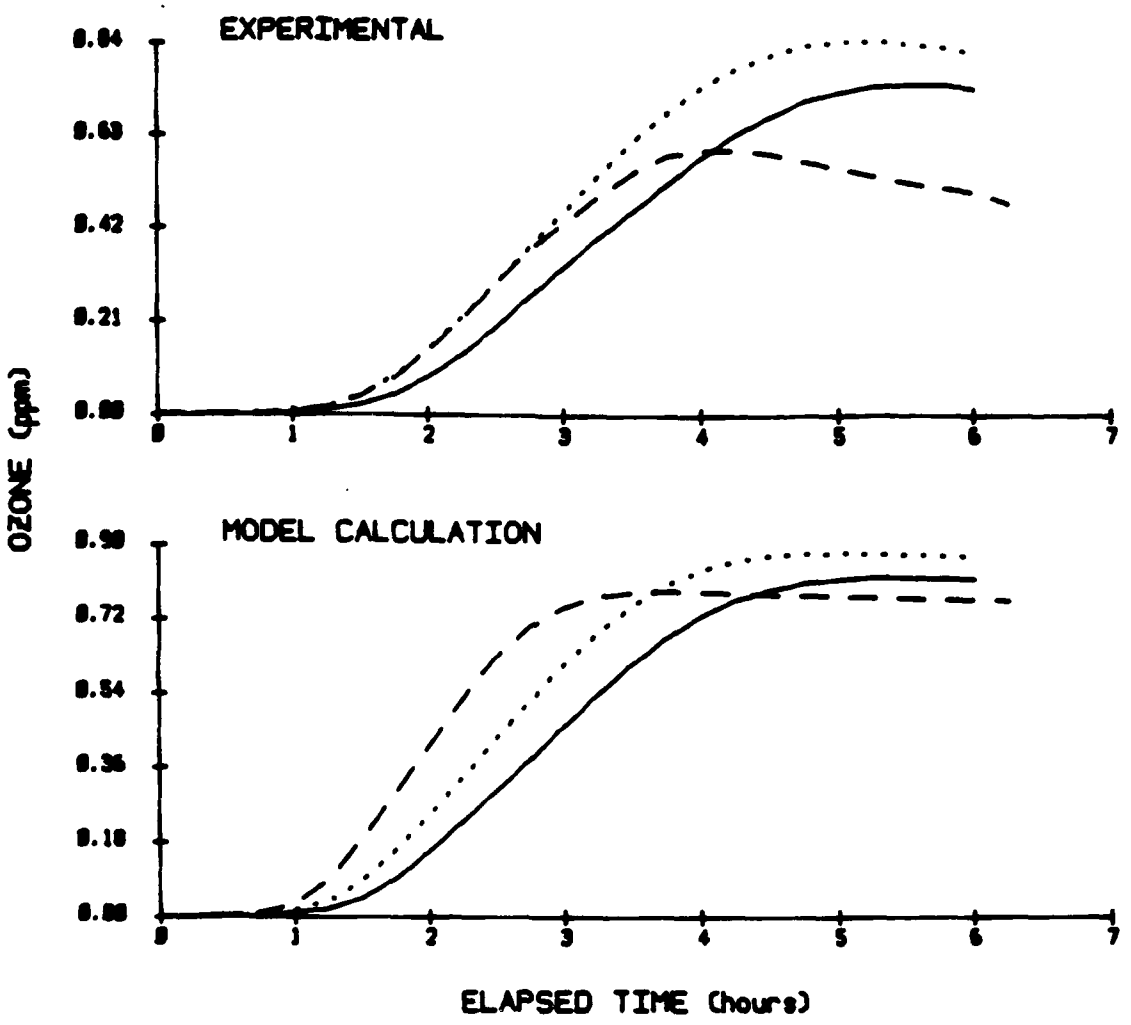

Figure 11. Comparison of Experimental and Calculated Ozone Concentration-Time Profiles for Three Experiments Employing Three Synthetic Fuels, with Initial NO_x = ~0.5 ppm and Initial Fuel = ~100 ppmC.

_____ = "Standard" Fuel Run ITC-784.
- - - = "High-Aromatics" Fuel Run ITC-796.
····· = "Modified-Aromatics" Fuel Run ITC-801.

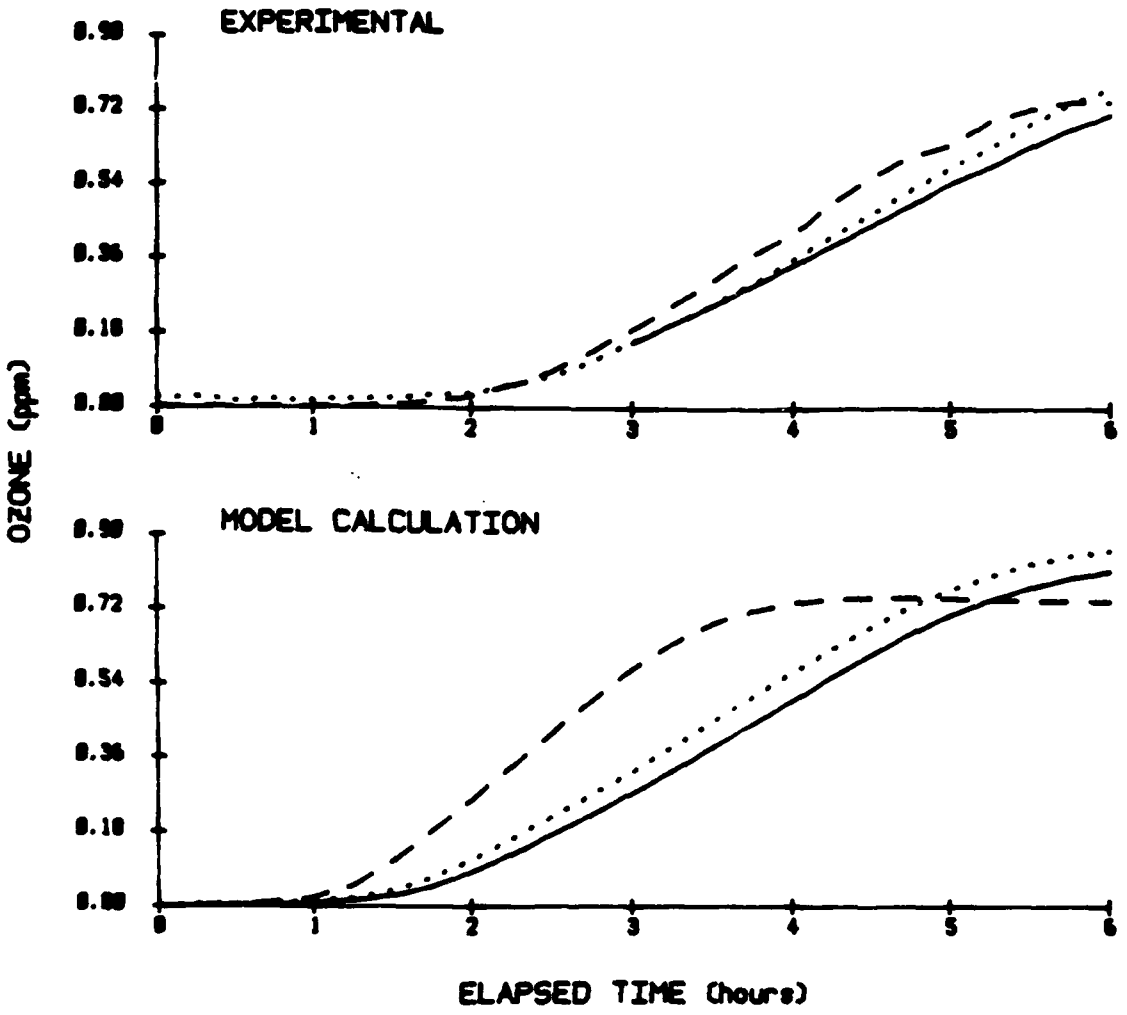

Figure 12. Comparison of Experimental and Calculated Ozone Concentration-Time Profiles for Three Experiments Employing Three Synthetic Fuels, with Initial NO_x = 0.5 ppm and Initial Fuel = 50 ppmC.

_____ = "Standard" Fuel Run ITC-781.
\- - - = "High-Aromatics" Fuel Run ITC-795.
····· = "Modified-Aromatics" Fuel Run ITC-799.

observed when the total aromatic content of the fuel is increased, i.e., that higher aromatic levels increase the rates of ozone formation and NO oxidation, but that they also decrease the maximum ozone yields.

Experiments were also carried out in which ~(2-5) percent of furan, thiophene, or pyrrole was added to the standard synthetic fuel. The experimental and calculated effects of the addition of these "impurities" to the fuel on ozone profiles are shown in Figure 13. These results show that the model can qualitatively simulate the effects of the addition of these compounds to the synthetic fuel mixture, though it underpredicts the tendency of furan or thiophene to suppress maximum ozone levels. This tendency of these compounds to suppress maximum ozone yields is probably due to NO_x sinks in the reaction mechanisms of these compounds, which are not adequately represented in this model. The furan-NO_x-air or pyrrole-NO_x-air experiments used to derive the models for these compounds are not sensitive to this aspect of this mechanism, thus, this possibility is not unexpected. However, the model derived from simulations of the single component runs did accurately account for the observation that the addition of these compounds to the fuels have dramatic effects on enhancing the NO oxidation and ozone formation rates.

The addition of thiophene to the synthetic fuel was observed to have relatively little effect on the experimental results, and the model predictions are consistent with this. The much smaller effect of the addition of thiophene on synthetic fuel reactivity is because of its relatively low OH and NO_3 radical rate constants, compared to the other two heteroatom-containing organics studied in this program.

g. Synthetic Exhaust Runs

The ability of this model to simulate the reactivities of jet exhaust mixtures whose compositions are known are indicated by the simulations of the synthetic jet exhaust experiments. The model can simulate the maximum ozone yields and NO oxidation and ozone formation rates quite well, with the performance of the model in this regard being comparable to, or better than, its performance in simulating runs with other complex mixtures (References 26, 63, and Section IV.C.4). On the other hand, the

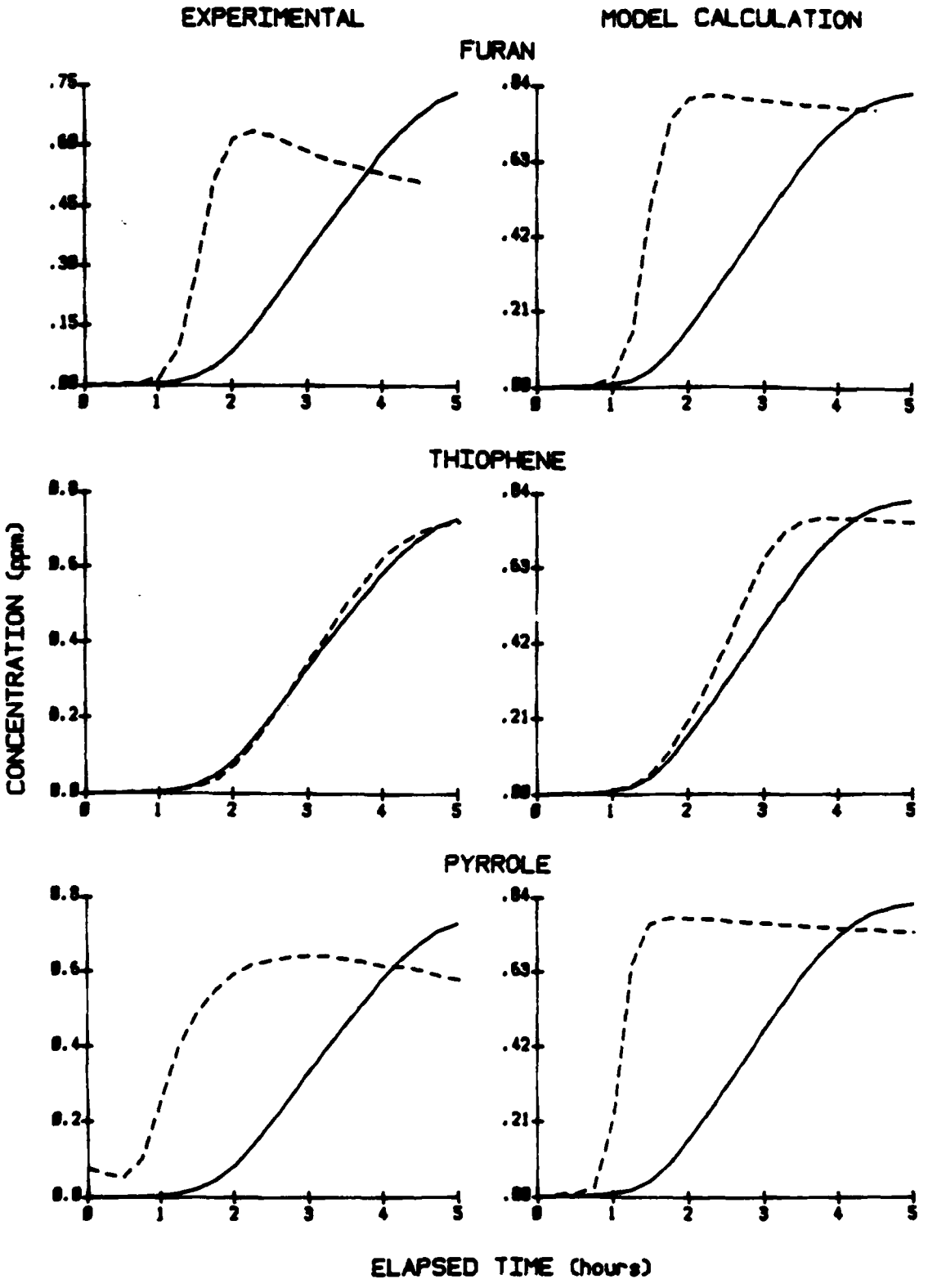

Figure 13. Comparison of Experimental and Calculated Effects on Ozone Concentration-Time Profiles of Addition of ~(2-5) Percent of Furan, Thiophene, or Pyrrole to a Synthetic Fuel Mixture.

model consistently underpredicted the PAN yields observed in this experiment, although poorer performance of this model in simulating PAN yields is also observed in the simulations of most other complex mixtures. Experimental and calculated concentration-time profiles for selected species in a representative synthetic exhaust run are shown in Figure 14.

3. Simulations of Experiments Employing the Reference JP-4 Fuel

Experiments employing three different types of JP-4 fuel and one type of JP-8 fuel were carried out in the SAPRC EC and ITC under this and previous (Reference 7) Air Force programs on fuel reactivity. In theory the results of these runs can be used for model testing. However, whole fuels such as JP-4 and JP-8 are complex mixtures of many organics, and if runs employing such fuels are to be useful for this purpose, detailed and accurate composition data for the fuel are required. Unfortunately, of the various whole fuels employed in this and our previous Air Force chamber studies (References 6, 7, 27) detailed composition data are available only for the "reference" JP-4 fuel sample. Therefore, only the runs employing that fuel could be used for model testing under this program. The methods used to derive the model inputs representing the composition of the "reference" JP-4 from the results of the available fuel composition analyses, the results of the model simulations of the runs employing this fuel, and the uncertainties and problems encountered in this effort, are discussed in this section.

a. Derivation of Model Input Representing Fuel Composition

The detailed composition of "reference" JP-4 fuel (also designated "Fuel 1A") used in our model simulations was derived, based on the results of gas chromatographic-mass spectrometric (GC-MS) analyses of this fuel carried out as part of the Monsanto fuel variability study (Reference 29). The results of detailed fuel composition analyses are reported in terms of mg mL^{-1} associated with each of ~300 GC "feature numbers" used in the Monsanto fuel analysis system. Separate tables are

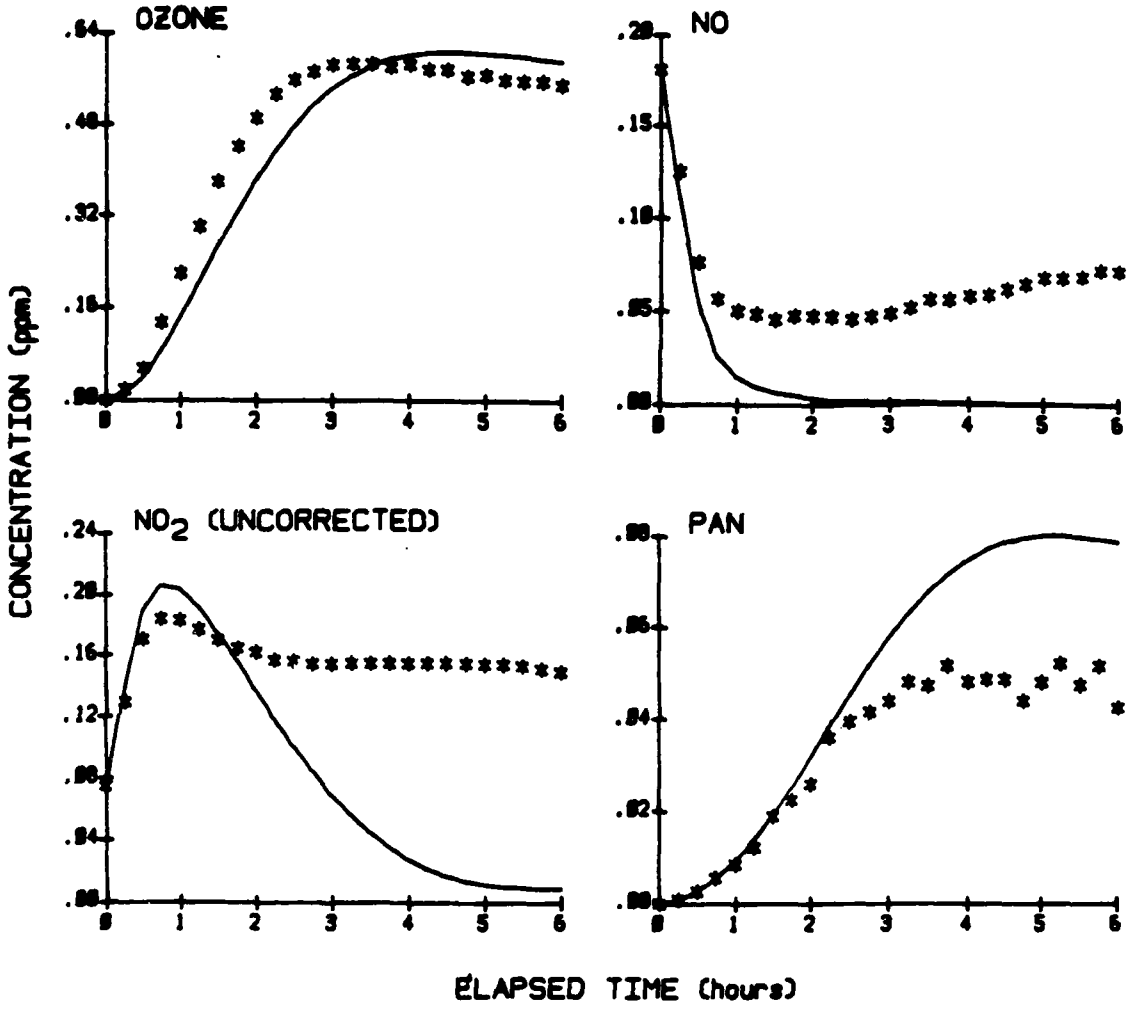

Figure 14. Experimental and Calculated Concentration-Time Profiles for Selected Species Observed in the Synthetic Jet Exhaust Experiment ITC-967.

included in the Monsanto report (Reference 29) giving the known or estimated assignments of fuel constituents associated with each of those feature numbers (Reference 29). Based on this information, we employed the following procedure to derive the fuel composition input data in the form required by the model:

- A computer file (named 1AJP4.GCD) giving the mg mL^{-1} for each GC-MS feature number was made by copying those data from the Monsanto (Reference 29) report. The data contained in this file are given in Table 21.

- A separate computer file (AFGC.PRM) giving the assignments made by Monsanto for the various GC-MS feature numbers was made by copying the relevant data from Tables 21-28 of the Monsanto (Reference 29) report. In some cases, more than one compound was assigned to a given feature. Therefore, an arbitrary judgment of the fractions of the contributions of each constituent to each GC peak was made (in most cases assuming equal contributions by each of the possible compounds assigned to it). The main exceptions were cases where a feature was identified as being either a cycloalkane or an alkene; in those cases, we usually assumed that ~80 percent of the peak was due to the cycloalkane, and ~20 percent to the alkene, based on the assumption that alkenes are less likely fuel constituents than cycloalkanes (see also below). When one of the peak constituents was identified as an n-alkane, it was also given higher weight.

- A data field was added to the AFGC.PRM file giving the compound in the model which is used to represent the reactions of each of the constituents assigned to the various GC peaks. The model compounds used, and the types of species each are used to represent, are given in Table 13 in Section IV.B. The complete AFGC.PRM data set, giving the Monsanto (Reference 29) peak assignments and other relevant data, our assigned fractions for peaks with more than one compound assigned to them, and the model species used to represent them, is given in Table 22. The heading of the table indicates the format of the data.

TABLE 21. COMPOSITION OF THE REFERENCE JP-4 FUEL, GIVEN IN TERMS OF MILLIGRAMS PER MILLILITER ASSOCIATED WITH MONSANTO'S GC-MS FEATURE NUMBERS (REFERENCE 29).

No.	$mg\ ml^{-1}$	No.	$mg\ ml^{-1}$	No.	$mg\ ml^{-1}$	No.	$mg\ ml^{-1}$	No.	$mg\ ml^{-1}$	No.	$mg\ ml^{-1}$
1	0.117	51	0.313	101	4.030	151	0.415	201	0.114	251	0.000
2	0.432	52	19.800	102	3.170	152	3.930	202	0.000	252	0.000
3	1.360	53	7.710	103	0.317	153	1.280	203	0.230	253	2.030
4	5.950	54	5.160	104	0.283	154	0.536	204	0.168	254	0.347
5	9.060	55	2.780	105	0.162	155	0.472	205	1.070	255	0.110
6	0.155	56	22.500	106	0.462	156	3.140	206	0.897	256	0.417
7	0.000	57	0.921	107	0.449	157	2.370	207	1.620	257	11.800
8	0.204	58	1.260	108	0.895	158	1.620	208	0.815	258	0.000
9	0.792	59	0.771	109	17.900	159	1.040	209	0.356	259	0.634
10	1.420	60	1.480	110	0.145	160	0.421	210	1.400	260	0.425
11	1.730	61	0.153	111	0.000	161	0.874	211	0.784	261	0.000
12	0.150	62	2.870	112	1.250	162	0.411	212	1.650	262	0.932
13	7.220	63	0.093	113	0.744	163	0.946	213	0.219	263	0.343
14	17.700	64	0.661	114	0.395	164	0.271	214	1.600	264	0.760
15	0.000	65	1.580	115	0.312	165	1.620	215	0.416	265	0.451
16	0.122	66	29.800	116	1.770	166	0.630	216	2.980	266	0.808
17	0.219	67	0.104	117	0.492	167	2.530	217	3.550	267	0.262
18	9.390	68	0.141	118	2.370	168	1.030	218	1.460	268	0.116
19	0.115	69	0.269	119	1.310	169	1.590	219	0.466	269	0.189
20	1.820	70	0.098	120	1.980	170	2.020	220	0.733	270	0.837
21	1.050	71	0.618	121	0.000	171	0.402	221	0.935	271	0.419
22	8.890	72	0.297	122	4.360	172	0.000	222	2.190	272	0.747
23	3.750	73	0.993	123	3.300	173	1.740	223	1.080	273	1.430
24	5.240	74	0.849	124	0.000	174	2.410	224	0.900	274	0.720
25	12.600	75	2.390	125	1.540	175	2.730	225	1.220	275	1.910
26	15.300	76	3.790	126	1.400	176	0.670	226	0.000	276	0.356
27	2.730	77	0.694	127	0.910	177	3.570	227	13.900	277	0.309
28	2.610	78	6.110	128	1.630	178	2.000	228	0.570	278	1.280
29	4.750	79	6.940	129	4.470	179	3.420	229	0.469	279	5.670
30	1.480	80	0.261	130	1.590	180	0.915	230	0.000	280	0.274
31	27.900	81	0.231	131	0.995	181	1.070	231	0.863	281	0.872
32	0.154	82	2.280	132	5.020	182	0.659	232	4.400	282	0.824
33	0.122	83	0.651	133	2.710	183	0.510	233	0.616	283	0.221
34	0.000	84	0.273	134	0.362	184	0.561	234	0.000	284	0.000
35	0.166	85	0.138	135	0.963	185	0.280	235	0.431	285	0.097
36	17.700	86	0.093	136	2.570	186	1.010	236	0.360	286	0.348
37	1.600	87	0.189	137	1.710	187	17.200	237	1.050	287	0.130
38	1.150	88	5.080	138	0.138	188	0.000	238	2.200	288	0.108
39	1.800	89	1.930	139	1.630	189	0.540	239	1.360	289	0.268
40	2.660	90	1.200	140	1.470	190	0.112	240	0.640	290	0.126
41	4.490	91	9.150	141	0.000	191	1.150	241	0.496	291	0.166
42	1.790	92	5.990	142	0.585	192	0.346	242	0.905	292	0.211
43	1.620	93	7.010	143	0.251	193	2.180	243	1.250	293	0.313
44	1.730	94	0.278	144	7.880	194	1.890	244	1.870	294	1.340

TABLE 21. COMPOSITION OF THE REFERENCE JP-4 FUEL, GIVEN IN TERMS OF MILLIGRAMS PER MILLILITER ASSOCIATED WITH MONSANTO'S GC-MS FEATURE NUMBERS (REFERENCE 29) (CONCLUDED).

No.	$mg\ ml^{-1}$	No.	$mg\ ml^{-1}$	No.	$mg\ ml^{-1}$	No.	$mg\ ml^{-1}$	No.	$mg\ ml^{-1}$	No.	$mg\ ml^{-1}$
45	0.554	95	1.520	145	0.916	195	0.861	245	1.430	295	0.289
46	0.515	96	7.890	146	1.050	196	0.134	246	1.870	296	1.600
47	0.157	97	0.370	147	0.327	197	0.000	247	0.685	297	0.254
48	0.659	98	0.450	148	0.261	198	0.309	248	1.250	298	0.000
49	4.730	99	3.180	149	14.400	199	1.170	249	3.780	299	0.000
50	9.400	100	1.240	150	0.765	200	1.710	250	0.000	300	0.000

TABLE 22. LISTING OF THE AFGC.PRM DATA SET, GIVING THE MONSANTO GC-MS FEATURE NUMBERS, THE MONSANTO FEATURE IDENTIFICATIONS AND RELATED DATA, AND THE MODEL COMPOUNDS ASSIGNED TO EACH FEATURE.

Data Format:

First record for each feature:	Feature No., Monsanto assignment[a]
Subsequent records for feature:	Feature No., fraction contribution; No. carbons; No. hydrogens; No. oxygens; 0; 0; 0; Monsanto code; model compound used

```
003   n-Butane
003    1.  4 10  0  0  0  0 NA   N-C4
004   2-Methylbutane
004    1.  5 12  0  0  0  0 BA   ISO-C5
005   n-Pentane
005    1.  5 12  0  0  0  0 NA   N-C5
009   2,3-Dimethylbutane
009    1.  6 14  0  0  0  0 BA   23-DMB
012   2-Methylpentane
012    1.  6 14  0  0  0  0 BA   2-ME-C5
013   3-Methylpentane
013    1.  6 14  0  0  0  0 BA   3-ME-C5
014   n-Hexane
014    1.  6 14  0  0  0  0 NA   N-C6
018   Methylcyclopentane
018    1.  6 12  0  0  0  0 C    CYC-C6
020   2,4-Dimethylpentane or isomer
020    1.  7 16  0  0  0  0 BA   BR-C7
```

TABLE 22. LISTING OF THE AFGC.PRM DATA SET, GIVING THE MONSANTO GC-MS FEATURE NUMBERS, THE MONSANTO FEATURE IDENTIFICATIONS AND RELATED DATA, AND THE MODEL COMPOUNDS ASSIGNED TO EACH FEATURE (CONTINUED).

Data Format:

First record for each feature:	Feature No., Monsanto assignment[a]
Subsequent records for feature:	Feature No., fraction contribution; No. carbons; No. hydrogens; No. oxygens; 0; 0; 0; Monsanto code; model compound used

021 3,3-Dimethylpentane
021 1. 7 16 0 0 0 0 BA BR-C_7
022 Cyclohexane
022 1. 6 12 0 0 0 0 C CYC-C_6
023 Benzene
023 1. 6 6 0 0 0 0 SB BENZENE
024 2,3-Dimethylpentane
024 1. 7 16 0 0 0 0 BA BR-C_7
025 2-Methylhexane
025 1. 7 16 0 0 0 0 BA BR-C_7
026 3-Methylhexane
026 1. 7 16 0 0 0 0 BA BR-C_7
027 1,3-Dimethylcyclopentane (trans)
027 1. 7 14 0 0 0 0 C CYC-C_7
028 1,3-Dimethylcyclopentane (cis)
028 1. 7 14 0 0 0 0 C CYC-C_7
029 1,2-Dimethylcyclopentane (trans)
029 1. 7 14 0 0 0 0 C CYC-C_7
030 3-Ethylpentane
030 1. 7 16 0 0 0 0 BA CYC-C_7
031 n-Heptane
031 1. 7 16 0 0 0 0 NA N-C_7
036 Methylcyclohexane
036 1. 7 14 0 0 0 0 C ME-CYCC$_6$
037 1,2,3-Trimethylcyclopentane or isomer
037 1. 8 16 0 0 0 0 C CYC-C_8
038 2,2,3,3-Tetramethylbutane
038 1. 8 18 0 0 0 0 BA BR-C_8
039 Ethylcyclopentane
039 1. 7 14 0 0 0 0 C CYC-C_7
040 2,5-Dimethylhexane or isomer + 4,5-Dimethyl-1-hexene or isomer
040 .5 8 18 0 0 0 0 BA BR-C_8
040 .5 8 16 0 0 0 0 E C_8-OLE1
041 2,4-Dimethlyhexane or isomer
041 1. 8 18 0 0 0 0 BA BR-C_8
042 1a,2b,4a-1,2,4-Trimethylcyclopentane or isomer
042 1. 8 16 0 0 0 0 C CYC-C_8

TABLE 22. LISTING OF THE AFGC.PRM DATA SET, GIVING THE MONSANTO GC-MS FEATURE NUMBERS, THE MONSANTO FEATURE IDENTIFICATIONS AND RELATED DATA, AND THE MODEL COMPOUNDS ASSIGNED TO EACH FEATURE (CONTINUED).

Data Format:

First record for each feature:	Feature No., Monsanto assignment[a]
Subsequent records for feature:	Feature No., fraction contribution; No. carbons; No. hydrogens; No. oxygens; 0; 0; 0; Monsanto code; model compound used

```
043   3,3-Dimethylhexane or isomer
043    1.  8 18  0  0  0  0 BA   BR-C8
044   1a,2a,3b-1,2,3-Trimethylcyclopentane or isomer
044    1.  8 16  0  0  0  0 C    CYC-C8
045   2,3,4-Trimethylpentane or isomer
045    1.  8 18  0  0  0  0 BA   BR-C8
046   2,3,3-Trimethylpentane or isomer
046    1.  8 18  0  0  0  0 BA   BR-C8
048   1,1,2-Trimethylcyclopentane
048    1.  8 16  0  0  0  0 C    CYC-C8
049   3-Ethyl-2-methylpentane or isomer
049    1.  8 18  0  0  0  0 BA   BR-C8
050   Toluene
050    1.  7  8  0  0  0  0 SB   TOLUENE
052   2-Methylheptane or isomer
052    1.  8 18  0  0  0  0 BA   BR-C8
053   4-Methylheptane or isomer
053    1.  8 18  0  0  0  0 BA   BR-C8
054   2,3,4-Trimethyl-2-pentene or isomer
054    1.  8 18  0  0  0  0 E    C8-OLE2
055   trans-1,4-Dimethylcyclohexane or isomer
055    1.  8 16  0  0  0  0 C    CYC-C8
056   3-Methylheptane or isomer
056    1.  8 18  0  0  0  0 BA   BR-C8
057   3-Methyl-1-butanol or isomer
057    1.  5 12  1  0  0  0 A    MEK
058   trans-1-Ethyl-3-methylcyclopentane or isomer
058    1.  8 16  0  0  0  0 C    CYC-C8
059   cis-1-Ethyl-3-methylcyclopentane or isomer
059    1.  8 16  0  0  0  0 C    CYC-C8
060   trans-4-Octene or isomer
060    1.  8 16  0  0  0  0 E    C8-OLE2
062   trans-1,2-Dimethylcyclohexane or isomer
062    1.  8 16  0  0  0  0 C    CYC-C8
064   cis-1,4-Dimethylcyclohexane or isomer
064    1.  8 16  0  0  0  0 C    CYC-C8
065   cis-1,4-Dimethylcyclohexane or isomer
065    1.  8 16  0  0  0  0 C    CYC-C8
```

TABLE 22. LISTING OF THE AFGC.PRM DATA SET, GIVING THE MONSANTO GC-MS FEATURE NUMBERS, THE MONSANTO FEATURE IDENTIFICATIONS AND RELATED DATA, AND THE MODEL COMPOUNDS ASSIGNED TO EACH FEATURE (CONTINUED).

Data Format:

First record for each feature:	Feature No., Monsanto assignment[a]
Subsequent records for feature:	Feature No., fraction contribution; No. carbons; No. hydrogens; No. oxygens; 0; 0; 0; Monsanto code; model compound used

066 n-Octane
066 1. 8 18 0 0 0 0 NA N-C_8
071 2,3,5-Trimethylhexane or isomer
071 1. 9 20 0 0 0 0 BA BR-C_9
073 cis-1,2-Dimethylcyclohexane or isomer
073 1. 8 16 0 0 0 0 C CYC-C_8
074 2,2-Dimethylheptane or isomer
074 1. 9 20 0 0 0 0 BA BR-C_9
075 Ethylcyclohexane or isomer
075 1. 8 16 0 0 0 0 C ET-CYCC_6
076 1,1,3-Trimethylcyclohexane or isomer
076 1. 9 18 0 0 0 0 C CYC-C_9
077 1a,3a,5a-1,3,5-Trimethylcyclohexane or isomer
077 1. 9 18 0 0 0 0 C CYC-C_9
078 2,6-Dimethylheptane or isomer
078 1. 9 20 0 0 0 0 BA BR-C_9
079 2,5-Dimethylheptane or isomer
079 1. 9 20 0 0 0 0 BA BR-C_9
082 1a,2b,4b-1,2,4-Trimethylcyclohexane or isomer
082 1. 9 18 0 0 0 0 C CYC-C_9
083 3-Ethyl-2-methylhexane or isomer
083 1. 9 18 0 0 0 0 BA BR-C_9
088 Ethylbenzene
088 1. 8 10 0 0 0 0 SB ALK1BENZ
089 2,3-Dimethylheptane or isomer
089 1. 9 20 0 0 0 0 BA BR-C_9
090 4-Ethylheptane or isomer
090 1. 9 20 0 0 0 0 BA BR-C_9
091 1,4-Dimethylbenzene or isomer
091 1. 8 10 0 0 0 0 SB P-XYLENE
092 4-Methyloctane or isomer
092 1. 9 20 0 0 0 0 BA BR-C_9
093 2-Methyloctane or isomer
093 1. 9 20 0 0 0 0 BA BR-C_9
095 3-Ethylheptane or isomer
095 1. 9 22 0 0 0 0 BA BR-C_9
096 3-Methyloctane or isomer
096 1. 9 20 0 0 0 0 BA BR-C_9

TABLE 22. LISTING OF THE AFGC.PRM DATA SET, GIVING THE MONSANTO GC-MS FEATURE NUMBERS, THE MONSANTO FEATURE IDENTIFICATIONS AND RELATED DATA, AND THE MODEL COMPOUNDS ASSIGNED TO EACH FEATURE (CONTINUED).

Data Format:

First record for each feature: Feature No., Monsanto assignment[a]

Subsequent records for feature: Feature No., fraction contribution; No. carbons; No. hydrogens; No. oxygens; 0; 0; 0; Monsanto code; model compound used

```
098   {C10-cycloalkane or alkene}
098    1. 10 22  0  0  0  0 C    CYC-C10
099   3,4,4-Trimethyl-2-hexene or isomer
099    1.  9 18  0  0  0  0 E    C9-OLE2
100   {C3-substituted hexene or cyclohexane}
100    1.  9 18  0  0  0  0 C    CYC-C9
102   1,2-Dimethylbenzene
102    1.  8 10  0  0  0  0 SB   O-XYLENE
106   {C10-cycloalkane or alkene}                        ???
106    1. 10 20  0  0  0  0 C    CYC-C10
107   1-Ethyl-4-methylcyclohexane (trans) or isomer
107    1.  9 18  0  0  0  0 C    CYC-C9
108   1-Ethyl-4-methylcyclohexane (cis) or isomer
108    1.  9 18  0  0  0  0 C    CYC-C9
109   n-Nonane
109    1.  9 20  0  0  0  0 NA   N-C9
112   2-Methyloctanhydropentalene or isomer              ??STRUCTURE??
112    1.  9 16  0  0  0  0 D    CYC-C9
113   (1-Methylethyl)cyclohexane or isomer
113    1.  9 18  0  0  0  0 C    CYC-C9
114   2-Methyl-4,5-nonadiene or isomer
114    1. 10 18  0  0  0  0 D    C9-OLE2
116   {C10-alkane} + (1-Methylethyl)benzene or isomer
116    .5 10 22  0  0  0  0 BA   BR-C10
116    .5  9 12  0  0  0  0 SB   ALK2BENZ
117   {Alkene >C7} {Cycloalkane >C7}                        ??
117    .8  9 18 00 00 00 00 E    CYC-C9
117    .2  9 18 00 00 00 00 C    C9-OLE2
118   Propylcyclohexane or isomer
118    1.  9 18  0  0  0  0 C    CYC-C9
119   2,5-Dimethyloctane or isomer
119    1. 10 22  0  0  0  0 BA   BR-C10
120   2,7-Dimethyloctane or isomer
120    1. 10 22  0  0  0  0 BA   BR-C10
122   2,6-Dimethyloctane or isomer
122    1. 10 22  0  0  0  0 BA   BR-C10
123   3-Ethyl-2-methylheptane or isomer
123    1. 10 22  0  0  0  0 BA   BR-C10
```

TABLE 22. LISTING OF THE AFGC.PRM DATA SET, GIVING THE MONSANTO GC-MS FEATURE NUMBERS, THE MONSANTO FEATURE IDENTIFICATIONS AND RELATED DATA, AND THE MODEL COMPOUNDS ASSIGNED TO EACH FEATURE (CONTINUED).

Data Format:

First record for each feature:	Feature No., Monsanto assignment[a]
Subsequent records for feature:	Feature No., fraction contribution; No. carbons; No. hydrogens; No. oxygens; 0; 0; 0; Monsanto code; model compound used

```
125   1,4-Dimethylcyclooctane or isomer
125    1. 10 20  0  0  0  0 C/E  CYC-C10
126   Propylbenzene or isomer
126    1.  9 12  0  0  0  0 SB   ALK1BENZ
127   1-Ethyl-2,3-dimethylcylcohexane or isomer
127    1. 10 20  0  0  0  0 C    CYC-C10
128   3-Ethyl-2-methylheptane or isomer
128    1. 10 22  0  0  0  0 BA   BR-C10
129   1-Ethyl-3-methylbenzene or isomer
129    1.  9 12  0  0  0  0 SB   O-XYLENE
130   3-(2-Methylpropyl)cyclohexene or isomer
130    1. 10 18  0  0  0  0 D    C10-OLE2
131   1,3,5-Trimethylbenzene or isomer
131    1.  9 12  0  0  0  0 SB   135-TMB
132   4-Methylnonane or isomer
132    1. 10 22  0  0  0  0 BA   BR-C10
133   2-Methylnonane or isomer
133    1. 10 22  0  0  0  0 BA   BR-C10
135   {C10-alkene} {C10-cycloalkane}
135    .2 10 20  0  0  0  0 E    C10-OLE2
135    .8 10 20  0  0  0  0 C    CYC-C10
136   3-Methylnonane or isomer + 1-Ethyl-2-methylbenzene or isomer
136    .5 10 22  0  0  0  0 BA   BR-C10
136    .5  9 12  0  0  0  0 SB   O-XYLENE
137   1-Methyl-4-(1-methylethyl)cyclohexane (cis) or isomer
137    1. 10 20  0  0  0  0 C    CYC-C10
139   4-Ethyl-2-octene or isomer
139    1. 10 20  0  0  0  0 C/E  C10-OLE2
140   5-Methyl-4-nonene or isomer
140    1. 10 20  0  0  0  0 C/E  C10-OLE2
142   1-Decene or isomer
142    1. 10 20  0  0  0  0 E    C10-OLE1
144   1,2,4-Trimethylbenzene or isomer
144    1.  9 12  0  0  0  0 SB   124-TMB
145   {C10-alkene} {C10-cycloalkane}
145    .2 10 20  0  0  0  0 E    C10-OLE2
145    .8 10 20  0  0  0  0 C    CYC-C10
```

TABLE 22. LISTING OF THE AFGC.PRM DATA SET, GIVING THE MONSANTO GC-MS FEATURE NUMBERS, THE MONSANTO FEATURE IDENTIFICATIONS AND RELATED DATA, AND THE MODEL COMPOUNDS ASSIGNED TO EACH FEATURE (CONTINUED).

Data Format:

First record for each feature: Feature No., Monsanto assignment[a]

Subsequent records for feature: Feature No., fraction contribution; No. carbons; No. hydrogens; No. oxygens; 0; 0; 0; Monsanto code; model compound used

```
146   4-Propyl-3-heptane or isomer
146    1. 10 20  0  0  0  0 E    BR-C10
149   n-Decane
149    1. 10 22  0  0  0  0 NA   N-C10
150   (1-Methylpropyl)benzene or isomer
150    1. 10 14  0  0  0  0 SB   ALK2BENZ
152   1,2,3-Trimethylbenzene or isomer
152    1.  9 12  0  0  0  0 SB   123-TMB
153   {Branched alkane + ?}                          ??
153    1. 11 24  0  0  0  0 BA   BR-C11
154   1-Methyl-4-(1-methylethyl)benzene or isomer
154    1. 10 14  0  0  0  0 SB   P-XYLENE
155   1-Methyl-2-(1-methylethyl)benzene or isomer
155    1. 10 14  0  0  0  0 SB   O-XYLENE
156   {Probably C11 branched alkane + C12 cycloalkane}
156    .8 11 24  0  0  0  0 BA   BR-C11
156    .2 12 24  0  0  0  0 C    C12-OLE2
157   {Probably C11 branched alkane + C12 cycloalkane}
157    .8 11 24  0  0  0  0 BA   BR-C11
157    .2 12 24  0  0  0  0 C    C12-OLE2
158   {Alkene, probably C11 (MW 154)}
158    1. 11 22  0  0  0  0 E    C11-OLE2
159   {Alkene, probably C11 (MW 154)}
159    1. 11 22  0  0  0  0 E    C11-OLE2
161   6-Ethyl-2-methyloctane or isomer (MW 156)
161    1. 11 24  0  0  0  0 BA   BR-C11
163   trans-Decahydronaphthalene + {C11 C/E}
163    1. 10 12  0  0  0  0 DC   CYC-C10
165   {Alkene, alkyne, or diene (MW 154-168)}        ???
165    1. 11 22  0  0  0  0 C/E  C11-OLE2
166   1,2-Diethylbenzene or isomer
166    1. 10 14  0  0  0  0 SB   O-XYLENE
167   1-Methyl-4-propylbenzene or isomer
167    1. 10 14  0  0  0  0 SB   P-XYLENE
168   1-Methyl-2-propylbenzene or isomer
168    1. 10 14  0  0  0  0 SB   O-XYLENE
169   {C4-benzene}
169    1. 10 14  0  0  0  0 SB   ALK2BENZ
```

TABLE 22. LISTING OF THE AFGC.PRM DATA SET, GIVING THE MONSANTO GC-MS FEATURE NUMBERS, THE MONSANTO FEATURE IDENTIFICATIONS AND RELATED DATA, AND THE MODEL COMPOUNDS ASSIGNED TO EACH FEATURE (CONTINUED).

Data Format:

First record for each feature:	Feature No., Monsanto assignment[a]
Subsequent records for feature:	Feature No., fraction contribution; No. carbons; No. hydrogens; No. oxygens; 0; 0; 0; Monsanto code; model compound used

```
170   1-Ethyl-2,4-dimethylbenzene or isomer
170    1. 10 14  0  0  0  0 SB   ALK3BENZ
173   5-Methyldecane or isomer + {C4-benzene}
173    .5 11 24  0  0  0  0 BA   BR-C11
173    .5 10 14  0  0  0  0 SB   ALK2BENZ
174   4-Methyldecane or isomer
174    1. 11 24  0  0  0  0 BA   BR-C11
175   2-Methyldecane or isomer
175    1. 11 24  0  0  0  0 BA   BR-C11
176   {Cycloalkane/alkene (MW=154)}
176    .8 11 22  0  0  0  0 C    CYC-C11
176    .2 11 22  0  0  0  0 E    C11-OLE2
177   3-Methyldecane or isomer + {C4-benzene}
177    .5 11 24  0  0  0  0 BA   BR-C11
177    .5 10 14  0  0  0  0 SB   ALK2BENZ
178   3-Methyldecane or isomer + {C4-benzene}
178    .5 11 24  0  0  0  0 BA   BR-C11
178    .5 10 14  0  0  0  0 SB   ALK2BENZ
179   6-Methyl-4-decene or isomer 2-Ethyl-1,3-dimethylbenzene or isomer
179    .5 11 22  0  0  0  0 E    C11-OLE2
179    .5 10 14  0  0  0  0 SB   ALK3BENZ
180   3-Methyl-4-decene or isomer
180    1. 11 22  0  0  0  0 E    BR-C11
181   1-Ethyl-2-propylcyclohexane or isomer
181    1. 11 22  0  0  0  0 C    CYC-C11
182   2,2-Dimethyl-3-decene or isomer
182    1. 12 24  0  0  0  0 E    C12-OLE2
183   3-Methyl-4-decene or isomer
183    1. 11 22  0  0  0  0 E    C11-OLE2
184   {Cycloalkane/alkene (MW=154)}
184    .8 11 22  0  0  0  0 C    CYC-C11
184    .2 11 22  0  0  0  0 E    C11-OLE2
186   1-Methyl-trans-bicyclo[4.4.0]decane + ?
186    1. 11 20  0  0  0  0 DC   CYC-C11
187   n-Undecane
187    1. 11 24  0  0  0  0 NA   N-C11
189   {Branched alkane}
189    1. 11 24  0  0  0  0 BA   BR-C12
```

TABLE 22. LISTING OF THE AFGC.PRM DATA SET, GIVING THE MONSANTO GC-MS FEATURE NUMBERS, THE MONSANTO FEATURE IDENTIFICATIONS AND RELATED DATA, AND THE MODEL COMPOUNDS ASSIGNED TO EACH FEATURE (CONTINUED).

Data Format:

First record for each feature: Feature No., Monsanto assignment[a]

Subsequent records for feature: Feature No., fraction contribution; No. carbons; No. hydrogens; No. oxygens; 0; 0; 0; Monsanto code; model compound used

```
191   C4-benzene + {unknown}
191    1. 10 14  0  0  0  0 SB   ALK2BENZ
193   C4-benzene + 2-Methyl-trans-bicyclo[4.4.0]decane or isomer
193    .5 10 14  0  0  0  0 SB   ALK2BENZ
193    .5 11 20  0  0  0  0 DC   CYC-C11
194   2,8-Dimethylundecane or isomer + {Cycloalkane or alkene}
194    1. 13 28  0  0  0  0 BA   BR-C11
195   2,7-Dimethylundecane or isomer + {unknown}
195    1. 13 28  0  0  0  0 BA   BR-C11
199   Pentylcyclohexane or isomer C12-Branched alkane
199    .5 11 22  0  0  0  0 C    CYC-C11
199    .5 12 26  0  0  0  0 BA   BR-C12
200   C12-Branched alkane
200    1. 12 26  0  0  0  0 BA   BR-C12
205   4-Methylindan or isomer + C5-Benzene + 5-Methyl-5-undecene or isomer
205 .3333 10 12  0  0  0  0 I    TETRALIN
205 .3333 11 16  0  0  0  0 SB   ALK3BENZ
205 .3333 12 24  0  0  0  0 E    C12-OLE2
206 X 1,2,3,4-Tetramethylbenzene or isomer + C5-Benzene + {Cycloalkane or
206   alkene}
206   .25 10 14  0  0  0  0 SB   ALK4BENZ
206   .25 11 16  0  0  0  0 SB   ALK3BENZ
206   .25 11 24  0  0  0  0 SB   ALK2BENZ
206   .25 12 24  0  0  0  0 E    CYC-C12
207   {Triply hydrogen-deficient molecule + cycloalkane or alkene}
207    .3 11 22  0  0  0  0 T    CYC-C11
207    .5 12 24  0  0  0  0 C    CYC-C12
207    .2 12 24  0  0  0  0 E    C12-OLE2
208 X p-Isobutyltoluene or isomer + {cycloalkane or alkene} +
208   Tetralin or isomer
208 .3333 11 16  0  0  0  0 SB   P-XYLENE
208 .3333 12 24  0  0  0  0 C    CYC-C12
208 .3333 10 12  0  0  0  0 TT   TETRALIN
210 X 2,2-Dimethyl-3-decene or isomer + C5-Benzene + {Doubly hydrogen-
210   deficient molecule}
210 .3333 12 24  0  0  0  0 C/E  C12-OLE2
210 .3333 11 16  0  0  0  0 SB   ALK3BENZ
210 .3333 12 22  0  0  0  0 D    CYC-C12
```

TABLE 22. LISTING OF THE AFGC.PRM DATA SET, GIVING THE MONSANTO GC-MS FEATURE NUMBERS, THE MONSANTO FEATURE IDENTIFICATIONS AND RELATED DATA, AND THE MODEL COMPOUNDS ASSIGNED TO EACH FEATURE (CONTINUED).

Data Format:

First record for each feature:	Feature No., Monsanto assignment[a]
Subsequent records for feature:	Feature No., fraction contribution; No. carbons; No. hydrogens; No. oxygens; 0; 0; 0; Monsanto code; model compound used

```
211   6-Methylundecane or isomer
211    1. 12 26  0  0  0  0 BA   BR-C12
212   C5-Benzene + 5-Methylundecane or isomer
212    .5 11 16  0  0  0  0 SB   ALK3BENZ
212    .5 12 26  0  0  0  0 BA   BR-C12
214   C5-Benzene + 4-Methylundecane or isomer
214    .5 11 16  0  0  0  0 SB   ALK3BENZ
214    .5 12 26  0  0  0  0 BA   BR-C12
216 X 2-Methylundecane or isomer + 2,3-Dimethyldecahydronaphthalene or
216   isomer + {cycloalkane or alkene}
216    .5 12 26  0  0  0  0 BA   BR-C12
216    .5 12 22  0  0  0  0 DC   CYC-C12
216    .0 12 24  0  0  0  0 E    C12-OLE2
217   Naphthalene
217    1. 10  8  0  0  0  0 SN   NAPHTHAL
218   3-Methylundecane or isomer
218    1. 12 26  0  0  0  0 BA   BR-C12
219   1,2-Dimethylindan + 4,6,8-Trimethyl-1-nonene or isomer
219    .5 11 14  0  0  0  0 I    TETRALIN
219    .5 12 24  0  0  0  0 E    C12-OLE1
220 X 1-Ethyl-2,4,5-trimethylbenzene or isomer +
220   1-Methyl-2-pentylcylohexane or isomer
220    .5 11 16  0  0  0  0 SB   ALK4BENZ
220    .5 12 24  0  0  0  0 C    CYC-C12
221   1-Dodecene or isomer + {1-ET-Indan or C1-tetralin} + ET-Decalin
221 .3333 12 24  0  0  0  0 C/E  C12-OLE1
221 .3333 11 14  0  0  0  0 I    TETRALIN
221 .3333 12 22  0  0  0  0 DC   CYC-C12
222 X 1-Ethyl-1-methylindan or isomer + {C2-Indan or C1-Tetralin +
222   unknown} + C6-Benzene
222 .3333 12 16  0  0  0  0 I    TETRALIN
222 .3333 11 14  0  0  0  0 I    TETRALIN
222 .3333 12 18  0  0  0  0 SB   ALK4BENZ
223   1-Methyl-4-(1-methylbutyl)cyclohexane or isomer
223    1. 12 24  0  0  0  0 C    CYC-C12
```

TABLE 22. LISTING OF THE AFGC.PRM DATA SET, GIVING THE MONSANTO GC-MS FEATURE NUMBERS, THE MONSANTO FEATURE IDENTIFICATIONS AND RELATED DATA, AND THE MODEL COMPOUNDS ASSIGNED TO EACH FEATURE (CONTINUED).

Data Format:

First record for each feature: Feature No., Monsanto assignment[a]

Subsequent records for feature: Feature No., fraction contribution; No. carbons; No. hydrogens; No. oxygens; 0; 0; 0; Monsanto code; model compound used

---

```
224   C5-Benzene + C6-Benzene + {C12-Cycloalkane or alkene}
224 .3333 11 16  0  0  0  0 SB   ALK4BENZ
224 .3333 12 18  0  0  0  0 SB   ALK4BENZ
224 .3333 12 24  0  0  0  0 C    CYC-C12
225   C5-Benzene + C12-Cycloalkane or alkene + C2-Decalin
225 .3333 12 16  0  0  0  0 SB   ALK4BENZ
225 .6667 12 24  0  0  0  0 C    CYC-C12
227   n-Dodecane
227    1. 12 26  0  0  0  0 NA   N-C12
228   {Bicycloalkane + ?}
228    1. 12 22  0  0  0  0 D    CYC-C12
231   6-Tridecene or isomer + 1,6-Dimethyldecahydronaphthalene or isomer
231    .5 13 26  0  0  0  0 E    C13-OLE2
231    .5 12 22  0  0  0  0 D    CYC-C12
232   2,6,7-Trimethyldecane or isomer
232    1. 13 26  0  0  0  0 BA   BR-C13
237   {Alkene or cycloalkane}
237    .2 12 24  0  0  0  0 E    C12-OLE2
237    .8 13 24  0  0  0  0 C    CYC-C13
238   (4-Methylpentyl)cyclohexane or isomer
238    1. 12 24  0  0  0  0 C    CYC-C12
239   1-Butyl-2-propylcyclopentane or isomer
239    1. 12 24  0  0  0  0 C/E  CYC-C12
240   {?}
240    1. 13 26  0  0  0  0 D    CYC-C12
241   1,2-Dibutylcyclopentane or isomer + ?
241    1. 13 26  0  0  0  0 C/E  CYC-C13
242   2,3-Dihydro-4,6-dimethyl-1H-indene or isomer + ?
242    1. 11 14  0  0  0  0 I    TETRALIN
243 X (2,2-Dimethylbutyl)benzene or isomer + 2,3,4-Trimethyldecane or
243   isomer
243    .5 12 18  0  0  0  0 SB   ALK1BENZ
243    .5 13 28  0  0  0  0 BA   BR-C13
244   5-Methyldodecane or isomer
244    1. 13 28  0  0  0  0 BA   BR-C13
245   2,3-Dimethylundecane or isomer
245    1. 13 28  0  0  0  0 BA   BR-C13
```

TABLE 22. LISTING OF THE AFGC.PRM DATA SET, GIVING THE MONSANTO GC-MS FEATURE NUMBERS, THE MONSANTO FEATURE IDENTIFICATIONS AND RELATED DATA, AND THE MODEL COMPOUNDS ASSIGNED TO EACH FEATURE (CONTINUED).

Data Format:

First record for each feature:	Feature No., Monsanto assignment[a]
Subsequent records for feature:	Feature No., fraction contribution; No. carbons; No. hydrogens; No. oxygens; 0; 0; 0; Monsanto code; model compound used

```
246   2-Methyldodecane or isomer
246    1. 13 28  0  0  0  0 BA   BR-C13
247   {Substituted benzene}
247    1. 11 20  0  0  0  0 SB   ALK3BENZ
248   3-Methyldodecane or isomer + ?
248    1. 13 28  0  0  0  0 BA   BR-C13
249   4,6-Dimethylundecane or isomer
249    1. 13 28  0  0  0  0 BA   BR-C13
253 X 2-Methylnaphthalene
253   1,1,3-Trimethyl-2,3-dihydro-1H-indene or isomer
253    1. 11 10  0  0  0  0 SN   TETRALIN
256   1-Methylnaphthalene
256    1. 11 10  0  0  0  0 SN   ME-NAPH
257   n-Tridecane
257    1. 13 28  0  0  0  0 NA   N-C13
259   {C14 Branched alkane + ?}
259    1. 14 30  0  0  0  0 BA   BR-C14
260   {Branched alkene or alkane + ?}
260    .2 12 24  0  0  0  0 BA+  C12-OLE2
260    .8 14 24  0  0  0  0 C/E  CYC-C14
261   6-Methyltridecane or isomer + {C/E}
261    1. 14 30  0  0  0  0 BA   BR-C14
262   6-Methyltridecane or isomer + {C/E}
262    1. 14 30  0  0  0  0 BA   BR-C14
264 X {Branched alkane + ?}
264   1-Heptylcyclohexane or isomer
264    1. 14 30  0  0  0  0 BA+  CYC-C14
266   {Cycloalkane or alkene}
266    .8 12 24  0  0  0  0 C    CYC-C12
266    .2 12 24  0  0  0  0 E    C12-OLE2
270 X 6-Methyltridecane or isomer
270   {Unknown}
270    1. 14 30  0  0  0  0 BA   BR-C14
272   4-Methyltridecane or isomer
272    1. 14 30  0  0  0  0 BA   BR-C14
```

TABLE 22. LISTING OF THE AFGC.PRM DATA SET, GIVING THE MONSANTO GC-MS FEATURE NUMBERS, THE MONSANTO FEATURE IDENTIFICATIONS AND RELATED DATA, AND THE MODEL COMPOUNDS ASSIGNED TO EACH FEATURE (CONCLUDED).

Data Format:

First record for each feature:	Feature No., Monsanto assignment[a]
Subsequent records for feature:	Feature No., fraction contribution; No. carbons; No. hydrogens; No. oxygens; 0; 0; 0; Monsanto code; model compound used

```
273   {Branched alkane}
273    .5 13 28  0  0  0  0 BA   BR-C13
273    .5 14 30  0  0  0  0 BA   BR-C14
274   {Branched alkane}
274    1. 15 32  0  0  0  0 BA   BR-C15
275   {Branched alkane} + 2-Ethylnaphthalene or isomer
275    .5 15 32  0  0  0  0 BA   BR-C15
275    .5 12 16  0  0  0  0 SN   ME-NAPH
278   {Cycloalkane or alkene} + 2,6-Dimethylnaphthalene or isomer
278    .5 14 28  0  0  0  0 C    CYC-C14
278    .5 12 16  0  0  0  0 SN   DM-NAPH
279   n-Tetradecane + 2,7-Dimethylnaphthalene or isomer
279    .8 14 28  0  0  0  0 NA   N-C14
279    .2 12 16  0  0  0  0 SN   DM-NAPH
281 X 1,5-Dimethylnaphthalene or isomer + {Diene, bicyclic or cyclic
281   alkene}
281    .5 12 16  0  0  0  0 SN   DM-NAPH
281    .5 15 28  0  0  0  0 D    CYC-C15
282 X 1,5-Dimethylnaphthalene or isomer + {Diene, bicyclic or cyclic
282   alkene}
282    .5 12 16  0  0  0  0 SN   DM-NAPH
282    .5 15 28  0  0  0  0 D    CYC-C15
285   {Unknown mixture}
285    1. 15 32 00 00 00 00 C/E  BR-C15
294   {Branched alkane}
294    .5 15 32  0  0  0  0 BA   BR-C15
294    .5 16 34  0  0  0  0 BA   BR-C16
296   n-Pentadecane
296    1. 15 32  0  0  0  0 NA   N-C15
297 X n-Hexadecane
297   Anthracene-d10
297    .0 00 34  0  0  0  0 NA   REF-STD.
```

[a]If an "X" is in Column 5, then the Monsanto assignment continues on to the next record.

• A computer program is then run which reads the 1AJP4.GCD and the AFGC.PRM data sets and uses the data there to determine the relative composition of the fuel in terms of the species in the model, and outputs these data in a form which can be read by the model calculation software. This same program can be run using .GCD files for other fuels, to derive the fuel composition in terms of the species in this model, provided that the GC feature numbers used are consistent with those used in the Monsanto study. However, we did not process such data for any other fuel, since the "reference" JP-4 fuel is the only one for which both environmental chamber data results and detailed GC-MS analyses are available.

The composition of the "reference" JP-4 fuel, given in terms of the species included in this model and derived using the procedure discussed, is shown in Table 23. This analysis accounts for 95.9 percent of the fuel (by weight); the remaining 4.1 percent was associated with GC feature numbers for which no assignment is given in the Monsanto report (Reference 29), and is not represented in the composition shown in Table 23. This analysis indicates that this fuel consists of ~80 percent (by carbon) alkanes, ~15 percent aromatics, and ~5 percent compounds which are identified as alkenes. However, as indicated by the question marks and other comments in Table 22, a number of the assignments are considered to be uncertain, particularly for the higher molecular weight constituents.

The result that the fuel contains ~5 percent (by carbon) alkenes is somewhat inconsistent with what would be expected from this type of fuel, and is subject to question. As far as we are aware, the alkene assignments are not based on any positive identification, and the GC-MS analysis in many cases cannot definitively distinguish between high molecular weight alkenes and cycloalkanes of the same molecular weight (Reference 66). In many cases, the Monsanto assignments indicate that a given GC feature may be either a cycloalkane, an alkene, or a mixture of the two, and we had to make an arbitrary assignment of the relative amounts of each. Thus, the possibility that many, if not most, of the components identified as alkenes may in fact be cycloalkanes cannot be ruled out. Indirect evidence that the actual alkene content of this fuel

TABLE 23. COMPOSITION OF THE "REFERENCE" JP-4 FUEL, GIVEN IN TERMS OF THE SPECIES NAMES USED IN THIS MODEL.

Name	ppb $ppmC^{-1}$	Mole %	Carbon %
n-Alkanes	31.97	27.02	26.37
$N\text{-}C_4$	0.53	0.44	0.21
$N\text{-}C_5$	2.83	2.39	1.41
$N\text{-}C_6$	4.62	3.91	2.77
$N\text{-}C_7$	6.27	5.30	4.39
$N\text{-}C_8$	5.87	4.96	4.70
$N\text{-}C_9$	3.14	2.65	2.83
N-C10	2.28	1.92	2.28
N-C11	2.48	2.09	2.72
N-C12	1.84	1.55	2.20
N-C13	1.44	1.22	1.87
N-C14	0.52	0.44	0.73
N-C15	0.17	0.14	0.25
Branched Alkanes	42.11	35.59	36.13
$ISO\text{-}C_5$	1.86	1.57	0.93
23-DMB	0.21	0.17	0.12
$2\text{-}ME\text{-}C_5$	0.04	0.03	0.02
$3\text{-}ME\text{-}C_5$	1.89	1.59	1.13
$BR\text{-}C_7$	8.09	6.84	5.66
$BR\text{-}C_8$	12.69	10.72	10.15
$BR\text{-}C_9$	7.14	6.03	6.43
BR-C10	3.72	3.15	3.72
BR-C11	2.68	2.27	3.02
BR-C12	1.09	0.92	1.30
BR-C13	1.95	1.65	2.54
BR-C14	0.44	0.37	0.61
BR-C15	0.26	0.22	0.39
BR-C16	0.07	0.06	0.11
Cycloalkanes	22.39	18.92	17.86
$CYC\text{-}C_6$	4.89	4.13	2.93
$CYC\text{-}C_7$	3.06	2.58	2.14
$ME\text{-}CYCC_6$	4.06	3.43	2.84
$CYC\text{-}C_8$	3.35	2.83	2.68
$ET\text{-}CYCC_6$	0.48	0.41	0.38
$CYC\text{-}C_9$	2.52	2.13	2.27
CYC-C10	1.22	1.03	1.22
CYC-C11	0.77	0.65	0.84
CYC-C12	1.60	1.35	1.93

TABLE 23. COMPOSITION OF THE "REFERENCE" JP-4 FUEL, GIVEN IN TERMS OF THE SPECIES NAMES USED IN THIS MODEL (CONCLUDED).

Name	ppb $ppmC^{-1}$	Mole %	Carbon %
CYC-C13	0.17	0.14	0.22
CYC-C14	0.20	0.17	0.28
CYC-C15	0.09	0.08	0.14
Alkyl-benzenes	14.85	12.55	12.73
BENZENE	1.08	0.91	0.65
TOLUENE	2.30	1.94	1.61
P-XYLENE	2.49	2.11	2.11
O-XYLENE	2.11	1.78	1.87
135-TMB	0.19	0.16	0.17
124-TMB	1.48	1.25	1.33
123-TMB	0.74	0.62	0.66
ALK1BENZ	1.43	1.21	1.20
ALK2BENZ	1.58	1.34	1.57
ALK3BENZ	1.13	0.96	1.18
ALK4BENZ	0.34	0.29	0.39
Tetralins and Naphthalenes	2.06	1.74	2.25
TETRALIN	0.87	0.73	0.95
NAPHTHAL	0.62	0.53	0.62
ME-NAPH	0.20	0.17	0.23
DM-NAPH	0.37	0.31	0.44
Identified as Alkenes	4.70	3.97	4.54
C_8-OLE1	0.27	0.22	0.21
C_8-OLE2	1.31	1.11	1.05
C_9-OLE2	0.65	0.55	0.59
C10-OLE2	0.82	0.69	0.82
C10-OLE1	0.09	0.08	0.09
C12-OLE2	0.45	0.38	0.54
C11-OLE2	0.98	0.83	1.08
C12-OLE1	0.07	0.06	0.09
Alcohol[a]			
MEK	0.23	0.20	0.12

[a]Represented by MEK in the model.

may in fact be much less than this analysis indicates comes from the results of the model simulations of the environmental chamber runs using this fuel, discussed in the following section.

b. Results of Simulations of the Fuel Experiments

A summary of the model predictions of the ozone yields and the ozone formation and NO oxidation rates for the "reference JP-4 experiments is shown in Table 19, and experimental and calculated concentration-time plots for selected species in representative ITC and EC runs employing this fuel are shown in Figures 15 and 16. Two sets of model calculations were carried out, one based on the composition derived as a result of the processing of the Monsanto GC-MS data and GC-MS peak assignments, and the other based on the assumption that fuel constituents identified by the Monsanto GC-MS assignments as alkenes are, in fact, their cycloalkane isomers. These results show that the assumptions made regarding the nature of the fuel constituents identified as alkenes have a significant effect on the result of these model calculations, despite the fact that they amount to only ~5 percent of the fuel. If alkenes are assumed to be present in this fuel at the ~5 percent level as indicated by the Monsanto GC-MS assignments, then this model significantly overpredicts the rates of ozone formation and NO oxidation observed in these chamber runs.

On the other hand, if the constituents identified as alkenes are assumed to be in fact cycloalkanes, then the model performs considerably better in the simulations of these experiments. However, even with this modification, the model performance in simulating the runs with the "reference" JP-4 fuel is not quite as good as the simulations of most of the runs with the synthetic fuels, whose compositions are (presumably) accurately known. The model consistently overpredicts the maximum ozone yields observed in the JP-4 experiments, and underpredicts the NO oxidation and ozone formation rates in the ITC experiments, and overpredicts them in the EC runs. It is difficult to determine to what extent these discrepancies are due to uncertainties regarding the exact composition of this fuel, as opposed to possible problems with the chemical model. However, in view of the significant effect on the model predictions of

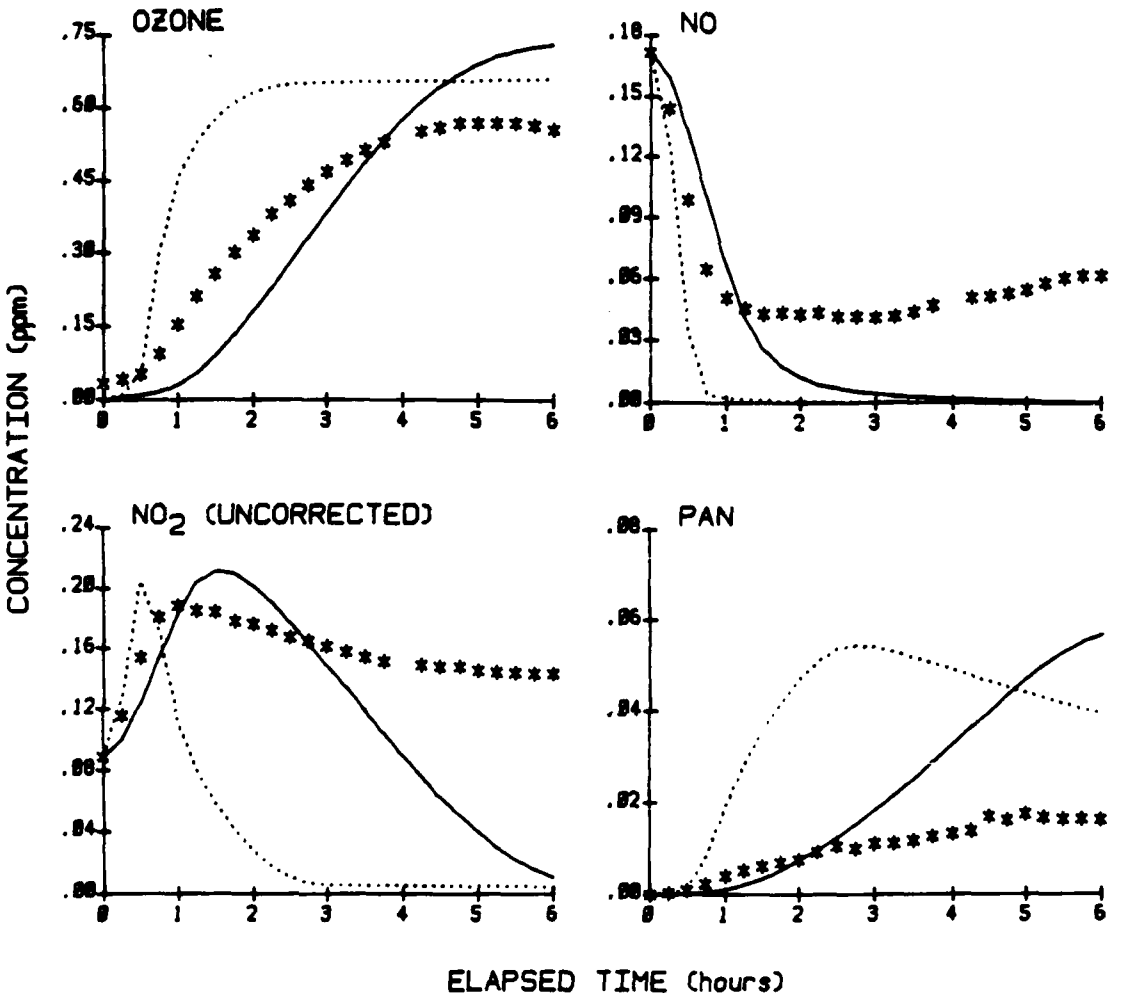

Figure 15. Experimental and Calculated Concentration-Time Profiles for Selected Species Observed in the "Reference" JP-4 Experiment ITC-966.

_____ = Model Calculation Using Fuel Alkenes Based on Monsanto GC-MS Assignments.

. . . = Model Calculation Assuming GC-MS Peaks Assigned as Alkenes are Actually Cycloalkanes.

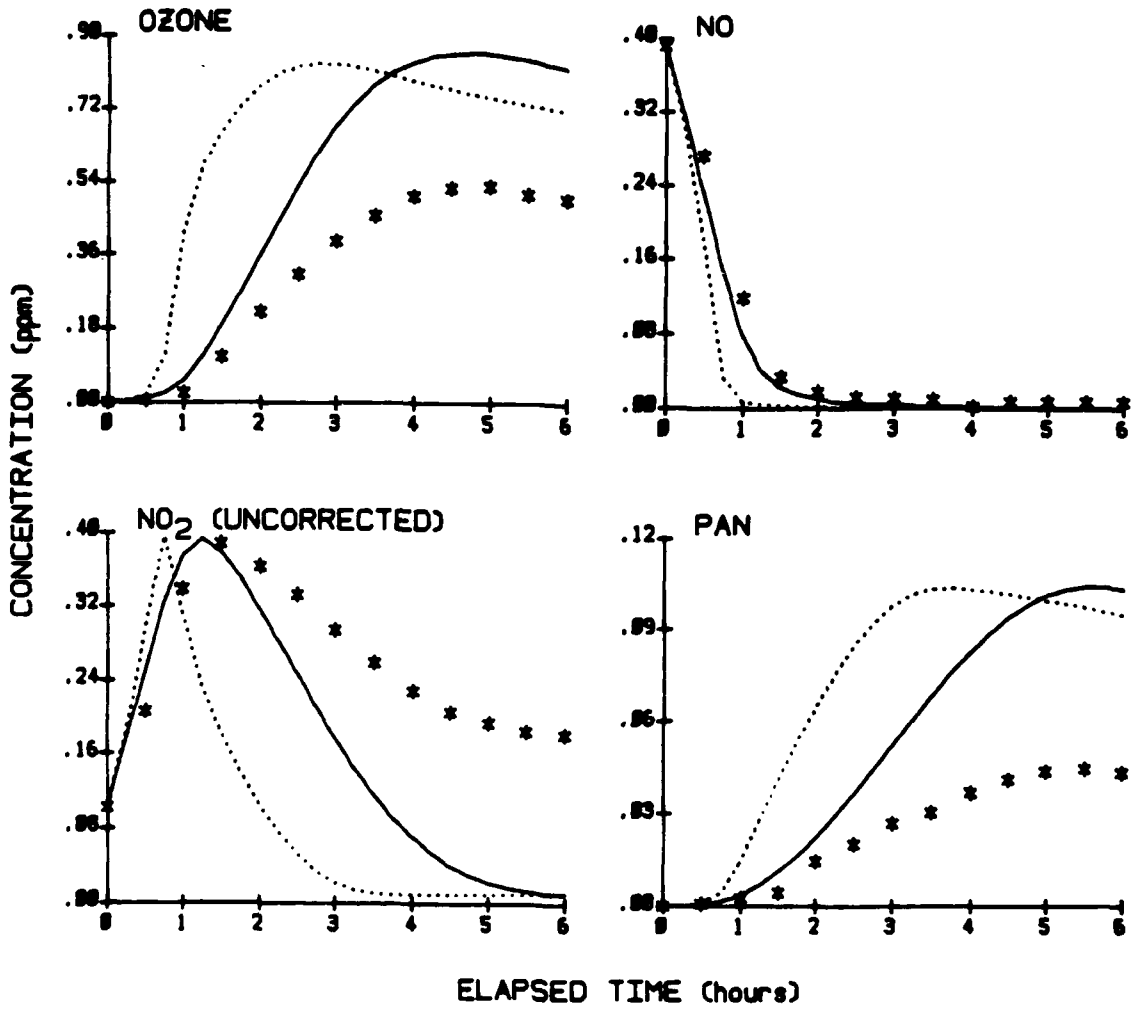

Figure 16. Experimental and Calculated Concentration-Time Profiles for Selected Species Observed in the "Reference" JP-4 Experiment EC-492.

_____ = Model Calculation Using Fuel Alkenes Based on Monsanto GC-MS Assignments.

. . . = Model Calculation Assuming GC-MS Peaks Assigned as Alkenes are Actually Cycloalkanes.

assumptions made regarding highly uncertain and questionable assignments of the ~5 percent of the fuel which were identified as alkenes, it appears more likely that the uncertainty regarding the composition of the fuel is the greater factor. Additional work is required to more firmly establish the chemical nature of these relatively minor fuel constituents before runs with real JP-4 fuels can be used for reliable model testing, or before the atmospheric reactivities of these fuels can be reliably predicted, based on results of detailed analyses of their constituents.

4. Summary of Model Performance in Simulations of Our Full EPA and USAF Environmental Chamber Data Base

The Air Force-funded experiments discussed previously were not the only runs used to test this chemical mechanism. As part of a related program carried out under EPA funding, the results of over 400 additional chamber experiments, conducted in four different chambers operated by two different research groups, were also used to test major portions of this model. The chambers whose data were employed include not only the SAPRC EC and ITC used for these Air Force runs, but also the ~50,000-liter SAPRC Outdoor Teflon® Chamber (OTC), and the University of North Carolina's (UNC) ~150,000-liter dual outdoor chamber. The results of this testing are documented in detail in two recent EPA reports (References 26, 63). These reports should be consulted for details concerning how the chamber characterization parameters were derived, and the results of simulations of individual experiments. However, these results are summarized briefly to give a more comprehensive view of the performance of this model in simulating the available data base of environmental chamber experiments. This includes results of simulations of experiments carried out in this Air Force program which were not given in the previous EPA reports.

Table 24 summarizes the number of the various types of runs which were modeled, and averages of the biases and errors in the simulations of the maximum ozone yields, the average initial NO oxidation and ozone formation rates, and the maximum PAN yields. In general, the quality of fits of the model simulations to the chamber experiments on our data set were found to be variable, although in most cases (with the alkane-NO_x-air runs being the major exception) the model could predict maximum ozone

TABLE 24. AVERAGES OF PERCENTAGE BIASES[a] AND ERRORS[b] IN MODEL SIMULATIONS OF MAXIMUM OZONE YIELDS, AVERAGE NO OXIDATION AND OZONE FORMATION RATES, AND MAXIMUM PAN YIELDS FOR ALL RUNS USED FOR MODEL EVALUATION[c].

Run type Run type	No. runs	Maximum ozone		Avg. d/dt ($[O_3]$-[NO])[d]		Maximum PAN	
		Bias	Err.	Bias	Err.	Bias	Err.
Formaldehyde	15	-1	19	24	26		
Acetaldehyde	5	-26	26	-13	13	1	20
Other Carbonyls	5	4	44	0	20	193	207
Ethene	14	12	23	6	22		
Propene	49	3	18	13	26	34	45
1-Butene	11	17	39	30	42	-34	34
1-Hexene	4	-1	4	14	14		
trans-2-Butene	3	-29	29	24	25	-13	23
Isobutene	1	7	7	46	46	-69	69
n-Butane	27	26	62	38	56	44	95
Branched Alkanes	7	34	49	18	19	-70	70
C_5-C_9 n-Alkanes	13	53	64	7	29		
Methylcyclohexane	4	198	[e]198	51	51		
Benzene	6	4	5	19	22		
Toluene	20	13	24	9	20	25	45
Xylenes	10	-9	16	12	22	-6	23
Mesitylene	8	-11	21	15	16	-42	45
Tetralin	5	-16	21	-18	18		
Naphthalene	5	4	25	-1	9		
2,3-Dimethyl-naphthalene	4	-1	14	4	10	-25	38
Furan	4	-2	24	-3	10		
Thiophene	4	10	12	-2	12		
Pyrrole	4	-6	20	-10	14		
Acrolein[f]	5	10	33	68	68		
Simple Mixtures[g]	40	11	36	-1	20	44	65
Surrogate Mixes[h]	146	5	22	10	26	27	46
Auto Exhaust	28	-1	21	5	17	-2	33
Synthetic Jet Fuel	11	10	11	31	31		
"Reference" JP-4[i]	6	46	46	46	71		
Synthetic Jet Exhaust	4	-6	8	-11	11	50	50

TABLE 24. AVERAGES OF PERCENTAGE BIASES[a] AND ERRORS[b] IN MODEL SIMULATIONS OF MAXIMUM OZONE YIELDS, AVERAGE NO OXIDATION AND OZONE FORMATION RATES, AND MAXIMUM PAN YIELDS FOR ALL RUNS USED FOR MODEL EVALUATION[c] (CONCLUDED).

[a]Bias = Average percent discrepancy. Positive number means model prediction is high.

[b]Error = Average of absolute values of percent discrepancies.

[c]Excluding characterization runs or runs with whole fuels.

[d]Average NO oxidation/ozone formation rate = one half of the maximum change in ($[O_3]$-[NO]), divided by the time required to achieve this change.

[e]Discrepancy shown is for only one experiment. The other methylcyclohexane experiments did not form enough ozone for meaningful comparison.

[f]Represented by propionaldehyde in the model.

[g]"Simple" mixtures = mixtures of more than one organic which do not have at least one each of an alkane, alkene, and aromatic.

[h]"Surrogate" mixtures = mixtures which have at least one each of an alkane, alkene, and aromatic.

[i]Model calculation assuming all GC peaks identified as "alkenes" are actually cycloalkanes.

yields and ozone formation and NO oxidation rates to within ± ~30 percent. The poorer performance of the model in simulating the alkane runs is due to the sensitivities of simulations of these runs to variabilities in chamber conditions, as discussed in Section IV.C.2.a. The model performed worse in simulations of PAN yields than in simulations of ozone yields or ozone formation and NO oxidation rates, as was also observed in the simulations of these Air force experiments. This was also the case for formaldehyde, where the model significantly underpredicted the formaldehyde yield observed in essentially all the UNC chamber experiments, at least when monitored by the usual technique employed at UNC, and was highly variable in the simulations of the SAPRC experiments (Reference 26). With formaldehyde, the poorer fits are almost certainly due to problems in accurately and precisely monitoring this compound in a routine manner; this may also be true for PAN.

Most of the discrepancies between model and experiments appeared to be random, with no apparent dependence of the quality of fits on initial reactant concentrations or ROG/NO_x ratios. In several cases, the

performance of the model depended on the time the experiment was carried out; this was observed in the simulations of the ethene runs carried out both in the EC and in the UNC chamber (Reference 26). In most other cases when a large number of comparable experiments were carried out, no such dependence could be determined.

In most cases, the model performed as well, if not better, in simulations of experiments with complex mixtures, as it did in simulations of runs with single organics or simple mixtures. This includes the UNC runs employing auto exhaust (Reference 67), the synthetic jet fuel and synthetic jet exhaust runs carried out in this study, as well as the many "urban surrogate"-NO_x-air irradiations which were modeled. It is not surprising that the model performance in simulations of complex mixtures is sometimes better than simulations of runs containing simpler mixtures or individual compounds because with many species present, the effects of uncertainties in the mechanism of any given compound would be relatively less important than when it is one of only a few reactants present. The possibility of cancellation of errors also becomes greater as the mixtures become more complex. This is why runs with mixtures were not used in optimizing uncertain mechanistic parameters during the course of the development of this model.

The apparent random nature of the discrepancies, and the apparent dependence in some cases on the time the experiments were carried out, suggests that problems in chamber characterization or characterization of the experimental conditions associated with the individual runs could account for some of the discrepancies observed. As previously discussed (Reference 26), characterization of chamber conditions remains a significant problem in comprehensive testing of atmospheric photochemical reaction mechanisms. The major uncertainties include, but are not limited to, problems in characterizing light intensity and spectral characteristics in outdoor chamber runs, and the variability of the chamber radical source. The results of appropriate characterization runs were used to determine appropriate values for chamber-dependent parameters, and factors which affect them, but the available characterization data are often limited. Even when available, such data are primarily useful in indicating the appropriate ranges for the values

of the chamber-dependent parameters, which may, in general, vary from run to run. No run to run optimization of chamber-dependent parameters was carried out as part of this model testing program. This would invalidate the purpose of such a study, because such optimization could mask problems with the chemical mechanism. Thus, variability in chamber characteristics not adequately represented in the model translates into variability in the quality of fits of the model predictions to the experimental results.

Even with the uncertainties and problems in accurate characterization of chamber effects, and the significant uncertainties in some areas of the reaction mechanism employed, it is encouraging that a current model can simulate at least the ozone yields and formation rates in most experiments to within ~30 percent. Since this is the only atmospheric photochemical mechanism which has been tested in a consistent manner against such a comprehensive data base, it is unclear whether any other current mechanism, based on alternative assumptions concerning the existing areas of uncertainty, can perform any better in simulations of the available data set. However, we believe that the mechanism developed and tested in this and our related EPA program represents the current state of the art, and that it is unlikely better results can be obtained without an improved understanding of atmospheric chemistry and chamber effects.

(The reverse of this page is blank)

SECTION V

ATMOSPHERIC PHOTOCHEMICAL REACTIVITY MODEL

The practical application of the chemical mechanism developed under this program for assessing atmospheric photochemical reactivities of fuels, exhausts, and other pollutants of interest to the Air Force requires use of air quality simulation models and associated software. Thus, as a second major component of Phase II of this program, an atmospheric photochemical reactivity modeling system was developed for use by the Air Force. This system consists of a series of computer programs and data files which can be used to conduct airshed model simulations of the type needed to assess photochemical reactivities of emitted pollutants under conditions representative of the atmosphere. This modeling system is discussed in detail in a separate User's Manual and associated appendixes (Reference 28). In this section, an overview of this airshed modeling system and associated software is given, with several examples of the types of reactivity assessment calculations for which it can be utilized.

A. OVERVIEW OF THE MODEL

Airshed models can vary greatly in complexity, ranging from simple "rollback" models which do not take into account the nature of the specific airshed involved or the chemical composition of the reactive organics emitted, to complex, multicelled "grid" models, which have large data requirements and require extensive computational resources. Except for the simplest versions, all airshed models have two major components: (1) the representation of the chemistry (i.e., the chemical nature of the emitted pollutants and the reactions they undergo), and (2) the representation of the physical conditions associated with the airshed into which the emissions are occurring, referred to as the model "scenario." Scenarios include such factors as atmospheric mixing heights, transport of pollutants, how emissions change with time and location, initial conditions, temperature, and relative humidity. In practice, because of computer constraints, to be useful airshed models must incorporate

extensive simplifications and approximations in at least one, if not both, of the major components. The nature of such simplifications determines the applications for which a given model is appropriate. For example, a model with extremely detailed representation of the chemistry but which represents the entire airshed as a single "box" would not be particularly useful in assessing effects of moving emissions sources from one area of the airshed to another. On the other hand, a model with a highly simplified representation of the chemistry would not be useful in assessing effects of changes in pollutant chemical composition, such as might occur, for example, if there were major changes in the formulation of fuels emitted into particular airsheds.

The essential purpose of the modeling system developed in this program is the estimation of the effects of changing the chemical composition of emitted mixtures, specifically turbine engine fuel and jet exhaust, on resulting photochemical air pollution levels. Therefore, this model is of the type which employs a highly detailed representation of the chemical transformations which occur in photochemical air pollution systems. The chemical mechanism incorporated in this model, discussed in the previous section of this report, is a much more comprehensive mechanism than usually employed in airshed models, and represents the atmospheric reactions of many different types of emitted ROG species, including those species representative of the major anthropogenic emissions into urban airsheds, as well as the major components of turbine engine fuels and jet exhaust. Because this model incorporates such a detailed representation of the chemical transformations, it contains a more approximate representation of the physical characteristics of each airshed whose air quality is being simulated.

The formulation of the physical scenarios which can be represented by this model is based on the "floating box" approach. In this approach, a single well-mixed air mass of constant volume but with variable area (determined by the mixing height which generally changes with time), moves from place to place, receiving emissions from the areas over which it moves. This formulation neglects exchange of pollutants from nearby air masses, other than input of pollutants aloft (if any) which are entrained into the air mass as the inversion height rises. It also assumes that

mixing of emitted pollutants between the ground and the inversion height is essentially instantaneous, and that a large air mass can retain its integrity throughout the day. The latter assumption neglects the possibility of wind shear and other factors which might result in much more complex mixing patterns. Although this formulation is obviously a simplification of reality, it does permit a relatively large degree of flexibility in representing conditions of particular airsheds. For example, it permits varying both the composition and the rates of pollutant emission with time, and can represent an air mass moving from an industrial to a nonindustrial area, or from a rural area to an Air Force base to another rural area, etc. It also permits variation in meteorological factors such as changes in inversion height with time and specification of dilution, temperature, and light intensity. This allows for a relatively wide degree of flexibility in the ranges of conditions which can be represented. In addition, it allows the effects of changes in the composition of emissions to be assessed under a range of conditions which can represent, at least semiquantitatively, the range of conditions which can occur in real airsheds.

This model uses essentially the same physical formulation as employed in the EPA's EKMA models, used to estimate the amount of total ROG control required to achieve a desired reduction in total ozone formation to comply with Federal air quality standards for ozone (References 68-71). In the case of the EKMA models, the EPA supplies a standard set of recommended "default" model inputs to be used where the appropriate input data are not known, but it recommends that local agencies use "city-specific" inputs to represent the conditions of the specific airsheds of interest, whenever possible. The problem of deriving the appropriate set of model inputs in this model for defining scenarios for reactivity assessment purpose under the conditions of a specific airshed of interest is entirely analogous, and the same types of input data are required. This modeling system could be used to carry out EKMA analyses, though it has not been specifically designed for this purpose.

The principal application for which this modeling system was designed is to assess the relative atmospheric reactivities of types of mixtures of reactive volatile organic compounds which can be emitted into the

atmosphere, and are of interest to the USAF and other potential users. In the context of this model, the "atmospheric reactivity" of a "test mixture" (or test compound) under the conditions of a given pollution scenario is defined as the effect on some measure of air quality. An example would be the maximum amount of photochemically formed ozone, caused by the emission of given amounts of the test mixture (or compound) when it is emitted into an air basin or an air parcel under a given set of conditions defined by the scenario. Note that the reactivity of the test compound or mixture will, in general, depend on these conditions (Reference 72); therefore, these conditions must be represented as accurately as possible to obtain an appropriate estimate of the effects of the emissions of the test substance. In particular, the air parcel of interest may already be polluted as a result of emissions from other sources besides those emitting the test compound or mixture whose reactivities are being assessed, and the presence of these other "base case" or "background" pollutants can have a significant effect on the calculated reactivities of the test substances (Reference 72). This reactivity assessment modeling system allows the presence of initial, "background" pollutants, and emissions of "base-case" (i.e., non "test") pollutants to be specified as parts of the overall airshed scenario, allowing these important effects to be taken into account.

This modeling system can be used to assess the reactivities of a variety of substances and test mixtures. Specific types of mixtures of particular interest to the Air Force for which this model has been developed include turbine engine fuels and jet exhaust, but this system can also be used for assessing the atmospheric reactivities of many other types of mixtures of hydrocarbons and oxygenated species, such as motor vehicle fuels and exhausts, hydrocarbon solvents, and other types of chemical compounds or mixtures which might be emitted into the atmosphere from military, governmental or private sector activities. The specific types of compounds and mixtures to which the present version of this atmospheric photochemical reactivity model can be applied are listed in Section IV.B. Several examples of reactivity assessment calculations, illustrating how this model can be applied, are given in the following section.

B. EXAMPLES OF ATMOSPHERIC REACTIVITY ASSESSMENT APPLICATIONS

The software and data files, as initially installed on the USAF computers at Tyndall AFB and Brooks AFB, include all the data files necessary to carry out example reactivity assessment calculations. These include data files defining the conditions of several representative idealized pollution scenarios which can be used for reactivity assessment calculations, and data files giving the compositions of the representative synthetic fuels and of the synthetic exhaust mixture which were employed in the chamber experiments. The conditions of several of the representative model scenarios are summarized in this section, and the calculated atmospheric reactivities for the representative surrogate fuel and exhaust mixtures are given.

The representative model scenarios included in the initial distribution of this model are based on the standard city-specific EKMA inputs recommended by Gipson and Freas (Reference 70) of the EPA for use in Regulatory Impact Analyses for the national ozone standard. These are designed to represent, though not replace, input data for the various city-specific EKMA models used in State Implementation Plans. For this purpose, Gipson and Freas divided the country into three regions on the basis of the mixing heights (i.e., the maximum amount of dilution occurring throughout the day), and specified inputs for EKMA model calculations designed to represent the conditions of those three regions. In the calculations reported here, the specific scenarios employed are designated EKMA1 and EKMA3. The EKMA1 scenario is based on the input data Gipson and Freas recommend for the low dilution region (Region I), and the EKMA3 scenarios employ the mixing height schedule they recommend for Region III, the highest dilution region.

The input data used to define these scenarios are summarized in Table 25. All of these "EKMA" scenarios are 1-day simulations [starting at 0800 Local Daylight Time (LDT) and ending at 2100 LDT], with a fraction of the reactive organics and NO_x assumed to be present initially and with the remainder being emitted at a constant rate until 1500 LDT, when it is assumed that the air parcel is transported out of the source region. The inversion height is assumed to increase throughout the day, based roughly

TABLE 25. SUMMARY OF THE INPUT DATA FOR THE "EKMA" SCENARIOS USED IN THE REACTIVITY ASSESSMENT EXAMPLES.

Scenario	EKMA-1	EKMA-3
Latitude	34.1	39.75
Date	June 21	June 21
Temperature (K)	300	300
Relative Humidity (%)	50	50
Calc. Sunrise (LDT)[a]	0552	0552
Sunset (LDT)	2008	2008
Inversion Height Schedule, ground[b]	(LDT) (m)	(LDT) (m)
	0552 250	0552 250
	0651 250	0651 250
	1247 492	1247 2492
	1613 600	1613 3500
	2100 600	2100 3500
Simulation Start Time (LDT)	0800	0800
Simulation End time (LDT)	2100	2100
Initial + Emitted ROG (millimoles C m^{-2} day^{-1})	12.0	12.0
Initial + Emitted NO_x	Varied from 0.3 to 3.0 millimoles m^{-2} day^{-1} Initial and Emitted $[NO_2]/[NO]$ = 3.0	
Initial Pollutants:		
ROG	67.1% of total ROG input	
NO_x	56.5% of total NO_x input	
ROG and NO_x Emissions Schedule[c]	(LDT) (fac)	(LDT) (fac)
	0800 1	0800 1
	1430 1	1430 1
	1530 0	1530 0
	2100 0	2100 0

[a]No correction made for latitude; i.e., differences between local sun time and standard clock time neglected.

[b]Values used for intermediate times obtained by interpolating between tabulated values.

[c]Emissions schedules are given as relative emission rates (factors) at various times, with factors for intermediate times obtained by interpolating between tabulated values. Absolute emissions rates are such that the total daily "initial + emitted" ROG and NO_x are as tabulated above.

AD-A190 690 ATMOSPHERIC PHOTOCHEMICAL MODELING OF TURBINE ENGINE FUELS AND EXHAUSTS P..(U) CALIFORNIA UNIV RIVERSIDE STATEWIDE AIR POLLUTION RESEARCH CE.. 3/3

UNCLASSIFIED W O CARTER ET AL. MAY 88 F/G 4/1 NL

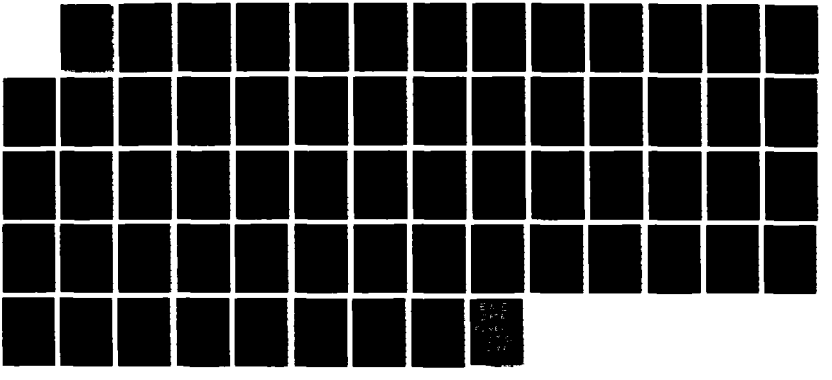

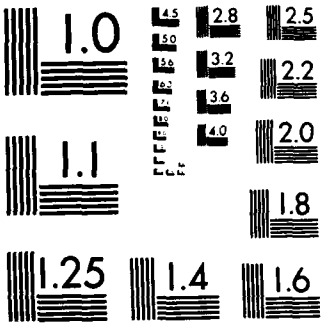
1.0
1.1
1.25
1.4
1.6
1.8
2.0
2.2
2.5
2.8
3.2
3.6
4.0
4.5
5.0
5.6

on the "characteristic curve" used as the default in the OZIPP software (Reference 73) with the main difference between these two scenarios being the maximum inversion height attained. As the inversion height increases, pollutants present in the air mass aloft are mixed into the ground layer and can affect the reactions occurring there. In standard EKMA calculations, the composition of the pollutants aloft (presumed to result from previous days pollution or transport from downwind source areas) must be specified in the input data. Gipson and Freas (Reference 70) recommend assuming 0.07 ppm ozone aloft, and Gipson (Reference 74) considers approximately 20 ppbC of ROG and negligible NO_x aloft to be typical of many situations; this was assumed in both these scenarios. The composition of the aloft ROG is based on the recommendation given by the EPA (Reference 71) for use as defaults when employing the Carbon Bond mechanism (References 22, 23) for EKMA calculations; since these are given as carbon bond species, they were translated into the representative molecular species utilized by the present model. The composition of the aloft species used in the EKMA scenarios are given in Table 26.

Most polluted airsheds have ROG emissions from other sources besides that producing the mixture whose reactivities are being assessed, and the presence of these additional pollutants can significantly affect calculated reactivities of the test mixtures (Reference 72). In the

TABLE 26. COMPOSITION OF ALOFT MIXTURE USED IN THE REACTIVITY ASSESSMENT EXAMPLES.

Species	Concentration (ppb)
Ozone	70
n-Butane	2.51
Ethene	0.60
Propene	0.30
Benzene	0.125
Toluene	0.375
Formaldehyde	1.50
Acetaldehyde	1.50

context of this model, these are designated the "base case" ROG emissions, since they would occur even if the pollution source whose reactivity is being assessed were removed. In these EKMA scenarios, the surrogate mixture used to represent base case ROG emissions is that designed by the researchers at Systems Applications, Inc. (SAI) to represent current emissions into the California South Coast Air Basin. In terms of "Carbon Bond" species (References 22, 23), the composition of this surrogate is almost identical with that recommended by the EPA for use in EKMA calculations in cases where no composition data are available (Reference 71). This mixture has been employed in a number of environmental chamber studies as a representative of current urban ROG emissions (References 31, 38, 75). The composition of this surrogate is given in Table 27.

The emission of NO_x is another very important component in the "base case" emissions into the reactivity assessment scenarios. The reactivity assessment calculations in this example were carried out with the initial NO_x level varied, corresponding to base case ROG/NO_x ratios of 4, 8, 15, and 40 ppmC ROG/ppm NO_x. (The software included with this model allows a series of calculations with one parameter varied to be carried out automatically, without having to give separate commands for each calculation. The emitted NO_x level is the varied parameter in all the scenarios delivered with this model, although other scenario parameters could be varied if desired.) The NO_x level is varied because the ROG/NO_x ratio is extremely important in affecting reactivities of organics (Reference 72). The ratios of 4-40 ppmC ROG/ppm NO_x represents the typical range of NO_x conditions encountered in urban airsheds, from NO_x-rich to NO_x-poor, with the middle ratios generally representing the range of conditions most favorable to ozone formation.

As indicated above, the test mixtures for which composition data are included in the distribution of this model include the six synthetic jet fuels and one synthetic jet exhaust mixture employed in the experiments carried out under this program. These composition files are designated FUEL1, FUEL2 FUEL1F, FUEL1T, FUEL1P, and AFSYNEXH, respectively. The composition of FUEL1 was designed by USAF scientists to represent JP-4 fuels currently in use; FUEL2 is similar to FUEL1 but the total aromatic

TABLE 27. COMPOSITION OF THE SURROGATE MIXTURE USED TO REPRESENT BASE CASE ROG EMISSIONS IN THE REACTIVITY ASSESSMENT EXAMPLES.

Component	PPB in 1 ppmC Mixture
n-Butane	37.5
n-Pentane	40.0
iso-Octane	18.75
Ethene	25.0
Propene	16.7
Toluene	17.86
m-Xylene	15.63
Formaldehyde	37.5
Unreactive	112.5

content is increased; FUEL3 is also similar to FUEL1 except that the ratio of alkylbenzenes to bicyclic aromatics was increased, while keeping the total aromatic content the same; and FUEL1F, FUEL1T, and FUEL1P are the same as FUEL1, except that they contain ~1 percent (on a mole carbon basis) of furan, thiophene, or pyrrole, respectively, to represent fuels with these potential impurities. The composition of the mixture designated AFSYNEXH is the synthetic jet exhaust mixture which was designed by USAF scientists, based on the results of the jet exhaust analyses carried out at Battelle (Reference 41). The compositions of the surrogate fuel mixtures are summarized in Table 28; the composition of the synthetic exhaust mixture is given in Table 7, Section III.B.4.

The reactivity assessment calculations in this example consist of carrying out model simulations of the base case scenarios, i.e., the scenarios without any added test mixture, and then calculations in which the test mixture in amounts equal to 10 percent of the base case ROG emissions were added. The results of these calculations are summarized in Table 29, which gives the maximum ozone concentrations calculated for the base case simulations, and the increase (or decrease) in maximum ozone caused by the addition of the test mixtures. The latter quantities reflect the reactivities, with respect to atmospheric ozone formation, of these mixtures under the conditions of these scenarios.

TABLE 28. COMPOSITIONS OF THE REPRESENTATIVE SURROGATE JET FUELS USED IN THE REACTIVITY ASSESSMENT EXAMPLES.

Compound	ppb Compound/ppmC surrogate fuel					
	FUEL1	FUEL2	FUEL3	FUEL1F	FUEL1T	FUEL1P
n-Hexane	18.98	16.50	19.48	18.79	18.79	18.79
n-Heptane	25.40	21.71	25.97	25.15	25.15	25.15
n-Octane	23.36	19.88	23.85	23.12	23.12	23.12
n-Tetradecane	2.57	2.07	2.36	2.54	2.54	2.54
Cyclohexane	10.82	9.33	10.99	10.72	10.72	10.72
Methylcyclohexane	17.84	15.29	18.27	17.66	17.66	17.66
Ethylcyclohexane	3.12	2.50	3.00	3.09	3.09	3.09
Toluene	11.27	16.86	14.56	11.16	11.16	11.16
p-Xylene	2.50	3.75	3.25	2.47	2.47	2.47
Isopropylbenzene	2.11	2.89	2.55	2.09	2.09	2.09
1,3,5-Trimethylbenzene	3.33	4.56	3.89	3.30	3.30	3.30
Tetralin	4.40	5.90	2.70	4.35	4.35	4.35
Naphthalene	3.00	4.20	1.80	2.97	2.97	2.97
2-Methylnaphthalene	3.27	4.09	1.91	3.24	3.24	3.24
2,3-Dimethylnaphthalene	1.08	1.42	0.67	1.07	1.07	1.07
Furan				2.50		
Thiophene					2.50	
Pyrrole						2.50

TABLE 29. MAXIMUM BASE CASE OZONE LEVELS CALCULATED FOR THE EXAMPLE EKMA SCENARIO, AND CALCULATED CHANGES IN MAXIMUM OZONE CAUSED BY THE ADDITION OF REPRESENTATIVE TEST MIXTURES.

Scen.	ROG/NO_x	Base O_3 (ppb)	Change in maximum ozone (ppb)[a]						
			FUEL1	FUEL2	FUEL3	FUEL1F	FUEL1T	FUEL1P	SYNEXH
EKMA1	4	67	7.6	9.0	7.9	7.9	7.6	7.8	32.2
	8	204	9.1	9.6	9.4	9.3	9.0	9.2	26.4
	16	186	1.0	0.7	1.1	1.1	1.0	1.0	7.2
	40	132	-1.1	-1.3	-1.0	-1.1	-1.1	-1.1	1.6
EKMA3	4	82	3.4	3.8	3.5	3.5	3.4	3.5	11.7
	8	98	1.6	1.7	1.7	1.7	1.6	1.7	4.6
	16	88	0.6	0.6	0.6	0.6	0.6	0.6	2.5
	40	74	-0.1	-0.1	-0.1	-0.1	-0.1	-0.1	0.8

[a]Added test mixture = 10 percent of base case ROG emissions.

The results of these calculations show that the effect of the addition of these mixtures depend significantly on the ROG/NO_x ratio, being the greatest (on a percentage basis) at the lowest ratios. Indeed, the fuels are negatively reactive at the highest ROG/NO_x ratios; this can be attributed to the NO_x sinks in the reaction mechanisms of aromatic hydrocarbons and high molecular weight alkanes (Reference 72), which are the major constituents of these fuels. In line with the results of the chamber experiments, the synthetic exhaust mixture is seen to be much more reactive, at least in atmospheric ozone formation, than are the synthetic fuels. There appears to be relatively little difference between the fuels in their reactivities in these scenarios, even among those which are quite different in reactivity when irradiated by themselves in the environmental chamber experiments. For example, the addition of ~1 percent furan or pyrrole to the "standard" fuel had a very large effect on the rate of ozone formation when the fuel is irradiated by itself in the chamber experiments (see Figure 13, in Section IV.C.2.f), yet it had a relatively small effect on maximum ozone yields under the conditions of these scenarios, even at the lowest ROG/NO_x ratios. This illustrates that extrapolating relative reactivities observed in chamber experiments to conditions more representative to real airsheds, without taking the effects of differences between the conditions of the experiments and the airshed scenarios into account, can cause misleading results. Utilization of this model can provide a means to estimate atmospheric reactivities which can potentially take these differences into account.

This example focuses on the applications of this modeling system for reactivity assessment purposes, since the level of detail of the chemical model it employs makes it particularly suitable for this purpose. However, this model can be employed for other applications where box model airshed simulations might be useful, such as carrying out EKMA analyses, assessing the effects of proposed control strategies, assessing atmospheric impacts of proposed new emissions sources, or assessing the contribution of one particular emissions source (such as an Air Force base) on overall pollution levels in surrounding areas. Some of these applications require much more detailed information regarding the exact conditions of the airshed of interest and its various pollution sources

than is required for reactivity assessment calculations. For some purposes, models with more complex representations of spatial variations, meteorology, and transport conditions (and thus, necessarily more simplified representations of the chemical transformations than would be appropriate for reactivity assessment models), might be more appropriate. The user must be aware of the relative strengths and weaknesses of any model in determining whether it is the most appropriate model for his particular application.

C. MAJOR COMPONENTS OF THE MODEL SOFTWARE

The USAF atmospheric photochemical reactivity modeling system developed for this program incorporates a series of related computer programs and data files whose interrelationships are shown diagrammatically in Figure 17. Some of these programs and data files (e.g., the Model Preparation and Integration Programs, and the batch model input files) are transparent to the user. However, a general familiarity with the entire system is useful in understanding how the system works, and what can be done with it. The major components of the system are described below.

1. User Interface Program

The User Interface is an interactive program which the user can employ to conduct a wide variety of airshed model simulations employing "floating box" type scenarios. A minimum amount of training is required beyond an understanding of the principles involved in airshed model calculations, and appropriate values for the required input data. For reactivity assessment calculations, knowledge is also required of the chemical composition of the substances whose atmospheric reactivities are being assessed. The User Interface program is not strictly necessary to operate this modeling system, but is designed to simplify its use for the applications of interest. In particular, it is sufficiently flexible to be employed in the various applications mentioned earlier in the Introduction.

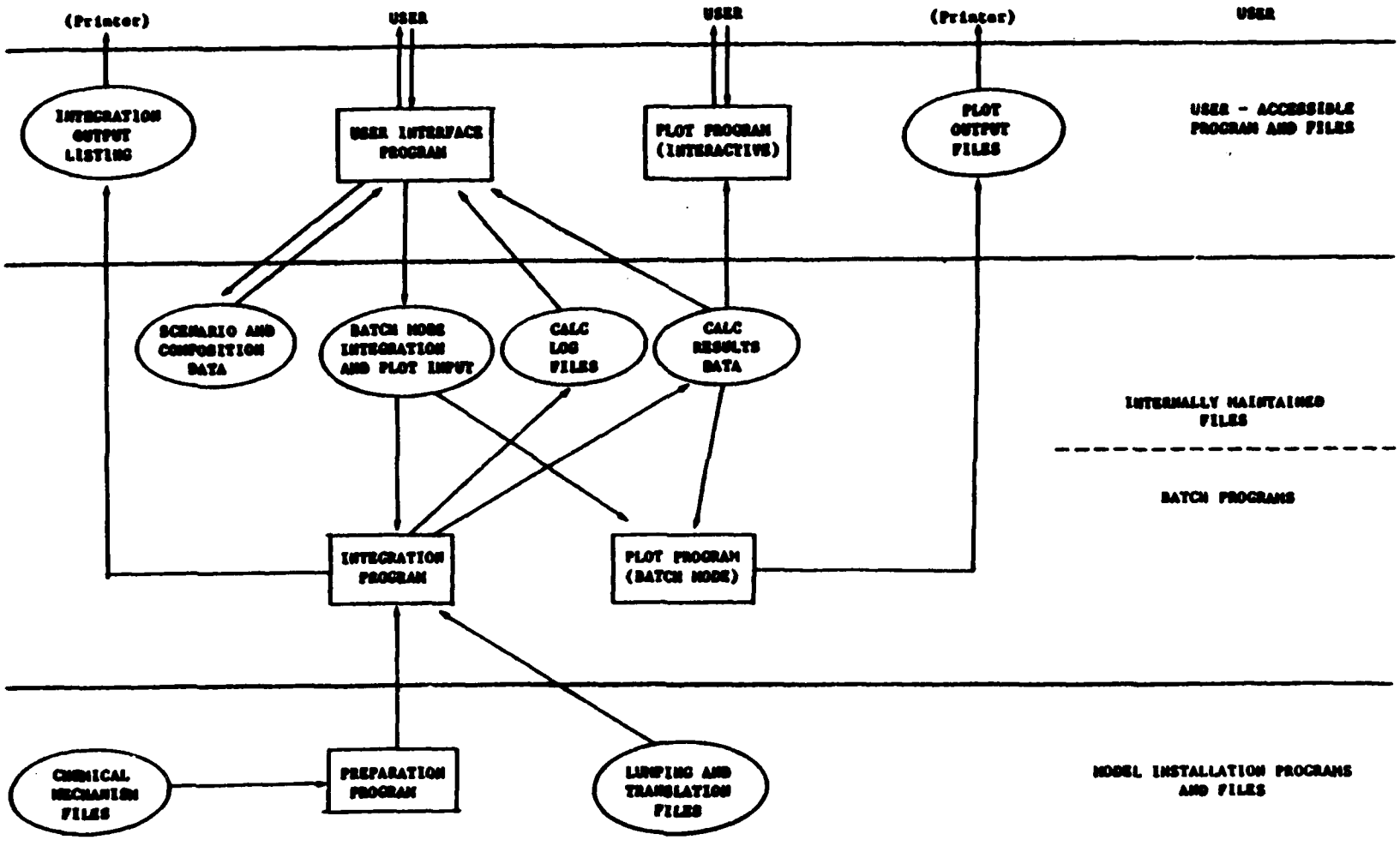

Figure 17. Components of the SAPRC-USAF Atmospheric Photochemical Modeling System and their Interrelationship.

The user can employ the User Interface program to carry out the following operations: (1) The user can define or modify conditions of model scenarios for airshed calculations, including (for example), amounts of base case ROG and NO_x emitted, schedules for base case ROG, NO_x, and test mixture emissions, schedules for how inversion height changes with time, the date and the latitude used in calculating the light intensity, the composition of base case ROG emissions, the composition of species present initially (background species), the composition of species present aloft which are entrained into the air mass as the inversion height increases, etc. (2) The user can define or modify "composition files," which are used to specify compositions of the test mixtures whose reactivities are to be assessed, the mixtures used to represent the base case ROG emissions, of the background species, and of the aloft species. (3) The user can give commands to cause the model simulations employing specified model scenarios and test mixtures to be conducted. The calculations are carried out externally to the program, using the model integration program discussed. (4) The user can examine, print, plot, or tabulate selected results of these calculations, once they have been completed.

The User Interface program indicates the type of input it expects at various points, checks for appropriate input, has a "HELP" feature to assist the user when necessary, and can optionally prompt the user for values for each of the various parameters required to define scenarios, leading the user through the process in a stepwise manner. The program allows named scenarios and compositions of mixtures to be saved for subsequent calculations employing different mixtures, scenarios, or relative emission levels. Calculations employing scenarios and mixtures which have already been defined can be started using single commands. The system is delivered with several representative scenarios and mixtures already defined. The user can employ these to carry out calculations immediately, or use these as starting points to define scenarios or mixtures of interest with respect to particular applications.

2. Plotting Program

The Plotting program can be used to produce page plots of concentration-time data calculated by the model for selected pollutants, and also to tabulate selected results of these calculations. It can also be used to plot results of chamber experiments, model simulations of chamber experiments, or the results of one model simulation against another. The features of the plot program are also available as part of the User Interface program. To use the Plotting program, the user must know the calculation number assigned to the particular simulation. The calculation number is given by the User Interface when the user issues the CALC command, and is also given in the output of the Integration program. The user can also use the LOG command in the User Interface, or examine the calculation logging file which gives the calculation numbers for the various simulations carried out. Alternatively, if the calculation was recently conducted, the user can employ zero or a negative number as a "relative" calculation number, which indicate the calculation number relative to the last calculation carried out.

The Plotting program can be used in three ways: (1) On an interactive basis, the user gives the list of compounds to be plotted or tabulated, and the calculation numbers (or chamber runs) whose data are to be plotted. The output will then go to the user's terminal, unless it is specified explicitly to produce the output in a file. This can be done either by invoking the PLOT feature of the User Interface, or by giving the system command to run the Plotting program externally to the User Interface. (2) The user can use the system editor to create an input file to the Plotting program, and then give the system command to run the program using that file as input. The program then produces an output file whose name is determined by the name of the input file (see Section IV). (3) If the user is doing the model calculations through the User Interface program, he can include as Output Options names of pollutants to plot and/or tabulate, and this will cause the User Interface to automatically run the Plotting program in batch mode. The Plotting output file so produced will either be automatically sent to the system line printer, or saved as a file (referenced by the calculation number), depending on the output options given to the User Interface.

3. Model Integration Program

The Model Integration program actually conducts the model simulations. It requires input data describing the conditions of the model scenario and the chemical species emitted or initially present. It utilizes these data, and the various data files implementing the chemical mechanism, to carry out the simulation by numerically integrating the differential equations involved. The results of the calculations are tabulated in an output file and are stored on disk for subsequent plotting or tabulation. Each calculation whose results are saved on disk are assigned a sequential "calculation number," which is used to reference the results of the calculation when using the User Interface or the Plotting program.

The user can utilize the Integration program in two ways: (1) by utilizing the User Interface program to produce the Integration program's input file and to automatically give the system commands to run the Integration program in batch mode or real time, or (2) by using the system editor to create or modify the Integration program input file specifying the model scenario and emitted species, and then explicitly giving the system commands to cause the program to be run. This program is usually run in a batch mode since, depending on the computer used and the complexity of the calculation being conducted, running this program can take significant computer time.

In either case, the Integration program does not prompt for any input from the user except for the name of the input file (if it was not given on the command line) and it normally does not produce any output to the user's terminal, other than a message indicating how many calculations were conducted. Explicitly creating the Integration program input file and running the program allows for full capability of the Integration program, but requires a detailed knowledge of the input requirements of this complex program, and is mainly for the advanced user. Using the User Interface to create the integration input file and run the program is designed to be much more suitable for use by the more inexperienced user, and is sufficiently flexible for most routine applications. It is the second method which is documented in this User's Manual.

4. Model Preparation Program

The Model Preparation program is used to process data files describing the chemical mechanism to produce the model-specific subroutines required by the Integration program (see below). It also produces other data files required to conduct model simulations using the chemical mechanism. The Model Preparation program needs to be run only when installing this system on a new computer, or when the chemical mechanism needs to be changed, and will not normally be run by the user of this modeling system. It is not an interactive program; the user must use the system editor to create or modify the input files, and its only normal output to the terminal is a simple message indicating that it is finished.

Making changes to the chemical mechanism may not only require running the Model Preparation program, but may also require changes in other data sets in this system (particularly if species are added or removed from the model). Thus, such changes should only be made by users who thoroughly understand all components of this system. In addition, making changes to the chemical mechanism without a knowledge of the relevant laboratory data which the existing mechanism is based, or without testing the revised model against the appropriate data base, may affect the validity of the model's predictions, and should be done with care.

(The reverse of this page is blank)

SECTION VI

CONCLUSIONS AND RECOMMENDATIONS

The ultimate goal of this 3-year program was to develop a computer model for the Air Force which can be used to predict the impacts on air quality of turbine engine fuel and exhaust emissions, and to predict the atmospheric impacts of future changes in jet fuel or exhaust compositions. This program has been successful in meeting this objective, and the Air Force now has a user-oriented computer model which can be applied to these and to other air pollution modeling applications. For example, this model can be used to predict the atmospheric reactivities of a wide variety of other types of VOC emissions, in addition to jet fuels and jet exhaust, including those classes of organic compounds for which environmental chamber data are available. Thus, the Air Force now has a useful tool in complying with local and Federal air quality regulations.

The most important part of this computer model is the chemical mechanism which describes the atmospheric transformations of the chemical components of jet fuels and/or jet exhaust. This chemical mechanism represents the current state of the art in our present understanding of atmospheric chemistry. It is an extension of the detailed mechanism we recently developed for the EPA, which was tested against data from almost 500 environmental chamber experiments, making it the most comprehensively tested photochemical transformation mechanism presently in existence. The ability to include in the model developed for the Air Force classes of compounds not previously included in atmospheric transformation models (e.g., naphthalenes and N, O- and S-heterocycles) is a major contribution of this program.

However, despite the significant advances resulting from this program in our ability to model the atmospheric photochemical transformations and atmospheric reactivities of complex organic mixtures such as the turbine engine fuels, it must be recognized that parts of the chemical mechanism developed in this study require further experimental study. In particular, significant uncertainties remain in our understanding of certain details of the photochemical transformations of the aromatic hydrocarbons under atmospheric conditions. In the case of the alkylbenzenes, which are

the most well-studied, very little is known concerning the details of the aromatic ring-opening processes, and the nature and reactions of the fragmentation products formed, beyond the fact that the products formed are obviously highly reactive. Additionally, very little is known about the atmospheric reactions, subsequent to the initial OH and NO_3 radical reactions, of tetralin, the naphthalenes, and the heteroatom-containing organics included in this model.

The reaction mechanisms of the alkanes with six or more carbon atoms are also not well-understood. Most of the higher alkanes undergo a significant degree of isomerization, resulting in the predicted formation of a large number of bi- and polyfunctional products. Although we have developed (in part for this program and in part for our related EPA programs) a predictive scheme for estimating the detailed processes involved and the products formed, no detailed product or mechanistic data presently exist to validate this scheme. In addition, the nitrate yields formed from the reactions of NO with the hydroxy-substituted peroxy radical intermediates predicted to be important in the photooxidations of the higher alkanes are unknown, and assumptions made concerning this have significant impacts on model predictions of alkane reactivity.

As noted above, the present atmospheric photochemical computer model developed for the Air Force represents the current state of the art, given the necessary tradeoffs between detailed chemical representation and computation time. However, a number of areas of uncertainty should be addressed to produce a new generation of more powerful and effective predictive models. Thus, a carefully designed and integrated program of experimental and modeling research should be undertaken toward this goal. Specifically, further research should focus on elucidating the atmospheric photooxidation reactions of aromatic compounds, heteroatom-containing organics and the long-chain alkanes.

In the meantime, to keep the present model current, it should be periodically updated to reflect new kinetic and mechanistic data from laboratories around the world. The Air Force may wish to contract for such updates either on an ongoing basis or about every 2 years.

Similarly, as computational methods become more efficient and powerful, the software associated with this model should be periodically

upgraded. For example, there is significant potential for software enhancement in the following areas: representing more complex scenarios, interfacing the output of analytical systems to the input of this model, expanding the present model to the full capabilities of the EPA's OZIPP programs (Reference 73), and implementing the model on other types of computers such as IBM PC/AT or System 2 type microcomputers.

(The reverse of this page is blank)

REFERENCES

1. Clewell, H.J., III, Fuel Jettisoning U. S. Air Force Aircraft, Volume 1, Summary and Analysis, ESL-TR-80-17, Engineering and Services Laboratory, Air Force Engineering and Services Center, Tyndall AFB, Florida, March 1980.

2. Conkle, J.P., Lackey, W.W., Martin, C.L., and Richardson, A., III, Organic Compounds in the Exhaust of a J85-5 Turbine Engine, Report No. SAM-TR-80-29, September 1980.

3. Churchill, A.V., Delaney, C.L., and Lander, H.R., "Future Aviation Turbine Fuels," Paper No. 78-268, presented at American Institute of Aeronautics and Astronautics 16th Aerospace Sciences Meeting, Huntsville, Alabama, 16-18 January 1978.

4. Bouble, R.W. and Martone, J.A., USAF Aircraft Engine Emission Goal: An Initial Review, ESL-TR-79-30, Engineering and Services Laboratory, Air Force Engineering and Services Center, Tyndall AFB, Florida, September 1979.

5. Scott, A.H., Jr., The Implications of Alternative Aviation Fuels on Airbase Air Quality, ESL-TR-80-38, Engineering and Services Laboratory, Air Force Engineering and Services Center, Tyndall AFB, Florida, August 1980.

6. Carter, W.P.L., Ripley, P.S., Smith, C. G., and Pitts, J.N., Jr., Atmospheric Chemistry of Hydrocarbon Fuels, ESL-TR-81-53, Engineering and Services Laboratory, Air Force Engineering and Services Center, Tyndall AFB, Florida, November 1981.

7. Winer, A.M., Atkinson, R., Carter, W.P.L., Long, W.D., Aschmann, S.M., and Pitts, J.N., Jr., High Altitude Jet Fuel Photochemistry, ESL-TR-82-38, Engineering and Services Laboratory, Air Force Engineering and Services Center, Tyndall AFB, Florida, October 1982.

8. Sickles, J.E., II, Eaton, W.C., Ripperton, L.A., and Wright, R.S., Literature Survey of Emissions Associated with Emerging Energy Technologies, EPA-600/7-77-104, 1977.

9. Falls, A.H. and Seinfeld, J.H., "Continued Development of a Kinetic Mechanism for Photochemical Smog," Environ. Sci. Technol., vol 12, pp. 1398-1406, 1978.

10. Hendry, D.G., Baldwin, A.C., Barker, J.R., and Golden, D.M., Computer Modeling of Simulated Photochemical Smog, EPA-600/3-78-059, June 1978.

11. Carter, W.P.L., Lloyd, A.C., Sprung, J.L., and Pitts, J.N., Jr., "Computer Modeling of Smog Chamber Data: Progress in Validation of a Detailed Mechanism for the Photooxidation of Propene and n-Butane in Photochemical Smog," Int. J. Chem. Kinet., vol 11, pp. 45-101, 1979.

12. Whitten, G.Z., Killus, J.P., and Hogo, H., Modeling of Simulated Photochemical Smog with Kinetic Mechanisms, Volume 1, EPA-600/3-80-028A, February 1980.

13. Atkinson, R., Carter, W.P.L., Darnall, K.R., Winer, A.M., and Pitts, J.N., Jr., "A Smog Chamber and Modeling Study of the Gas Phase NO_x-Air Photooxidation of Toluene and the Cresols," Int. J. Chem. Kinet., vol 12, pp. 779-836, 1980.

14. Atkinson, R. and Lloyd, A.C., "Smog Chemistry and Urban Airshed Modeling," pp. 559-592. In Oxygen and Oxy-Radicals in Chemistry and Biology, Rodgers, M.A.J. and Powers, E.L. (Eds.), Academic Press, 1981.

15. Atkinson, R., Lloyd, A.C., and Winges, L., "An Updated Chemical Mechanism for Hydrocarbon/NO_x/SO_2 Photooxidations Suitable for Inclusion in Atmospheric Simulation Models," Atmos. Environ., vol 16, pp. 1341-1355, 1982.

16. Leone, J.A. and Seinfeld, J.H., "Updated Chemical Mechanism for Atmospheric Photooxidation of Toluene," Int. J. Chem. Kinet., vol 16, pp. 159-193, 1984.

17. Atkinson, R. and Lloyd, A.C., "Evaluation of Kinetic and Mechanistic Data for Modeling of Photochemical Smog," J. Phys. Chem. Ref. Data, vol 13, pp. 315-444, 1984.

18. Lurmann, F.W., Lloyd, A.C., and Atkinson, R., Gas Phase Chemistry, ADOM/TADAP Model Development Program, vol 6, ERT Document No. P-B980-530, July 1984.

19. Atkinson, R. and Carter, W.P.L., "Kinetics and Mechanisms of the Gas-Phase Reactions of Ozone with Organic Compounds under Atmospheric Conditions," Chem. Rev., vol 84, pp. 437-470, 1984.

20. Leone, J.A., Flagan, R.C., Grosjean, D., and Seinfeld, J.H., "An Outdoor Smog Chamber and Modeling Study of Toluene-NO_x Photooxidation," Int. J. Chem. Kinet., vol 17, pp. 177-216, 1985.

21. Lurmann, F.W., Lloyd, A.C., and Atkinson, R., "A Chemical Mechanism for Use in Long-Range Transport/Acid Deposition Computer Modeling," J. Geophys. Res., in press, 1986.

22. Whitten, G.Z., Killus, J.P., and Johnson, R.G., Modeling of Auto Exhaust Smog Chamber Data for EKMA Development, EPA-600/3-85-025, 1985.

23. Whitten, G.Z., Johnson, R.G., and Killus, J.P., Development of a Chemical Kinetic Mechanism for the U. S. EPA Regional Oxidant Model, EPA-600/3-85-026, April 1985.

24. Carter, W.P.L. and Atkinson, R., "Atmospheric Chemistry of Alkanes," J. Atmos. Chem., vol 3, pp. 377-405, 1985.

25. Atkinson, R., "Kinetics and Mechanisms of the Gas-Phase Reactions of the Hydroxyl Radical with Organic Compounds Under Atmospheric Conditions," Chem. Rev., vol 86, pp. 69-201, 1986.

26. Carter, W.P.L., Lurmann, F.W., Atkinson, R., and Lloyd, A.C, Development and Testing of a Surrogate Species Chemical Reaction Mechanism, EPA-600/3-86-031, August 1986.

27. Carter, W.P.L., Winer, A.M., Atkinson, R., Dodd, M.C., Long, W.D., and Aschmann, S.M., Atmospheric Photochemical Modeling of Turbine Engine Fuels, Phase I. Experimental Studies, Vol. I, Results and Discussion, ESL-TR-84-32, Engineering & Services Laboratory, Air Force Engineering & Services Center, Tyndall Air Force Base, FL, July 1984.

28. Carter, W.P.L., Winer, A.M., Atkinson, R., Heffron, S.E., Poe, M.P., and Goodman, M.A., User's Manual for the USAF Atmospheric Photochemical Reactivity Modeling System, USAF Contract No. F08635-83-0278, Engineering and Services Laboratory, Air Force Engineering and Services Center, Tyndall AFB, Florida, May 1986.

29. Hughes, B.M., Hess, G.G., Simon, K., Mazer, S., Ross, W.D., and Wininger, M.T., Variability of Major Organic Components in Aircraft Fuels, ESL-TR-84-02, Engineering and Services Laboratory, Air Force Engineering and Services Center, Tyndall Air Force Base, Florida, June 1984.

30. Darnall, K.R., Atkinson, R., Winer, A.M. and Pitts, J.N., Jr., "Effects of Constant versus Diurnally-Varying Light Intensity and Ozone Formation," J. Air Pollut. Contr. Assoc., vol 31, pp. 262-264, 1981.

31. Carter, W.P.L., Atkinson, R., Long, W.D., Parker, L.N., and Dodd, M.C., Effects of Methanol Fuel Substitution on Multi-Day Air Pollution Episodes, Final Report, California Air Resources Board Contract No. A3-125-32, September 1986.

32. Doyle, G.J., Bekowies, P.J., Winer, A.M., and Pitts, J.N., Jr., "Charcoal-Adsorption Air Purification System for Chamber Studies Investigating Atmospheric Photochemistry," Environ. Sci. Technol., vol 11, pp. 45-51, 1977.

33. Plum, C.N., Sanhueza, E., Atkinson, R., Carter, W.P.L. and Pitts, J.N., Jr., "OH radical Rate Constants and Photolysis Rates of α-Dicarbonyls," Environ. Sci. Technol., vol 17, pp. 479-484.

34. Winer, A.M., Peters, J.M., Smith, J.P., Pitts, J.N., Jr., "Response of Commercial Chemiluminescent NO-NO_2 Analyzers to Other Nitrogen-Containing Compounds," Environ. Sci. Technol., vol 8, pp. 1118-1121, 1974.

35. Stephens, E.R., Burleson, F.R., and Cardiff, E.A., "The Production of Pure Peroxyacyl Nitrate," J. Air Pollut. Control Assoc., vol 15, pp. 87-89, 1965.

36. Stephens, E.R. and Price, M.A., "Analysis of an Important Air Pollutant: Peroxyacetyl Nitrate," J. Chem. Educ., vol 50, pp. 351-354, 1973.

37. Zafonte, L., Rieger, P.L., and Holmes, J.R., "Nitrogen Dioxide Photolysis in the Los Angeles Atmosphere," Environ. Sci. Technol., vol 11, pp. 483-487, 1977.

38. Carter, W.P.L., Dodd, M.C., Long, W.D., and Atkinson, R., Outdoor Chamber Study to Test Multi-Day Effects, EPA-600/3-84-115.

39. Carter, W.P.L., Atkinson, R., Winer, A.M., and Pitts, J.N., Jr., "Experimental Investigation of Chamber-Dependent Radical Sources," Int. J. Chem. Kinet., vol 14, pp. 1071-1103, 1982.

40. Pitts, J.N., Jr., Atkinson, R., Carter, W.P.L., Winer, A.M., and Tuazon, E.C., Chemical Consequences of Air Quality Standards and of Control Implementation Programs, Final Report, California Air Resources Board Contract No. A1-030-32, April 1983.

41. Spicer, C.W., Holdren, M.W., Lyon, T.F., and Riggin, R.M., Composition and Photochemical Reactivity of Turbine Engine Exhaust, Final Report, F-98635-82-C-0131, Engineering and Services Laboratory, Air Force Engineering and Services Center, Tyndall Air Force Base, Florida, May 1984.

42. Altshuller, A.P. and Bufalini, J.J., "Photochemical Aspects of Air Pollution: A Review," Environ. Sci. Technol., vol 5, pp. 39-64, 1971, and references therein.

43. Finlayson-Pitts, B.J. and Pitts, J.N., Jr., Atmospheric Chemistry: Fundamentals and Experimental Techniques, John Wiley & Sons, Inc., 1098 pp., 1986.

44. Stockwell, W.R., "A Homogeneous Gas Phase Mechanism for Use in a Regional Acid Deposition Model," Atmos. Environ., vol 20, pp. 1615-1632, 1986.

45. Molina, M.J. and Arguello, G., "Ultraviolet Absorption Spectrum of Methylhydroperoxide Vapor," Geophys. Res. Lett., vol 6, pp. 953-955, 1979.

46. Atkinson, R., Aschmann, S.M., and Winer, A.M., "Alkyl Nitrate Formation from the Reaction of a Series of Branches RO_2 Radicals with NO as a Function of Temperature and Pressure," J. Atmos. Chem., vol 5, pp. 91-102, 1987.

47. Atkinson, R., Aschmann, S.M., Carter, W.P.L., Winer, A.M., and Pitts, J.N., Jr., "Alkyl Nitrate Formation from the NO_x-Air Photooxidations of C_2-C_8 n-Alkanes," J. Phys. Chem., vol 86, pp. 4563-4569, 1982.

48. McRae, G.J., Leone, J.A., and Seinfeld, J.H., Evaluation of Chemical Reaction Mechanisms for Photochemical Smog. Part I. Mechanism Description and Documentation, U. S. Environmental Protection Agency, Report No. EPA-600/3-83-086, 1983.

49. Killus, J.P. and Whitten, G.Z., "Comments on 'Formation of Chemical Compounds from Irradiated Mixtures of Aromatic Hydrocarbons and Nitrogen Oxides'", by Besemer, A.C. Atmos. Environ., vol 16, pp. 1599-1602, 1982, Atmos. Environ., vol 17, pp. 1597-1604, 1983.

50. Hoshino, M., Akimoto, H., and Okuda, M., "Photochemical Oxidation of Benzene, Toluene, and Ethylbenzene Initiated by OH Radicals in the Gas Phase," Bull. Chem. Soc. Japan, vol 51, pp. 718-724, 1978.

51. Tuazon, E.C., Mac Leod, H., Atkinson, R., and Carter, W.P.L., "α-Dicarbonyl Yields from the NO_x-air Photooxidations of a Series of Aromatic Hydrocarbons in Air," Environ. Sci. Technol., vol 20, pp. 383-387, 1986.

52. Bandow, H., Washida, N., and Akimoto, H., "Ring-Cleavage Reactions of Aromatic Hydrocarbons Studied by FT-IR Spectroscopy. I. Photooxidation of Toluene and Benzene in the NO_x-Air System," Bull. Chem. Soc. Jpn., vol 58, pp. 2531-2540, 1985.

53. Bandow, H. and Washida, N., "Ring-Cleavage Reactions of Aromatic Hydrocarbons Studied by FT-IR Spectroscopy. II. Photooxidation of o-, m-, and p-Xylenes in the NO_x-Air System," Bull. Chem. Soc. Jpn., vol 58, pp. 2541-2548, 1985.

54. Bandow, H. and Washida, N., "Ring-Cleavage Reactions of Aromatic Hydrocarbons Studied by FT-IR Spectroscopy. III. Photooxidation of 1,2,3-, 1,2,4- and 1,3,5-Trimethylbenzenes in the NO_x-Air System," Bull. Chem. Soc. Jpn., vol 58, pp. 2549-2555, 1985.

55. Dumdei, B.E. and O'Brien, R.J., "Toluene Degradation Products in Simulated Atmospheric Conditions," Nature, vol 311, pp. 248-250, 1984.

56. Shepson, P.B., Edney, E.O., and Corse, E.W., "Ring Fragmentation Reactions in the Photooxidations of Toluene and o-Xylene," J. Phys. Chem., vol 88, pp. 4122-4126, 1984.

57. Atkinson, R. and Aschmann, S.M., "Kinetics of the Reactions of Naphthalene, 2-Methylnaphthalene and 2,3-Dimethylnaphthalene with OH Radicals and with O_3 at 295 ± 1 K," Int. J. Chem. Kinet., vol 18, pp. 569-573, 1986.

58. Atkinson, R., Aschmann, S.M., and Carter, W.P.L., "Kinetics of the Reactions of O_3 and OH Radicals with Furan and Thiophene at 298 ± 2 K," Int. J. Chem. Kinet., vol 15, pp. 51-61, 1983.

59. Atkinson, R., Aschmann, S.M., Winer, A.M., and Carter, W.P.L., "Rate Constants for the Gas Phase Reactions of NO_3 Radicals with Furan, Thiophene and Pyrrole at 295 ± 1 K and Atmospheric Pressure," Environ. Sci. Technol., vol 19, pp. 87-90, 1985.

60. Atkinson, R., Aschmann, S.M., Winer, A.M., and Carter, W.P.L., "Rate Constants for the Gas Phase Reactions of OH Radicals and O_3 with Pyrrole at 295 ± 1 K and Atmospheric Pressure," Atmos. Environ., vol 18, pp. 2105-2107, 1984.

61. Tuazon, E.C., Atkinson, R., and Carter, W.P.L., "Extent of H-Atom Abstraction from the Reaction of the OH Radical with 1-Butene under Atmospheric Conditions, Int. J. Chem. Kinet., vol 17, pp. 725-734, 1985.

62. Killus, J.P. and Whitten, G.Z., A New Carbon-Bond Mechanism for Air Quality Simulation Modeling, EPA-600/3-82-041, April 1982.

63. Lurmann, F.W., Carter, W.P.L., and Coyner, L.A., A Surrogate Species Chemical Reaction Mechanism for Urban-Scale Air Quality Simulation Models. Volume 1 - Adaptation of the Mechanism, Final Report to EPA Contract No. 68-02-4104, Atmospheric Sciences Research Laboratory, Office of Research and Development, U.S. EPA Research Triangle Park, NC, 1987.

64. Pitts, J.N., Jr., Darnall, K., Carter, W.P.L., Winer, A.M., and Atkinson, R., Mechanisms of Photochemical Reactions in Urban Air, EPA-600/3-79-110, November 1979.

65. Pitts, J.N., Jr., Sanhueza, E., Atkinson, R., Carter, W.P.L., Winer, A.M., Harris, G.W., and Plum, C.N., "An Investigation of the Dark Formation of Nitrous Acid in Environmental Chambers," Int. J. Chem. Kinet., vol 16, pp. 919-939, 1984.

66. Mayfield, H., AFESC/RDVS, personal communication, 1986.

67. Jeffries, H.E., Sexton, K.G., Morris, T.P., Jackson, M., Goodman, R.G., Kamens, R.M., and Holleman, M.S., Outdoor Smog Chamber Experiments Using Automobile Exhaust, EPA-600/3-85-032, March 1985.

68. Dodge, M.C. "Combined Use of Modeling Techniques and Smog Chamber Data to Derive Ozone-Precursor Relationships," in Proceedings, International Conference on Photochemical Oxidant Pollution and Its Control, EPA-300/3-77-001, 1977.

69. Gipson, G.L., Freas, W.P., Kelly, K.R., and Meyer, E.L., Guideline for Use of City-Specific EKMA in Preparing Ozone SIP's, EPA-450/4-80-027, March 1981.

70. Gipson, G.L. and Freas, W.P., Use of City-Specific EKMA in the Ozone RIA, U. S. Environmental Protection Agency, July 1983.

71. U.S. Environmental Protection Agency, Guideline for Using the Carbon Bond Mechanism in City Specific EKMA, EPA-450/4-84-005, February 1984.

72. Carter, W.P.L. and Atkinson, R., A Computer Modeling Study of Incremental Hydrocarbon Reactivity, Final Report to EPA Cooperative Agreement No. CR810214, Atmospheric Sciences Research Laboratory, Office of Research and Development, U. S. EPA, Research Triangle Park, NC, March 1987.

73. Gipson, G.L., Users Manual for OZIPM-2: Ozone Isopleth Plotting with Optional Mechanisms/Version 2, EPA-450/4-84-024, August 1984.

74. Gipson, G.L., U. S. Environmental Protection Agency, personal communication, 1985.

75. Pefley, R.K., Pullman, J.B., and Whitten, G.Z., The Impact of Alcohol Fuels on Urban Air Pollution: Methanol Photochemistry Study, Final Report, U. S. Department of Energy, Office of Vehicle and Engine R&D, Washington, D.C., 1984.

76. Peterson, J.T., Calculated Actinic Fluxes (290-700 nm) for Air Pollution Photochemistry Applications, EPA-600/4-76-025, June 1976.

(The reverse of this page is blank)

APPENDIX A

COMPUTER TAPE CONTAINING RESULTS OF THE AIR FORCE CHAMBER EXPERIMENTS

The results of all environmental chamber experiments carried out under both phases of this program, and of the chamber runs carried out under a previous Air Force contract (Reference 7) used for testing this model, are available on magnetic tape in computer-readable format. The format of the data on this tape, and descriptions of the data sets on the tape, are given in this Appendix. This tape was submitted to the United States Air Force along with this report, and copies of the tape are available from SAPRC for handling and distribution costs (plus the cost of the tape). Requests for copies of this tape should be addressed to:

Dr. William P. L. Carter
Statewide Air Pollution Research Center
University of California
Riverside, CA 92521

The computer tape has a data density of 1600 BPI, uses ASCII character format, and has a maximum blocksize of 5280 bytes. The tape contains 321 files, of three different types. File 1, which has a logical record length of 80 bytes, is the same as Table A-1 in this Appendix, and contains the complete list of run numbers, run types, and file numbers for the chamber runs carried out in this program. Files 2-161, which have logical record lengths of 132 bytes, consist of "printout images" of the tabulated data formatted in a manner most suitable for obtaining hardcopy printouts for manual inspection. A description of the data contained in these "printout" files is given in Section A, below. Files 162-321, which have logical record lengths of 80 bytes, contain the data in a compressed format which is more suitable for being read by computer programs for purposes of, for example, data manipulation or plotting. The format of these these compressed data sets is described in Section B. The data set numbers for the printout and the compressed data sets for each of the runs included on the tape are given in Table A-1.

TABLE A-1. RUN NUMBERS, RUN TYPES, AND FILE NUMBERS FOR ALL CHAMBER RUNS ON THE DATA TAPE.

Run ID.	Run type	File numbers[a]	
		Printout format	Compressed format
Selected Runs Carried out Under Contract USAF-F08635-80-C-0359			
EC-489	JP-4(1A) - NO_x	2	162
EC-490	JP-4(1A) - NO_x	3	163
EC-491	JP-4(1A) - NO_x	4	164
EC-492	JP-4(1A) - NO_x	5	165
Runs Carried out Under Phase I of Contract USAF-F08635-83-0278			
EC-900	Mesitylene - NO_x	6	166
EC-901	Mesitylene - NO_x	7	167
EC-903	Mesitylene - NO_x	8	168
ITC-690	Propene - NO_x (New Reactor)	9	169
ITC-692	Tracer - NO_x	10	170
ITC-693	Propene - NO_x	11	171
ITC-694	Isobutene - NO_x	12	172
ITC-695	Tracer - NO_x	13	173
ITC-697	Ozone Dark Decay	14	174
ITC-698	Benzene - NO_x	15	175
ITC-699	Toluene - NO_x	16	176
ITC-700	Tracer - NO_x	17	177
ITC-702	m-Xylene - NO_x	18	178
ITC-703	Mesitylene - NO_x	19	179
ITC-704	Tracer - NO_x	20	180
ITC-706	Mesitylene - NO_x	21	181
ITC-707	Tracer - NO_x	22	182
ITC-709	Mesitylene - NO_x	23	183
ITC-710	Benzene - NO_x	24	184
ITC-711	Furan - NO_x	25	185
ITC-712	Tracer - NO_x	26	186
ITC-713	Furan - NO_x	27	187
ITC-714	Tracer - NO_x	28	188
ITC-715	Furan - NO_x	29	189
ITC-716	Propene - NO_x	30	190
ITC-717	Tracer - NO_x	31	191
ITC-721	JP-4(Shale) - NO_x	32	192
ITC-722	JP-4(Shale) - NO_x	33	193
ITC-723	Tracer - NO_x	34	194
ITC-724	Tracer - NO_x	35	195

TABLE A-1. RUN NUMBERS, RUN TYPES, AND FILE NUMBERS FOR ALL CHAMBER RUNS ON THE DATA TAPE (CONTINUED).

Run ID.	Run type	File numbers[a]	
		Printout format	Compressed format
ITC-725	JP-4(Shale) - NO_x	36	196
ITC-726	Tracer - NO_x	37	197
ITC-728	Propene - NO_x	38	198
ITC-729	Thiophene - NO_x	39	199
ITC-730	Thiophene - NO_x	40	200
ITC-731	Tracer - NO_x	41	201
ITC-733	Thiophene - NO_x	42	202
ITC-734	Tracer - NO_x	43	203
ITC-735	Pyrrole - NO_x	44	204
ITC-736	Propene - NO_x (New Reactor)	45	205
ITC-737	Tracer - NO_x	46	206
ITC-739	Tetralin - NO_x	47	207
ITC-740	Tracer - NO_x	48	208
ITC-742	Mesitylene - NO_x	49	209
ITC-743	Furan - NO_x	50	210
ITC-744	Thiophene - NO_x	51	211
ITC-745	Tracer - NO_x	52	212
ITC-747	Tetralin - NO_x	53	213
ITC-748	Tetralin - NO_x	54	214
ITC-749	Tracer - NO_x	55	215
ITC-750	Tetralin - NO_x	56	216
ITC-751	Naphthalene - NO_x	57	217
ITC-752	Tracer - NO_x	58	218
ITC-754	Propene - NO_x	59	219
ITC-755	Naphthalene - NO_x	60	220
ITC-756	Naphthalene - NO_x	61	221
ITC-757	Tracer - NO_x	62	222
ITC-759	Propene - NO_x	63	223
ITC-760	Tracer - NO_x	64	224
ITC-761	Tracer - NO_x + n-Octane	65	225
ITC-762	Tracer - NO_x + n-Octane	66	226
ITC-763	Tracer - NO_x + n-Octane	67	227
ITC-765	Tracer - NO_x + Methylcyclohexane	68	228
ITC-766	Tracer - NO_x + Methylcyclohexane	69	229
ITC-767	Tracer - NO_x + Methylcyclohexane	70	230
ITC-768	JP-4(Shale) - NO_x	71	231
ITC-770	Tracer - NO_x + n-Butane	72	232
ITC-771	2,3-Dimethylnaphthalene - NO_x	73	233
ITC-772	Tracer - NO_x	74	234
ITC-774	2,3-Dimethylnaphthalene - NO_x	75	235
ITC-775	2,3-Dimethylnaphthalene - NO_x	76	236
ITC-776	Tracer - NO_x	77	237

TABLE A-1. RUN NUMBERS, RUN TYPES, AND FILE NUMBERS FOR ALL CHAMBER RUNS ON THE DATA TAPE (CONTINUED).

Run ID.	Run type	File numbers[a]	
		Printout format	Compressed format
ITC-778	Pyrrole - NO_x	78	238
ITC-779	Pyrrole - NO_x	79	239
ITC-780	Tracer - NO_x + Pyrrole	80	240
ITC-781	Synthetic Fuel #1 - NO_x	81	241
ITC-782	Tracer - NO_x	82	242
ITC-784	Synthetic Fuel #1 - NO_x	83	243
ITC-785	Synthetic Fuel #1 - NO_x	84	244
ITC-786	Syn. Fuel #1 + Furan - NO_x	85	245
ITC-787	Tracer - NO_x	86	246
ITC-788	Syn. Fuel 1 + Thiophene - NO_x	87	247
ITC-789	Tracer - NO_x	88	248
ITC-791	Propene - NO_x	89	249
ITC-792	Propene - NO_x (New Reactor)	90	250
ITC-793	Tracer - NO_x	91	251
ITC-795	Synthetic Fuel #2 - NO_x	92	252
ITC-796	Synthetic Fuel #2 - NO_x	93	253
ITC-797	Tracer - NO_x + n-Octane	94	254
ITC-798	Naphthalene - NO_x	95	255
ITC-799	Synthetic Fuel #3 - NO_x	96	256
ITC-800	Tracer - NO_x + Methylcyclohexane	97	257
ITC-801	Synthetic Fuel #3 - NO_x	98	258
ITC-802	Naphthalene - NO_x	99	259
ITC-803	Tracer - NO_x	100	260
ITC-805	Synthetic Fuel #1 - NO_x	101	261
ITC-806	2,3-Dimethylnaphthalene - NO_x	102	262
ITC-807	Syn. Fuel #1 + Pyrrole - NO_x	103	263
ITC-808	Tracer - NO_x	104	264
ITC-810	Propene - NO_x	105	265
ITC-813	Tracer - NO_x	106	266
ITC-822	Ozone Dark Decay	107	267
ITC-824	Tracer - NO_x	108	268
ITC-825	Acetaldehyde - Air	109	269
ITC-826	Tracer - NO_x + Mesitylene	110	270
ITC-827	Tracer - NO_x + m-Xylene	111	271
ITC-828	Tracer - NO_x + Toluene	112	272
ITC-829	Tracer - NO_x	113	273
ITC-831	Tracer - NO_x + Benzene	114	274
ITC-832	Tracer - NO_x + Tetralin	115	275

TABLE A-1. RUN NUMBERS, RUN TYPES, AND FILE NUMBERS FOR ALL CHAMBER RUNS ON THE DATA TAPE (CONTINUED).

Run ID.	Run type	File numbers[a]	
		Printout format	Compressed format
Runs Carried out Under Phase II of Contract USAF-F08635-83-0278			
ITC-924	Tracer - NO_x	116	276
ITC-925	Propene - NO_x	117	277
ITC-926	Ethene - NO_x	118	278
ITC-927	1-Butene - NO_x	119	279
ITC-928	Tracer - NO_x + 1-Butene	120	280
ITC-929	1-Hexene - NO_x	121	281
ITC-930	1-Butene - NO_x	122	282
ITC-931	1-Hexene - NO_x	123	283
ITC-932	Tracer - NO_x	124	284
ITC-934	1-Hexene - NO_x	125	285
ITC-935	1-Butene - NO_x	126	286
ITC-936	Ethene - NO_x	127	287
ITC-937	Tracer - NO_x + 1-Hexene	128	288
ITC-938	Propene - NO_x	129	289
ITC-939	n-Butane - NO_x	130	290
ITC-940	Pure Air Irrad.	131	291
ITC-941	Acrolein - NO_x	132	292
ITC-942	Tracer - NO_x	133	293
ITC-943	Acrolein - NO_x	134	294
ITC-944	Acrolein - NO_x	135	295
ITC-945	Tracer - NO_x + Acrolein	136	296
ITC-946	Acrolein + Propene - NO_x	137	297
ITC-947	Propene - NO_x	138	298
ITC-948	n-Butane - NO_x	139	299
ITC-949	Tracer - NO_x	140	300
ITC-951	JP-4(Tank) - NO_x	141	301
ITC-952	JP-4(Tank) - NO_x	142	302
ITC-953	Tracer - NO_x	143	303
ITC-954	JP-4(Tank) - NO_x	144	304
ITC-955	Pure Air Irrad.	145	305
ITC-956	JP-4(Tank) - NO_x	146	306
ITC-957	Acetaldehyde - Air	147	307
ITC-958	Tracer - NO_x	148	308
ITC-960	Propene - NO_x	149	309
ITC-961	JP-4(Tank) - NO_x	150	310
ITC-963	Syn. Jet Exhaust - NO_x	151	311
ITC-964	Tracer - NO_x	152	312
ITC-965	Syn. Jet Exhaust - NO_x	153	313
ITC-966	JP-4(1A) - NO_x	154	314

TABLE A-1. RUN NUMBERS, RUN TYPES, AND FILE NUMBERS FOR ALL CHAMBER RUNS ON THE DATA TAPE (CONCLUDED).

Run ID.	Run type	File numbers[a]	
		Printout format	Compressed format
ITC-967	Syn. Jet Exhaust - NO_x	155	315
ITC-968	Syn. Jet Exhaust - NO_x	156	316
ITC-969	JP-4(1A) - NO_x	157	317
ITC-970	Tracer - NO_x	158	318
ITC-972	Propene - NO_x	159	319
ITC-973	Pure Air Irrad.	160	320
ITC-974	Acetaldehyde - Air	161	321

[a]File no. 1 consists of this table.

A. DATA SETS IN "PRINTOUT" FORMAT

The "printout format" data sets consist of tabluations of the results of the chamber experiments in a format suitable for manual inspection. If hard copies of these data sets are required, these can be printed out on any printer which can print 132 columns, has a page length of 60 lines or more, and which recognizes the "form feed" (ASCII code 12) character. Each of these "printouts" contains the following information (where applicable).

- The indoor Teflon® chamber (ITC) run number.
- A brief run description.
- The date the run was carried out (given below the run description).
- The date the printout files was created (given in right hand corner on each page).
- Comments for the run, including experimental operations and operator's comments taken from the log book, problems encountered (if any), etc.
- The initial concentrations of injected reactants which were monitored.

- Lists of all instruments used in these runs. For each instrument, this list indicates the ID number (used internally at SAPRC), the label identifying the instrument on the data tabulation, and a brief description giving information identifying the instrument and/or technique.
- The data tabulations. The tabulations indicate the compound or parameter measured, the units in which the measurements are reported, and the instrument. Because of space and format limitations, the compound names frequently had to be abbreviated on the tabulations. The meanings of representative abbreviations which may not be obvious are listed in Table A-2. For each data point, the clock time and (in most cases) the elapsed time (in minutes) since the irradiation began (or since the first measurement for dark runs) are indicated.
- If any of the data are flagged (indicated by an "A," or "B," etc., immediately to the right of the value), footnotes giving the reason it is flagged appear at the end of the tabulation for the run.

TABLE A-2. REPRESENTATIVE ABBREVIATIONS USED IN THE DATA TABULATIONS.

Abbreviation	Meaning
NO2-UNC	NO_2 readings, uncorrected for interferences by organic nitrates and HNO_3
N-C4	n-Butane
I-C4	Isobutane
ISO-C8	Iso-Octane (2,2,4-trimethylpentane)
I-C4=	Isobutene
M-XYL	m-Xylene
C5-K-3	3-Pentanone (diethyl ketone)
C5-N-2	2-Pentyl nitrate
ACETALD	Acetaldehyde[a]
MEK	Methyl ethyl ketone[a]
PROX	Propene oxide[a]
BUTY[illegible]	Butyraldehyde[a]
LN C[illegible]3=	ln([n-butane]/[propene]), whose rate of change is used to derive OH radical concentrations[b]
DEW PT	Dew point (units of degrees C)
K1	k_1, the NO_2 photolysis rate (units of min^{-1})
UV RAD	UV radiometer readings (units of mW cm^{-2})

[a]Or some other compound with the same retention time on the gas chromatographic system employed.

[b]Concentration units are arbitrary; only the slope of the log is of interest.

B. DATA SETS IN "COMPRESSED" FORMAT

If it is desired to use the data from these experiments as input to computer programs, for purposes such as data analysis, plotting, etc, then the data sets in the "compressed" format would be more useful. These data sets consists of records in card image format, and are organized as described in Table A-3. The following points should be noted regarding these data sets:

- Because this data format is used for a number of different types of experiments at SAPRC, the records contain provisions for data values which are not used in these particular runs. These should be ignored; usually (but not always) they are zero.

- The types of data on the data sets can be categorized by: (a) general information data, such as run title, date, number of instruments, comments, chambers, etc., (b) comments, (c) instrument descriptions, (d) channel parameters, and (e) channel data. By "channel" we mean the set of experimental measurements which depend on time, such as ozone concentrations, temperature readings, etc.

- Channels which have data have associated with them a "time set," which is an array of the times at which the measurements for that channel were made. The time sets are stored separately from the channel data because in general, more than one channel may have the same time set.

- T = 0 refers to the clock time at which the irradiation began; or, for dark runs, the time the first measurement was made.

- Some data points are "flagged" with a nonblank character (as indicated by the values in the "LFLGS" and "FLGS arrays in group 3 of Table A-3), which associates it with a comment which has the same character as its associated flag ("FLGCOM" in group 5 of Table A-3). These comments indicate problems, etc., with the "flagged" data point, or set of data points starting with the one which is flagged. If a comment has FLGCOM = "N," the comment line is a continuation of the previous flagged comment, and the character "N" does not appear on the "printout" format data sets.

TABLE A-3. ORGANIZATION OF THE COMPRESSED DATA FILES FOR CHAMBER RUNS.

Record	Column	Format[a]	Name	Description
Group 1. Four Records. General Information				
1	1-7	(1X,I6)	IRUNID	Run number + 10000 x chamber number (chamber numbers: 1 = EC, 2 = ITC, 4 = OTC)
	8-13	(I6)	FORM	File format; always 1.
	14-29	(A16)	UPDRUN	Date of last update (internal SAPRC use)
	30-69	(A40)	TITLE	Run title
	70-77	(A8)	DATE(1)	First half of run date
2	1-9	(1X,A8)	DATE(2)	Second half of run date
	10-25	(I6)	TZERO	Clock time at T = 0
	16-21	(I6)	PSTPDT	1 for PST, 2 for PDT
	22-39	(3I6)	-	(Ignore)
	40-45	(I6)	BAGNO	ITC or OTC reaction bag number (If zero, bag number is not specified)
	46-78	(3G11.4)	-	(Ignore)
3	1-57	(1X,6E11.4)	-	(Ignore)
	50-64	(I7)	-	(Ignore - should be zero)
	65-70	(I6)	NSIDES	Number of sides if chamber is divided applicable to outdoor chamber runs only (Note: "Side 3" always refers to ambient air outside chamber.)
4	1-7	(1X,I6)	NTS	Number of time sets
	8-13	(I6)	NCHN	Number of channels
	14-19	(I6)	NWL	Number of wavelenths in spectral distribution (evacuable chamber only)
	20-25	(I6)	NINS	Number or instruments
	26-31	(I6)	NCOMS	Number of comments
	32-37	(I6)	-	(Ignore)
	38-48	(E11.4)	-	(Ignore)
	49-54	(I6)	-	(Ignore)
Group 2. One Record for Each Set of 4 Wavelengths in the Spectral Distribution. INT((NWL+3)/4) Records. No Records if NWL=0.				
1+	1-69	(1X,4(I6,E11.4))	WL,SDIST	WL = wavelength (in nm) SDIST = relative intensity at wavelength = WL

TABLE A-3. ORGANIZATION OF THE COMPRESSED DATA FILES FOR CHAMBER RUNS (CONTINUED).

Record	Column	Format[a]	Name	Description
Group 3. One Set of One or More Records for Each of the NTS Time Sets				
1	1-7	(1X,I6)	NPTS	Number of points in this time set
	8-73	(11I6)	TIMES	Clock times + 10000 x day number. (Day number: 0 = first day, 1 = second day, etc. E.G., 10930 = 9:30 AM on day 2 of the run.)
2+	1-73	(1X,12I6)	TIMES	Rest of clock times. (No records of this type if NPTS ≤11.)
Group 4. One Set of Three or More Records for Each of the NCHN Data Channels				
1	1-7	(1X,I6)	ID1	Data type identification number (internal SAPRC use).
	8-13	(I6)	INST	Instrument number - i.e., record number in group 4 that describes the instrument used for this channel. (0 = instrument undefined)
	14-19	(I6)	SIDE	Side number (3 = outside). Ignore if NSIDES = 0 or 1.
	20-25	(I6)	TIMSET	Time set number. (If TIMSET = 0, there are no data for this channel.)
	26-31	(I6)	NP	Number of data points (ignore if TIMSET = 0)
	32-37	(I6)	NF	Number of flagged data points (Ignore if TIMSET = 0)
	38-67	(5I6)	-	(Ignore)
	68-73	(I6)	PRTORD	If >0, determines order channel appears on printouts - lower number printed first. If PRTORD = -1, channel is not printed. If PRTORD is -2, the data for this channel are printed out separately at the end.

TABLE A-3. ORGANIZATION OF THE COMPRESSED DATA FILES FOR CHAMBER RUNS (CONTINUED).

Record	Column	Format[a]	Name	Description
	74-79	(I6)	DIG	(DIG-2) = number of digits to the right of the decimal point that appears on printouts. If DIG = ≥0 or ≤7, data prints out in exponential notation.
2	1-7	(1X,I6)	UNTS	Code number for units of data: 1 = ppm, 2 = degree C, 7 = mw-cm^{-2}, 8 = blank (no units), 9 = ppmC, 10 = ppb, 11 = degree F, 14 = "raw data," 17 = min^{-1}.
	8-19	(2I6)	-	(Ignore)
	20-41	(2E11.4)	FAC,ZERO	Factor and zero corrections. Data values = factor x (raw data - zero) (Note however that data values stored on the data sets are already calculated, so these quantities can be ignored.)
	42-52	(E11.4)	-	(Ignore)
	53-63	(E11.4)	CONCØ	Initial concentration (if SDEV, below, <0) or average (if SDEV ≥0) to appear at the start of the printouts. If CONCØ = -9.9999E+9, initial concentration or average is not used. If CONCØ = -9.9999E+9, it needs to be calculated from the data.
	64-74	(E11.4)	SDEV	If SDEV <0, CONCØ is an initial concentration. If SDEV = -1, the initial concentration was assigned; if SDEV = -9.9999E+9, the data value at T = 0 is used as the initial concentration. If SDEV ≥0, CONCØ is the average of the data, and SDEV is the (1σ) standard deviation. If SDEV = 9.999E+9, the standard deviation is unknown.
3	1-9	(1X,A8)	NAME	Channel name
4+	1-78	(1X,7E11.4)	DATA	The data values. As many records as needed for the NP values. A data value of

TABLE A-3. ORGANIZATION OF THE COMPRESSED DATA FILES FOR CHAMBER RUNS (CONCLUDED).

Record	Column	Format[a]	Name	Description
				9.9999E+9 means no data is available for that time point. No records if TIMSET = 0.
5+	1-73	(1X,9(I6,A2))	LFLCS, FLGS	For each of the NF flagged data points, LFLGS is the index number for the point, and the first byte of FLGS is the flag character. As many records as needed for the NF values; no record if NF = 0.
Group 5. One Record for Each of the NINS Instruments				
1	1-7	(1X,I6)	INSCOD	Instrument code number
	7-19	(6A2)	-	(Ignore)
	20-27	(A8)	INSLBL	Instrument label
	28-67	(A40)	INSDSC	Instrument description
	68-78	(E11.4)	-	(Ignore)
Group 6. One Record for Each of the NCOMS Comments				
1	1-3	(2X,A1)	FLGCOM	If blank, the comment appears on the first page of the printouts. If not blank, the comment is a footnote which is printed along with the first byte of FLGCOM at the end of the printout.
	4-80	(A77)	COMENT	The comment line

[a]FORTRAN format code.

(The reverse of this page is blank)

APPENDIX B

FULL LISTING OF THE CHEMICAL MECHANISM

This Appendix gives a full listing of the reactions and the kinetic parameters in the chemical mechanism used in the model developed under this contract. The development and testing of this mechanism is discussed in Section IV of this report. The reactions and kinetic parameters used are given in Table B-1, while Table B-2 lists the species used in the mechanism. For the alkanes, the aromatic hydrocarbons and the higher alkenes, the reactions used in the mechanism are all of the same general form, shown in Table B-1. The values of the mechanistic and kinetic parameters for those species are given in Tables 9, 10, and 12 in Section IV of this volume, and are thus not reproduced in this Appendix.

Rate constants for photolysis reactions are calculated from the products of the absorption coefficients and quantum yields, given as a function of wavelength for each type of photolysis reaction in Table B-3, and the intensity and spectral distribution of the light source. For simulations of the ITC and the EC chamber experiments, the spectral distribution of the light sources for the respective chambers are given in our previous EPA report (Reference 26), and the photolysis rates were normalized so that the calculated NO_2 photolysis rate (k_1) corresponded to the values measured in the NO_2 actinometry experiments. For the ITC experiments, only one relative spectral distribution was used, and the calculated photolysis rates corresponding to a typical ITC NO_2 photolysis rate of 0.325 min^{-1} is given in Table B-4. For experiments with different NO_2 photolysis rates, the values used for all the photolysis rates are proportional to those given in Table B-4. For the EC experiments, the spectral distributions varied with time (Reference 26), and thus, the photolysis rates depended on the times in which the experiments were carried out. Photolysis rates for representative EC experiments used for model testing in this program are also shown in Table B-4. Photolysis rates used in simulations of EC experiments carried out around the same time (as shown in Table B-4) are similar.

When this mechanism is used in airshed simulations, such as in the applications described in Section V of this report, the photolysis rate constants are calculated using the absorption coefficients and quantum yields shown in Table B-3, and the ground-level solar actinic irradiances given by Peterson (Reference 76). Calculated solar photolysis rate constants for selected zenith angles are given in Table B-5. The details of the methods used to calculate these ambient air photolysis rates, and the values of the parameters employed, are given in our previous EPA report (Reference 26). These methods for calculating photolysis rates in airshed simulations are implemented in the atmospheric photochemical reactivity modeling software developed under this program (Reference 28).

TABLE B-1. REACTIONS AND RATE CONSTANTS USED IN THE PHOTOCHEMICAL MODEL.

Label[a]	Kinetic parameters[b]			Reaction[c]
				Inorganic Reactions
1	PHOT. = NO2			NO2 + HV = NO + O
2	2.155E-05	0.00	-4.300	O + O2 + M = O3 + M
3A	1.365E+04	0.00	-1.000	O + NO2 = NO + O2
3B	3.232E-03	0.00	-4.000	O + NO2 + M = NO3 + M
4	2.642E+03	2.72	-1.000	O3 + NO = NO2 + O2
5	1.761E+02	4.87	-1.000	O3 + NO2 = O2 + NO3
6	1.174E+04	-0.50	-1.000	NO + NO3 = #2 NO2
7	1.185E-10	-1.05	-2.000	NO + NO + O2 = #2 NO2
8	FALLOFF F= 0.600, N= 0.972			NO2 + NO3 = N2O5
	0: 7.182E-02	0.00	-6.300	
	I: 2.055E+03	0.00	-1.500	
9	4.333E+13	22.55	0.000	N2O5 + #RCON8 = NO2 + NO3
10	1.468E-06	0.00	-1.000	N2O5 + H2O = #2 HONO2
11	3.670E+01	2.44	-1.000	NO2 + NO3 = NO + NO2 + O2
12A	PHOT. = NO3NO			NO3 + HV = NO + O2
12B	PHOT. = NO3NO2			NO3 + HV = NO2 + O
13A	PHOT. = O3O3P			O3 + HV = O + O2
13BL	PHOT. = O3T270			O3 + HV + #T270 = O*1D2 + O2
13BM	PHOT. = O3T300			O3 + HV + #T300 = O*1D2 + O2
13BH	PHOT. = O3T330			O3 + HV + #T330 = O*1D2 + O2
14	3.229E+05	0.00	-1.000	O*1D2 + H2O = #2 HO.
15	4.257E+04	0.00	-1.000	O*1D2 + M = O + M
16	FALLOFF F= 0.600, N= 1.000			HO. + NO = HONO
	0: 2.406E-02	0.00	-5.300	
	I: 4.404E+04	0.00	-2.000	
17	PHOT. = HONO			HONO + HV = HO. + NO
18	FALLOFF F= 0.600, N= 1.000			HO. + NO2 = HONO2
	0: 9.337E-02	0.00	-5.200	
	I: 3.523E+04	0.00	-2.300	
19	1.380E+01	-1.55	-1.000	HO. + HONO2 = H2O + NO3
21	3.200E+02	0.00	-1.000	HO. + CO = HO2. + CO2
22	2.349E+03	1.87	-1.000	HO. + O3 = HO2. + O2
23	5.431E+03	-0.48	-1.000	HO2. + NO = HO. + NO2
24	FALLOFF F= 0.560, N= 1.000			HO2. + NO2 = HO2NO2
	0: 8.260E-03	0.00	-6.600	
	I: 6.165E+03	0.00	-0.800	
25	1.754E+13	21.60	1.000	HO2NO2 + #RCON24 = HO2. + NO2
27	5.872E+03	0.00	-1.000	HO2NO2 + HO. = H2O + NO2 + O2
28	2.055E+01	1.15	-1.000	HO2. + O3 = HO. + #2 O2
29A	3.229E+02	-1.23	-1.000	HO2. + HO2. = HO2H + O2
29B	6.823E-05	-1.95	-2.000	HO2. + HO2. + M = HO2H + O2
29C	1.113E-05	-5.60	-2.000	HO2. + HO2. + H2O = HO2H + O2 + H2O
29D	2.370E-06	-6.32	-2.000	HO2. + HO2. + H2O = HO2H + O2 + H2O

TABLE B-1. REACTIONS AND RATE CONSTANTS USED IN THE PHOTOCHEMICAL MODEL (CONTINUED).

Label[a]	Kinetic parameters[b]			Reaction[c]
30A	SAME K AS 29A			NO3 + HO2. = HONO2 + O2
30B	SAME K AS 29B			NO3 + HO2. + M = HONO2 + O2
30C	SAME K AS 29C			NO3 + HO2. + H2O = HONO2 + O2 + H2O
30A	SAME K AS 29D			NO3 + HO2. + H2O = HONO2 + O2 + H2O
31	PHOT. = H2O2			HO2H + HV = #2 HO.
32	4.550E+03	0.37	-1.000	HO2H + HO. = HO2. + H2O
				Chamber Dependent Reactions
				(Not used in airshed model simulations. Values of chamber-dependent parameters used in simulations of EC and ITC experiments are given in Tables 17 and 18 Section IV.C.1)
O3W	0.000E-01	0.00	0.000	O3 =
HPW	0.000E-01	0.00	0.000	HO2H =
N25I	0.000E-01	0.00	0.000	N2O5 = #2 NOX-WALL
N25S	0.000E-01	0.00	-1.000	N2O5 + H2O = #2 NOX-WALL
NAW	0.000E-01	0.00	0.000	HONO2 = NOX-WALL
NO2W	0.000E-01	0.00	0.000	NO2 = #YHONO HONO + #1-YHONO NOX-WALL
RSI	PHOT. = NO2			HV + #RS-I = HO.
RSS	PHOT. = NO2			NO2 + HV + #RS-S = #.5 HONO + #.5 NOX-WALL
ONO2	PHOT. = NO2			#E-NO2/K1 = NO2 + #-1 NOX-WALL
OALD	PHOT. = NO2			#E-ALD/K1 = HCHO + #-1 -C
XSHC	0.000E-01	0.00	0.000	HO. = HO2.
				General Peroxy Radical Reactions
				(See Section IV.A.1 for a description of how the reactions of preoxy radicals are represented in this mechanism.)
B1	6.165E+03	-0.36	-1.000	RO2. + NO = NO
B2	6.165E+03	-0.36	-1.000	RCO3. + NO = NO
B4	4.110E+03	-0.36	-1.000	RCO3. + NO2 = NO2
B5	4.404E+03	0.00	-1.000	RO2. + HO2. = HO2.
B6	4.404E+03	0.00	-1.000	RCO3. + HO2. = HO2.
B8	1.468E+00	0.00	-1.000	RO2. + RO2. =
B9	4.404E+03	0.00	-1.000	RO2. + RCO3. =
B10	3.670E+03	0.00	-1.000	RCO3. + RCO3. =

TABLE B-1. REACTIONS AND RATE CONSTANTS USED IN THE PHOTOCHEMICAL MODEL (CONTINUED).

Label[a]	Kinetic parameters[b]			Reaction[c]
B7	PHOT. = CO2H			-OOH + HV = HO2. + HO.
B11	SAME K AS B1			RO2-R. + NO = NO2 + HO2.
B12	SAME K AS B5			RO2-R. + HO2. = -OOH
B13	SAME K AS B8			RO2-R. + RO2. = RO2. + #.5 HO2.
B14	SAME K AS B9			RO2-R. + RCO3. = RCO3. + #.5 HO2.
B15	SAME K AS B1			R2O2. + NO = NO2
B16	SAME K AS B5			R2O2. + HO2. =
B17	SAME K AS B8			R2O2. + RO2. = RO2.
B18	SAME K AS B9			R2O2. + RCO3. = RCO3.
B19	SAME K AS B1			RO2-N. + NO = RONO2
B20	SAME K AS B5			RO2-N. + HO2. = -OOH + MEK + #1.5 -C
B21	SAME K AS B8			RO2-N. + RO2. = RO2. + #.5 HO2. + MEK + #1.5 -C
B22	SAME K AS B9			RO2-N. + RCO3. = RCO3. + #.5 HO2. + MEK + #1.5 -C
G2	SAME K AS B1			RO2-NP. + NO = NITROPHEN
G3	SAME K AS B5			RO2-NP. + HO2. = -OOH + #6 -C
G4	SAME K AS B8			RO2-NP. + RO2. = RO2. + #.5 HO2. + #6 -C
G5	SAME K AS B9			RO2-NP. + RCO3. = RCO3. + HO2. + #6 -C
				Reactions of Formaldehyde
C1	PHOT. = HCHOR			HCHO + HV = #2 HO2. + CO
C2	PHOT. = HCHOM			HCHO + HV = H2 + CO
C3	1.321E+04	0.00	-1.000	HCHO + HO. = HO2. + CO + H2O
C4	1.468E+01	0.00	-1.000	HCHO + HO2. = -C + RO2-R. + RO2.
C9	8.807E+02	4.09	-1.000	HCHO + NO3 = HONO2 + HO2. + CO
				Reactions of Acetaldehyde and PAN
C10	1.013E+04	-0.50	-1.000	CCHO + HO. CCO-O2. + H2O + RCO3.
C11A	PHOT. = CCHOR			CCHO + HV = CO + HO2. + HCHO + RO2-R. + RO2.
C12	4.404E+02	2.84	-1.000	CCHO + NO3 = HONO2 + CCO-O2. + RCO3.
C13	SAME K AS B2			CCO-O2. + NO = CO2 + NO2 + HCHO + RO2-R. + RO2.
C14	SAME K AS B4			CCO-O2. + NO2 = C-PAN

TABLE B-1. REACTIONS AND RATE CONSTANTS USED IN THE PHOTOCHEMICAL MODEL (CONTINUED).

Label[a]	Kinetic parameters[b]			Reaction[c]
C15	SAME K AS B6			CCO-O2. + HO2. = -OOH + CO2 + HCHO
C16	SAME K AS B9			CCO-O2. + RO2. = RO2. + #.5 HO2. + CO2 + HCHO
C17	SAME K AS B10			CCO-O2. + RCO3. = RCO3. + HO2. + CO2 + HCHO
C18	1.200E+18	26.91	0.000	C-PAN = CCO-O2. + NO2 + RCO3.
				Reactions of Propionaldehyde and PPN
C25	1.248E+04	-0.50	-1.000	RCHO + HO. = C2CO-O2. + RCO3.
C26	PHOT. = RCHO			RCHO + HV + #.2 = CCHO + RO2-R. + RO2. + CO + HO2.
C27	4.404E+02	2.84	-1.000	NO3 + RCHO = C2CO-O2. + RCO3.
C28	SAME K AS B2			C2CO-O2. + NO = CCHO + RO2-R. + CO2 + NO2 + RO2.
C29	SAME K AS B4			C2CO-O2. + NO2 = C2-PAN
C30	SAME K AS B6			C2CO-O2. + HO2. = -OOH + CCHO + CO2
C31	SAME K AS B9			C2CO-O2. + RO2. = RO2. + #.5 HO2. + CCHO + CO2
C32	SAME K AS B10			C2CO-O2. + RCO3. = RCO3. + HO2. + CCHO + CO2
C33	1.200E+18	26.91	0.000	C2-PAN = C2CO-O2. + NO2 + RCO3.
				Reactions of Acetone
C38	1.468E+04	2.23	-1.000	C-CO-C + HO. = CCOCHO + RO2-R. + RO2.
C39	PHOT. = KETONE			C-CO-C + HV + #.07 = CCO-O2. + HCHO + RO2-R. + RCO3. + RO2.
				Reactions of Methyl Ethyl Ketone
C44	1.761E+04	1.48	-1.000	MEK + HO. = H2O + #.5 "CCHO + HCHO + CCO-O2. + C2CO-O2." + RCO3. + #1.5 "R2O2. + RO2."
C57	PHOT. = KETONE			MEK + HV + #.1 = CCO-O2. + CCHO + RO2-R. + RCO3. + RO2.

TABLE B-1. REACTIONS AND RATE CONSTANTS USED IN THE PHOTOCHEMICAL MODEL (CONTINUED).

Label[a]	Kinetic parameters[b]			Reaction[c]
				Reactions of Glyoxal and Its PAN Analogue
C58A	PHOT. = GLYOXAL1			HCOCHO + HV + #.029 = #.13 HCHO + #.87 H2 + #1.87 CO
C59	1.688E+04	0.00	-1.000	HCOCHO + HO. = #.63 HO2. + #1.26 CO + #.37 "HCOCO-O2. + RCO3."
C60	8.807E+02	4.09	-1.000	HCOCHO + NO3 = HONO2 + #.63 HO2. + #1.26 CO + #.37 "HCOCO-O2. + RCO3."
C62	SAME K AS B2			HCOCO-O2. + NO = NO2 + CO2 + CO + HO2.
C63	SAME K AS B4			HCOCO-O2. + NO2 = HCO-PAN
C64	1.200E+18	26.91	0.000	HCO-PAN = HCOCO-O2. + NO2 + RCO3.
C65	SAME K AS B6			HCOCO-O2. + HO2. = -OOH + CO2 + CO
C66	SAME K AS B9			HCOCO-O2. + RO2. = RO2. + #.5 HO2. + CO2 + CO
C67	SAME K AS B10			HCOCO-O2. + RCO3. = RCO3. + HO2. + CO2 + CO
				Reactions of Methylglyoxal
C68	PHOT. = MEGLYOX			CCOCHO + HV + #QY.MGL = HO2. + CO + CCO-O2. + RCO3.
C69	2.495E+04	0.00	-1.000	CCOCHO + HO. = CO + CCO-O2. + RCO3.
C70	4.404E+03	2.84	-1.000	CCOCHO + NO3 = HONO2 + CO + CCO-O2. + RCO3.
				Reactions of the Lumped Alkyl Nitrate
C95	3.216E+04	1.41	-1.000	RONO2 + HO. = NO2 + #.155 MEK + #1.05 RCHO + #.48 CCHO + #.16 HCHO + #.61 -C + #1.39 "R2O2. + RO2."
				Reactions of Benzaldehyde and PBzN
G30	1.761E+04	0.00	-1.000	BZ-CHO + HO. = BZ-CO-O2. + RCO3.
G31	PHOT. = BZCHO			BZ-CHO + HV + #QY.BZA = #7 -C
G32	4.404E+02	2.97	-1.000	BZ-CHO + NO3 = HONO2 + BZ-CO-O2.
G33	SAME K AS B2			BZ-CO-O2. + NO = BZ-O. + CO2 + NO2 + R2O2. + RO2.

TABLE B-1. REACTIONS AND RATE CONSTANTS USED IN THE PHOTOCHEMICAL MODEL (CONTINUED).

Label[a]	Kinetic parameters[b]			Reaction[c]
G34	SAME K AS B4			BZ-CO-O2. + NO2 = BZ-PAN
G35	9.600E+16	25.90	0.000	BZ-PAN = BZ-CO-O2. + NO2 + RCO3.
G36	SAME K AS B6			BZ-CO-O2. + HO2. = -OOH + CO2 + PHENOL
G37	SAME K AS B9			BZ-CO-O2. + RO2. = RO2. + #.5 HO2. + CO2 + PHENOL
G38	SAME K AS B10			BZ-CO-O2. + RCO3. = RCO3. + HO2. + CO2 + PHENOL
G43	2.202E+04	0.00	-1.000	BZ-O. + NO2 = NITROPHEN
G44	4.404E+03	0.00	-1.000	BZ-O. + HO2. = PHENOL
G45	6.000E-02	0.00	0.000	BZ-O. = PHENOL
				Reactions of Phenol
G46	4.154E+04	0.00	-1.000	HO. + PHENOL = #.15 RO2-NP. + #.85 RO2-R. + #.2 HCOCHO + #4.7 -C + RO2.
G51	5.578E+03	0.00	-1.000	NO3 + PHENOL = HONO2 + BZ-O.
				Reactions of Cresols
G52	6.018E+04	0.00	-1.000	HO. + CRES = #.15 RO2-NP. + #.85 RO2-R. + #.2 CCOCHO + #5.5 -C + RO2.
G57	3.229E+04	0.00	-1.000	NO3 + CRES = HONO2 + BZ-O. + -C
				Reactions of Nitrophenols
G58	5.578E+03	0.00	-1.000	NITROPHEN + NO3 = HONO2 + BZ(NO2)-O.
G59	2.202E+04	0.00	-1.000	BZ(NO2)-O. + NO2 = #2 -N + #6 -C
G60	4.404E+03	0.00	-1.000	BZ(NO2)-O. + HO2. = NITROPHEN
G61	6.000E-02	0.00	0.000	BZ(NO2)-O. = NITROPHEN
				Reactions of the Pseudospecies Used to Represent the Uncharacterized Aromatic Ring-Opened Products
G7	4.404E+04	0.00	-1.000	HO. + HCOCHO(X) = HCOCO-O2. + RCO3.
G8	PHOT. = AROMUNKN			HCOCHO(X) + HV + #ARP1/U = HO2. + HCOCO-O2. + RCO3.

TABLE B-1. REACTIONS AND RATE CONSTANTS USED IN THE PHOTOCHEMICAL MODEL (CONTINUED).

Label[a]	Kinetic parameters[b]	Reaction[c]
G9	4.404E+04 0.00 -1.000	HO. + CCOCHO(X) = C2CO-O2. + RCO3.
G10	PHOT. = AROMUNKN	CCOCHO(X) + HV + #ARP2/U = HO2. + CO + CCO-O2. + RCO3.
		General Alkane Reactions
		(The kinetic and mechanistic parameters for all the alkanes included in this model are given in Table 9 in Section IV.A.2, where the parameter p_{RR} in the table refers to #RR in the listing below, p_{NR} refers to #NN, etc. The value for #RO2 is calculated as shown below. Table 9 gives the values of the parameters at 270, 300, and 330 K. The values for intermediate temperatures are obtained by linear interpolation.)
kOH		HO. + Alkane = #RR RO2-R. + #NR RO2-N. + #R2 R2O2. + #A1 HCHO + #A2 CCHO + #A3 RCHO + #K3 C-CO-C + #K4 MEK + #CO CO + #C2 CO2 + #RO2 RO2. (Where #RO2 = #RR + #NR + #R2)
		General Aromatic Reactions
		(The kinetic and mechanistic parameters for all the aromatic hydrocarbons included in this model are given in Table 10 in Section IV.A.3, where the parameter p_{RR} in the table refers to #RR in the listing below, etc. The values for #RO2 and #RH are calculated as shown below. The mechanistic parameters are temperature independent.)

TABLE B-1. REACTIONS AND RATE CONSTANTS USED IN THE PHOTOCHEMICAL MODEL (CONTINUED).

Label[a]	Kinetic parameters[b]			Reaction[c]
kOH				HO. + Aromatic = #RR RO2-R. + #NP RO2-NP. + #R2 R2O2. + #PH PHENOL + #CR CRES + #BZ BZ-CHO + #GL HCOCHO + #MG CCOCHO + #U1 HCOCHO(X) + #U2 CCOCHO(X) + #RH HO2. + #RO2 RO2. (Where #RO2 = #RR + #NP + #R2, and #RH = 1 - #RO2)
				Reactions of Ethene
D1	3.156E+03	-0.82	-1.000	C:C + HO. = #.22 CCHO + #1.56 HCHO + RO2-R. + RO2.
D6	1.761E+01	5.23	-1.000	C:C + O3 = HCHO + (HCHO2)
D8	1.527E+04	1.57	-1.000	C:C + O = HCHO + CO + HO2. + RO2-R. + RO2.
D9	2.936E+03	5.81	-1.000	C:C + NO3 = NO2 + #2 HCHO + R2O2. + RO2.
				Reactions of Propene
D14	7.119E+03	-1.00	-1.000	C:CC + HO. = HCHO + CCHO + RO2-R. + RO2.
D19	1.938E+01	4.18	-1.000	C:CC + O3 = #.5 "CCHO + (HCHO2) + HCHO + (CCHO2)"
D21	1.732E+04	0.64	-1.000	C:CC +O = #.6 C-CO-C + #.4 CO + #.4 HCHO + #.2 CCHO + #.2 HO2. + #.6 "RO2-R. + RO2."
D22	7.340E+03	3.84	-1.000	C:CC + NO3 = NO2 + CCHO + HCHO + R2O2. + RO2.
				Reactions of trans-2-Butene
D40	1.483E+04	-1.09	-1.000	CC:CC + HO. = #2 CCHO + RO2-R. + RO2.
D45	1.333E+01	2.26	-1.000	CC:CC + O3 = CCHO + (CCHO2)
D46	3.317E+04	-0.02	-1.000	CC:CC +O = MEK + #.4 HO2.
D47	1.468E+04	1.94	-1.000	CC:CC + NO3 = NO2 + #2 CCHO + R2O2. + RO2.

TABLE B-1. REACTIONS AND RATE CONSTANTS USED IN THE PHOTOCHEMICAL MODEL (CONTINUED).

Label[a]	Kinetic parameters[b]			Reaction[c]
				Reactions of 1-Butene
D27	9.585E+03	-0.93	-1.000	C:CCC + HO. = HCHO + RCHO + RO2-R. + RO2.
D32	5.079E+00	3.40	-1.000	C:CCC + O3 = #.5 "RCHO + (HCHO2) + HCHO + (C2CHO2)"
D34	1.835E+04	0.65	-1.000	C:CCC + O = #.44 MEK + #.39 "RCHO + -C" + #.17 "CO + HCHO + CCHO" + #.34 HO2.
D35	7.340E+03	3.70	-1.000	C:CCC + NO3 = NO2 + RCHO + HCHO + R2O2. + RO2.
				Reactions of Isobutene
D52	1.396E+04	-1.00	-1.000	ISOBUTEN + HO. = HCHO + C-CO-C + RO2-R. + RO2.
D57	5.211E+00	3.36	-1.000	ISOBUTEN + O3 = #.5 "C-CO-C + (HCHO2) + HCHO + (C(C)CO2)"
D59	2.584E+04	0.09	-1.000	ISOBUTEN + O = #.5 "MEK + RCHO + -C" + #.4 HO2.
D60	1.468E+04	2.14	-1.000	ISOBUTEN + NO3 = NO2 + HCHO + C-CO-C + R2O2. + RO2.
				Reactions of 1-Hexene
D71	9.571E+03	-1.00	-1.000	1-HEXEN + HO. = #.775 "HCHO + RCHO + RO2-R. + #2 -C" + #.225 "RO2-N. + #.5 -C" + RO2.
D72	5.079E+00	3.37	-1.000	1-HEXEN + O3 = #.5 "RCHO + (HCHO2) + HCHO + (C2CHO2)" + #2 -C
D74	1.835E+04	0.65	-1.000	1-HEXEN + O = #.44 MEK + #.39 RCHO + #.17 "CO + HCHO + CCHO" + #.34 HO2. + #2.39 -C
D75	7.340E+03	3.70	-1.000	1-HEXEN + NO3 = NO2 + RCHO + HCHO + R2O2. + RO2. + #2 -C
				General Higher Alkene Reactions
				(Mechanistic and kinetic parameters for the higher alkenes are given in Table 12 in Section IV.A.5. The

TABLE B-1. REACTIONS AND RATE CONSTANTS USED IN THE PHOTOCHEMICAL MODEL (CONTINUED).

Label[a]	Kinetic parameters[b]			Reaction[c]
				P1, ..., P5 parameters refer to the structure of the molecule, as follows: P1 = number of $=CH_2$ groups P2 = number of $=CHCH_3$ groups P3 = number of =CHR groups P4 = number of $=C(CH_3)2$ groups P5 = number of $=C(CH_3)R$ or $=CR_2$ groups. where R is any alkyl substituent other than CH_3)
kOH				Alkene + HO. = #P1R HCHO + #P2R CCHO + #P3R RCHO + #P4R C-CO-C + #P5R MEK + #PR RO2-R. + #PN RO2-N. + RO2. [Where #P1R = (1 - #PN) * #P1, etc., and #PR = 1 - #PN]
kO3				Alkene + O3 = #P1/2 "HCHO + (HCHO2)" + #P2/2 "CCHO + (CCHO2)" + #P3/2 "RCHO + (C2CHO2)" + #P4/2 "C-CO-C + (C(C)CO2)" + #P5/2 "MEK + (C(R)CO2)" (Where #P1/2 = 0.5 * #P1, etc.)
kO3P				Alkene + O = #.4 HO2. + #.5 "MEK + RCHO" + #O-C -C + #.8 MEK
kNO3				Alkene + NO3 = NO2 + #P1 HCHO + #P2 CCHO + #P3 RCHO + #P4 C-CO-C + #P5 MEK + R2O2. + RO2.
				Reactions of Alkene Ozonolysis Intermediates
D7	6.000E+01			(HCHO2) = #.4 HCHO2 + #.18 CO2 + #.42 CO + #.12 H2 + #.42 H2O + #.12 HO2.
D65	7.927E-03	0.00	-1.000	HCHO2 + H2O = -C
D20	6.000E+01			(CCHO2) = #.2 CCHO2 + #.14 CH4 + #.29 CO2 + #.15 CO + #.03 HCHO + #.27 "HCHO + RO2-R. + RO2." + #.21 HO2. + #.12 HO. + #.72 -C
D66	7.927E-03	0.00	-1.000	CCHO2 + H2O = #2 -C

TABLE B-1. REACTIONS AND RATE CONSTANTS USED IN THE PHOTOCHEMICAL MODEL (CONTINUED).

Label[a]	Kinetic parameters[b]			Reaction[c]
D33	6.000E+01			(C2CHO2) = #.2 C2CHO2 + #.14 C2 + #.29 CO2 + #.15 CO + #.3 CCHO + #.27 "RO2-R. + RO2." + #.21 HO2. + #.12 HO. + #1.08 -C
D67	7.927E-03	0.00	-1.000	C2CHO2 + H2O = #3 -C
D58	6.000E+01			(C(C)CO2) = #.2 "HO. + CCOCHO + RO2-R. + RO2." + #.8 MEK + #-.8 -C
D58B	6.000E+01			(C(R)CO2) = #.2 "HO. + RCO3." + #.1 "CCHO + HCHO + CCO-O2. + C2CO-O2." + #.3 "R2O2. + RO2." + #.8 MEK
				Reactions of Furan
K1	1.938E+04	-0.66	-1.000	HO. + FURAN = #FUR-V "R2O2. + RO2." + HO2. + #FUR-P HET-UNKN
K2	2.055E+03	0.00	-1.000	NO3 + FURAN = HO2. + HONO2
				Reactions of Thiophene
K1	4.697E+03	-0.64	-1.000	HO. + THIOPHEN = HO2. + #THI-PU HET-UNKN + HET-UNK2 + #THI-U1 HCOCHO(X)
K6	4.697E+01	0.00	-1.000	NO3 + THIOPHEN = HO2. + HONO2
				Reactions of Pyrrole
K11	1.761E+05	0.00	-1.000	HO. + PYRROLE = #PYR-P HET-UNKN + HO2. + #PYR-V "R2O2. + RO2." + HET-UNK2
K12	7.193E+04	0.00	-1.000	NO3 + PYRROLE = HO2. + HONO2
				Reactions of the Pseudospecies Used to Represent the Uncharacterized Reactive Products of Furan, Thiophene and Pyrrole
K3	PHOT. = AROMUNKN			HET-UNKN + HV + #HETP/U = #2 HO2.
K14	3.596E+02	0.00	-1.000	HET-UNK2 + NO3 = NO

TABLE B-1. REACTIONS AND RATE CONSTANTS USED IN THE PHOTOCHEMICAL MODEL (CONTINUED).

[a]Reaction label notation of Carter et al. (Reference 26).

[b]The kinetic parameters in this mechanism, which are used by the computer modeling software to define the rate constants as a function of temperature, light intensity and spectral distribution, or rate constants for other reactions, are specified in one of four ways:

1. Simple Thermal Reactions:

If the kinetic parameters are given as three numbers without any additional notation, then the numbers given are (in order) A, Ea, and B, and the rate constant, k, is calculated by the modified Arrhenius expression.

$$k = A \times (T/300)^{B} \times \exp\left[-Ea / (0.0019872 \times T)\right]$$

where T is the temperature in K, Ea is given in kcal $mole^{-1}$, and the units of k and A are min^{-1} for first order reactions, ppm^{-1} min^{-1} for second order reactions, or min^{-1} for third order reactions. (The order of the reaction is determined by the number of non-coefficient reactants.)

[If a reaction has the symbol "#RCONxxxx as one of the "reactants" (where "xxxx" is the reaction label of some previous input reaction which should be the reverse of this reaction), then the "k" calculated as given above is actually an equilibrium constant, since the rate constant for this reaction is given by "k" times the rate constant for reaction "xx." See footnote c for a discussion of coefficients as reactants.]

2. "Falloff" Thermal Reactions:

If the kinetic parameters are given as seven numbers in the following format,

FALLOFF F= f, N= n

k_0: A_0, Ea_0, B_0

k_I: A_I, Ea_I, B_I

then the rate constant, k is calculated by

$$k = \left[(k_0 \times M)/(1 + [k_0 \times M / k_I])\right] * f^{g}$$

where

$$g = 1/[1 + (\log10\,[k_0 \times M / k_I] / n)^2]$$

and

TABLE B-1. REACTIONS AND RATE CONSTANTS USED IN THE PHOTOCHEMICAL MODEL (CONTINUED).

$$k_0 = A_0 \times (T/300)^{B0} * \exp(-Ea_0 / [0.0019872 \times T])$$
$$k_I = A_I \times (T/300)^{BI} * \exp(-Ea_I / [0.0019872 \times T])$$

and T is the temperature in K. and M is the concentration of the constant species "M", which is the the total pressure in ppm. In this model, M is always 10^6 ppm.

Reactions of this type are always second order, so the units of k, k_I and A_I are ppm^{-1} min^{-1}, and the units of k_0 and A_0 are ppm^{-2} min^{-2}. The units of Ea_0 and Ea_I are kcal/mole.

3. Reactions with Same Rate Constants as Other Reactions

The notation "SAME K AS xxxx," where "xxxx" is the reaction label for some other reaction, means that the reaction always has the same rate constant as reaction "xxxx."

4. Photolysis Reactions

Photolysis reactions are indicated by the notation "PHOT. = filename," where "filename" refers to a "photolysis file," which gives the absorption coefficients and quantum yields, as a function of wavelength, which are used to calculate the photolysis rate constants given the spectral distribution of the light source. The contents of the photolysis files used in this mechanism are given in Table B-3.

[c]The following examples indicate the notation used to define the reactants, products, and (where applicable) coefficients involved in the reactions in the mechanism:

```
reactant1 + reactant2 + ... = product1 + product2 + ...
reactant1 + ... = #coef1 product1 + ...
reactant1 + ... = #coef2 "product1 + product2 + ..." + ...
reactant1 + #coef3 + ... = product1 + ...
```

The first example is a simple reaction without any coefficients. The second and third have product coefficients which give the yield of the products. The notation in the third reaction is used to indicate that both "product1" and "product2" have the same coefficient, and thus, that reaction is equvalent to

```
reactant1 + ... = #coef2 product1 + #coef2 product2 + ...
```

When a coefficient is shown as a "reactant," as in the fourth example, the coefficient is multiplied by the rate constant calculated from the kinetic parameters (as described in footnote b, above), to give the rate constant of the reaction. For example, one of the reactions used to represent the chamber radical source is

TABLE B-1. REACTIONS AND RATE CONSTANTS USED IN THE PHOTOCHEMICAL MODEL (CONCLUDED).

RSI) PHOT. = NO2 HV + #RS-I = HO.

and for this reaction, the rate constant, defining the rate of OH generation, is given by the photolysis rate of NO_2 multiplied by the value of the coefficient specified, which in this case is the value assigned to the parameter RS-I. A special kind of reactant coefficient is that of the form "#RCONxxxx," whose value is the rate constant for the reaction labeled "xxxx."

Regardless of how the coefficients are used, they can be either constant as indicated by numbers, or variable coefficients, which have non-numeric names. In some cases the coefficients can depend on other coefficients or on temperature. The values of the variable coefficients are given in the tables in Section IV as indicated in the reaction list.

If the list of reactants, products, and coefficients do not fit on one line, they are continued on the following line.

TABLE B-2. LIST OF SPECIES USED IN THE PHOTOCHEMICAL MODEL.

Species name	Compound or use
Species Integrated Explicitly	
Inorganic Reactants and CO	
O3	Ozone
NO	Nitric Oxide
NO2	Nitrogen Dioxide
NO3	Nitrate Radical
N2O5	N_2O_5
HONO2	Nitric Acid
HONO	Nitrous Acid
HO2.	HO_2 Radicals
HO2NO2	Peroxy Nitric Acid
HO2H	Hydrogen Peroxide
CO	Carbon Monoxide
Peroxy and Hydroperoxy Pseudo-Species	
RO2.	Lumped Alkyl Peroxy Radicals (sum of all alkyl peroxy radicals)
RCO3.	Lumped Acyl Peroxy Radicals (sum off all acyl peroxy radicals)
-OOH	Lumped Hydroperoxide Group (used to represent photolizable hydroperoxide groups formed when peroxy radicals react with HO_2)
Organic Oxygenate and Nitrate Products	
HCHO	Formaldehyde
CCHO	Acetaldehyde
C-PAN	PAN
RCHO	Propionaldehyde and Lumped Higher Aldehydes
C2-PAN	PPN (and PAN analogues formed from higher aldehydes)
C-CO-C	Acetone
CCOCHO	Methyl Glyoxal
MEK	Methyl Ethyl Ketone and Lumped Higher Ketones
HCOCHO	Glyoxal
HCO-PAN	HCO-CO-OONO$_2$ (PAN analogue formed from glyoxal)
RONO2	Lumped Alkyl Nitrates
BZ-CHO	Benzaldehyde
BZ-PAN	PBzN
PHENOL	Phenol

TABLE B-2. LIST OF SPECIES USED IN THE PHOTOCHEMICAL MODEL (CONTINUED).

Species name	Compound or use
CRES	Cresols and other alkyl phenols
NITROPHEN	Nitrophenols
HCOCHO(X)	Pseudo-Species Used to Represent the Reactions of Uncharacterized Aromatic Ring-Opened Products Which Do Not Have Methyl Groups
CCOCHO(X)	Pseudo-Species Used to Represent the Reactions of Uncharacterized Aromatic Ring-Opened Products Which Which Have Methyl Groups
HET-UNKN	Pseudo-Species Used to Represent the Reactions of Uncharacterized Photoreactive Products Formed in Reactions of Furan, Thiophene, and Pyrrole
HET2-UNKN	Pseudo-Species Used to Represent the Reactions of Uncharacterized Products, Formed in the Reactions of Thiophene and Pyrrole, Which React with NO_3 Radicals
Alkanes	
Alkane	Any alkane in the model. The names used for specific alkanes are listed in Table 9 in Section IV.A.2.
Aromatic Hydrocarbons	
Aromatic	Any aromatic hydrocarbon in the model. The names used for specific aromatic hydrocarbons are listed in Table 10 in Section IV.A.3
Alkenes	
C:C	Ethene
C:CC	Propene
C:CCC	1-Butene
CC:CC	trans-2-Butene
ISOBUTEN	Isobutene
1-HEXEN	1-Hexene
Alkene	Any higher alkene in the model. The names used for specific higher alkenes are listed in Table 12 in Section IV.A.5.

TABLE B-2. LIST OF SPECIES USED IN THE PHOTOCHEMICAL MODEL (CONTINUED).

Species name	Compound or use
Other Organic Reactants	
FURAN	Furan
THIOPHEN	Thiophene
PYRROLE	Pyrrole
Species Held Constant in the Calculations	
HV	Total Light Intensity. Always 1.0 in these calculations
O2	Oxygen in Air (always 2.090E+05 PPM)
M	Total Pressure (always 1.000E+06 PPM)
H2O	Water Concentration. 2.0E+04 ppm used for ITC simulations, and 2.08E+04 used for simulations of airshed scenarios
Product-Only and Counter Species (species which are formed, but which do not react, or pseudo-species used to keep track of carbon, nitrogen, etc.)	
-C	"Lost" or Unreactive Product Carbon (used to check for carbon balance, and to determine the extent of species whose reactions are ignored)
-N	"Lost" or Unreactive Product Nitrogen (used to check for nitrogen balance)
NOX-WALL	NO_x Absorbed on the Walls (used primarily to check for nitrogen balance)
CO2	Carbon Dioxide
CH4	Methane (reactions ignored)
H2	Hydrogen (reactions ignored)
C2	Ethane
Species for which the Steady State Approximation is Applied	
Inorganic Radicals and Atoms	
O	$O(^3P)$ Atoms
O*1D2	$O(^1D)$ Atoms
HO.	Hydroxyl Radicals

TABLE B-2. LIST OF SPECIES USED IN THE PHOTOCHEMICAL MODEL (CONTINUED).

Species name	Compound or use
Pseudo-Species Used in the Representation of Peroxy Radical Reactions	
RO2-R.	Pseudospecies Used to Represent the Conversion of NO to NO_2 and the Formation of HO_2 Resulting from the Reactions of Most Peroxy Radicals
R2O2.	Pseudospecies Used to Represent the Additional NO to NO_2 Conversion Resulting from the Reactions of Certain Peroxy Radicals
RO2-N.	Pseudospecies Used to Represent the Conversion of NO to NO_2 and the Formation of $RONO_2$ Resulting from the Reactions of Certain Peroxy Radicals
RO2-NP.	Pseudospecies Used to Represent the Conversion of NO to NO_2 and the Formation of Nitrophenol Resulting from the Reactions of Some Aromatic Peroxy Radicals
Acyl Peroxy Radicals	
CCO-O2.	Acetyl Peroxy Radicals
C2CO-O2.	Propionyl Peroxy Radicals
HCOCO-O2.	Acyl Peroxy Radical Formed when O_2 Reacts with HCOCO.
BZ-CO-O2.	Benzoyl Peroxy Radical
Alkene Ozonolysis Intermediates	
(HCHO2)	"Hot" Criegee Biradical Formed in the Reactions of Ozone with Alkenes with $=CH_2$ Groups
HCHO2	Stabilized Criegee Biradical Formed in the Reactions of Ozone with Alkenes with $=CH_2$ Groups
(CCHO2)	"Hot" Criegee Biradical Formed in the Reactions of Ozone with Alkenes with $=CHCH_3$ Groups
CCHO2	Stabilized Criegee Biradical Formed in the Reactions of Ozone with Alkenes with $=CHCH_3$ Groups
(C2CHO2)	"Hot" Criegee Biradical Formed in the Reactions of Ozone with Alkenes with =CHR Groups (where R is any alkyl group other than CH_3)
C2CHO2	Stabilized Criegee Biradical Formed in the Reactions of Ozone with Alkenes with =CHCHR Groups (where R is any alkyl group other than CH_3)

TABLE B-2. LIST OF SPECIES USED IN THE PHOTOCHEMICAL MODEL (CONCLUDED).

Species name	Compound or use
(C(C)CO2)	"Hot" Criegee Biradical Formed in the Reactions of Ozone with Alkenes with $=C(CH_3)_2$ Groups
(C(R)CO2)	"Hot" Criegee Biradical Formed in the Reactions of Ozone with Alkenes with $=C(CH_3)R$ or $=CR_2$ Groups (where R is any alkyl group other than CH_3)
Other Organic Intermediates	
BZ-O.	Phenoxy Radical

TABLE B-3. ABSORPTION COEFFICIENT x QUANTUM YIELD PRODUCTS USED TO CALCULATE THE PHOTOLYSIS REACTION RATE CONSTANTS.

PHOT. name[a]	(Wavelength, absorption coefficient x quantum yield) (microns) (cm^2 $molec^{-1}$, base e)		
NO2	(0.250 2.830E-20)	(0.255 1.450E-20)	(0.260 1.900E-20)
	(0.265 2.010E-20)	(0.270 3.130E-20)	(0.275 4.020E-20)
	(0.280 5.540E-20)	(0.285 6.990E-20)	(0.290 8.180E-20)
	(0.295 6.970E-20)	(0.300 1.156E-19)	(0.305 1.619E-19)
	(0.310 1.695E-19)	(0.315 2.137E-19)	(0.320 2.383E-19)
	(0.325 2.581E-19)	(0.330 2.730E-19)	(0.335 3.105E-19)
	(0.340 3.445E-19)	(0.345 3.561E-19)	(0.350 3.538E-19)
	(0.355 4.361E-19)	(0.360 3.779E-19)	(0.365 4.768E-19)
	(0.370 4.406E-19)	(0.375 3.906E-19)	(0.380 4.852E-19)
	(0.385 4.158E-19)	(0.390 4.440E-19)	(0.395 4.771E-19)
	(0.400 4.394E-19)	(0.405 2.022E-19)	(0.410 8.078E-20)
	(0.415 4.221E-20)	(0.420 1.433E-20)	(0.425 0.000E-01)
NO3NO	(0.585 0.000E-01)	(0.590 1.285E-18)	(0.595 1.632E-18)
	(0.600 7.075E-19)	(0.605 6.900E-19)	(0.610 2.960E-19)
	(0.615 1.960E-19)	(0.620 3.580E-19)	(0.625 4.625E-19)
	(0.630 2.830E-19)	(0.635 4.350E-20)	(0.640 0.000E-01)
NO3NO2	(0.400 0.000E-01)	(0.405 3.000E-20)	(0.410 4.000E-20)
	(0.415 5.000E-20)	(0.420 8.000E-20)	(0.425 1.000E-19)
	(0.430 1.300E-19)	(0.435 1.800E-19)	(0.440 1.900E-19)
	(0.445 2.200E-19)	(0.450 2.800E-19)	(0.455 3.300E-19)
	(0.460 3.700E-19)	(0.465 4.300E-19)	(0.470 5.100E-19)
	(0.475 6.000E-19)	(0.480 6.400E-19)	(0.485 6.900E-19)
	(0.490 8.800E-19)	(0.495 9.500E-19)	(0.500 1.010E-18)
	(0.505 1.100E-18)	(0.510 1.320E-18)	(0.515 1.400E-18)
	(0.520 1.450E-18)	(0.525 1.480E-18)	(0.530 1.940E-18)
	(0.535 2.040E-18)	(0.540 1.810E-18)	(0.545 1.810E-18)
	(0.550 2.360E-18)	(0.555 2.680E-18)	(0.560 3.070E-18)
	(0.565 2.530E-18)	(0.570 2.540E-18)	(0.575 2.740E-18)
	(0.580 3.050E-18)	(0.585 2.770E-18)	(0.590 3.855E-18)
	(0.595 2.448E-18)	(0.600 1.556E-18)	(0.605 1.380E-18)
	(0.610 4.350E-19)	(0.615 4.900E-19)	(0.620 7.160E-19)
	(0.625 1.388E-18)	(0.630 2.830E-19)	(0.635 0.000E-01)
O3O3P	(0.260 1.070E-08)	(0.270 7.740E-19)	(0.280 3.790E-19)
	(0.290 1.340E-19)	(0.300 3.160E-20)	(0.310 4.341E-20)
	(0.320 2.600E-20)	(0.330 6.700E-21)	(0.340 1.700E-21)
	(0.350 4.000E-22)	(0.355 0.000E-01)	(0.400 0.000E-01)
	(0.450 1.600E-22)	(0.500 1.340E-21)	(0.550 3.320E-21)
	(0.600 5.060E-21)	(0.650 2.450E-21)	(0.700 8.700E-22)
	(0.750 3.200E-22)	(0.800 1.600E-22)	(0.900 0.000E-01)

TABLE B-3. ABSORPTION COEFFICIENT x QUANTUM YIELD PRODUCTS USED TO CALCULATE THE PHOTOLYSIS REACTION RATE CONSTANTS (CONTINUED).

PHOT. name[a]	(Wavelength, absorption coefficient x quantum yield) (microns) (cm^2 $molec^{-1}$, base e)		
O3T270	(0.260 9.630E-18)	(0.270 6.966E-18)	(0.280 3.411E-18)
	(0.290 1.206E-18)	(0.300 3.420E-19)	(0.305 1.617E-19)
	(0.310 4.508E-20)	(0.313 1.200E-20)	(0.315 3.640E-21)
	(0.317 1.248E-21)	(0.320 0.000E-01)	
O3T300	(0.260 9.630E-18)	(0.270 6.966E-18)	(0.280 3.411E-18)
	(0.290 1.206E-18)	(0.300 3.420E-19)	(0.305 1.673E-19)
	(0.310 5.488E-20)	(0.313 1.950E-20)	(0.315 6.760E-21)
	(0.317 2.080E-21)	(0.320 0.000E-01)	
O3T330	(0.260 9.630E-18)	(0.270 6.966E-18)	(0.280 3.411E-18)
	(0.290 1.206E-18)	(0.300 3.420E-19)	(0.305 1.692E-19)
	(0.310 6.174E-20)	(0.313 2.700E-20)	(0.315 1.144E-20)
	(0.317 4.992E-21)	(0.320 7.800E-22)	(0.322 0.000E-01)
HONO	(0.311 0.000E-01)	(0.312 2.000E-21)	(0.313 4.200E-21)
	(0.314 4.600E-21)	(0.315 4.200E-21)	(0.316 3.000E-21)
	(0.317 4.600E-21)	(0.318 3.600E-20)	(0.319 6.100E-20)
	(0.320 2.100E-20)	(0.321 4.270E-20)	(0.322 4.010E-20)
	(0.323 3.930E-20)	(0.324 4.010E-20)	(0.325 4.040E-20)
	(0.326 3.130E-20)	(0.327 4.120E-20)	(0.328 7.550E-20)
	(0.329 6.640E-20)	(0.330 7.290E-20)	(0.331 8.700E-20)
	(0.332 1.380E-19)	(0.333 5.910E-20)	(0.334 5.910E-20)
	(0.335 6.450E-20)	(0.336 5.910E-20)	(0.337 4.580E-20)
	(0.338 1.910E-19)	(0.339 1.630E-19)	(0.340 1.050E-19)
	(0.341 8.700E-20)	(0.342 3.350E-19)	(0.343 2.010E-19)
	(0.344 1.020E-19)	(0.345 8.540E-20)	(0.346 8.320E-20)
	(0.347 8.200E-20)	(0.348 7.490E-20)	(0.349 7.130E-20)
	(0.350 6.830E-20)	(0.351 1.740E-19)	(0.352 1.140E-19)
	(0.353 3.710E-19)	(0.354 4.960E-19)	(0.355 2.460E-19)
	(0.356 1.190E-19)	(0.357 9.350E-20)	(0.358 7.780E-20)
	(0.359 7.290E-20)	(0.360 6.830E-20)	(0.361 6.900E-20)
	(0.362 7.320E-20)	(0.363 9.000E-20)	(0.364 1.210E-19)
	(0.365 1.330E-19)	(0.366 2.130E-19)	(0.367 3.520E-19)
	(0.368 4.500E-19)	(0.369 2.930E-19)	(0.370 1.190E-19)
	(0.371 9.460E-20)	(0.372 8.850E-20)	(0.373 7.440E-20)
	(0.374 4.770E-20)	(0.375 2.700E-20)	(0.376 1.900E-20)
	(0.377 1.500E-20)	(0.378 1.900E-20)	(0.379 5.800E-20)
	(0.380 7.780E-20)	(0.381 1.140E-19)	(0.382 1.400E-19)
	(0.383 1.720E-19)	(0.384 1.990E-19)	(0.385 1.900E-19)
	(0.386 1.190E-19)	(0.387 5.650E-20)	(0.388 3.200E-20)
	(0.389 1.900E-20)	(0.390 1.200E-20)	(0.391 5.000E-21)
	(0.392 0.000E-01)		

TABLE B-3. ABSORPTION COEFFICIENT x QUANTUM YIELD PRODUCTS USED TO CALCULATE THE PHOTOLYSIS REACTION RATE CONSTANTS (CONTINUED).

PHOT. name[a]	(Wavelength, absorption coefficient x quantum yield) (microns) (cm^2 $molec^{-1}$, base e)		
H2O2	(0.250 8.300E-20)	(0.255 6.700E-20)	(0.260 5.200E-20)
	(0.265 4.200E-20)	(0.270 3.200E-20)	(0.275 2.500E-20)
	(0.280 2.000E-20)	(0.285 1.500E-20)	(0.290 1.130E-20)
	(0.295 8.700E-21)	(0.300 6.600E-21)	(0.305 4.900E-21)
	(0.310 3.700E-21)	(0.315 2.800E-21)	(0.320 2.000E-21)
	(0.325 1.500E-21)	(0.330 1.200E-21)	(0.335 9.000E-22)
	(0.340 7.000E-22)	(0.345 5.000E-22)	(0.350 3.000E-22)
	(0.355 0.000E-01)		
CO2H	(0.210 3.750E-19)	(0.220 2.200E-19)	(0.230 1.380E-19)
	(0.240 8.800E-20)	(0.250 5.800E-20)	(0.260 3.800E-20)
	(0.270 2.500E-20)	(0.280 1.500E-20)	(0.290 9.000E-21)
	(0.300 5.800E-21)	(0.310 3.400E-21)	(0.320 1.900E-21)
	(0.330 1.100E-21)	(0.340 6.000E-22)	(0.350 4.000E-22)
	(0.360 0.000E-01)		
HCHOR	(0.240 6.300E-23)	(0.250 3.120E-22)	(0.260 1.410E-21)
	(0.270 3.440E-21)	(0.280 1.097E-20)	(0.290 1.782E-20)
	(0.300 2.044E-20)	(0.310 1.886E-20)	(0.320 1.147E-20)
	(0.330 5.456E-21)	(0.340 0.000E-01)	
HCHOM	(0.240 1.260E-22)	(0.250 5.980E-22)	(0.260 2.256E-21)
	(0.270 3.956E-21)	(0.280 6.510E-21)	(0.290 6.526E-21)
	(0.300 5.764E-21)	(0.310 5.635E-21)	(0.320 7.030E-21)
	(0.330 1.214E-20)	(0.340 8.142E-21)	(0.350 1.680E-21)
	(0.360 7.200E-23)	(0.370 0.000E-01)	
CCHOR	(0.260 6.696E-21)	(0.270 1.315E-20)	(0.280 2.549E-20)
	(0.290 2.618E-20)	(0.295 2.181E-20)	(0.300 1.672E-20)
	(0.305 1.111E-20)	(0.310 6.392E-21)	(0.315 3.135E-21)
	(0.320 1.200E-21)	(0.325 3.390E-22)	(0.330 0.000E-01)
RCHO	(0.280 5.260E-20)	(0.290 5.770E-20)	(0.300 5.050E-20)
	(0.310 3.680E-20)	(0.320 1.660E-20)	(0.330 6.490E-21)
	(0.340 1.440E-21)	(0.345 0.000E-01)	
KETONE	(0.210 1.100E-21)	(0.220 1.200E-21)	(0.230 4.600E-21)
	(0.240 1.300E-20)	(0.250 2.680E-20)	(0.260 4.210E-20)
	(0.270 5.540E-20)	(0.280 5.920E-20)	(0.290 5.160E-20)
	(0.300 3.440E-20)	(0.310 1.530E-20)	(0.320 4.600E-21)
	(0.330 1.100E-21)	(0.340 0.000E-01)	

TABLE B-3. ABSORPTION COEFFICIENT x QUANTUM YIELD PRODUCTS USED TO CALCULATE THE PHOTOLYSIS REACTION RATE CONSTANTS (CONTINUED).

PHOT. name[a]	(Wavelength, absorption coefficient x quantum yield) (microns) (cm^2 $molec^{-1}$, base e)		
GLYOXAL	(0.230 2.867E-21)	(0.235 2.867E-21)	(0.240 4.301E-21)
	(0.245 5.735E-21)	(0.250 8.602E-21)	(0.255 1.147E-20)
	(0.260 1.434E-20)	(0.265 1.864E-20)	(0.270 2.294E-20)
	(0.275 2.581E-20)	(0.280 2.867E-20)	(0.285 3.298E-20)
	(0.290 3.154E-20)	(0.295 3.298E-20)	(0.300 3.584E-20)
	(0.305 2.724E-20)	(0.310 2.724E-20)	(0.312 2.867E-20)
	(0.315 2.294E-20)	(0.320 1.434E-20)	(0.325 1.147E-20)
	(0.327 1.434E-20)	(0.330 1.147E-20)	(0.335 2.867E-21)
	(0.340 0.000E-01)	(0.355 0.000E-01)	(0.360 2.294E-21)
	(0.365 2.867E-21)	(0.370 8.029E-21)	(0.375 1.004E-20)
	(0.380 1.720E-20)	(0.382 1.577E-20)	(0.384 1.491E-20)
	(0.386 1.491E-20)	(0.388 2.867E-20)	(0.390 3.154E-20)
	(0.391 3.242E-20)	(0.392 3.040E-20)	(0.393 2.229E-20)
	(0.394 2.634E-20)	(0.395 3.040E-20)	(0.396 2.634E-20)
	(0.397 2.432E-20)	(0.398 3.242E-20)	(0.399 3.040E-20)
	(0.400 2.837E-20)	(0.401 3.242E-20)	(0.402 4.458E-20)
	(0.403 5.269E-20)	(0.404 4.255E-20)	(0.405 3.040E-20)
	(0.406 3.040E-20)	(0.407 2.837E-20)	(0.408 2.432E-20)
	(0.409 2.837E-20)	(0.410 6.079E-20)	(0.411 5.066E-20)
	(0.412 6.079E-20)	(0.412 4.863E-20)	(0.413 8.308E-20)
	(0.414 6.484E-20)	(0.414 7.497E-20)	(0.414 8.105E-20)
	(0.415 8.105E-20)	(0.415 6.890E-20)	(0.416 4.255E-20)
	(0.417 4.863E-20)	(0.418 5.876E-20)	(0.419 6.687E-20)
	(0.420 3.850E-20)	(0.421 5.674E-20)	(0.421 4.458E-20)
	(0.422 5.269E-20)	(0.423 1.054E-19)	(0.423 8.511E-20)
	(0.424 6.079E-20)	(0.425 7.295E-20)	(0.426 1.175E-19)
	(0.426 1.297E-19)	(0.427 1.074E-19)	(0.428 1.662E-19)
	(0.429 4.053E-20)	(0.430 5.066E-20)	(0.431 4.863E-20)
	(0.432 4.053E-20)	(0.433 3.647E-20)	(0.434 4.053E-20)
	(0.435 6.079E-20)	(0.435 5.066E-20)	(0.436 8.105E-20)
	(0.437 1.135E-19)	(0.437 5.269E-20)	(0.438 1.013E-19)
	(0.438 1.378E-19)	(0.439 7.700E-20)	(0.440 2.472E-19)
	(0.441 8.105E-20)	(0.442 6.079E-20)	(0.443 7.497E-20)
	(0.444 9.321E-20)	(0.445 1.135E-19)	(0.446 5.269E-20)
	(0.447 2.432E-20)	(0.448 2.837E-20)	(0.449 3.850E-20)
	(0.450 6.079E-20)	(0.451 1.094E-19)	(0.451 9.321E-20)
	(0.452 1.216E-19)	(0.453 2.391E-19)	(0.454 1.702E-19)
	(0.455 3.404E-19)	(0.456 4.053E-19)	(0.456 1.013E-19)
	(0.457 1.621E-20)	(0.458 1.216E-20)	(0.458 1.418E-20)
	(0.459 4.053E-21)	(0.460 4.053E-21)	(0.461 6.079E-21)
	(0.461 2.026E-21)	(0.462 0.000E-01)	

TABLE B-3. ABSORPTION COEFFICIENT x QUANTUM YIELD PRODUCTS USED TO CALCULATE THE PHOTOLYSIS REACTION RATE CONSTANTS (CONCLUDED).

PHOT. name[a]	(Wavelength, absorption coefficient x quantum yield) (microns) (cm^2 $molec^{-1}$, base e)		
MEGLYOX	(0.220 2.103E-21)	(0.225 2.103E-21)	(0.230 4.206E-21)
	(0.235 7.570E-21)	(0.240 9.252E-21)	(0.245 8.411E-21)
	(0.250 9.252E-21)	(0.255 9.252E-21)	(0.260 9.673E-21)
	(0.265 1.051E-20)	(0.270 1.262E-20)	(0.275 1.430E-20)
	(0.280 1.514E-20)	(0.285 1.430E-20)	(0.290 1.472E-20)
	(0.295 1.178E-20)	(0.300 1.136E-20)	(0.305 9.252E-21)
	(0.310 6.308E-21)	(0.315 5.467E-21)	(0.320 3.365E-21)
	(0.325 1.682E-21)	(0.330 8.411E-22)	(0.335 0.000E-01)
	(0.350 0.000E-01)	(0.354 4.206E-22)	(0.358 1.262E-21)
	(0.360 2.103E-21)	(0.362 2.103E-21)	(0.364 2.944E-21)
	(0.366 3.365E-21)	(0.368 4.206E-21)	(0.370 5.467E-21)
	(0.372 5.888E-21)	(0.374 7.570E-21)	(0.376 7.991E-21)
	(0.378 8.832E-21)	(0.380 1.009E-20)	(0.382 1.093E-20)
	(0.384 1.346E-20)	(0.386 1.514E-20)	(0.388 1.724E-20)
	(0.390 2.061E-20)	(0.392 2.103E-20)	(0.394 2.313E-20)
	(0.396 2.481E-20)	(0.398 2.607E-20)	(0.400 2.776E-20)
	(0.402 2.986E-20)	(0.404 3.196E-20)	(0.406 3.785E-20)
	(0.408 3.953E-20)	(0.410 4.332E-20)	(0.412 4.710E-20)
	(0.414 4.794E-20)	(0.416 4.879E-20)	(0.418 5.047E-20)
	(0.420 5.215E-20)	(0.422 5.299E-20)	(0.424 5.173E-20)
	(0.426 5.299E-20)	(0.428 5.215E-20)	(0.430 5.551E-20)
	(0.432 5.131E-20)	(0.434 5.678E-20)	(0.436 6.224E-20)
	(0.438 6.056E-20)	(0.440 5.467E-20)	(0.441 6.140E-20)
	(0.442 5.467E-20)	(0.443 5.551E-20)	(0.433 6.813E-20)
	(0.444 5.972E-20)	(0.445 5.131E-20)	(0.446 4.879E-20)
	(0.447 5.720E-20)	(0.448 5.467E-20)	(0.449 6.561E-20)
	(0.450 5.047E-20)	(0.451 3.028E-20)	(0.452 4.290E-20)
	(0.453 2.776E-20)	(0.454 2.271E-20)	(0.456 1.766E-20)
	(0.458 8.411E-21)	(0.460 4.206E-21)	(0.464 1.682E-21)
	(0.468 0.000E-01)		
BZCHO	(0.299 1.776E-19)	(0.304 7.400E-20)	(0.306 6.910E-20)
	(0.309 6.410E-20)	(0.313 6.910E-20)	(0.314 6.910E-20)
	(0.318 6.410E-20)	(0.325 8.390E-20)	(0.332 7.650E-20)
	(0.338 8.880E-20)	(0.342 8.880E-20)	(0.346 7.890E-20)
	(0.349 7.890E-20)	(0.354 9.130E-20)	(0.355 8.140E-20)
	(0.364 5.670E-20)	(0.368 6.660E-20)	(0.369 8.390E-20)
	(0.370 8.390E-20)	(0.372 3.450E-20)	(0.374 3.210E-20)
	(0.376 2.470E-20)	(0.377 2.470E-20)	(0.380 3.580E-20)
	(0.382 9.900E-21)	(0.386 0.000E-01)	
AROMUNKN	(0.200 3.950E-20)	(0.350 3.950E-20)	(0.360 0.000E-01)

[a]PHOT. Name is the photolysis file name referenced by the PHOT. entry given for photolysis reactions in the reaction list in Table B-1.

TABLE B-4. PHOTOLYSIS RATE CONSTANTS CALCULATED FOR INDOOR TEFLON® CHAMBER (ITC) RUNS WHERE K1 = 0.235 MIN^{-1}, AND FOR REPRESENTATIVE EVACUABLE CHAMBER (EC) RUNS.

PHOT. name[a]	ITC	EC-266	EC-340	EC-345	EC-901
NO2	0.3250	0.3500	0.4000	0.3900	0.4100
NO3NO	0.0000	0.4134	0.6379	0.5805	0.7325
NO3NO2	1.0848E-02	3.904	5.980	5.453	6.879
O3O3P	1.5196E-03	1.1303E-02	1.6236E-02	1.4996E-02	1.7091E-02
O3T270	3.1942E-04	1.5393E-03	6.4003E-04	1.0079E-03	2.5276E-06
O3T300	3.6890E-04	1.6362E-03	7.1883E-04	1.0950E-03	3.8897E-06
O3T330	4.2684E-04	1.7324E-03	8.0185E-04	1.1834E-03	6.1323E-06
HONO	9.8416E-02	6.9451E-02	7.6641E-02	7.5026E-02	7.1373E-02
H2O2	2.6320E-04	2.3037E-04	2.1040E-04	2.1777E-04	5.4987E-05
CO2H	2.7481E-04	2.2944E-04	2.1238E-04	2.1875E-04	6.4287E-05
HCHOR	7.0554E-04	8.3117E-04	7.4194E-04	7.7322E-04	8.8945E-05
HCHOM	2.2469E-03	1.4974E-03	1.4903E-03	1.4864E-03	5.4396E-04
CCHOR	6.4621E-05	1.4533E-04	1.0202E-04	1.2060E-04	3.1325E-06
RCHO	1.1271E-03	1.3778E-03	1.1963E-03	1.2650E-03	1.4562E-04
KETONE	2.7789E-04	4.5473E-04	3.5602E-04	3.9659E-04	2.5364E-05
GLYOXAL	1.0646E-02	6.8151E-02	8.8730E-02	8.4709E-02	0.1046
MEGLYOX	6.8765E-03	4.2249E-02	5.4453E-02	5.2132E-02	6.4954E-02
BZCHO	5.1362E-02	3.3363E-02	3.5383E-02	3.4896E-02	2.7002E-02
AROMUNKN	1.5164E-02	9.1904E-03	9.2649E-03	9.2306E-03	4.5425E-03

[a]PHOT. Name is the photolysis file name referenced by the PHOT. entry given for photolysis reactions in the reaction list in Table B-1.

TABLE B-5. PHOTOLYSIS RATE CONSTANTS CALCULATED FOR AMBIENT AIR SIMULATIONS FOR SOLAR ZENITH ANGLES OF 0, 30, 60, AND 80 DEGREES.

PHOT. name	Z=0	Z=30	Z=60	Z=80
NO2	0.4974	0.4587	0.3003	6.8382E-02
NO3NO	1.118	1.072	0.8492	0.2912
NO3NO2	10.14	9.708	7.627	2.522
O3O3P	2.9380E-02	2.7750E-02	2.0943E-02	6.9760E-03
O3T270	2.0321E-03	1.4416E-03	3.1129E-04	1.0821E-05
O3T300	2.2697E-03	1.6309E-03	3.7284E-04	1.4326E-05
O3T330	2.5105E-03	1.8273E-03	4.4416E-04	1.9475E-05
HONO	9.7642E-02	8.9586E-02	5.6944E-02	1.2482E-02
H2O2	4.5195E-04	3.8702E-04	1.8679E-04	2.9300E-05
CO2H	4.4349E-04	3.8110E-04	1.8659E-04	2.9882E-05
HCHOR	1.8149E-03	1.5376E-03	6.9645E-04	9.4492E-05
HCHOM	2.7772E-03	2.4637E-03	1.3501E-03	2.4718E-04
CCHOR	2.9228E-04	2.2986E-04	7.6966E-05	6.1656E-06
RCHO	2.9553E-03	2.4783E-03	1.0841E-03	1.4174E-04
KETONE	9.5019E-04	7.7296E-04	3.0064E-04	3.2774E-05
GLYOXAL	0.1361	0.1286	9.4830E-02	2.6271E-02
MEGLYOX	7.9919E-02	7.5519E-02	5.5558E-02	1.5162E-02
BZCHO	5.1595E-02	4.6606E-02	2.7840E-02	5.7093E-03
AROMUNKN	1.5856E-02	1.4105E-02	7.8665E-03	1.4868E-03

[a]PHOT. Name is the photolysis file name referenced by the PHOT. entry given for photolysis reactions in the reaction list in Table B-1.